POLITECNICO DI MILANO

Scuola di Ingegneria Industriale e dell'Informazione

Corso di Laurea Magistrale in
Ingegneria Energetica

LUMPED PARAMETER AND CFD MODELLING OF EJECTORS FOR REFRIGERATION APPLICATIONS

Relatore: Prof. Fabio Inzoli
Correlatore: Ing. Giorgio Besagni

Tesi di Laurea di:
Giuseppe Di Leo
Matricola 801073

Anno Accademico 2013 - 2014

Acknowledgments

Desidero innanzitutto ringraziare Giorgio Besagni per i suoi preziosi consigli, per tutto il tempo che mi ha dedicato e per avermi seguito costantemente durante tutto il percorso che ha portato alla stesura di questo lavoro.

Un doveroso ringraziamento va anche al Professor Fabio Inzoli e a tutto il gruppo di ricerca CFDLab per la loro disponibilità e il loro aiuto.

Inoltre desidero ringraziare lo staff del Sistema Bibliotecario di Ateneo per l'ottimo servizio di reperimento degli articoli scientifici e per il prezioso lavoro che svolgono per gli studenti.

Il ringraziamento più grande lo devo alla mia famiglia, per il loro sostegno e per aver sempre creduto in me.

Un grande ringraziamento va anche a tutti i miei amici. Se sono arrivato fino a questo punto è anche merito del loro incoraggiamento che mi ha aiutato a dare sempre il meglio di me. Nonostante alcuni di loro siano lontani, li ho sempre sentiti al mio fianco.

Grazie anche ai miei compagni di Università per questi anni trascorsi insieme. Vi auguro di intraprendere una brillante carriera lavorativa.

Grazie a tutti voi,

Giuseppe

Abstract

Most of the actual refrigeration systems are activated by electricity and their use has increased during the recent years so much to move the peak electricity consumptions from winter to summer seasons. A possible solution to reduce electricity consumptions is the use of thermal refrigeration systems, such as those based on ejectors. The ejector refrigeration systems are characterized by high reliability and low costs and can exploit low-grade energy sources (i.e. solar energy or waste heat from industrial processes). The ejector is the most critical component of these systems and modelling techniques able to provide accurate information about its performance are needed for a proper evaluation of the refrigeration system operation. The ejector modelling techniques can be divided into lumped parameter models (based on thermodynamic equations) and Computational Fluid Dynamics (CFD) models. The aims of this thesis are to analyze and apply both modelling techniques to case studies and to propose an integrated lumped parameter-CFD model for supersonic ejector. This modelling technique could combine the simplicity of the lumped parameter models with the detailed description of local fluid dynamics phenomena provided by the CFD models. The thesis is structured in five chapters. In the first and in the second chapter, the state of the art of ejector technology and ejector modelling are presented and discussed. The third chapter concerns the analysis of the lumped parameter models and their implementation to examine the influence of the operating conditions and working fluids on ejector performance. The fourth chapter concerns the CFD modelling technique and is composed of two parts. In the first part, a CFD approach is validated comparing the performance of the main RANS turbulence models and their different wall treatments. In the second part, the validated CFD approach is used to examine the performance of three different ejector geometric shapes as a function of the operating conditions. In the fifth chapter, the integrated lumped parameter-CFD model is presented for supersonic ejectors.

Keywords: ejectors; ejector refrigeration systems; supersonic ejector modelling; lumped parameter models; CFD modelling; RANS turbulence models

Italian abstract

La maggior parte dei sistemi di refrigerazione esistenti è attivata da energia elettrica e il loro utilizzo è diventato talmente importante da spostare il picco di consumi di energia elettrica dai mesi invernali a quelli estivi. Una possibile soluzione per ridurre i consumi sono i sistemi di refrigerazione attivati da energia termica, come gli impianti basati su eiettori. Questi sistemi, oltre ad avere un'affidabilità molto elevata e bassi costi, possono essere progettati per utilizzare energia termica di basso pregio (come può essere quella derivante da pannelli solari o il calore di scarto dei processi industriali). L'eiettore è il componente critico di questi impianti ed è quindi necessario avere a disposizione strumenti che possano fornire informazioni precise sulle sue prestazioni. Le tecniche utilizzate per la modellazione degli eiettori comprendono i modelli termodinamici a parametri concentrati e i modelli di termofluidodinamica computazionale (CFD). Questa tesi si pone come obiettivi l'analisi e l'impiego di entrambi gli approcci nello studio di concreti casi applicativi e proporre un modello integrato termodinamico-CFD per eiettori supersonici. Questa tecnica modellistica può unire la semplicità di implementazione dei modelli a parametri concentrati con la descrizione dettagliata dei fenomeni fluidodinamici locali fornita dai modelli CFD. La tesi è strutturata in cinque capitoli. Nel primo e nel secondo capitolo vengono presentati, rispettivamente, lo stato dell'arte della tecnologia basata sugli eiettori e delle tecniche di modellazione utilizzate. Il terzo capitolo riguarda l'analisi dei modelli a parametri concentrati e la loro implementazione per esaminare l'influenza delle condizioni operative e dei fluidi di lavoro sulle prestazioni dell'eiettore. Il quarto capitolo riguarda l'approccio CFD ed è suddiviso in due parti. La prima parte è costituita da un'analisi di validazione dell'approccio CFD, confrontando le prestazioni dei principali modelli di turbolenza RANS e dei diversi trattamenti a parete. Nella seconda parte, il modello CFD validato viene utilizzato per esaminare le prestazioni di tre diverse configurazioni geometriche di un eiettore al variare delle condizioni operative. Nel quinto capitolo viene presentato il modello integrato termodinamico-CFD per eiettori supersonici.

Italian keywords: eiettori; sistemi di refrigerazione con eiettori; modellazione degli eiettori supersonici; modelli a parametri concentrati; modellazione CFD; modelli di turbolenza RANS

Italian extended abstract

Negli ultimi anni le caratteristiche della domanda e dei consumi di energia elettrica stanno subendo molti cambiamenti. In particolare, il settore terziario e il settore residenziale stanno assumendo un peso sempre più rilevante sul bilancio elettrico, principalmente a causa del crescente utilizzo degli impianti di climatizzazione e condizionamento dell'aria negli edifici pubblici, commerciali e residenziali. L'*International Institute of Refrigeration in Paris* (IIF/IIR) ha stimato che nel 2012 il 15% dell'energia elettrica prodotta a livello mondiale è stata impiegata in impianti di refrigerazione e di condizionamento dell'aria. La maggior parte dei sistemi di refrigerazione esistenti è infatti attivata da energia elettrica e il loro utilizzo è diventato talmente importante da spostare il picco di consumi di energia elettrica dai mesi invernali a quelli estivi. Tale tendenza avrà effetti importanti nel settore elettrico che quindi dovrà essere interessato non solo da un adeguamento infrastrutturale, ma anche da interventi significativi sul fronte della domanda di energia elettrica. Una possibile soluzione a questi problemi può essere l'impiego di sistemi di refrigerazione attivati da energia termica, come gli impianti basati su eiettori.

Gli eiettori sono dei dispositivi costituiti da un ugello, una camera di aspirazione, una camera di miscelazione e un diffusore. Un flusso primario ad alta pressione accelera ed espande attraverso l'ugello, creando una zona di bassa pressione in prossimità della sezione di uscita. Questo consente l'aspirazione di un flusso secondario, il quale, passando attraverso la camera di aspirazione, viene introdotto all'interno dell'eiettore. Grazie alla sua elevata energia cinetica, il flusso primario trascina quello secondario lungo la camera di miscelazione, nella quale ha luogo il trasferimento di quantità di moto e di energia tra i due flussi. Il flusso miscelato è anche interessato da onde d'urto che determinano un incremento di pressione. Il completo recupero di energia di pressione, a scapito dell'energia cinetica, avviene nel diffusore divergente.

Negli impianti di refrigerazione, gli eiettori sostituiscono, completamente o in parte, il compressore, riducendo notevolmente i consumi di energia elettrica e i costi d'investimento. Inoltre l'eiettore non ha organi in movimento e questo determina un incremento della disponibilità e dell'affidabilità dell'intero impianto. Un ulteriore vantaggio di questi sistemi consiste nel fatto che possono essere progettati per utilizzare energia termica di basso pregio (come può essere quella derivante da pannelli solari o il calore di scarto dei processi industriali). Questa importante caratteristica è in linea con la direttiva europea 2009/28/EC, la quale prevede che, entro il 2020, il 25% dell'energia destinata ai sistemi di riscaldamento e refrigerazione dovrà provenire da fonti energetiche rinnovabili. Tuttavia, i sistemi di refrigerazione con eiettore non sono riusciti ad affermarsi sul mercato a causa del basso coefficiente di prestazione (*COP*) rispetto ai sistemi di refrigerazione tradizionali a compressione di vapore. Pertanto l'interesse della ricerca scientifica nei confronti degli eiettori è volto a studiare il suo comportamento fluidodinamico al fine di incrementare le prestazioni.

Le tecniche utilizzate per la modellazione degli eiettori comprendono i modelli a parametri concentrati e i modelli di termofluidodinamica computazionale (CFD). I modelli a parametri concentrati si basano su alcune ipotesi (p. es. flusso monodimensionale, adiabatico e stazionario) al fine di semplificare il problema e agevolarne la risoluzione, tramite semplici equazioni che derivano dai bilanci di massa, quantità di moto ed energia. L'approccio CFD, invece, utilizza il metodo ai volumi finiti e opportuni algoritmi numerici per risolvere le equazioni differenziali alle derivate parziali che descrivono il problema fluidodinamico. I modelli a parametri concentrati

hanno un ridotto onere computazionale, mentre i modelli CFD sono in grado di descrivere in modo molto dettagliato il comportamento locale del fluido.

La tesi è strutturata in cinque capitoli. Il primo capitolo illustra in modo molto dettagliato lo stato dell'arte dei sistemi di refrigerazione con eiettori, descrivendo le diverse configurazioni impiantistiche e le prestazioni ottenute. L'analisi mostra che negli anni si è riusciti ad incrementare le performance di questi impianti, attraverso una progettazione dell'eiettore più accurata e grazie all'introduzione di nuove tipologie di impianto. Per esempio i sistemi standard di refrigerazione con eiettore sono passati da $COP = 0.12$ nel 1964 a $COP = 0.75$ ottenuto in anni più recenti. I sistemi ibridi eiettore-compressore, invece, sono oggi in grado di ottenere un coefficiente di prestazione compreso nell'intervallo $COP = 5 \div 7$, risultando molto competitivi rispetto ai sistemi tradizionali a compressione di vapore e ai cicli frigoriferi ad assorbimento.

Il secondo capitolo riguarda le tecniche di modellazione degli eiettori. Per ogni tipologia di approccio modellistico (parametri concentrati, CFD) vengono riportate le equazioni costitutive dei modelli, le condizioni al contorno e le ipotesi semplificative comunemente utilizzate nella risoluzione del problema. Entrambi gli approcci si suddividono in base a due sottocategorie: (i) fluido monofase o bifase e (ii) fluido ideale o reale. Le tecniche di risoluzione sono diverse a seconda della categoria presa in esame.

Il terzo capitolo riguarda l'analisi dei modelli a parametri concentrati. Sono stati selezionati dalla letteratura cinque modelli termodinamici e sono stati validati tramite il confronto con alcuni studi sperimentali provenienti dalla letteratura. Al fine di esaminare l'influenza delle condizioni operative e dei fluidi di lavoro sulle prestazioni dell'eiettore, uno dei modelli analizzati è stato implementato al variare delle condizioni termodinamiche del fluido primario, secondario e di uscita. L'analisi ha mostrato che le prestazioni del sistema dipendono molto dal refrigerante utilizzato, anche in funzione delle condizioni operative dell'impianto. Per temperature di generazione maggiori di 100°C, gli idrocarburi R600 e R601 raggiungono le prestazioni migliori ($COP = 0.3 \div 0.4$), mentre per temperature più basse i refrigeranti migliori sono R134a e R152a ($COP = 0.15 \div 0.25$).

Il quarto capitolo riguarda l'approccio CFD ed è suddiviso in due parti. La prima parte è costituita da un'analisi di validazione dell'approccio CFD, confrontando le prestazioni dei principali modelli di turbolenza RANS e dei diversi trattamenti a parete. In particolare, i modelli di turbolenza scelti sono: *Spalart-Allmaras*, *Standard k-*ε, *RNG k-*ε, *Realizable k-*ε, *Standard k-*ω, *SST k-*ω e *Reynolds Stress Model*. Lo studio ha mostrato che il modello *SST k-*ω permette di ottenere i risultati migliori e una buona descrizione del campo di moto all'interno dell'eiettore. Per ogni modello di turbolenza, sono stati utilizzati diversi trattamenti a parete al fine di testare la loro influenza sui risultati. Per i modelli *RSM* e *k-*ε, la funzione di parete "*Enhanced wall function*" ha consentito un miglioramento dei risultati, mentre i modelli *Low-Reynolds* (*Spalart-Allmaras* e *k-*ω) hanno risentito in maniera minore dell'effetto del raffinamento della griglia in prossimità della parete. Nella seconda parte, il modello CFD validato è stato utilizzato per esaminare le prestazioni di tre diverse configurazioni geometriche di un eiettore al variare delle condizioni operative. Lo studio sperimentale di riferimento di questa analisi aveva evidenziato alcuni comportamenti da parte dei tre eiettori ai quali non era stato possibile fornire delle spiegazioni plausibili. Lo studio CFD e l'analisi dei campi di moto degli eiettori sono stati in grado di risolvere queste problematiche.

Nel quinto capitolo viene presentato il modello integrato termodinamico-CFD per eiettori supersonici. Questa tecnica modellistica può unire la semplicità di implementazione dei modelli a parametri concentrati con la descrizione dettagliata dei fenomeni fluidodinamici locali fornita dai

modelli CFD. Infatti, le simulazioni CFD vengono utilizzate per definire delle mappe di efficienza per ogni componente dell'eiettore, dalle quali è poi possibile ricavare delle correlazioni facilmente implementabili in un modello a parametri concentrati.

Contents

List of Figures

List of Tables

Introduction

The characteristics of the electricity demand are rapidly changing. This involves significant rearrangements of the entire electrical system [1, 2]. In the present study, we take as a reference Italy. Here we present and discuss primary energy and electricity consumption.

Historically, the primary energy and electricity use have grown: final primary energy consumption (FPEC) in 2005 was 146.6 million tonnes of oil equivalent (Mtoe) and between 1995 and 2005 FPEC increased by 17%. Then it decreased steadily until 2008 and the following year it has fallen by 6%, in correspondence with the global economic crisis [3].

The electricity has followed this growth trend too: from 1997 to 2008 it has risen about 26%, reaching 319 TWh, but in 2009 it began to drop [4]. The latest available statistics date back to 2012, in the course of Eurozone crisis: total electricity consumption reached 307.2 TWh (-2.1% from the previous year).

Table 1: Primary energy consumptions [4].

	Gross consumption [Mtoe]	Final consumption [Mtoe]
1995	171.69	125.60
1996	171.69	125.90
1997	174.37	127.70
1998	179.43	131.16
1999	182.67	134.09
2000	185.90	134.85
2001	188.77	137.47
2002	188.07	136.29
2003	194.38	142.26
2004	196.83	144.00
2005	197.78	146.59
2006	196.19	145.66
2007	193.69	142.91
2008	191.30	141.12
2009	180.34	132.71
2010	187.79	138.58
2011	183.89	134.49

Table 2: Electricity consumptions (GRTN - Terna).

	Demand [TWh]	Consumption [TWh]
1997	271.4	253.7
1998	279.3	260.8
1999	285.8	267.3
2000	298.5	279.3
2001	304.8	285.5
2002	310.7	291.0
2003	320.7	299.8
2004	325.4	304.5
2005	330.4	309.8
2006	337.5	317.5
2007	339.9	319.0
2008	339.5	319.0
2009	320.3	299.9
2010	330.5	309.9
2011	334.6	313.8
2012	328.2	307.2

Subdividing by different sectors, the reduction in industry consumptions was the worst since post-war; while in the civil one, fluctuations in its trend were probably due to climatic factors that have influenced room air-conditioning [5]. The tertiary sector has registered the highest increment (+3.4%), exceeding 100 TWh [6].

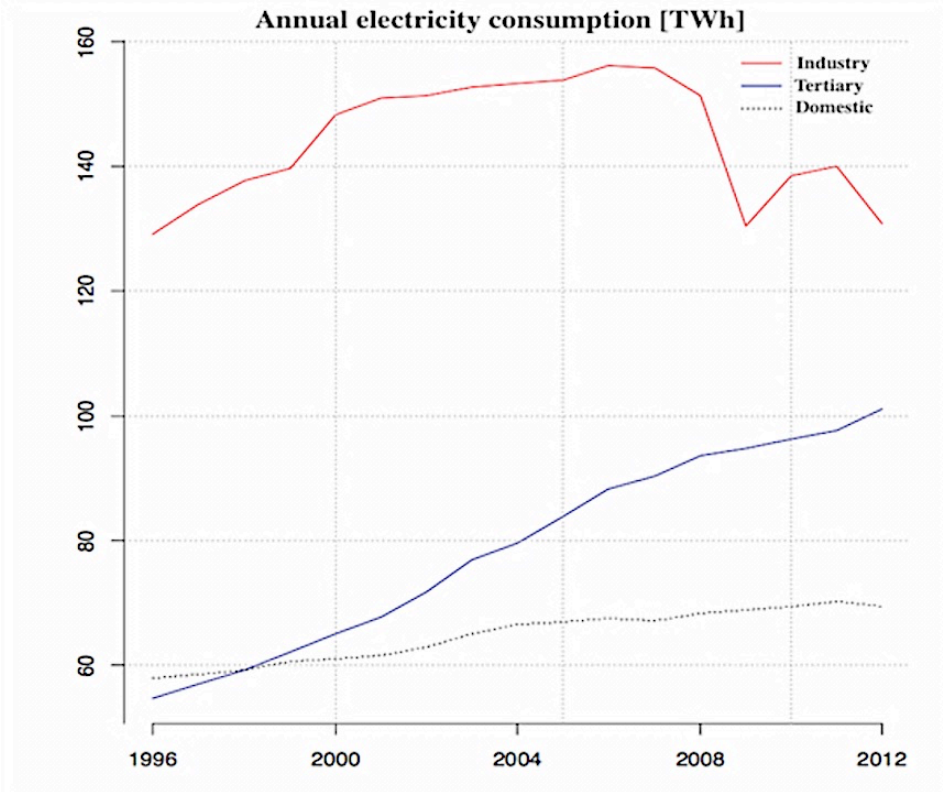

Figure 1: Electricity consumption by sector – modified from [1].

In this framework, it is interesting to analyse the future tendencies of electricity. The Italian electricity transmission system operator, Terna S.p.A., has redacted a report [1] that shows new previsions about future electricity demand, in terms of energy and power. Terna expects a "demand's electrification", consequent widening of electricity application in many new sectors. According to their analysis, in fact, it will be a growth of primary energy demand but electricity requirement will increase more, raising its relative weight. Particularly influential will be the development of electric vehicles and air-conditioning systems for summer and winter use. Therefore, there will be a continuous increase of demand of electricity.

Another aspect to take into account is the peak power demand. In the past the highest value was recorded in winter, but for some year is summer that requires maximum power: in 2012 the peak was equal to 54.1 GW, requests on 10 July. Also in the future it is expected that the highest power demand continue to grow, but with a largest growth rate in summery month and it is estimated that in 2023 will need a total available generation capacity equal to 83 GW to offset the maximum load [1]. This is mainly due to the consumption development in tertiary and residential sectors, essentially caused by widespread of some technologies, such as air conditioning units and cold chain [2]. These areas will weigh increasingly on national electric budget, also resulting in structural changes on electricity sector. Consequently, electrical system will need not only new power plants, but also strong measures in the matter of energy demand.

One of these interventions will certainly affect the refrigeration field and thermal energy refrigeration may be the solution to many problems [7-9]. Cold production is useful in many human and industrial necessities, like air-conditioning and conservation of foods and other products. However, conventional refrigeration cycles are driven by mechanical vapour compressors, using large amounts of electricity provides by fossil-fuel power plants. This involves a high load on the power transmission grid and, on the other hand, air pollution and greenhouse gases emissions, causing global warming. The estimates of The International Institute of Refrigeration in Paris (IIF/IIR) say that 15% of all the electricity produced in the world is employed for refrigeration and air-conditioning processes [10], with a great impact.

Thermal energy refrigeration, using low-grade heat or solar energy for cooling purposes, would allow a significant reduction of these drawbacks: it can provide cheap and clean energy for refrigeration all over the world [11]. Moreover, an additional advantage is that the heat source is widely available where it has required (i.e. chemical and food processing plants, hot places) [12] and their use is important not only for ecological aspects, but also for energy and cost savings [13]: the Mediterranean countries could save approximately 50% of their costs [11]. A final important aspect to consider is that electricity is not easily accessible everywhere, thus the employment of solar energy represents a good alternative solution [10].

The European directive to promote renewable energy 2009/28/EC [14] calls for 25% of EU heating and cooling to be supplied by renewable in 2020. It is an onerous object consider also that the EU project SACE (Solar Air Conditioning in Europe) predicted for the following years a strong increase in the demand for building cooling and air-conditioning, by a factor 4 in the 2020 [15]. To achieve this ambitious target, it is essential to increase the use of renewable energy sources, coupled with efficiency measures and each member state is authorized to support demand also through financial incentives.

Various technologies have been proposed, very different from each other but all of them are intended to reduce electricity consumption and environmental impact. However, several factors such as initial and capital cost, the availability of energy sources, performance and operating conditions must be considered to properly design and compare energy-efficient refrigeration systems [16]. A more detailed analysis will be carried out in the following chapter; in general, thermal energy refrigeration devices can reach a coefficient of performance COP less than the vapour-compression systems, but producing refrigeration from thermal energy remains an inviting prospect and the attractiveness of “free” cooling has stimulated research in recent years [17].

Among the most promising technologies, the heat-driven ejector refrigeration systems (ERS) appear like an attractive solution to use heat supply and they have several advantages over conventional compression systems: except for a small pump, the cycle has no moving parts, low capital cost, simplicity of operation, reliability and low maintenance cost [18]. ERS possible applications are [19]:

- In buildings, solar-driven ejectors may be used for heating and cooling purpose or in distributed tri-generation systems;
- In industry, they represent an attractive solution for waste heat upgrading and new opportunities for their integration in innovative cycle based on the combinations of ejectors with vapour compression or absorption systems.

Nevertheless, ERS have not yet been able to penetrate the market because of their low coefficient of performance, mainly due to fluid dynamic losses occurring inside the ejector. Thus, many

researchers have been engaged in improving it and combining ERS with other refrigeration systems in order to enhance the overall system performance [7].

In the present thesis, the modelling techniques of ejectors for refrigeration systems will be presented and discussed. It is structured as follow: the first two chapters are detailed reviews concerning respectively heat-driven refrigeration systems, focusing on jet refrigeration devices, and ejectors numerical modelling, explaining several approaches that are used in the last years. The third chapter talks about the Lumped Parameter Model (LPM) of ejectors. Five thermodynamic models, taken from literature, have been implemented and validated and an applicative case is analyzed in order to enquire into several parameters that can affect the ejector performance. The fourth chapter concerns the Computational Fluid Dynamic (CFD) models. Many ejector configurations and operating conditions have been analyzed through several CFD turbulence models and the predicted results have been compared with experimental data. The validated model is then used to examine some fluid dynamic aspects that occur in the ejector. In the fifth chapter the integrated lumped parameter-CFD model (ILPM-CFD) is presented. The ILPM-CFD purpose is to exploit the advantages of both the approaches, using the validated CFD model to generate efficiency maps and correlations for employ them in the LPM models. The thesis structure is summarized in the Figure 2.

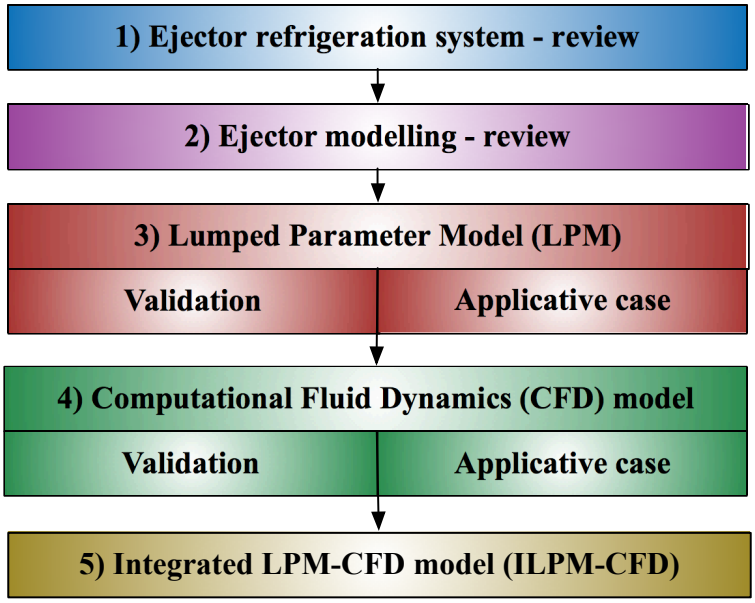

Figure 2: Schematic representation of the thesis structure.

Chapter 1

Jet refrigeration: a comprehensive review

In this chapter we present and discuss the jet refrigeration technologies and the role of working fluid on their performance. The present chapter is organized as follow. The first part concerns a brief overview of thermal energy refrigeration systems. In the second part we describe ejector's technology and behaviour. The third part concerns a detailed description of refrigerant properties, in order to justify the choices on their selection that have been made over the years by the authors. The fourth part is a review focused on the main jet refrigeration cycle proposed and analysed in literature. Finally, an overview over the whole ejector technology is presented with a focus on the past, present and future trends with the purpose to illustrate the progresses made and the evolution of ejector refrigeration systems.

1.1 Thermal energy refrigeration systems

When referring to thermal refrigeration technologies, a system where thermal power is used for cooling purposes is concerned [1, 2]. To use the energy source in the form of heat is, in general, simple. Instead, the generation of refrigerating effect is a much more complex operation because it implies the reduction of the entropy of a cold body by means of a series of thermo-mechanical or thermo-chemical processes [3]. The thermal energy refrigeration system has attracted many attentions in the recent years. Indeed, researchers are increasingly focusing on renewable energy sources [1], particularly solar energy [4] due to its cleanliness and natural availability. In this sense, thermal energy refrigeration may contribute to [1, 5]:

- the replacement of fossil fuel demand by the use of solar heat and by this, contributing to the European policy targets on the increased use of renewable energy [6];
- the support in stability of electricity grid by less electrical energy and peak power demand [7, 8];
- the reduction of greenhouse effect emissions through both saving in primary energy and avoidance of environmental harmful refrigerants;
- the optimized use of solar thermal systems through use of solar heat for combined assistance of space heating, cooling and domestic hot water preparation.

As shown in Figure 1-1, the various solar energy refrigeration systems can be divided into two families, according to the way in which solar energy is used:

- photovoltaic cells [9] produce electricity in order to move the compressor (vapour compression or Stirling cycle) or to exploit Peltier effect [10] (thermo-electric effect). Their operation is equal to traditional systems, but they make use of renewable energy, with all the

advantages and disadvantages that this entails. In general, they have a high *COP* but penalized by low PV cells efficiency. They are significantly more expensive (as shown in Ref. [11]).

- solar thermal collectors provide, directly or indirectly, the thermal energy required to evaporate working fluid. These devices are very different from each other; normally they are cheaper but with a lower *COP*.

In the refrigeration field, the photovoltaic systems and the solar thermal energy plants have been used over the last few decades to meet the cold needs for both domestic and industrial purposes [1]. The main refrigeration systems that make use of solar energy as cycle source are:

- vapour absorption/adsorption refrigeration;
- vapour jet refrigeration;
- solar vapour compression refrigeration;
- photovoltaic vapour compression refrigeration;
- photovoltaic thermoelectric refrigeration;
- photovoltaic Stirling cycle.

As in the mechanical compression systems, the mentioned tools are based on the refrigerant evaporation method, but consuming much less or not at all electricity. All these refrigeration systems have their own application field, marked by the temperature at which they can produce the cooling capacity. For further information the reader may refer to [1, 9, 12].

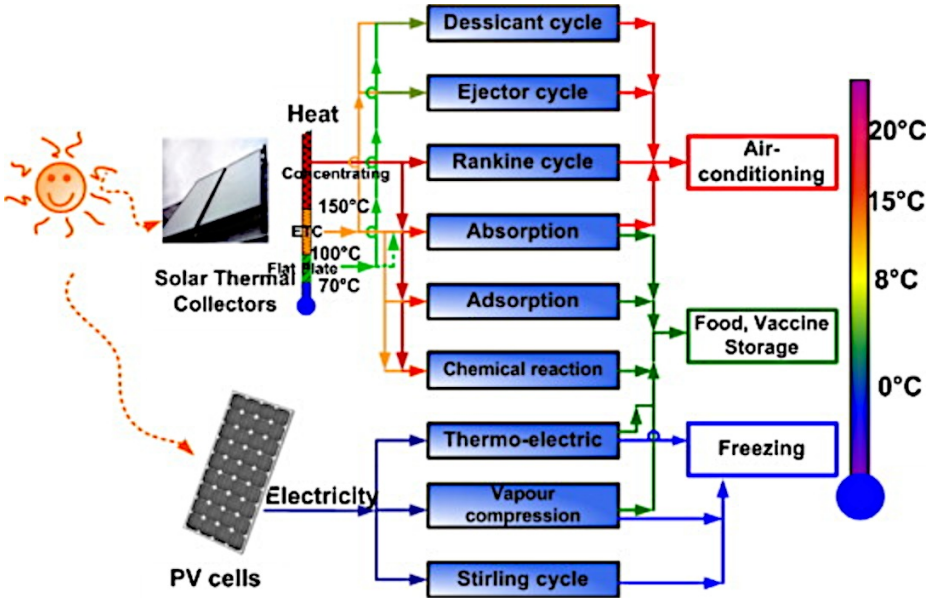

Figure 1-1: Solar cooling paths – taken from [10].

Generally speaking, the thermal cooling technology is preferred to the PV-based cooling systems because it can utilize more incident sunlight and thus it provides greater energy conversion efficiency than a PV system [1].

In the following sections, a detailed ejector description will be provided and a wide review about the main ejector refrigeration systems and the refrigerant fluids used will be presented.

1.2 Ejectors technology

1.2.1 Technology

Ejectors are devices constituted by a motive nozzle, a suction chamber, a mixing chamber and a final diffuser (Figure 1-2). A high-pressure primary flow, passing through the nozzle, accelerates and expands. This produces a lower pressure region near the nozzle exit, allowing the entrance of a secondary fluid. Thus, primary fluid entrains the secondary fluid in the suction chamber and, being faster, it drags the entrained fluid throughout the mixing chamber, in virtue of the momentum and energy transfer. Indeed, the large velocity difference between the two streams produces the "shear stress layer" interface and shear mixing occurs. In a given section, the two flows will be completely mixed and the remaining kinetic energy must be recovered. This happens in the diffuser, where the mixed stream is compressed and kinetic energy is converted into pressure energy.

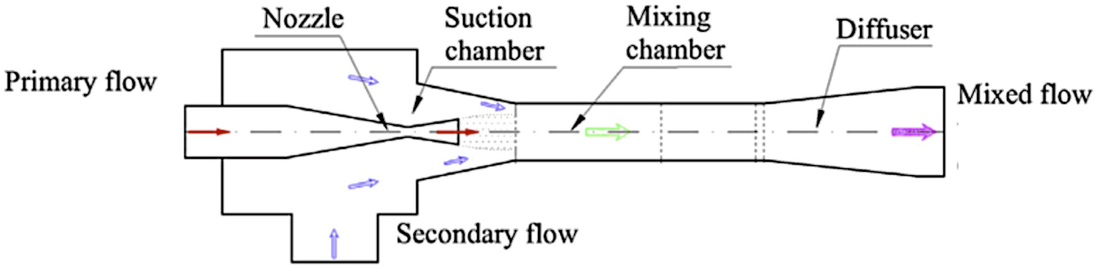

Figure 1-2: Schematic view of an ejector structure – modified from [13].

1.2.2 Ejector classification

The ejector can be classified accordingly with (i), (ii) and (iii) in Table 1-1. In the following paragraphs those classifications will be detailed.

Table 1-1: Ejector classification – taken from [14].

Parameters	Condition	Classification
Nozzle position	Inside suction chamber	CPM ejector
	Inside constant-area section	CAM ejector
Nozzle design	Convergent	Subsonic ejector
	Convergent-divergent	Supersonic ejector
Number of Phases	Single phase flow	Single phase ejector
	Two phase flow	Two phase ejector

1.2.2.1 Nozzle position

According to the position of the nozzle, the ejector design is classified in [15-17]:

- Constant-pressure mixing ejector (CPM), in which the nozzle exit plane is located within the converging area throat. It was assumed that the mixing of the primary and entrained flows occurs in the suctions chamber with a uniform pressure.

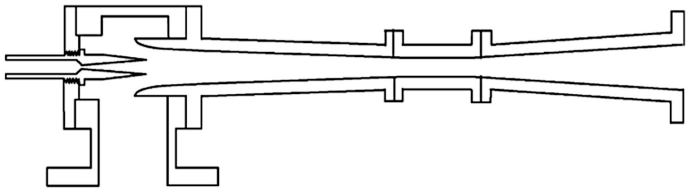

Figure 1-3: Schematic view of a CPM ejector – taken from [10].

- Constant-area mixing ejector (CAM), in which the nozzle exit plane is placed within the constant-area section. The mixing of the primary and secondary flows occurs inside the constant-area section.

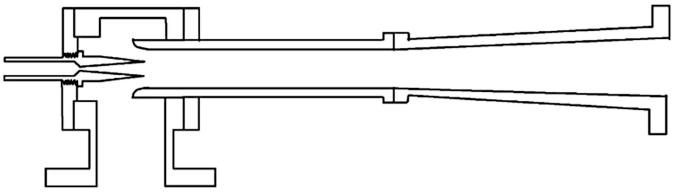

Figure 1-4: Schematic view of a CAM ejector – taken from [10].

CPM ejectors are widely used because are more flexible to operate in larger backpressure ranges and so they generally performed better than CAM ejectors, even if CAM is capable of drawing more mass flow rate [17].

It should not escape notice that Eames [18] recently proposed a new approach towards project ejector, called "constant rate of Momentum Change" (CRMC): its purpose is to combine the benefits of CPM and CAM ejectors. Most of all, CRMC scheme replaces the constant area section employed in traditional ejectors with a variable area section, producing a geometry that can provide the optimum flow passage area and reduce the thermodynamic shock process, increasing ejectors performance. The method assumes a constant rate of momentum change within the duct [19, 20].

However, for the sake of clearness, in the following we refer to CPM and CAM ejectors, accordingly with the literature.

1.2.2.2 Nozzle design

Nozzle geometry affects ejector operation. In particular nozzle shape can be:

- convergent, hence ejector works in subsonic field and it can reach at most sonic condition into exit suction

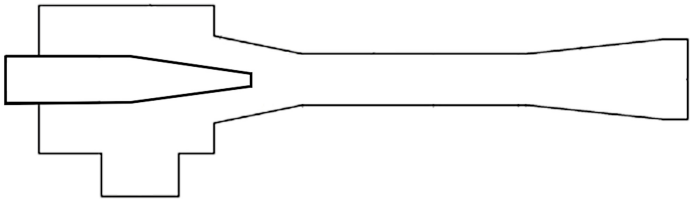

Figure 1-5: Schematic view of a subsonic ejector.

- convergent-divergent, thus flow through the ejector will be able to reach supersonic velocity

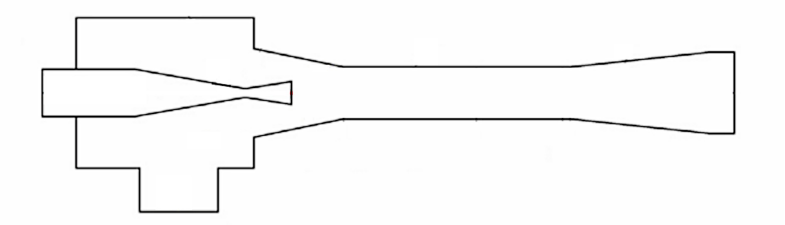

Figure 1-6: Schematic view of a supersonic ejector.

The choice between the two kinds of ejector is based on the specific requests of the different application [14]. Subsonic ejectors are not designed to produce a great fluid compression, but they must win low pressure loss. In energy field they can be employed in:

- Proton Exchange Membrane Fuel Cell (PEMFC) systems [21, 22];
- Chemical Looping Combustion (CLC) power plants [23, 24];
- Transcritical CO_2 Ejector Refrigeration Systems (TERS) [25, 26].

On the other hand, supersonic ejectors are used when there is the need to generate a high pressure difference: at supersonic velocities, the primary flow can entrain more suction flow both with greater momentum transfer and a lower-pressure region at the entrance of the mixing section [27]. The main energy applications are:

- Solid Oxide Fuel Cell (SOFC) systems [28, 29] and Molten Carbonate Fuel Cell (MCFC) systems [30, 31];
- ejector metal topping power plants [32, 33];
- ejector Organic Rankine Cycle (ORC) [34];
- Ejector Refrigeration Systems (ERS) [10, 35, 36].

A description of the main technologies is shown in Ref. [37].

The actual operating conditions will depend, however, on the backpressure value, fixed primary and secondary flow operating conditions. In the following, the operating conditions of subsonic and supersonic ejector are described and details on their fluid dynamics are outlined.

Subsonic ejector. In this regard, the subsonic ejector performance can be divided in three working modes:

1) Critical mode, in which primary flow is chocked and secondary mass flow rate is constant;
2) Subcritical mode, in which primary flow are not chocked and the secondary mass flow rate is very sensitive to the backpressure value;
3) Malfunction mode (back-flow), in which the secondary flow is reversed, causing a malfunction of ejector.

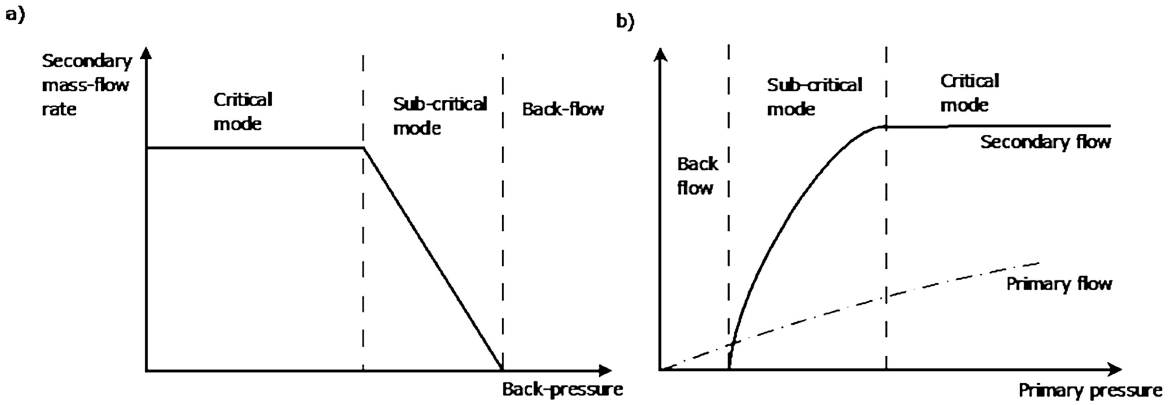

Figure 1-7: Subsonic ejector operational mode (a) fixed primary pressure, (b) fixed backpressure.

Supersonic ejector. As for the supersonic ejector, it can work in three operating conditions:

1) Critical mode (double-chocking), in which the entrainment ratio is constant because primary and secondary flows are both chocking;
2) Subcritical mode (single chocking), in which only the primary flow are chocked and so the entrained ratio changes linearly with the backpressure;
3) Malfunction mode (back-flow), in which the secondary flow is reversed, causing a malfunction of ejector.

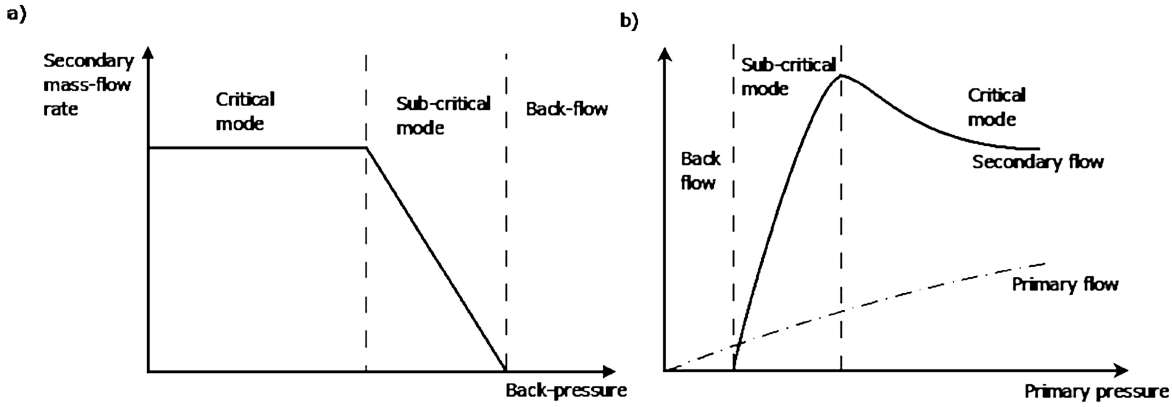

Figure 1-8: Supersonic ejector operational mode (a) fixed primary pressure, (b) fixed backpressure.

It is useful to highlight the phenomenon of the secondary flow chocking that, in critical mode, limited the maximum flow rate through the ejector and thus *CC* and *COP* remain constants. More precisely, primary fluid's expanded waves, due to under-expansion nozzle, form a converging duct without mixing with the secondary flow. The entrained flow sees the cross-section constriction, reaches sonic speed and chocks [38]. This area is not in a fixed position in the duct, but varied with the operating conditions [39, 40]. Thus, the flow rate of the secondary flow is independent from the condenser pressure and can only be raised by an increase of the evaporator pressure.

In subcritical mode, instead, the subsonic secondary flow provides a channel for pressure upstream communication making ejectors reactive to the backpressure [41]. The shock tends to move backward into the mixing chamber and interferes with the mixing of primary and secondary fluid [16].

If the backpressure is further increased, the flow will reverse back into the secondary inlet and the ejector loses its function completely.

In order to obtain a better efficiency, ejectors must work in critical mode [15], but generally ejectors operating in single chocking mode and only in particular applications (i.e. refrigeration applications) they work in double-chocking condition [41].

However, in supersonic ejectors is very complicated to describe in detail the flow characteristics, because a series of oblique or normal shock waves occur and interact with shear layers: this complex fluid dynamics influence the functioning and performance of ejectors [41]. Particularly relevant is the dissipative effect of the shock trains occurring by the end of the mixing chamber: it produces a major fluid compression and a sudden drop in the mixed flow speed from supersonic to subsonic.

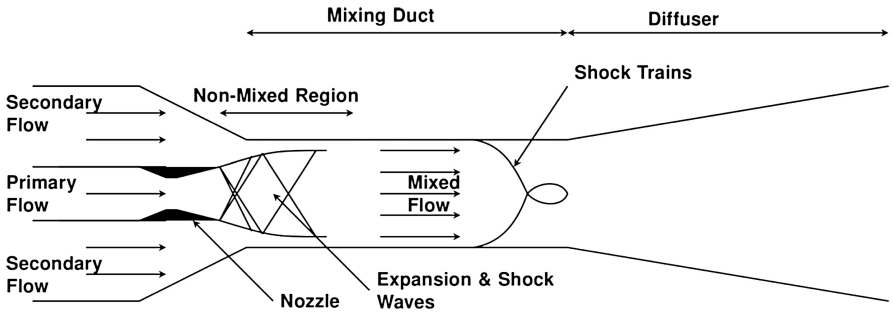

Figure 1-9: Schematic view of fluid dynamic behaviour of a supersonic ejector – taken from [41].

A more detailed description of the flow field inside an ejector will be presented later, also through the analysis of the results of the mathematical models used.

1.2.2.3 Number of phases

The working fluid's state of matter has a significant impact on fluid dynamics [42], especially on shock waves that can take place inside the ejectors.

Table 1-2: Ejector classification according to state of matter of the working fluid – taken from [42].

	Primary flow	Secondary flow	Exit flow	Remarks
Vapour jet ejector	Vapour	Vapour	Vapour	Two-phase flow can occur; Shock waves possible
Liquid jet ejector	Liquid	Liquid	Liquid	Single-phase flow without shock waves
Condensing ejector	Vapour	Liquid	Liquid	Two-phase flow with primary flow condensation; Strong shock waves
Two-phase ejector	Liquid	Vapour	Two-phase	Two-phase flow; Shock waves possible

In particular, the complete details of the fluid flow in a condensing ejector are not well understood and are complex to model [43]. The condensing ejector combines a subcooled liquid stream and a vapour stream and utilizes the beneficial thermodynamics of condensation to produce a liquid stream with a stagnation pressure that can be higher than the pressure of either of the two inlet flows. The phase change process is driven by both mixing and interphase heat transfer, favoured by the high relative velocity and the large temperature difference between vapour and liquid streams: vapour condenses onto the liquid stream, and the momentum of the liquid increases accordingly. The rapid condensation process causes shock waves and a completely liquid state results downstream of the shock [43, 44].

The possibility of working with two-phase flows is a further reason for preferring ejector-based systems and this is especially important for refrigeration systems using water as refrigerant fluid. Even though condensation is very likely, a perfect gas behaviour is often assumed for steam in ejector analysis. This schematization is simple but its results are far from reality. Only a metastable behaviour of steam is a reliable fluid description and can be taken as a reference. In fact, thermodynamic equilibrium can hardly be established in the short timeframe of the expansion in a supersonic nozzle and thus metastable states are very likely to occur [45]. Moreover, droplet nucleation and the subsequent development of condensation result in an energy transfers that cannot be accurately simulated if the steam behaves assuming is a perfect gas. Therefore, recent CFD simulations of steam ejector performance have incorporated droplet nucleation and condensation models [46]. From the point of view of the ejector shape, a redesign of the nozzle is necessary, in order to move the nucleation downstream of the throat by a suitable length, avoiding flow oscillations across the sonic section [45].

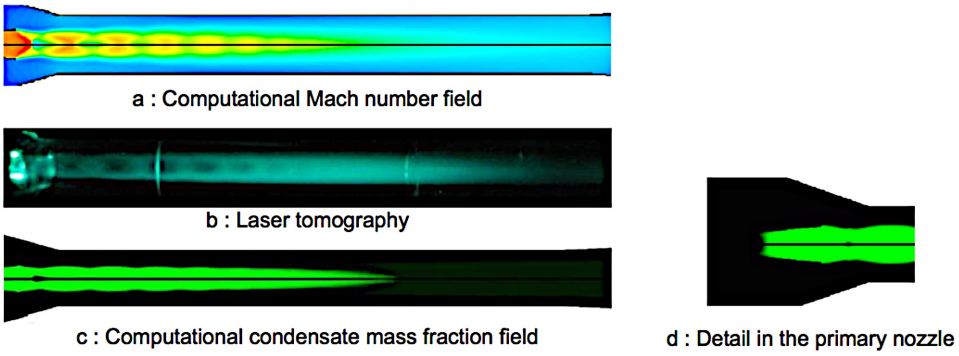

Figure 1-10: Flow visualizations of condensation process in the ejector mixing chamber – taken from [47].

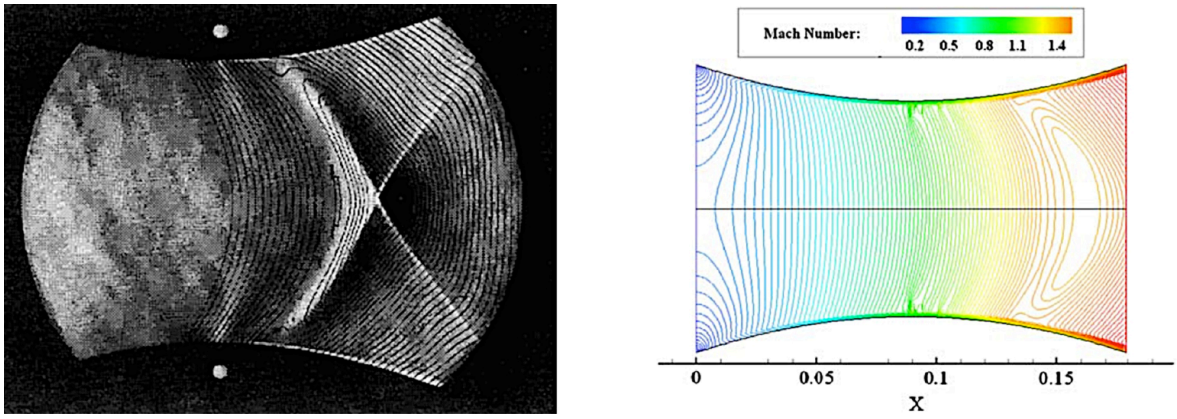

Figure 1-11: Schlieren image and CFD result of condensation shock with Iso-Mach Lines – taken from [48].

1.3 Ejector Refrigeration Systems: working fluid

The selection of the appropriate refrigerant is one of the most important stages in the design of ejector refrigeration systems [10, 16, 35]. In this section we will present and discuss the main working fluid operating in the ejector refrigeration systems.

1.3.1 Working fluid: presentation

The most common way of classifying the working fluid of a refrigeration cycle is by the chemical compounds in the refrigerant molecules. They can be classified into three main groups [10]:

- halocarbon group, in which carbon atoms are linked by covalent bonds with one or more halogen atoms, as chlorofluorocarbons (CFCs), hydrochlorofluorocarbons (HCFCs), hydrofluorocarbons (HFCs) and hydrofluoroolefin (HFO);
- hydrocarbon group (HC), organic compounds consisting of hydrogen and carbon (i.e. R290, R600, R600a);
- other refrigerant (i.e. water R718b, ammonia R717, carbon dioxide R744).

Table 1-3: Refrigerants classification and safety characteristics.

Group		Safety group [49] (toxicity/flammability)	Example
Halocarbon compounds	CFC	A1	R11, R12, R113, R114
	HCFC	A1 – B1	R21, R22, R123, R141b, R142b, R500, R502
	HFC	A1 – A2	R134a, R152a, R236fa, R245fa
	HFO	A2L	R1234yf
Hydrocarbon compounds	HC	A3	R290, R600, R600a
Other refrigerants		B1	CH_3OH
		B2L	R717
		A1	R718b, R744

1.3.2 Thermodynamic properties and fluid dynamics behaviour

Considering the differential entropy equations for an ideal gas:

$$dS = C_p \frac{dT}{T} - R\frac{dp}{p} \tag{1.1}$$

Increasing the temperature or decreasing the pressure will raise the fluid entropy. Depending on which effect prevails between temperature and pressure, the saturated vapour line in the *T-s* diagram can be negative slope or positive slope. In a simple molecular compound dominates the effect of pressure, while in a complex molecular compound, due to its high molar heat capacity, the thermal effect has a greater influence.

According to the saturated vapour line slope in the *T-s* diagram, a working fluid can be categorized as [10, 35, 50]:

- Wet vapour, for which the saturated vapour line forms a negative slope (low molecular complexity);
- Isentropic vapour, for which the saturated vapour line is approximately vertical;
- Dry vapour, for which the saturated vapour line forms a positive slope (high molecular complexity).

In light of this, for a dry or isentropic vapour fluid, in most cases, there is no phase change during the expansion process through the primary nozzle. Contrariwise, for a wet vapour fluid, small drops may be formed at the nozzle exit, blocking the effective area and cause periodically oscillating unsteady flow in the ejector and unstable system operation [45], affecting the working conditions of the ejector. Similarly to what happens in steam turbines, superheating the fluid before entering the nozzle may be a solutions [10]. However, in this case the use of superheated motive steam causes a slight decrease in ejector efficiency [10, 51]: a large superheat will not benefit the system *COP*, just waste energy [52], while a too small superheat may not eliminate the droplet formation [50].

Therefore, dry vapour is more desirable than wet vapour fluid. However, it is noted that also for the dry and isentropic fluids, the isentropic expansion could occur in the two-phase region, as well as shown the blue lines in Figure 1-12b and Figure 1-12c. When the saturation temperature is close to the critical temperature the expansion may lead to the same problems that are inherent to wet fluids [50]. As a result, for some dry and isentropic fluids, the extremely high temperature that approaches to the critical value should be avoided for ejector refrigeration systems.

Fluid dynamic losses will actually reduce the problem since the state at the nozzle exit is much closer to the vapour saturation line. However, losses are never desired due to the negative influence on the system performance [13].

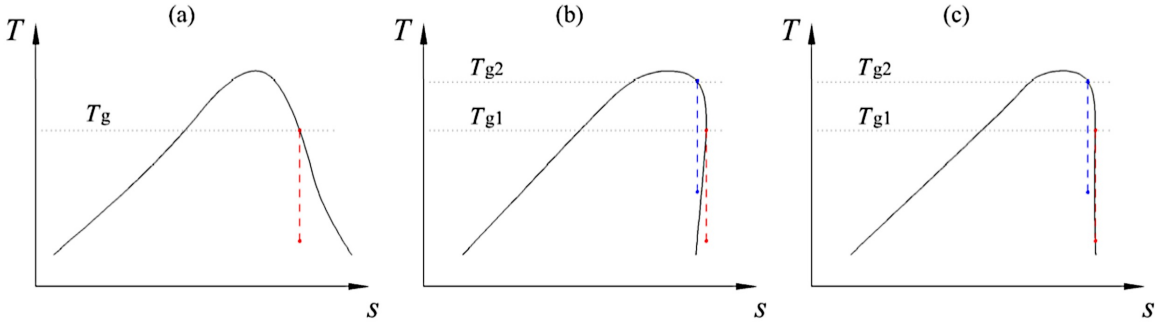

Figure 1-12: Expansion process through the primary nozzle for (a) wet fluids, (b) dry fluids, (c) isentropic fluids – taken from [50].

1.3.3 Employment in the ejector refrigeration systems

Generally speaking, a suitable refrigerant for refrigeration system should yield good performance in the selected operating ranges and the following requirements must be taken into account [10, 16, 35]:

- thermo-physical properties:

  [i] the fluid should have a large latent heat of vaporization in the evaporator and generator temperature range in order to minimize circulation rate per unit of cooling capacity;

[ii] the fluid should have a relatively high critical temperature to adapt large variations of generator temperatures;

[iii] the fluid pressure at the generator temperature should not be too high in order to avoid heavy construction of the pressure vessel and to minimize the power required by pump;

[iv] viscosity, thermal conductivity and the other transport properties that influence heat transfer should be favourable;

[v] higher molecular mass fluid leads to an increase in entrainment ratio and ejector efficiency [53]; however, working fluid with bigger molecular mass value requires comparatively smaller ejectors for the same system capacity and the difficulties of constructing small-scale ejector components should be considered;

- environmental impact: the fluid should be environmental friendly with relatively low ozone depletion potential (ODP, a measure of the impact on the stratospheric ozone layer compared to R11) and global warming potential (GWP, a factor indicating the relative effect on global warming compared to CO_2);
- safety: the fluid should be chemically stable, non-toxic, non-explosive, non-corrosive;
- economics and availability: the fluid should be low cost and available on the market.

When speaking of ejector refrigeration system, the following point has to be taken into account. The ejectors are versatile enough to operate with an assorted variety of fluids. The possibility of using a wide range of refrigerants is another advantage of the ejector refrigeration system. Clearly, different refrigerants have distinct characteristics and perform differently in a selected range of operating conditions [10].

Using water (R718b) as the working fluid for a jet refrigerator [54-77] provides many advantages. It has a high heat of vaporization, is inexpensive and has minimal environment impact. However, there are some drawbacks. In fact, using water as a refrigerant limits the cooling temperature to above 0°C and the system must be under vacuum condition. Moreover, water has very large specific volume at typical evaporator conditions and to minimize the pressure loss, pipe diameter must be large [78]. Experiments show that a steam-jet refrigerator requires a boiler temperature between 100 and 160°C. Thus, with water as a refrigerant, the useful range of operating temperature is thermodynamically restricted [16, 35]. The obtainable *COP* is not high (less than 0.5) and the absence of any pollution problem and the universal availability of the fluid are the only reasons for which some applications could accept a performance lower than optimum [3]. Therefore, water is often employed in experimental device but is rarely used in real refrigeration systems.

The working fluids most used in refrigeration field are halocarbon compounds [39, 50, 54, 61, 73, 79-128] and ejector refrigeration systems using them can provide cooling temperature below 0°C and can exploit low-grade thermal energy (such as solar energy, waste heat and exhaust gas) as low as 60°C [35] producing an acceptable *COP* (0.4÷0.6) and cooling temperature. For example, R113 is a low-pressure refrigerant having high molecular mass able to produce a high mass ratio (0.5÷0.6), good ejector efficiency (0.5÷0.55) and high compressibility factor (0.9÷0.995) [87].

However, several halocarbon refrigerants yielding high performance are not environmentally friendly, included R113: some have a high ODP or a high GWP. The environmental problem is caused by working fluids that escaped through leakages from cooling equipment during normal

operation (filling or empting) or after accidents (damages) gather in significant quantities at high levels of the atmosphere. Through catalytically decompounding linked to the presence of chlorine and bromine in the stratosphere, pollutant gasses deplete the ozone layer that normally filters the ultraviolet radiation from the sun [129] and thus contributing to the greenhouse effect and global warming.

In order to protect the environment, in 1989 entered into forced "The Montreal Protocol on Substances that Deplete the Ozone Layer" [130], an agreement ratified by all the member states of the United Nations that was designed to reduce the production and consumption of ozone depleting substance. Among the banned products, there are several halocarbon compounds, widely used in refrigeration applications until then, like chlorofluorocarbon (CFCs) and hydrochlorofluorocarbon (HCFCs).

The new generation of refrigerants includes very different kinds of working fluid. The HFCs do not deplete the ozone layer and have many of the desirable properties of CFCs and HCFCs. They have significant benefits regarding safety, stability and low toxicity, being appropriate for large-scale applications [129]. Even more promising for the future are the HFOs. They can offer balance among performance, environmental impact, safety and durability. However, they belong to A2L safety group and thus they will require changes to equipment safety standards.

In additions to the new halocarbon compounds, also the HCs with low environment impact are considered as potential alternatives [50, 96, 98, 101, 108, 109, 123, 131-140]. Unfortunately, HC refrigerant are highly flammable, which limits the usage in large capacity systems [129, 141]. The explosion risk may be reduced by hermetically designing the system for minimum charge of refrigerant, by use of spark-proof electric components and by ventilation of confined spaces [141]. These concerns can be relieved with additional research about new mixture between HCs and HFCs [129].

New halocarbon compounds and HCs are ozone-friendly, but they have significant GWP. Instead, the advantages of ammonia NH_3 (R717) [61, 83, 91, 96, 98, 101, 109, 133, 142-145] over the other refrigerants are its low cost, high performance (and thus low energy cost), more favourable thermodynamic properties and it does not create environmental problems. However, it likely will remain restricted to industrial applications and unsuitable for domestic use due to its toxicity [35].

Another interesting option is the methanol [64, 146-149]. Increasingly, the methanol is being employed in a number of applications and, in the energy field, is becoming above all a viable alternative to conventional fuels. It can also be a valid solution in refrigeration systems thanks to its appropriate thermo-physical properties, low environmental impact (no damage to the ozone layer) and low cost. Moreover, it allows to produce cooling effect at an evaporation temperature below the freezing point of water [146]. On the other hand, the methanol is toxic and highly flammable and important preventive measures should be taken.

Recent research [145, 150-156] has shown an increasing interest in carbon dioxide (R744) as a refrigerant because of CO_2 is a non-flammable natural substance with zero ODP and a negligible GWP. Owing to the fact that the critical temperature of CO_2 (30.85°C) is lower than the environment temperature that can be achieved in a summer day, a supercritical heat rejection temperature is required in the ERS. This requires the system to work under a transcritical thermodynamic cycle.

With regard to development of ejector refrigeration systems, many working fluids suggested in early works are now forbidden due to their environmental effect, such as R11, R12 or R113. New refrigerants are now studied, for example, R134a, R152a and carbon dioxide.

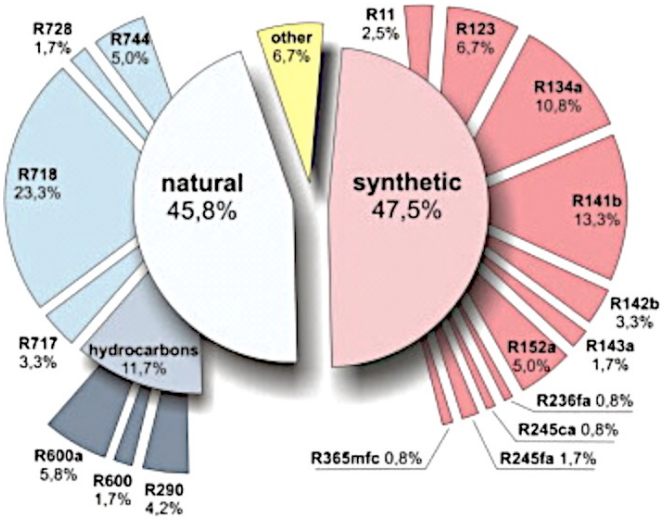

Figure 1-13: Refrigerant used in ejector refrigeration systems – taken from [132].

1.3.4 Working fluid: summary

The great versatility of the ejectors has allowed to test many working fluids, also very different each other. Over the years, the selection strategy of the refrigerants has changed a lot. In fact, in the past the main principle of selection was the maximization of the performance and this especially rewarded fluids such as R11 and R113. Considering the lack of technological maturity of ERS and the lack of powerful computing means like CFD, the performance in terms of *COP* that was reached with those fluids (*COP* = 0.3÷0.4) was considerable. Nowadays, instead, we must consider several factors (safety, cost…) and the final choice will depend primarily on the compromise between the performance and the environmental impact.

According to the results of the literature studies, the best working fluids are the HFC halocarbon compounds and, in particular, the R134a seems to be able to ensure the best performance (*COP* = 0.5÷0.6), respecting the environment. Even the hydrocarbon compounds can achieve good performance (*COP* =0.4÷0.5) and they have neither ozone depletion potential (ODP = 0) nor significant direct global warming potential (GWP < 20) [129]. However, their flammability is a disadvantage compared to the halocarbon.

For the future development of the ERS, however, the carbon dioxide in transcritical cycles seems to be the best compromise between performance (*COP* =2÷3) and environmental impact (ODP = 0, GWP = 1). Some experiments are still needed and the technical and economical feasibility of this choice on a large scale is to be evaluated.

The Table 1-4 lists some fluids commonly considered for ejector refrigeration systems.

Table 1-4: Working fluids for ejector refrigeration systems [157, 158].

	Wet/Dry vapour	Molecular mass [kg/kmol]	Boiling point [°C]	Latent heat at 10°C [kJ/kg]	GWP (100yr)	ODP	Employment in ERS Ref.
R11	Wet	137.4	23.7	186.2	4750	1	[54, 61, 73, 79-83]
R12	Wet	120.9	-29.8	147.8	10900	1	[54, 61, 73, 79, 83, 84]
R22	Wet	86.5	-40.8	196.8	1790	0.05	[82-86]
R113	Dry	187.4	47.6	155.9	6130	0.85	[39, 54, 73, 80, 83, 87, 88]
R114	Dry	170.9	3.8	133.7	9180	0.58	[82, 83, 89, 90]
R123	Dry	152.9	27.9	177.5	77	0.01	[54, 61, 73, 82, 91-97]
R134a	Wet	102.0	-26.1	190.9	1370	0	[50, 54, 61, 73, 82, 86, 91, 96, 98-114]
R141b	Dry	116.9	32.1	233.1	717	0.12	[82, 96, 101, 109, 113, 115-122]
R142b	Dry	100.5	-9.2	212.0	2220	0.06	[54, 73, 82, 101, 113, 123-127]
R152a	Wet	66.1	-24.0	295.8	133	0	[50, 54, 73, 82, 86, 91, 96, 98, 101, 108, 109]
R245fa	Dry	134.1	15.1	199.0	1050	0	[50, 101, 122, 128]
RC318	Dry	200.0	-6.0	110.7	10300	0	[54, 73, 82]
R290	Wet	44.1	-42.1	360.3	20	0	[50, 96, 98, 101, 108, 109, 131-133]
R500	Wet	99.3	-33.6	-	8100	0.61	[54, 73, 83]
R502	Wet	111.6	-45.3	-	4600	0.31	[61, 83]
R600	Dry	58.1	-0.5	376.1	20	0	[50, 98, 101, 108, 132, 134, 135]
R600a	Dry	58.1	-11.8	344.6	20	0	[50, 96, 108, 109, 123, 132, 133, 136-139]
CH_3OH		32.0	64.7	1194.5	-	-	[64, 146-149]
R717	Dry	17.0	-33.3	1226.1	0	0	[61, 83, 91, 96, 98, 101, 109, 133, 142-145]
R718b	Wet	18.0	100	2477.2	0	0	[54-77]
R744	Wet	44.0	-78.5	197.7	1	0	[145, 150-156]

1.4 Ejector Refrigeration Systems: technologies

In the present section a review on ejector refrigeration systems are provided after an introduction on the technology and the performance parameters.

1.4.1 Ejector refrigeration technology

The ejectors have found applications in several sectors as aeronautic, maritime and process industry (i.e. chemical, petrochemical, food and drugs...). In energy field, they are going to assume a rising importance in numerous energetic appliances, like fuel cells power plants [21, 22, 28-31], chemical looping combustion plants [23, 24] and, above all, in refrigeration technology. In the recent years, refrigeration field is subjected to a rapid evolution in order to reduce electricity consumptions (please refer to the introduction for a detailed discussion of this framework). In this framework, the ejector refrigeration system (ERS) is one of the most promising technologies because of simplicity in construction, installation and maintenance of ejector [35]. Indeed, the ejector has not moving parts, as instead happens in traditional vapour-compression systems, and this guarantees a long life cycle, high availability and low maintenance costs. Another considerable advantage over its competitors is the chance to use practically any working fluid. Moreover, utilization of low-grade thermal energy, like solar energy or exhaust heat, instead of electricity, provides economical, energetic and environmental benefits. Indeed, in additions to energy savings, they can help to mitigate the problem related to CO_2 emissions. On the other hand, these systems have some drawbacks. The coefficient of performance *COP* of the ejector refrigeration systems is relatively low and these systems are very sensible to off design conditions. Low *COP* means high cost of the refrigeration system for achieving the same cooling capacity, in compared to conventional refrigeration systems. In this framework, considerable efforts are required to increase the performance of these systems, studying their fluid dynamics and carefully designing them, in order to make them economically more attractive. Recent studies have shown that the operation and performance of ejector-based cycles largely depend on appropriate and careful overall design [105]. In addition, ejectors are designed to operate in a narrow range of operating conditions; deviation from this optimum results in a significant deterioration of the ejector performance [159].

1.4.2 Ejector refrigeration: performance parameters

There are several parameters employed to describe ejectors performance. For refrigeration application the most important are:

- Entrainment ratio ω, given by the ratio between mass of secondary flow $\dot{m}_e$ and mass of primary flow $\dot{m}_g$

$$\omega = \frac{\dot{m}_e}{\dot{m}_g} \tag{1.2}$$

- Compression ratio R_c, equal to the static pressure at diffuser exit p_c (condensation) divided by the static pressure of the secondary flow p_e (evaporation)

$$R_c = \frac{p_c}{p_e} \tag{1.3}$$

The entrainment ratio evaluates the refrigeration cycle efficiency, while the pressure lift ratio is a measure of operative range at which the cycle works. Thus, ejector must provide the highest entrainment ratio and the maximum possible discharged pressure, at given inlet thermodynamic conditions [16, 35].

- Coefficient of performance *COP*, defined as the ratio between evaporation heat energy $\dot{Q}_e$ (cooling effect) and the total incoming energy in the cycle $\left(\dot{Q}_g + \dot{L}_p\right)$; work consumed by the mechanical pump $\dot{L}_p$ can often be neglected.

$$COP = \frac{\dot{Q}_e}{\dot{Q}_g + \dot{L}_p} \cong \frac{\dot{Q}_e}{\dot{Q}_g} = \omega \frac{h_{e,out} - h_{c,out}}{h_{g,out} - h_{c,out}} \tag{1.4}$$

  The numerator is often called cooling capacity *CC*:

$$CC = \dot{m}_e \cdot \left(h_{e,out} - h_{e,in}\right) \tag{1.5}$$

Concerning the ejector itself, there are many way to define ejector efficiency $\eta_{ejector}$, but the one used by ASHRAE (American Society of Heating, Refrigerating and Air Conditioning Engineers) is as follows [27]:

$$\eta_{ejector} = \frac{\left(\dot{m}_g + \dot{m}_e\right) \cdot \left(h_{c,in} - h_{e,out}\right)}{\dot{m}_g \cdot \left(h_{g,out} - h_{e,out}\right)} \tag{1.6}$$

equal to the ratio between the actual compression energy recovered and the theoretical energy available in the motive stream.

Usually ejector efficiency is not a high value, due to the friction, mixing and shocks losses [27]. The main source of irreversibility can be classified as loss of interaction of primary flow with secondary flow in the mixing chamber, kinetic energy losses and shock wave losses [20]:

- the interaction between the two inlets flows produces friction and mixing losses;
- the kinetic energy losses mainly occur within the convergent part of the nozzle and within the diffuser and are due to the frictional effects caused by flow separation. These losses can be reduced with a good surface finish and using a nozzle large enough.
- The shock waves occurring in the mixing chamber are responsible for the losses of total pressure of the mixed stream. Thus, they have a direct effect on reducing the maximum backpressure that the ejector can overcome. However, to improve the system efficiency the shock effect must be minimized in order to maintain the highest critical pressure.

For the above mentioned reasons, ejectors are not a very efficient compressor, but it is useful to remember that the compression effect is obtained without consuming electricity. According to Equation (1.6), a typical efficiency value is approximately 0.25 [27].

The main jet refrigeration cycles reported in literature will be discussed, due to providing a complete survey about the development of the research.

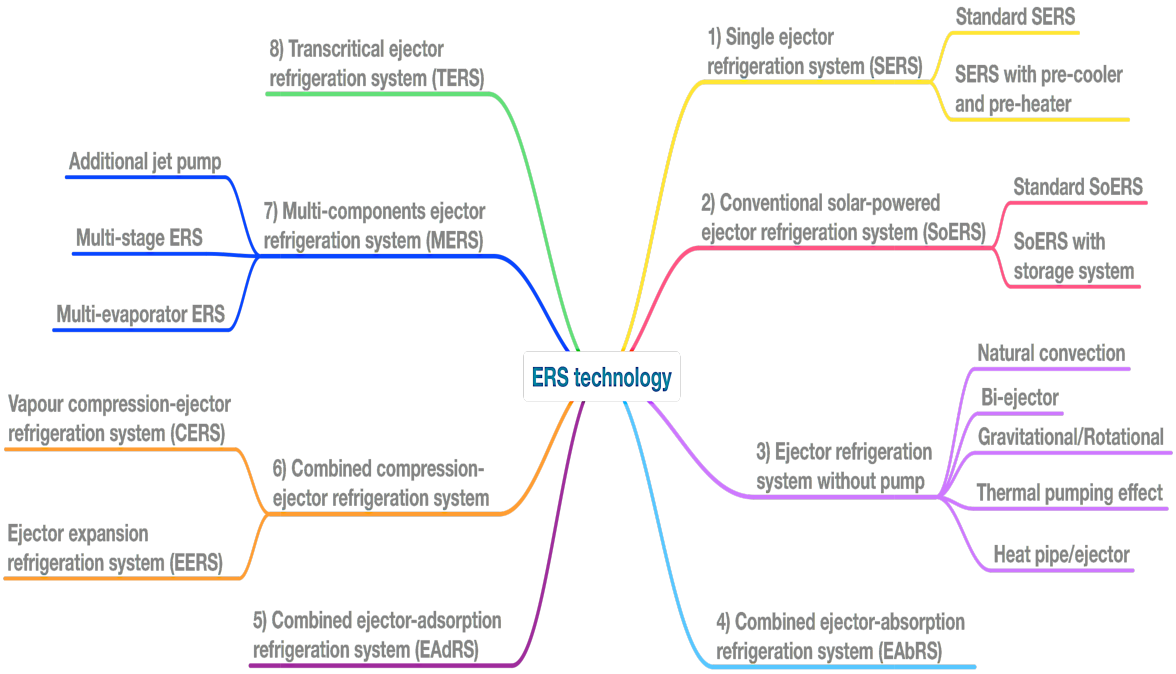

Figure 1-14: Overview of ejector refrigeration systems.

1.4.3 Single ejector refrigeration system (SERS)

Single ejector refrigeration system (SERS) may be divided in two sub-categories: (i) standard SERS and (ii) SERS with pre-cooler and pre-heater. In the following for each section, after a brief description of the working cycles, we will present a comprehensive collection of all the literature studies regarding these systems.

1.4.3.1 Standard SERS

The standard cycle is structured as detailed in Figure 1-15:

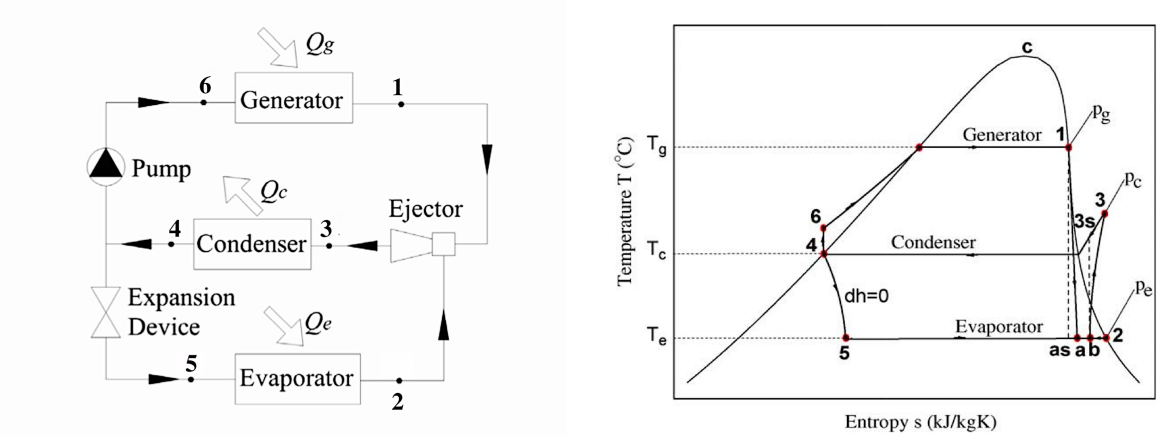

Figure 1-15: Typical ejector refrigeration system and T-s chart of the cycle – modified from [13, 100].

The generator supplies low-grade heat energy for working fluid vaporization (*6→1*). Reached saturation conditions, the high-pressure flow, i.e. the primary flow, is sent to the ejector nozzle (*1→a*) and entrains the low-pressure vapour from the evaporator, i.e. secondary flow (*2→b*). The two streams mix and the resulting mixed flow (*b→3*) leaves the ejector and is despatched to

condenser, where condensation takes place by rejecting heat to the environment (*3→4*). Suddenly the liquid is split: one part expands isenthalpically through the valve (*4→5*) and then is fed into the evaporator, producing the cooling effect (*5→2*); the other one is pumped back to the generator (*4→6*). Thus, the generator is used to produce high-pressure vapour to drive the ejector. The tasks of the ejector are the "entrainment" and recompression of the vapour leaving the evaporator to be discharged at the condenser. The main features of a Standard SERS are [35, 160, 161]:

- setting of generator and evaporator working conditions, when the ejector operates in critical mode, provide constant *COP* and *CC*; exceeded the critical pressure, secondary flow is reduced and thus ω and *COP* decrease significantly;
- increasing generator pressure will decrease ω but enhance the critical condenser pressure, fixed evaporator pressure. In fact, the primary mass flow increases and the growth of expansion angle causes a reduction of the annulus effective area; thus, less secondary flow can be entrained. However, this causes the momentum of the jet core and of the mixed flow to increase, the shock wave position moves downstream and so the critical pressure grows. The *CC* and the *COP* diminish.
- once the generator conditions are fixed, an increase in evaporator pressure will increase *ω* and the critical condenser pressure. This is due to the reduction of the under-expanded wave's angle: a larger effective area results and so the secondary flow increases. Momentum of the jet core is reduced but the total momentum of the mixed flow becomes higher thanks to the great secondary pressure. The shocking position moves downstream and the ejector can be operated at higher backpressure. Thus, increases of *CC* and *COP* result.

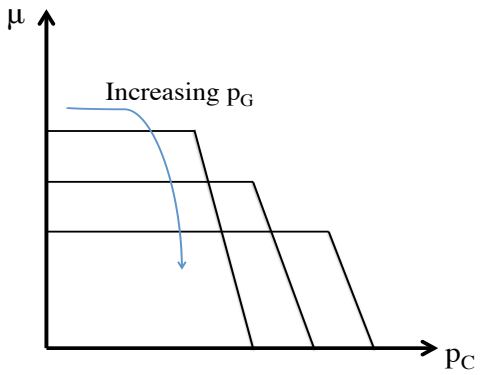

Figure 1-16: Effect of the primary flow pressure.

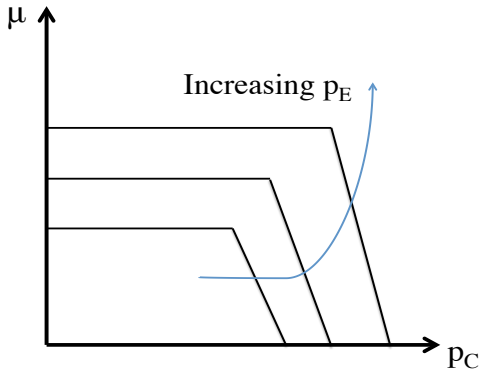

Figure 1-17: Effect of the secondary flow pressure.

In 1858, Henry Giffard invented the first condensing ejector to feed liquid water and replenish the reservoir of a steam engine boiler [162]. Since then, ejectors have been studied for a large number of different applications. On the early 20th century, Sir Charles Parsons employed an ejector for removing air from a steam engine's condenser [163], while Maurice Leblanc used the first steam ejector in a refrigeration system to reduce the need for mechanical energy input [164, 165], replacing with low-grade energy [27, 42]. However, the advent of vapour compression systems in 1930s has checked ejector progress, because of their greater efficiency [27].

In the 1950s, the growing nuclear industry began to be interested in ejectors for emergency cooling systems in nuclear reactors [27]. As a result, much research about ejector flow field got going, including the important academic works by Keenan et al. about the performance investigation of a simple air ejector (1942) [166] and a one-dimensional method of analysis of ejectors (1950) [167].

De Frate et al. (1959) [168] wanted to evaluate the optimum design of ejectors using a computational method. In the same period, Martynowsky (1954) [79] carried out the first investigation on ERS using R11 and R12 instead of water as working fluid, while Mizrahi et al. (1957) [84] used different refrigerants (R11, R12, R21, R22, R40, R764) and they found that R22 (COP = 0.2) and R12 (COP = 0.18) gave the best performance. They concluded that ejector system is a feasible way to produce cooling effect with a low temperature heat source (T_e = -15°C).

Heymann and Resnick (1964) [131] applied and modified the previous one-dimensional analysis of ejector performance [167, 168]. They concluded that a generation temperature which could be provided by solar collectors was appropriate for the operation of an ejector system: a propane designed for T_g = 85°C, T_e = -15°C and T_c = 30°C provided a COP = 0.12. The performance coefficients increase substantially as the evaporator temperature is increased (+50% for T_e = 10°C) but the operation at off-design conditions can have a profound effect on ω and COP of an ejector system. The authors suggested that this factor could be overcome by designing the system with several ejectors working in parallel and the requisite number operated in accordance with the varying load and temperature conditions.

Later, in the 1970s, and again more recently in the 2000s, the rising cost of fuel and the growing attention toward the environmental aspects sparked a new interest in ejector technology [27].

Chen (1978) [88] employed a numerical 1D method in order to optimize an ejector driven with the waste heat form the cooling system of an internal combustion engine: for a conventional 2000 c.c. automobile, the available cooling effect produced from engine waste heat using R113 refrigerant is equal to 8 kW and the required pump power consumption is only 0.1% of the engine power. The waste heat is able to withstand a T_g = 76°C and the other operating conditions are T_e = 27°C and T_c = 67°C, giving a COP = 0.24.

Tyagi and Murty (1985) [80], following strict selection criteria (such as those listed in section 1.3.3), chose R11 and R113 for their analysis, because satisfy the requirements best. After a parametric study of the ejector system, for different generator, evaporator and condenser temperature, they conclude that COP increases with growth of generator and evaporator temperature, while it diminishes with increase of condenser temperature. A similar study was conducted by Chen and Hsu (1987) [81] who used R11 as working fluid. The analysis indicates that the COP varies greatly with the off-design operating conditions (COP = 0.15÷0.42).

The entry into force of "The Montreal Protocol on Substances that Deplete the Ozone Layer" [130] in the 1989 raised the need to study the behaviour of new environmentally friendly refrigerants, as hydrofluorocarbon (HFCs) and other fluids (for further details, please refer to the section 1.3).

Dorantes and Lallemand (1995) [82] proposed the use of non-azeotropic mixtures [169, 170] in order to take advantages of their thermodynamic characteristics in the heat exchanger. They investigated a simple model of an ejector-compression refrigeration cycle and its applications to air conditioning, using classical refrigerants (R11, R22, R114), pure and cleaner refrigerants (R123, R133a, R134a, Rl41b, R142b, R152a, RC318) or non-azeotropic mixtures. The results suggest that, for different temperatures of the heat source (T_g = 90÷130°C) and the heat sink (T_e = 10÷20°C), the entrainment ratio and the system efficiency depend mainly on the fluid type and the mixture composition. R141b (COP = 0.21), R123 (COP = 0.20) and RC318 (COP = 0.20) gave the best performance.

A comparison of the performance of various working fluids was carried out by Sun (1999) [54], through a computer simulation program for ERS based on a thermodynamic model. Among the

eleven fluids tested (water, several halocarbon compounds, an organic fluid and an azeotrope R500), the best results were obtained with R152a (*COP* = 0.09÷0.50) and R500 (*COP* = 0.09÷0.47), while the steam jet systems had very low performance (*COP* = 0÷0.35). The variation of the *COP* values for various working fluids is more or less the same for entrainment ratio: this confirms the importance of improving ejector design for maximum ω in order to maximize the ejector performance.

A CFD analysis and experimental investigation of an ejector refrigeration system using methanol was presented by Riffat and Omer (2001) [146]. Further details on the CFD technique will be provided in the next section. The results showed that a methanol ERS could produce cooling effect to temperatures below the freezing point of water (T_e = -2÷14°C), achievable using low-grade heat (T_g = 80÷100°C), such as solar energy and waste heat.

Cizungu et al. (2001) [91] theoretically compared the performance of an ejector using the environmentally friendly working fluids R123, R134a, R152a and R717 (ammonia). The results suggested that, for different generator temperatures, the entrainment ratio and *COP* depend mainly on the ejector geometry and the compression ratio. It was also found that, with the same ejector, R134a and R152a were suitable for 70-80°C heat sources, while R717 was suitable for the heat source whose temperature was greater than 90°C. However, the authors found R134a as the best working fluid, giving a *COP* = 0.1÷0.45.

Selvaraju and Mani (2004) [98] presented similar information comparing ERS performance using R134a, R152a, R290, R600 and R717. Their analysis confirmed that R134a could provide the best system COP (0.12÷0.40) and the highest critical entrainment ratio (0.20÷0.45).

The work done by Alexis and Katsanis (2004) [147] concerned the behaviour of methanol through an ejector operating in a refrigeration system with a medium temperature thermal source (superheated temperature equal to 150°C). It was found that there are three independent variables for an ejector system, namely (i) the generator, (ii) the evaporator and (iii) the condenser conditions. This study showed that the maximum *COP* is a linear function of generator temperature (T_g = 117.7÷132.5°C) and a cubic function of the condenser temperature (T_c = 42÷50°C) and evaporator temperature (T_e = -10÷5°C):

$$COP_{max} = \sum_{i=0}^{1} B_i T_g^i \tag{1.7}$$

$$B_0 = \sum_{i=0}^{3} T_e^i \sum_{j=0}^{3} \alpha_{ij} T_c^j \tag{1.8}$$

$$B_1 = \sum_{i=0}^{2} T_e^i \sum_{j=0}^{3} \beta_{ij} T_c^j \tag{1.9}$$

One of the first exergy analyses of ERS was presented by Alexis (2005) [56]. The results showed that a better quality of the ejector has more effect on the system performance than the better quality of other components, because the ejector has the greater exergy loss of the system, equal to 54% of the total irreversibility loss. The other exergy losses are due to the condenser (26.9%), the generator (10.8%), the evaporator (7.4%) and the expansion valve (1%). At design conditions, the second law efficiency remains close to 17%.

In order to make the ejector system more economically attractive, a number of researches have investigated the optimization of the ejector geometry on system performance, i.e. nozzle exit position (*NXP*) and the area ratio. Several ejector designs were modelled using finite volume CFD techniques with this purpose [160, 171-174]. It is found that the position of the nozzle is an important ejector design parameter.

The experimental and theoretical analysis presented by Sun (1996) [75] shown the limitations of fixed-geometry ejector refrigeration cycles for low *COP* values (of the order of 0.2÷0.3) and difficulty in achieving optimum performance under various operating conditions. From this study, it is clear that the geometry of an ejector in the refrigeration cycle should be variable in order to cope with variations of working conditions and maintain optimum performance and constant cooling capacity of the system. With a fixed-geometry ERS, optimum performance of the system will be very difficult to achieve when operating conditions vary. In general, variable-geometry ejector-refrigeration systems will demonstrate better performance than conventional ejector systems and could become competitive with other refrigeration and air- conditioning systems.

Aphornratana and Eames (1997) [74] found that the ejector performance, i.e. cooling capacity, *COP* and critical condenser pressure of a jet refrigerator can be varied by changing the position of the primary nozzle. Retracting the nozzle into the mixing chamber causes the *CC* and *COP* to increase with the expenses of critical condenser pressure. According to their tests, each ejector required a particular optimum nozzle position and a single optimum nozzle position cannot be defined to meet all operating conditions.

Chunnanond and Aphornratana (2004) [55] have analyzed the static pressure trend through the ejector, changing the operating conditions T_g = 120÷140°C, T_e = 5÷15°C and T_c = 22÷36°C, the superheated level of primary flow (heat input of 0÷100W) and the geometry and positions of the nozzle *NXP* = -10÷20mm (by changing the spindle position, the area ratio can be changed). The authors concluded that there are two parameters involved with the performance of an ejector refrigerator, that are the amount of secondary flow, which determines the *COP* and *CC* of the system and the momentum of the mixed stream, which indicates the critical condenser pressure $p_{c,cr}$. This work yielded that:

- A decrease in the boiler pressure (primary flow decrease and secondary flow increase) caused the *COP* and *CC* to rise (*COP* = 0.25÷0.48); this results in a decrease of the momentum of the mixed flow and so the critical condenser pressure was reduced ($p_{c,cr}$ = 40÷65mbar).
- An increase in evaporator pressure (this would sacrifice the desired cooling temperature) increased the critical condenser pressure ($p_{c,cr}$ = 48÷55mbar); this also increased the total mass flow and consequently increased *COP* and *CC* (*COP* = 0.28÷0.48).
- The superheated level of motive fluid before entering the nozzle, have not much influence in cycle performance.
- Retracting the nozzle out of mixing chamber can increase the *COP* and *CC*; on the other hand, the critical condenser pressure is reduced ($p_{c,cr}$ = 41÷47mbar).

In the study of Aidoun and Ouzzane (2004) [51] several important features of ejector operation characteristics were simulated by using a thermodynamic model. The fluid mixing conditions dictated by the fluid type, the mixing chamber geometry, the inlet and outlet constraints, may lead to off design operation with performance deterioration. Moreover, the internal superheat

generation, due to inefficient mixing and normal shock waves is very important in off design operation; the authors concluded that some degree of inlet superheat (around 5 °C) is necessary to prevent internal condensation but excess superheat is detrimental to the condenser efficiency at the exit.

Selvaraju and Mani (2006) [99] studied 6 different geometrical configurations of the ejectors switching generator, evaporator and condenser temperatures. For a given ejector configuration and fixing evaporator and condenser temperature, exists an optimum temperature of primary flow which yields maximum ω and *COP*. They obtained by regression analysis some correlations to calculate *COP* and ω at critical conditions. The *COP* can be evaluated by the following relation:

$$COP = -0.27238\, R_d - 0.37332\, R_c + 0.202621\,\phi + 0.968945 \tag{1.10}$$

Where R_d is the expansion ratio (p_g/p_c), R_c is the compression ratio (p_c/p_e) and ϕ is the ejector area ratio (A_m/A_t).

An important non-dimensional factor affecting the ejector performance is thus the area ratio. Considering that the secondary fluid is entrained into the region between the primary fluid and the ejector wall, an ejector of fixed primary pressure, secondary pressure and nozzle geometry, increasing the mixing section area will result in a greater flow area for the secondary stream. The entrainment ratio will therefore increase but since the compression work available from the primary flow is unchanged, the ejector is unable to compress to higher discharge pressures. In this case, according to Varga et al. (2009) [175], increasing the area ratio increases entrainment ratio and decreases the critical back-pressure and therefore an optimal value should exist, depending on operating conditions.

Cizungu et al. (2005) [143] modelled a two-phase ejector with ammonia as working fluid and found out a quasi linear dependence between the area ratio and the expansion ratio. This result was suitable for the rough draft of sizing and operational behaviour of the refrigerator. Moreover, the authors stated that the optimum primary nozzle diameter decreased with increase in the boiler temperature.

The influence of the area ratio (ϕ = 4, 5.76 and 8.16), compression ratio (R_c = 1.6÷2.25) and expansion ratio (R_d = 2.1÷2.6) on ejectors performance (*COP* = 0.12÷0.30) has been studied by Sankarlal and Mani (2007) [142]:

- *COP* and ω of the system increase with increase in ejector area ratio and expansion ratio; they increase with decrease in compression ratio.
- Performance of the ejector refrigeration system depends on area ratio alone, not on nozzle and mixing chamber diameters.
- *COP* increased with increase in expansion ratio and decreased with compression ratio.

Another experimental analysis was presented by Eames et al. (2007) [128]. They described and evaluated the design and construction of a jet-pump refrigerator and the effect of operational parameters on the performance of the system using R245fa. Performance maps, useful for practical design and control, are also provided. The nozzle geometry and position have strong influence on system entrainment ratio and coefficient of performance: these were found to vary by as much as 40% by changing the nozzle exit position from -10mm to 0mm. The results showed that R245fa is a practical working fluid for jet-pump refrigeration systems.

Yapici et al. (2008) [97] determined experimentally and theoretically the optimum generator temperature as a function of the ejector area ratio at given evaporator and condenser conditions, using R123 as working fluid. For a given ejector area ratio, there exist an optimum generator temperature at which maximum *COP* is obtained from the ejector refrigeration system. The system *COP* undergoes a rather sharp drop when the generator temperature is lowered from the optimum temperature corresponding to its area ratio. The optimum area ratio nearly linearly increases with the generator temperature in the studied range.

Yapici (2008) [92], analysing ejectors with movable primary nozzle, came to the following concluisions:

- The performance of the system could be improved if its ejector was designed carefully and manufactured by using good manufacturing technique.
- To obtain a better performance, the position of the nozzle should be determined; the results show that the optimum position is 5 mm outwards from the mixing chambers.
- For generator temperature higher than 97°C, *CC* remains constant but *COP* decreases.

The numerical analysis conducted by Boumaraf and Lallemand (2009) [123] evaluates the performance and the characteristics of the operating cycle of ERS with the working fluids R142b and R600a, in dimensioning and off-dimensioning conditions. The results of the calculation suggest the following comments:

- At fixed geometry and evaporator temperature, the *COP* of the system with ejector operating at critical mode decreases when the generator temperature is higher than that of the dimensioning of the system (T_g = 120÷135°C). Therefore, it is preferable to dimension the ejector at the highest possible temperature in order to guarantee better performance at lower source temperature.
- For ERS dimensioned for the working fluids R142b and R600a at the same temperatures, the system *COP* operating with R142b is better (round about +70%).

The simulation with a validated one-dimensional mathematical model, carried out by Roman and Hernandez (2011) [108] with low ecological impact refrigerants, indicated that R290 demonstrated better performance, because had the highest system *COP* and its ejector had the maximum entrainment ratio value, the least area ratio value and the highest efficiency value. In order, R152a, R134a, R600a and R600 followed it in terms of performance.

Kasperski and Gil (2014) [132] presented a theoretical analysis based on 1D model of Huang et al. (1999) [15]. Nine heavier hydrocarbons have been tested and optimal temperature range of vapour generation for each fluid was calculated: each hydrocarbon has its own maximum entrainment ratio at its individual temperature of the optimum. Moreover, optimal temperature of vapour generation and maximum values of the entrainment ratio increase according to the hydrocarbon heaviness but peak values of the *COP* do not follow the same trend. The highest *COP* equal to 0,32 is achieved for R600a at the temperature of 102 °C and the *COP* equal to 0.28 for R601 at 165°C. R603 and R604 can be ignored.

Recently, Chen et al. (2014) [122] carried out a detailed investigation of ejector working characteristics with the aim of generalize the interactions and relationships of various ejector parameters to get better understanding of the ejector working characteristics in the refrigeration system. External parameters (generator T_g = 75÷125°C, evaporator T_e = 0÷16°C, condenser

temperature T_c = 27÷43°C and superheat of primary and secondary flow ΔT = 0÷10°C) and internal parameters (ejector component efficiencies 0.7÷0.98) were studied separately. All external, internal, and geometric parameters eventually impact the ejector performance, such as *COP*, entrainment ratio ω, and ejector internal entropy production:

- *COP* and ω increase with an increase in generator and evaporator temperature but decrease with increasing of condenser temperature. Although a higher generator temperature has a positive effect on *COP*, a very high T_g could lead the Carnot efficiency to decrease. Thus, there exists an optimum generator temperature where the Carnot efficiency reaches to maximum (optimum T_g is 100°C, 95°C and 110°C for R141b, R245fa and R600a respectively), while a lower condenser temperature and a higher evaporator temperature always benefit the ejector performance in terms of reducing the ejector irreversibility.
- the ejector component efficiencies have dramatic effects on the system *COP* and ejector behaviour.
- different refrigerants perform distinctively and R141b has highest system *COP*.
- although the superheats of the primary flow or the secondary flow are not economically justifiable for R141b, R245fa and R600a because of insignificant improvement on the ejector and system performance, they might be very critical for the other working fluid, especially the wet working fluid.

The latter aspect was further investigated by Chen et al. (2014) [50]. Four wet fluids (R134a, R152a, R290 and R430A), four dry fluids (R245fa, R600, R600a and R1234ze) and one isentropic fluid (R436B) were tested in a numerical model to compare their performance and applicability in an ejector refrigeration system. To avoid droplet formation inside the ejector working with wet fluids, it is suggested superheat the primary flow before entering ejector nozzle. In some cases, superheat may also be employed to dry fluids and isentropic fluids. The authors proposed a numerical approach for deciding the minimum superheat before entering ejector nozzle, because it is unclear that how much superheat for the primary flow is appropriate. For wet fluid, the task is to find the exact amount of superheat to avoid the droplet formation, obtained when the expansion process in the ejector nozzle ends at saturation condition. The minimum superheat relies on both the generator saturation temperature and the nozzle efficiency: excessive superheat of the ejector primary flow only slightly improves the entrainment ratio, and its effects on *COP* are insignificant, while an increase in the excessive superheat results in a decrease of Carnot efficiency. Using the same method for dry and isentropic fluids, the superheat can be prevented as long as fluids are not operating at the high temperatures adjacent to their critical values. In light of all, R600 is recommended as a good candidate for the ejector refrigeration system from perspectives of system performance and environmental concern. However, its flammability requires extra considerations.

1.4.3.2 SERS with pre-cooler and pre-heater

In some studies the pre-cooler and the pre-heater (also called regenerator) are added to the conventional system in order to improve the system efficiency [16]. The regenerator is used to pre-heat liquid refrigerant returning to the generator using the hot refrigerant from the ejector exhaust. The pre-cooler is used to cool the refrigerant liquid before it enters the evaporator using the cold refrigerant vapour leaving the evaporator. The temperature of the refrigerant from the condenser is slightly increased and decreased before entering the boiler and evaporator, respectively. Therefore, the effect is to reduce the heat input to the generator and the cooling load to the evaporator of the

system. The schematic diagram of a typical SERS with a pre-cooler and a pre-heater is shown in Figure 1-18:

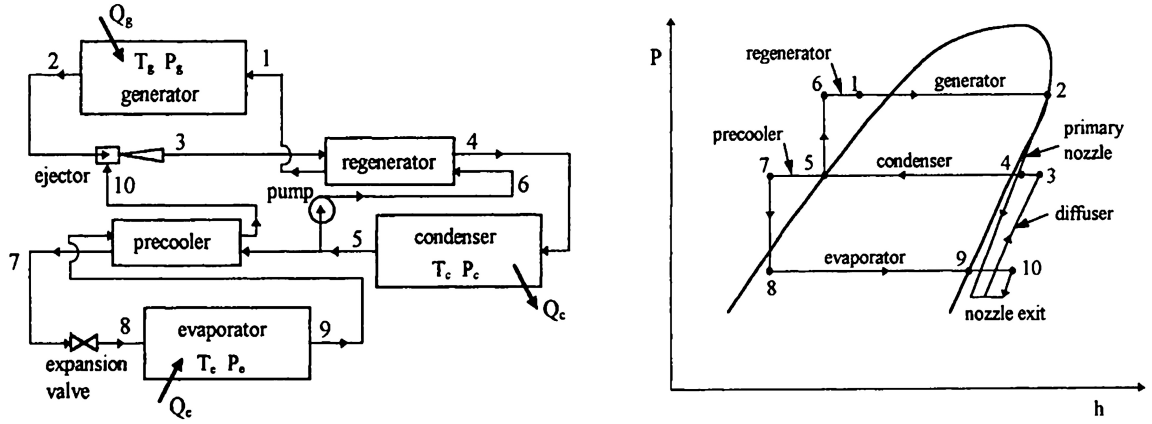

Figure 1-18: Typical SERS with a pre-cooler and a pre-heater and p-h chart of the cycle – taken from [93].

Huang and Jiang (1985) [39] used the R113 as the working fluid in their experimental study, including a regenerator and a pre-cooler to improve the behaviour of the system. A performance map was constructed to show the ejector characteristics and from which the design analysis of ERS was carried out. They experimentally have shown that the choking phenomena in the secondary flow play a very important role in ejector performance. In fact, the effective area for the secondary flow in the mixing chamber, associated to the ejector chocking, was shown not to be a constant but to vary with operating conditions. Moreover, the authors found that for a certain condenser pressure, called critical, and below it, the cooling capacity and *COP* remained constant: the system has to work at this critical pressure to avoid primary vapour waste. Thus, to achieve highest operating efficiency, it is better to design jet refrigeration system at critical points with a design safety factor according with the performance map and to automatically control operating conditions such that the system always works at critical conditions.

Sun and Eames (1996) [93] presented a computer simulation model for ERS based on a thermodynamic model. If regenerators are introduced into the cycle, the required heat input and the cooling load of the system are reduced and the *COP* can be improved by about 20%. Other two heat exchanged are needed, thus costs and plant complication rise. However, the introduction of a regenerator can bring about a significant improvement in system *COP*, but the addition of a pre-cooler has much less effect. Its addition may not be economically justifiable.

Therefore, we may conclude that the introduction of the pre-cooler and the pre-heat in the refrigeration systems seems to be a bad technical-economical choice. It could be taken into account only in particular applications, i.e. automobile air conditioning like [88, 176].

1.4.3.3 Summary

All the above mentioned studies are summarized in the Table 1-5. In this table particular attention is given to the working fluids, operating conditions and performances. SERS performances depend strongly on working fluid and for each refrigerant there are appropriate operating conditions. In addition, it is very important the effect of some geometric parameters, like the position of the nozzle and the area ratio.

Searching appropriate refrigerants, some theoretical and experimental studies show the advantages of using R134a [91, 98], R152a [54], R141b [82], R142b [123] and finally R600a [132] to obtain

high COP, working under the typical operating conditions of the ejectors. The search of new working fluids with low environmental impact and good performance has not ended and it is clear that finding the working fluids with these characteristics will not be easy. However, the use of hydrocarbon refrigerants can be a good technical and environmental option, although research and some safety procedures, due to their flammability, have to be developed before applying these environmental friendly refrigerants [36].

Although the single ERS has an interesting range of applications, it cannot reach compression ratio values higher than 4, reducing its application range only to air-conditioning [36]. In order to improve ERS performance and their market appeal, on the one hand it must exploit the heat source, on the other hand new plant configuration need to be studied.

Table 1-5: State of art of SERS operating conditions and performance. (T) Theoretical study, (E) Experimental study.

Ref.	Working Fluid	Generator temperature [°C]	Evaporator temperature [°C]	Condenser temperature [°C]	*COP* [-]	*CC* [kW]
[131] T	R290	85	-15	30	0.12	na
[88] T	R113	76	27	67	0.24	3.5
[80] T	R11 R113	70 – 90	0 – 5	30 – 35	0.08 – 0.65 0.10 – 0.60	na
[81] T	R11	80 – 104	-1 – 20	30 – 55	0.15 – 0.42	na
[82] T	R11 R22 R114 R123 R133a R134a R141b R142b R152a RC318	90 – 130	10 – 20	25	0.10 – 0.25	na
[54] T	H_2O R11 R12 R113 R21 R123 R142b R134a R152a RC318 R500	80 – 90	-5 – 5	25 – 35	0.02 – 0.50	na
[146] E	CH_3OH	80 – 100	-2 – 14	16 – 28	0.20 – 0.40	0.5
[91] T	R123 R134a R152a R717	60 – 90	-5 – 14	25 – 40	0.05 – 0.45	na
[98] T	R134a R152a R290 R600a NH_3	60 – 90	5	24 – 36	0.05 – 0.40	na
[147] T	CH_3OH	150	-10 – 5	42 – 50	0.14 – 0.47	na
[75] E	H_2O	95 – 130	5 – 15	25 – 45	0.24 – 0.31	5
[74] E	H_2O	120 – 140	5 – 10	22 – 32	0.10 – 0.40	2
[55] E	H_2O	120 – 140	5 – 15	22 – 36	0.28 – 0.48	3
[56] T	H_2O	165	4 – 8	44 – 50	0.40 – 0.60	100
[99] E	R134a	65 – 90	2 – 13	26 – 38	0.03 – 0.16	0.5
[142] E	R717	62 – 72	5 – 15	30 – 36	0.12 – 0.29	2
[128] E	R245fa	110 – 120	10 – 15	30 – 40	0.30 – 0.70	4
[97] E	R123	80 - 105	9 – 15	32 – 37	0.22 – 0.50	na

[92] E	R123	83 – 103	0 – 14	29 – 38	0.12 – 0.39	2
[123] T	R142b R600a	120 – 135	10	20 – 35	0.11 – 0.13 0.06 – 0.08	10
[108] T	R600 R600a R134a R152a	70 – 100	5 – 15	25 – 35	0.30 – 0.75	1
[132] T	R290 R600 R600a R601 R601a R602 R602a R603 R604	70 – 200	10	40	0.05 – 0.32	na
[122] T	R141b R245fa R600a	75 – 125	0 – 16	27 – 43	0.35 – 0.42	na
[50] T	R134a R152a R290 R430A R600 R245fa R600a R1234ze R436B	75 – 125	0 – 16	27 – 43	0.05 – 0.50	5
[39] E	R113	65 – 80	7 – 12	28 – 45	0.16 – 0.24	1.6
[93] T	R123	80 – 90	5 – 10	30	0.19 – 0.29	na

1.4.4 Conventional Solar-powered ejector refrigeration system (SoERS)

The configuration of solar-powered ejector refrigeration system (SoERS) is equal to the previous one. In this case, the thermal source is constituted by solar thermal energy: heat from the solar collector is carried by the intermediate medium and transferred to the refrigerant by the heat exchanger. The heat transfer mediums should have the boiling point higher than the possible temperature in the system, low viscosity and good heat transfer properties. Water with a corrosion inhibitor additive and transforming oil are recommended for operating temperature below and above 100°C, respectively [35].

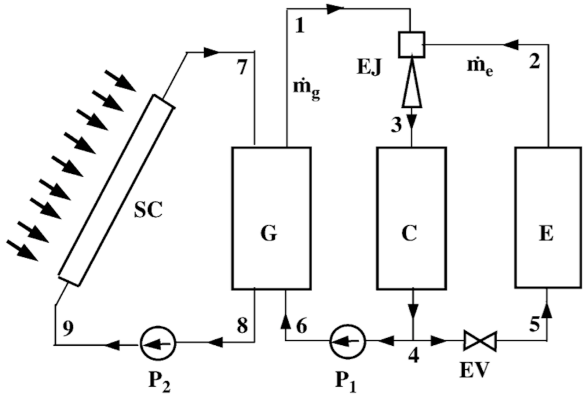

Figure 1-19: Solar-driven ejector refrigeration system.

The behaviour of these systems depends first on the external environment and solar collector efficiency. Generator temperature will not be too high: for example, [99, 142] can give indications about their performance. In order to evaluate SoERS performance, further efficiency definition is introduced. The overall efficiency of the solar ejector refrigeration cycle can be expressed as the product between the solar collector efficiency and the ejector *COP* [16]:

$$COP_{overall} = \eta_{solar} \cdot COP_{ejector} \tag{1.11}$$

It is obvious that not only the performance of the refrigeration system itself, but also the thermal efficiency of solar collector, are the parameters affecting on the overall performance of solar jet refrigerator. In particular, the efficiency of a solar system depends on the collector type, the solar radiation intensity and the system operating conditions. Further details on solar collectors may be found in [177]. The installation of a very high efficiency solar collector may give the significant increase of overall efficiency but, on the other hand, the unit cost per watt of cooling is also increased and the break-even point may not be met [16].

With the diffusion of renewable energy technology, this system has been widely studied and now many analyses that make explicit reference to solar thermal source are available in literature. We may divide the solar-powered ejector refrigeration systems in two sub-categories: (i) standard SoERS and (ii) SoERS with storage system.

1.4.4.1 Standard SoERS

Al-Kahlidy (1998) [87] carried out a theoretical analysis to select a suitable refrigerant for the system and proposed certain refrigerant selection criteria, concluding that the molecular weight was an important parameter. Refrigerant R113 was chosen for the experimental solar-driven ERS because it has a high molecular weight, then the mixing ratio can be increased, and the greater compressibility factor. The ejector *COP* reaches 0.42 for T_g = 100°C, T_e = 18°C and T_c = 50°C.

In the same year, a high-performance solar ejector cooling system using R141b was developed by Huang et al. (1998) [115]: the *COP* obtained exceeds the 0.5 and the overall *COP* of the system can reach as high as 0.22. Moreover, the design of the solar ejector cooling system is very simple and it has only four major components (solar collector, ejector, condenser and evaporator). Thus, the installation cost can be lowed as compared to the absorption cooling system. However, the performance of the solar-driven ejector needs to be improved further in order to compete with the other thermal refrigeration systems. In a following work [178], the performance of the solar ERS was simulated using three different collectors: a little difference on solar collector efficiency can determine a larger difference on overall *COP*.

Pridasawas and Lundqvist (2004) [134] carried out an exergy analysis and optimized the operating conditions using this method. Irreversibility depends on the operating temperatures and the most significant losses in the system are in the solar collector and in the ejector, equal to 51% and 16% of the overall system losses, respectively. However, the optimum generating temperature is about 80-100°C, depending on the evaporator temperature. Thus, the high temperature solar collector is not necessary for the solar-driven ERS for the given conditions. The overall thermal energy efficiency at the generating temperature T_g = 90°C is about 11%.

Alexis and Karayiannis (2005) [100] evaluated the performance of an ejector cooling system driven by solar thermal energy and R134a as working fluid. The Athens area in summer months was taken as reference. The solar collector efficiency varied from 0.319 to 0.507 and the overall *COP* was equal to 0.011-0.101. At last, this study showed that the *COP* of ejector cooling system is an exponential function of generator, evaporator and condenser temperature.

Ersoy et al. (2007) [94] conducted a numerical investigation on the performance of solar ERS under Turkish climatic conditions. The evacuated tube solar collector efficiency varied very much depending on the solar radiation rather than the ambient temperature for the day. Therefore, in order to operate with continuity the system, an auxiliary heat source should be employed. When generator, condenser, and evaporator temperatures were taken, namely, T_g = 85°C, T_c = 30°C and

T_e = 12°C, the maximum overall *COP* and the *CC* were obtained as 0.197 and 178.26 W/m^2, respectively, at 12:00 in August for Aydin (Turkey).

A comparison of solar-driven ERS with air-conditioning purpose, using several environment friendly working fluids, was carried out by Nehdi et al. (2008) [101]. The comparative calculation showed that R717 provided the highest *COP*. For the solar air-conditioning application, the *COP* of the overall system varied from 0.21 to 0.28 and the exergy efficiency varied from 0.14 to 0.19.

Ma et al. (2010) [57] controlled the primary flow using a spindle (the function of the spindle is to provide a fine tuning and an optimum *COP* for the ejector operation) and, changing the generator and evaporator temperatures, they observed:

- When the spindle position moved toward the nozzle, the primary nozzle throat area increases, and consequently the mass flow rate; exists an optimum entrainment ratio and *COP* related to the optimum area ratio.
- Increasing the boiler temperature did not always increase system efficiency; the maximum cooling capacity was found at generator temperature of 92.8°C and maximum ω and *COP* were found at 90°C.
- The system performance (*CC*, ω and *COP*) increases significantly with evaporator temperature; however, the critical backpressure increases slowly with the increase of the evaporator temperature.

Smierciew et al. (2014) [136, 137] carried out an experimental investigation on ejector air-conditioning system driven by low temperature solar heat, below 75°C. Under this range, the ejector cycles can be considered very competitive with absorption refrigeration systems. In fact, 80°C can be considered as the minimum value at which the absorption cycle can still operate, while there is no physical limitation for operation of the ejector systems at lower temperatures. The results confirmed that the ejector cycle operating with R600a may be effectively driven by low temperature heat source and this system may be successfully used for air conditioning purposes, either for individual or commercial households.

The variations in solar irradiation intensity not allow maintaining a steady generator temperature. Thus, in order to improve ejector performance, Yen et al. (2013) [58] proposed a variable throat ejector and analyzed its behaviour using CFD simulations (please refer to the next section for further details on the CFD approach). An ejector with a greater throat area and larger solar collector allows a wider operating range of generator temperatures, but may be overdesigned and expensive. Conversely, decreasing the throat area limits the operating range of the generator temperature, and the resulting system may be unable to use solar energy as a heat source.

1.4.4.2 SoERS with storage system

The major technical problem of solar-powered ERS is the strongly reliant of the system on ambient conditions, like solar radiation, air temperature, wind speed and other transient factors [35]. In order to mitigate these negative aspects, the main intervention is to introduce an integrated thermal storage system. This solution is becoming a hot research topic [35]. Thermal energy storage is essential in applications with intermittent energy supply and continuous cooling demand. In solar air conditioning applications two form of energy storage can be considered [179]:

- hot storage, in which high temperature energy from the solar collector is stored in a tank;
- cold storage, in which low temperature energy from the evaporator is stored in a tank.

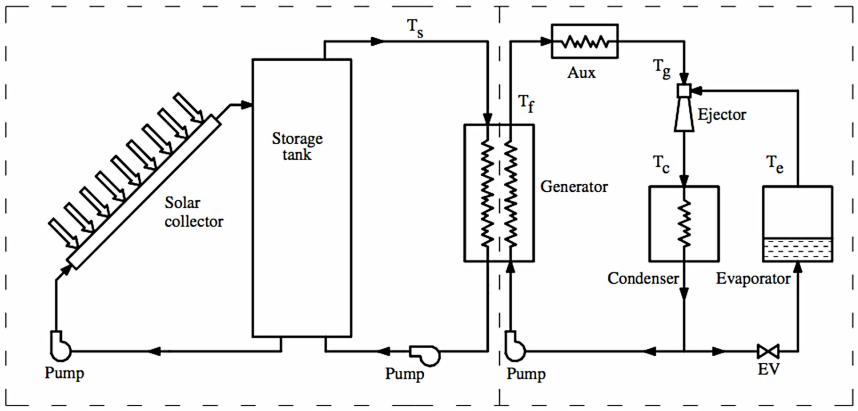

Figure 1-20: Solar-driven ejector refrigeration system with hot storage tank [116].

Dorantes et al. (1996) [124] developed a mathematical model to simulate the dynamic thermal behaviour of a solar ejector-compressor refrigeration systems for icemaker usage. As Sokolov and Hershgal (1990) [89] suggested in order to enhance efficiency, they decided on a hybrid cycle using a booster: in this way the vapour coming from the evaporator is compressed in two steps. Moreover, a storage unit coupled to the solar-collector is used. Due to the discontinuous features of solar energy, the authors evaluated the performance of the system in design conditions and for a whole year: the nominal *COP* was equal to 34%, while the annual average efficiency was 11%. However, the model allows establishing the limits of the system optimum performance and the importance of the use of the storage tank. Moreover, the authors compared their result with the performance of an intermittent single effect absorption system, finding that jet compression COP values were very competitive and with an advantage of the simplicity of this kind of systems.

An hourly simulation of an ejector cooling system moved by solar energy was proposed by Vidal et al. (2006) [116]. Its major components include solar collector, a hot water storage tank, an ejector cycle and an auxiliary heat supply (an additional source of energy to ensure the design operating conditions required by ejector). The parametric study to select the optimum system size leaded to a collector area of 80 m^2 with a solar fraction of 42% and thermal capacity of 10.5 kW. The size of the storage tank influences only slightly the useful heat gain of the system and has a greater effect on the auxiliary heat.

Pridasawas and Lundqvist (2007) [138] developed another theoretical model about the same system pattern as the previous, selecting Bangkok as simulation location. They found solar collector area of around 80 m^2 for a solar fraction of 75% and a thermal cooling capacity of 2.5-3.5 kW, using the evacuated tube solar collector. Even if the installation cost of the system using flat plate collector is cheaper than the evacuated tube, it is not economically competitive due to the high amount of auxiliary heat required.

Varga et al. (2009) [59] carried out a theoretical analysis of a solar ERS with storage tank and aux heater in the Mediterranean, based on a simplified 1D model. The results indicated that in order to achieve an acceptable *COP*, generator temperature should not fall below 90°C. The required solar collector area and the ejector dimensions to provide 5 kW of cooling effect was calculated for different conditions.

An application case for office buildings air conditioning in Shanghai was proposed by Guo and Shen (2009) [102]. Employing a vacuum tube collector of 15 m^2, the results indicate that during the office working-time, the average *COP* and the average solar fraction of the system were 0.48 and

0.82 respectively. Moreover, compared with traditional compressor based air conditioner, the solar-powered ERS could conserve more than 75% of electric energy.

In the case of ejector cooling, it can be interesting to store low temperature thermal energy with a temperature variation as small as possible, in order to ensure nearly constant conditions in the evaporator and thus a high cooling cycle *COP* [180]. Thus, several authors proposed also a solar-driven ERS with a cold storage tank with the help of phase changing materials, cold water or ice storage, as recommended by Bejan et al. [181].

Diaconu et al. (2011) [179] simulated a solar-assisted ejector cooling system with cold storage located in a hot location (Algeria). In order to get a complete view of the problem, a system without energy storage was compared to the system with cold storage. The first system was not capable of ensuring reasonable comfort conditions during the interval of time when solar radiation was not available, while the system with cold storage substantially improved internal comfort conditions. The following years, Diaconu (2012) [180] continued his work presenting a quantitative energy analysis about an office building with cooling requirements during working hours only. For the best configuration tested, the maximum value of the cooling load was 6.6 kW, the *COP* of the ejector and the overall efficiency of the system were 0.61 and 0.3 respectively.

In order to provide better compliance with varying ambient conditions, a variable geometry ejector with cold storage was investigated by Dennis et al. (2011) [117]. The study concluded that with no energy storage, both fixed and variable ejector systems had poor solar fractions, 4% and 17% respectively; with a cold storage, instead, a variable geometry ejector is able to increase yield by 8-13% compared to a fixed geometry ejector. The modelling showed how the solar collector area may be decreased if a cold store is used and this may benefit the capital and operating cost of the system.

Eames et al. (2013) [76] carried an experimental investigation of a novel ejector refrigeration cycle with a jet spray thermal ice storage system, in which a steam driven jet- pump is used to create a vacuum pressure in a hermetic vessel into which water is sprayed through a nozzle. The effect creates ice in the vessel under normal operation and acted as a coolth storage medium. The low evaporator temperature resulted in a relatively low overall *COP* equal to 0.162. The authors argued that such system powered by solar energy would help to store the coolth to level out the off-peak conditions.

1.4.4.3 Other SoERS

The scientific research is constantly looking for new plant configurations in order to improve the performance of the ejector-based systems. Recently, a solar-powered combined Rankine and ejector refrigeration cycle has been proposed for the production of power and refrigeration output.

Kumar et al. (2014) [77] carried out a thermodynamic analysis in order to find out the effect on the performance of the combined cycle of the follow parameters: the turbine inlet pressure (0.9÷1.3 MPa), the evaporator temperature (-11÷-3°C), the condenser temperature (24÷30°C), the extraction ratio (0.2÷0.8) and the direct normal radiation per unit area (0.8÷0.9 kW/m^2). The Figure 1-21 shows the schematic diagram of the cycle proposed by the authors:

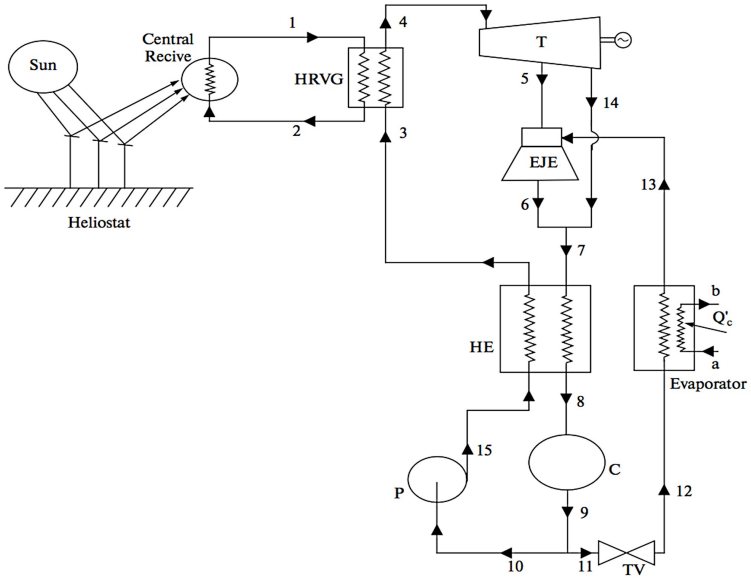

Figure 1-21: Schematic diagram of solar-powered combined Rankine and ejector refrigeration cycle – taken from [77].

The solar energy is exploited by means of the concentrating solar power tower system (solar tower CSP [182]). The oil (Duratherm600) is heated by passing through the central receiver (*1→2*) and transfers the thermal energy from central receiver to the refrigerant in the HRVG (*3→4*). The superheated refrigerant vapour (*4*) is expanded in a turbine to generate work. The extracted vapour from the turbine (*5*) passes through the supersonic nozzle of ejector, while as usual the secondary flow comes from the evaporator (*13*). The stream out of the ejector (*6*) mixed with turbine exhaust (*14*) is cooled in the heat exchanger (*7→8*) and enters the condenser. The saturated liquid (*9*) is divided in two streams: the first one (*11*) is sent to the evaporator and produces the cooling effect; the second one (*10*) is pumped to the heat exchanger (*15*) and to the HRVG. The authors carried out an energy analysis (applied to find out the energy distribution of solar heat source) and an exergy analysis (applied to find out the exergy destruction in each component of the system). The results reveal that, out of 100% energy (solar heat source) supplied to the system, around 14.81% is available as useful energy output: 10.62% is the net power output and 4.19% is the refrigeration output. Moreover, about 88.1% of the input (solar heat) exergy is destructed and lost due to irreversibilities; the remainder is available as an exergy output: 11.36% of exergy is associated with the net power output and 0.54% exergy is associated with the refrigeration output.

Zhang and Mohamed (2014) [140] proposed a very similar plant configuration where, however, the steam extraction to supply the ejector is downstream of the turbine. Moreover, the system has been designed to work in hot climates and to harness low-grade solar energy or any other low-grade thermal energy, without specifying the particular technology adopted. The authors have also introduced a latent heat storage unit, a thermal buffer between solar receiver and the combined cycle, which compensates for the daily solar incident change and releases the thermal energy to the combined cycle at night. In this paper, several typical alternative refrigerants (R1234yf, R1234ze, R290, R600, R600a, R601, R744) are evaluated and compared to the most commonly used HFC refrigerant (R134a). From this analysis it appears that the pentane-based (R601) combined power and ejector cooling cycle has great potential of harnessing low-grade thermal energy in hot climates due to the relatively high critical temperature (196.7°C) of the pentane, which provides

vapour expansion a wide operating temperature range above the ambient temperature of 40°C. A thermodynamic analysis of the combined system has been performed and the thermal and exergy efficiencies resulted equal to 15.06% and 19.43%, respectively, at T_e = 12°C and T_g = 148.83°C. According to the authors, this system provides an alternative environment-friendly solution to utilize hydrocarbons for sustainable energy production and more research efforts are needed to optimize the design and performance of the proposed stand-alone solar thermal power and cooling system for its successful application in hot climates.

In the solar-powered combined Rankine and ejector cooling cycle no compressor is needed and the solar thermal cycle does not need any external power input; thus, it is expected to be energy-efficient and reliable [140]. This combined cycle also provides great flexibility for operation. Indeed, when cooling is not needed, the combined cycle can function at the sole power generation opening the ejector-bypass valve. On the other hand, when the cooling demand is dominant, the expander and generator set can be regulated to reduce power output, thereafter the vapour after expansion has more exergy to entrain cooling refrigerants from the evaporator [140].

1.4.4.4 Summary

The Table 1-6 provides a general overview about solar-driven ERS performance and operating conditions. It should be noted that selection of the working fluid for the solar refrigeration or air-conditioning system is the crucial problem because of the strong influence of the thermodynamic fluid properties on the system efficiency.

In the Table 1-7 have been reported the characteristics of the solar collector used in the literature studies and, where required, the kind of storage system. The information contained in this table can help to understand the influence of the efficiency of the solar collector on the *COP* of the system.

Table 1-6: State of art of conventional SoERS operating conditions and performance. (T) Theoretical study, (E) Experimental study.

Ref.	Working Fluid	Generator temperature [°C]	Evaporator temperature [°C]	Condenser temperature [°C]	$COP_{ejector}$ [-]	CC [kW]
[87] E	R113	60 – 100	5 – 18	40 – 50	0.42 (max)	0.21
[115] T	R141b	80 – 120	-6 – 8	30 – 36	0.20 – 0.50	10.5
[134] T	R600	85 – 125	5 – 15	37	0.20 – 0.40	5
[100] T	R134a	82 – 92	-10 – 0	32 – 40	0.04 – 0.20	na
[94] T	R123	85	12	30	0.20	3.7
[101] T	R134a R141b R142b R152a R245fa R290 R600 R717	90	15	35	0.30 – 0.41	na
[57] E	H_2O	84 – 96	6 – 13	21 – 38	0.17 – 0.32	5
[136] E	R600a	50 – 64	4 – 7	22 – 32	0.15 – 0.20	2
[58] T	H_2O	90 – 110	8 – 20	35 – 40	0.2 – 0.55	10.5
[124] T	R142b	105	-10	30	0.34	2
[116] T	R141b	80	8	32	0.39	10.5
[138] T	R600a	70 – 120	5 – 15	T_{amb} + 5	0.35 – 0.48	3.5

[59] T	H_2O	90 – 110	5 – 15	30 – 40	0.10 – 0.55	5
[102] T	R134a	85	8	$T_{amb} + \Delta T$	0.30 – 0.53	6
[117] T	R141b	80 – 110	2 – 14	20 – 40	1.5 (max)	3.5
[76] E	H_2O	110 – 135	2.5 – 10	21 – 30	0.5 (max)	na
[77] T	H_2O	150	-11 – -3	24 – 30	$\eta_I = 0.148$	na
[140] T	R601	150	12	50	$\eta_I = 0.151$	na

Table 1-7: Characteristics of the solar collector used and the kind of storage system (where required) in the previous literature studies.

Ref.	Solar collector and Storage system	Solar radiation intensity [kW/m^2]	Efficiency [%]	Area [m^2]
[87]	Parabolic trough concentrator	0.762 – 0.874	20	15
[115]	Double-glazed selective surface flat-plate solar collector	0.7	50	68
[134]	Double-glazed selective surface flat-plate solar collector	0.7	48	-
[100]	Evacuated-tube solar collector	0.536 – 0.838	31.9 – 50.7	-
[94]	Evacuated-tube solar collector	0.200 – 0.896	28 – 36	19.7 – 21.5
[101]	Single-glazed selective surface flat-plate solar collector	0.351 – 0.875	40	-
	Double-glazed selective surface flat-plate solar collector		50	
	Evacuated-tube solar collector		65	
[57]	Evacuated-tube solar collector	-	-	-
[124]	Evacuated-tube solar collector + Hot liquid storage tank	0.311	52	18
[116]	Single-glazed selective surface flat-plate solar collector + Hot liquid storage tank	-	-	80
[138]	Evacuated-tube solar collector + Hot liquid storage tank	-	47	50
[59]	Evacuated-tube solar collector + Hot liquid storage tank	0.8	-	50
[102]	Evacuated-tube solar collector + Hot liquid storage tank	0.2 – 0.9	-	15
[117]	Evacuated-tube solar collector + Cold storage system	-	-	12 – 22
[77]	Heliostat for solar tower CSP	0.8 – 0.9	75	3000

1.4.5 Ejector refrigeration system without pump

The pump does not determine a high growth in cost or electricity consumption (i.e. in Ref. [134] the required pump power consumption is only 0.18% of the total energy received from the solar collector). However, it needs more maintenance than other parts because it is the only moving part in the system. Hence, in order to dismiss the pump, several solutions have been found:

[i] Natural convection ejector refrigeration system;

[ii] Bi-ejector refrigeration system;

[iii] Gravitational/Rotational ejector refrigeration system;

[iv] ERS with thermal pumping effect;

[v] Heat pipe/ejector refrigeration system.

In this way, the ejector refrigeration systems acquire additional benefits, such as the potential for a very long lifetime with minimal maintenance requirement, low risk of breakdown and no associated noise or vibration [60].

Natural convection ejector refrigeration system. One of the first works about ERS without a pump was carried out by Nguyen et al. (2001) [60] who proposed an ERS powered by solar thermal energy. The elimination of the pump was achieved by transferring liquid from the condenser to the boiler, using gravity head. The system used water as refrigerant for an air-conditioning application that also provide heating in the winter season, evaluated and installed in an office building in England. The prototype system had a nominal cooling capacity of 7 kW and operated with a *COP* of up to 0.3. An economical comparison between this system and a conventional one of the same thermal capacity was presented, finding that the investment payback period was 33 years. A reduction in capital cost must be achieved if commercial viability is to be enhanced. In addition to the economic aspects, this system has other criticalness. The main problem lies in their large thermal inertia, which affects the start-up and shut-down performance. In particular, the boiler takes approximately 20 minutes to achieve working temperature from cold under strong sun. Indeed, the thermal inertia of the boiler and hot water circulation system should be reduced to increase the speed of response. Moreover, during off-design operating conditions (i.e. periods of reduced solar irradiation) use of a propane burner is necessary for supplementary heating and avoid thermal transient.

Bi-ejector refrigeration system. In the bi-ejector refrigeration system (BERS), a second ejector replaces the mechanical pump: it carries the liquid condensate to the generator, thanks to the entrainment of the primary vapour flow. Therefore, the ejector added is a condensing ejector (vapour/liquid). The remarkable characteristic of a bi-ejector solar refrigeration system is that during ideal operation, the system will not consume electricity.

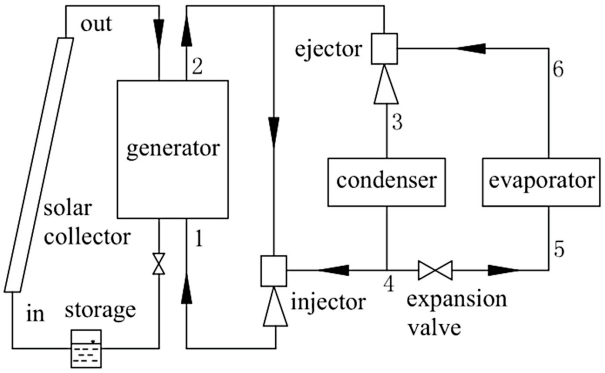

Figure 1-22: Bi-ejector refrigeration system without pump proposed by Wang and Shen (2009) – taken from [95].

Shen et al. (2005) [61] studied this kind of configuration and the numerical results showed that the cycle *COP* value at a given operating condition is mainly influence by the gas-gas ejector entrainment ratio: this trend is more or less the same for all the tested refrigerants. The condensing ejector entrainment ratio of R718 was relatively high. However, the best overall system COP achieved was 0.26 using R717 as the refrigerant.

Wang and Shen (2009) [95] investigated a novel solar bi-ejector refrigeration system using R123. With increasing generation temperature, the entrainment ratio of ejector improved, while that of condensing ejector became worse. Thus, the overall thermal efficiency of the solar bi-ejector refrigeration system first increases and then decreases with an optimum value of 0.13 at T_g = 105°C, T_c = 35°C and T_e = 10°C. However, with increasing condensation temperature, the entrainment ratios of the two ejectors and the overall system efficiency all become worse.

Gravitational/Rotational ejector refrigeration system. Kasperski (2009) [62], proposed a gravitational ejector as an alternative solution for a pump ejector refrigerator. The vertical arrangement of the heat exchangers on different levels allows to equalize the pressure differences between the exchangers with the help of the refrigerant hydrostatic pressure. The highest pressure is obtained in the steam generator, which forces the lowest liquid level. The lowest pressure obtained in the evaporator causes the inflow of liquid to the highest installation level. There are then complex mechanisms of self-regulation of generator, evaporator and condenser. The limitation of this system lies in its requirement of great height differences (which depends on the applied refrigerant and on levels of temperature in particular parts of the device) and the length of pipe work, which increases friction and heat losses. At T_g = 80°C, T_c = 35°C and T_e = 15°C, the coefficient of performance reached is *COP* = 0.16.

Kasperski (2010) [63] developed the concept of the gravitational ejector into a rotating ejector. The application of rotary motion causes the axis-symmetric arrangement of liquid levels: similarly to the gravitational refrigerator, higher steam pressure pushes the liquid level outside and the lower steam pressure sucks the liquid inside. With lager accelerations of rotary motion (order of 1000 rpm), this roto-gravitational refrigerator significantly decreased the size of the gravitational refrigerator and the amount of working fluid. The performance are similar to those of the gravitational ejector [62]: *COP* = 0.16 at T_g = 90°C, T_c = 35°C and T_e = 15°C.

The author identifies a number of applications for this device: food storage, air-conditioning, internal cooling of rotors (generators, pump), compact cooling fans or pumps. However, the main problem of experimental research concerning rotary refrigerators is the limited possibility to

observe the occurring processes, the damage of measurement sensors caused by centrifugal acceleration and the disturbance of electric signals transmitted by sliding contacts.

ERS with thermal pumping effect. The fourth plant configuration was proposed by Huang et al. (2006) [118] and involved the use of a multi-function generator (MFG) to eliminate the mechanical pump. The MFG serves as both a pump and a vapour generator. The system includes two generators and each generator consists of a vapour generator (boiler) and an evacuation chamber. The vapour generator is a heat exchanger like a conventional boiler for heating the liquid in order to pressurize the whole generator and to generate vapour; while the evacuation chamber provides a cooling effect to depressurize the whole generator in order to intake the liquid from condenser. The system has not moving parts, but it is composed of too many elements, which will lead to inevitable consumption of available thermal energy. The experimental results showed that the system coefficient of performance was 0.22 at T_g = 90°C, T_c = 32.4°C and T_e = 8.2°C, while taking into account the extra heat needed for the MFG operation, the total coefficient of performance is 0.19.

In order to replace R141b, Huang et al. (2009) [183] redesigned the ejector for working with R365mfc. They showed experimentally that R365mfc could replace R141b and no drop of system performance occurs as long as the ejector design is optimized. At generator temperature 90 °C, $COP_{ejector}$ = 0.182÷0.371, the total COP = 0.137÷0.298, and CC = 0.56 kW÷1.20 kW for T_e = 6.7÷21.3°C.

Heat pipe/ejector refrigeration system. Finally, the integration of the heat pipe with an ejector results in a compact and high performance system, which does not require additional pump work. This system can also utilize solar energy or hybrid sources. The heat pipes are devices with high thermal conductance and may consist of a sealed tube provided with an internal wick. In operation, heat applied to one end of the pipe causes the liquid refrigerant to evaporate and the resulting vapour travels to the cool end where it condenses, surrendering energy. The basic cycle of the heat pipe/ejector system consists of a heat pipe, ejector nozzle, evaporator and expansion valve. When heat is supplied to the generator section of the heat pipe, the working fluid evaporates and expands through the primary nozzle of the ejector, thereby entraining low-pressure refrigerant from the evaporator section producing a refrigeration effect. The ejector exhaust is discharged into the condenser section of the heat pipe where heat is removed using air or water. From the condenser, some of the liquid refrigerant is returned to the generator by the wick action, while the remainder is expanded through the expansion valve (or capillary tube) to the evaporator.

Riffat and Holt (1998) [64] carried out a computer modelling using water, methanol and ethanol as working fluids. The COP of methanol was found to be higher then the other fluids, around 0.7. In general, COP of approximately 0.5 is achievable using operating conditions practicable using low-grade heat.

An applicable heat pipe/ejector system for building cooling and air-conditioning was proposed by Ziapour and Abbasy (2010) [65] who carried out an energy and exergy analysis. The simulation results indicate that COP = 0.30 at T_e = 10°C, T_c = 30°C and T_g = 100°C. The authors indicated that the maximum heat pipe cooling capacity could be obtained for large heat pipe diameters, near the small heat pipe lengths.

The performances of all the plant configurations that do not involve the use of a mechanical pump are recapitulated in the Table 1-8. The most promising system seems to be the integrate heat pipe/ejector system: achievable COP is similar to that of absorption refrigeration systems, whilst

still maintaining the benefits of significantly cheaper capital, maintenance and operating costs [64]. However, experimental investigations are not available.

Table 1-8: State of art of ERS without mechanical pump operating conditions and performance. (T) Theoretical study, (E) Experimental study.

Ref.	Working Fluid	Generator temperature [°C]	Evaporator temperature [°C]	Condenser temperature [°C]	*COP* [-]	*CC* [kW]
[60] E	H_2O	90	10	35	0.30	7
[103] E	R134a	75 - 80	10 – 18	31 – 36	ω=0.08÷0.13	1.5
[61] T	R11 R12 R22 R134a R123 R502 R717 H_2O	75 – 100	3 – 15	28 – 40	0.04 – 0.26	na
[95] T	R123	80 – 95	7 – 15	30 – 39	0.15 – 0.30	na
[62] T	H_2O	80	15	35	0.16	0.12
[63] T	H_2O	90	15	35	0.16	0.08
[118] E	R141b	90	8	32	0.22	0.8
[183] E	R365mfc	90	8 – 25	32	0.10 – 0.45	1.7
[64] T	H_2O CH_3OH C_2H_5OH	80 – 100	5	24 – 32	0.40 – 0.70	na
[65] T	H_2O	90 – 100	10 – 15	30 – 32	0.30 – 0.50	1 – 5.5

1.4.6 Combined ejector-absorption refrigeration system (EAbRS)

Absorption is the process in which a substance assimilates from one state into a different state [184]. These two states create a strong attraction to make a strong solution or mixture. The increase of heat or the effect of the partial pressure difference in a solution can reverse the process. The absorption refrigeration technology consists of a generator, a pump and an absorber that are capable of compressing the refrigerant vapour. The evaporator draws the vapour refrigerant by absorption into the absorber and the extra thermal energy separates the refrigerant vapour from the solution. The condenser liquefies the refrigerant and then the evaporator expands the cooled liquid refrigerant [4, 35]. The attractive feature of the absorption system is that any types of heat source, including solar heat and waste heat, can be utilized in the desorber. However, because of its complex configuration and low *COP*, it is less competitive than the conventional vapour compression system. Adding ejector to the conventional absorption systems and an appropriate installation configuration can help to improve the system performance, almost similar to multi-effect absorption cycle machine. Moreover, due to the simplicity of the combined ejector-absorption refrigeration machine, its capital investment cost is lower [35]. Substantially, the combination brings together the advantages of absorption and ejector refrigeration systems and provides high COP for refrigeration and air-conditioning.

Chen (1988) [85] presented and analyzed a modified ejector-absorber absorption cycle in which the ejector outflow is sent to the absorber. Practically, for a limited absorber temperature, the absorption efficiency increases with increasing absorber pressure and an energy-recovery process can be accomplished by using an ejector instead of a pressure-reducing valve. From the results, it is

observed that a considerable improvement in *COP* is obtained compared with that of the conventional cycle. The present study also shows that the geometric parameters of the ejector design have considerable effects on the system's performance and it is recommended that the detailed analysis be used in conjunction with coupled ejector-parameters to arrive at optimum operating conditions. The optimum area ratio gives a maximum *COP* = 0.85, while the performance of a conventional cycle is *COP* = 0.68 under the same conditions T_g = 120°C, T_c = 40°C and T_e = 5°C. By reducing the condenser temperature to T_c = 30°C, the coefficient of performance of the combined cycle can reach the maximum value *COP* = 1.5.

Sun, Eames et al. (1996) [66] proposed to integrate the ejector in an absorption cycle in order to increase the refrigerant flow rate from the evaporator and thus raises the cooling capacity of the machines (Figure 1-23). The combined cycle provides potentially high coefficient of performance (*COP* = 2.4) that intrinsically could be twice that of a conventional single-effect absorption machine. Despite the obvious improvements in efficiency, the required generator temperatures were too high (T_g = 220°C) to be handled by low-grade energy sources.

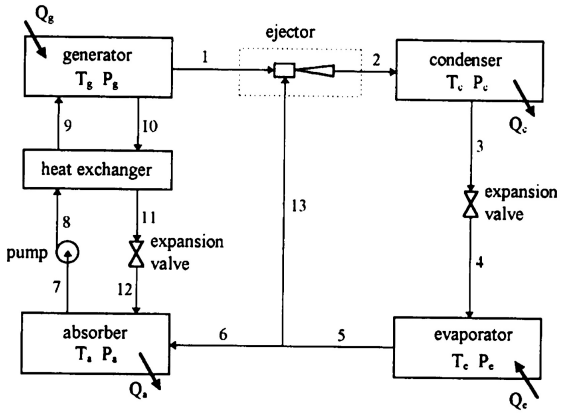

Figure 1-23: Combined ejector-absorption refrigeration system – taken from [66].

A thermo-economical comparative analysis between a three-pressure ejector-absorption refrigeration cycle and a double-effect absorption cycle was carried out by Jiang et al. (2002) [148]. The *COP* of the three-pressure absorption–ejector refrigeration system is up to 0.9–1.0 and it is slightly lower than that of the commercial double-effect absorption refrigeration system, but the annual total cost of the first system is competitive to that the second one.

Sozen and Ozalp (2005) [67] proposed a solar-driven ejector-absorption system operated with aqua-ammonia situated in Turkey. Ejector was located at the absorber inlet, which helped the pressure recovery from the evaporator. As a result of the analysis, using the ejector, the *COP* improved by about 20%.

Jaya et al. (2005) [104] made a comparative study of EAbRS operating with new working fluid pairs such as R124-DMAC, R134a-DMAC and R32-DMAC. Results show that R124-DMAC and R134a-DMAC give good performance (*COP* of order of 1.0) at low values of generator temperature (T_g = 100÷110°C) and evaporator temperature (T_e = 5°C). R32-DMAC has drawbacks such as high generator pressures and high circulation ratios.

Hong et al. (2011) [68] proposed a novel ejector-absorption combined refrigeration cycle. When the temperature of the heat source is high enough, this cycle will work as a double-effect cycle. If the temperature of the heat source is lower than that required to drive conventional double-effect absorption refrigeration cycle but much higher to drive conventional single-effect absorption

refrigeration cycle, the *COP* of new cycle will also be higher than that of conventional single-effect absorption refrigeration cycle. The ejector is the key component in the combined cycle. Obviously, the *COP* of the system depends strongly on the performance of the ejector. Simulation results show that the *COP* of the cycle is 30% higher than that of the conventional single-effect cycle.

Wang et al. (2009) [69] presented a combined power and ejector-absorption refrigeration cycle with aqua-ammonia as working fluids. This system combined the Rankine cycle with ejector-absorption refrigeration cycle, and could produce both power output (P = 612.12 kW) and refrigeration output (CC = 245.97 kW) simultaneously. This combined cycle introduces an ejector between the rectifier and the condenser, and provides a performance improvement without greatly increasing the complexity of the system. The results of the parametric analysis showed that generator, condenser and evaporator temperature, turbine inlet and outlet pressure and solution ammonia concentration have significant effects on the net power output, refrigeration output and exergy efficiency of the combined cycle.

Sirwan et al. (2013) [144] proposed a modification in the combined absorption–ejector cooling system in order to enhance efficiency of the system components, essential to increase the *COP* of the system. In fact, the absorption cooling cycles can be powered by solar but the performance is limited by heat source temperature (solar collector) and high ambient temperature that can affect the condensation process. Adding a removable flash tank between the condenser and evaporator could improve entrainment ratio of the ejector, along with improving the cooling effect inside the evaporator. A computer simulation program is developed to evaluate the performance of the modified combined cycle using NH_3–H_2O refrigerant. The performance of the proposed combined cooling cycle is compared with basic absorption, and combined absorption–ejector cooling cycles. Results showed a significant improvement in the *COP* of the modified cycle at different operating conditions: the overall *COP* ranges are found higher at the modified combined cycle (0.49–0.86) compare to combined cycle (0.42–0.75), and basic cycle (0.18–0.575). Cooling effect and capacity of the evaporator is enhanced due to the reduction of flash gas delivered to the evaporator. Furthermore, the flash tank optimized the ejector entertainment ratio and consequently increasing the condenser pressure. This optimization will enable the system to perform well in hot climates where the condenser efficiency is limited by ambient temperature.

Table 1-9: State of art of EAbRS operating conditions and performance. (T) Theoretical study, (E) Experimental study.

Ref.	Working Fluid	Generator temperature [°C]	Evaporator temperature [°C]	Condenser temperature [°C]	*COP* [-]	*CC* [kW]
[85] T	DME-R22	120 – 180	5	30 – 50	0.5 – 1.5	na
[66] T	LiBr-H_2O	190 - 220	5 – 15	22 – 40	0.7 – 2.4	na
[148] T	LiBr-$ZnCl_2$-CH_3OH	170	7	42	0.9 – 1.0	30
[67] T	NH_3-H_2O	50 – 130	-5 – 5	25 – 40	0.6 – 0.8	na
[104] T	DMAC-R32 DMAC-R124 DMAC-R134a	70 – 140	-5 – 15	20 – 34	0.4 – 1.2	na
[68] T	LiBr-H_2O	120 – 150	5	40	0.8 – 1.2	na

[69] T	NH_3-H_2O	62	-5	31	-	858 ($CC+P_{el}$)
[144] T	NH_3-H_2O	65 – 120	-15 – 15	20 – 40	0.4 – 0.85	na

1.4.7 Combined ejector-adsorption refrigeration system (EAdRS)

The adsorption process differs from the absorption process in that absorption is a volumetric phenomenon, whereas adsorption is a surface phenomenon [4]. The primary component of an adsorption system is a solid porous surface with a large surface area and a large adsorptive capacity. Initially, this surface remains unsaturated. When a vapour molecule contacts the surface, an interaction occurs and the molecules are adsorbed on to the surface. The molecules do not perform any chemical reaction, but they discard energy when attached to the surface: the phase change (from fluid to adsorbate) is exothermic and the process is fully reversible [1, 4]. In an adsorption cycle there are the adsorption process and the desorption process. Because the refrigeration is intermittent, a system with two beds out of phase is necessary to realize the continuity. However, if solar energy is used as thermal source, other measures, i.e. cooling storage, must be taken.

The novel combined cycle of a solar-powered adsorption–ejection refrigeration system provided by Li et al. (2002) [70] may overcome the intermittence of adsorption refrigeration. During the daytime, the adsorber is in the desorption process and simultaneously the ejector is in refrigeration; at night, adsorption refrigeration begins with heat recovery to heat water for the next day's ejection cycle. Using zeolite 13X-water, it was demonstrated that the *COP* of the ejector sub-system improved when the temperature of the adsorbent increased or when the pressure decreased. It was further concluded that by increasing the temperature or reducing the pressure within the adsorbent bed, the *COP*s of the ejection sub-system could be improved slightly, but if much more adsorbent is used, a better result might be obtained.

To improve the *COP* and cooling capacity effectively, and to overcome the intermittence of such refrigeration systems, Zhang et al. (2002) [71] presented a theoretical analysis of a solar-driven continuous combined solid adsorption-ejector refrigeration and heating hybrid system. This system is working on the same principle as the previous system but in this case, when the temperature in the adsorber is high enough, the adsorber is used as a thermal collector for heating up tap water. However, compared with an adsorption system without an ejector, the combined system's COP was improved by 10% totally and reached 0.33. A prototype of the combined adsorption–ejector refrigeration and heating hybrid system was being designed and the authors are confident that much more detailed performance information of the combined system could be acquired from the prototype.

Table 1-10: State of art of EAdRS operating conditions and performance. (T) Theoretical study, (E) Experimental study.

Ref.	Working Fluid	Generator temperature [°C]	Evaporator temperature [°C]	Condenser temperature [°C]	*COP* [-]	*CC* [MJ/kg]
[70] T	13X-H_2O	120	10	40	0.4	na
[71] T	13X-H_2O	150 – 200	5	30	0.33	0.3

1.4.8 Combined compression-ejector refrigeration system

According to the function performed by the ejector, there are two kinds of combined compression-ejector refrigeration systems. In the first one, the ejector still has the aim of raising the pressure level of the working fluid in the refrigeration cycle. In the second one, a two-phase ejector is used as an expansion device in order to enhance performance of a vapour compression refrigeration system. In the following will be presented these two sub-categories in their own section: (i) vapour compression-ejector refrigeration system (CERS) and (ii) ejector expansion refrigeration system (EERS).

However, a brief explanation is required in order to clarify some aspects concerning the approach followed in this paragraph.

With regard to the vapour compression-ejector refrigeration system, in the 1990 Sokolov and Hershgal (1990) [89] first proposed the CERS in various plant configurations. What was more successful was a combined ejector-compressor refrigeration cycle, which consists in a standard ejector refrigeration system and a vapour compression refrigeration system in cascade. Later, several authors suggested some changes (that will be illustrated next) in order to improve the system performance.

The second sub-category is made up of the ejector expansion refrigeration system. In this plant configuration, in which the ejector has assumed a new role, the compressor is a key component of the system and it cannot be replaced. Therefore, the EERS will be presented inside this section.

1.4.8.1 Vapour compression-ejector refrigeration system (CERS)

The *COP* of a CERS is still defined as the ratio between the cooling effect and the total incoming energy in the cycle, which in this case also includes the electric work consumed by the compressor or the booster. Neglecting the power consumption of the pump, it becomes:

$$COP = \frac{\dot{Q}_e}{\dot{Q}_g + \dot{L}_c} \tag{1.12}$$

However, in the CERS, for which the heat supply to the generator is available at very little or no charge, this conventional definition of *COP* does not necessarily reflect the real economics [89]. Under these circumstances, COP_{mec} has a more direct economic implication defined by:

$$COP_{mec} = \frac{\dot{Q}_e}{\dot{L}_c} \tag{1.13}$$

The result is that on one side, the ERS opens its application range and increases its efficiency; on the other hand, the mechanical compression refrigeration system reduces its electrical energy requirements.

Sokolov and Hershgal (1990) [89] suggested two basically different way in order to improve *COP* of ejector refrigeration system. All proposed improved *COP* cycles are based on the fact that the ejector performance is highly dependent on the secondary flow pressure and, if all other cycle parameters remain unchanged, an increase in secondary flow pressure will cause an increase in either condenser pressure or entrainment ratio.

The first configuration proposed is the booster assisted ejector cycle. It is very similar to the conventional ERS, but a pressure booster compresses the secondary flow before entering in the ejector (as Dorantes et al. [124]). The *COP* is improved (*COP* = 0.767, more than double the *COP*

of the SERS) but in view of the sensitivity of the ejector's operation to its inlet conditions, matching the booster and ejector in series may cause control problems.

The second configuration proposed is a combined ejector-compressor refrigeration cycle. The bottoming cycle is a conventional ERS or a booster ERS, while the topping cycle is a vapour compression cycle moved by a compressor. The heat (and eventually the mass) was transferred between the two cycles in an inter-cooler, which replaces the evaporator of the ejector cycle (it can be seen as the evaporator of the ERS and as the condenser of the mechanical compression system). This arrangement can reduce fluctuation in working conditions and assure smooth running conditions of the system. Moreover, if a single refrigerant is used, the intercooler may combine both heat and mass transfer and thus provide inter-balancing effects of the thermodynamic state in each of the cycles. Otherwise, the intercooler is only a heat exchanger, but it allows the use of two different refrigerants a time, selecting the most convenient thermo-physical refrigerant properties for each subsystem.

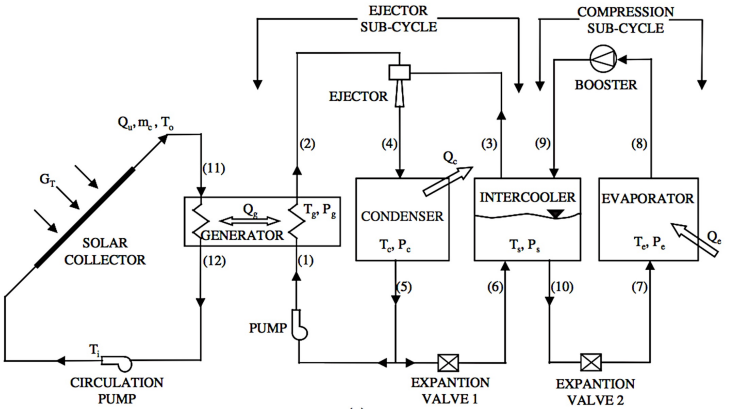

Figure 1-24: Vapour compression-ejector refrigeration system proposed by Arbel and Sokolov (2004) – taken from [125].

Three years later, Sokolov and Hershgal (1993) [90] developed a single-refrigerant compression enhanced refrigeration system, in which the inter-cooler allows both the heat and mass transfer. They demonstrated that this system could work with solar energy, but in order to enhance the system availability, storage is recommended. In particular, the authors suggested the employment of a cold storage tank, because the hot storage would be a wasteful method, due to the low thermal efficiency of the system.

Sun (1997) [72] proposed a solar-driven combined CERS for air-conditioning and refrigeration purpose. H_2O is used as the refrigerant in the ejector sub-cycle and R134a in the vapour compression sub-cycle. The study showed that the combined cycle is a potentially high performance system with an increase in system *COP* by more than 50% over the conventional cycles and the electrical energy requirements were reduced to half.

Sun (1998) [73] evaluated a combined CERS for refrigeration and air-conditioning. It could operate with a single refrigerant or dual refrigerants and in order to identify suitable dual refrigerants, water (R718), CFCs (R11, R12, R113), HCFCs (R21, R123, R142b), HFCs (R134a, R152a), organic compound RC318, and azeotrope R500 are chosen as refrigerants in the combined system. The simulation results showed that the combined cycle has a significant increase in system performance and its *COP* values (*COP* = 0.8) are competitive to the single-effect absorption systems (*COP* = 0.6÷0.8 [11, 185]). If the system is powered by waste heat and the cost of its

supply can be neglected, the *COP* values will be much higher. The system performance can be further improved if dual refrigerants are used: it was identified that the optimum pair of the dual refrigerants is R718 for the ejector cycle and R21 for the vapour compression one. The use of recovery heat exchangers was evaluated, concluding that the superheating of the fluid to the jet compressor reduces ω as a consequence of the specific volume decreasing reducing the overall performance.

A combined CERS moved by waste heat and with a pre-cooler in the bottom cycle was built and tested by Huang et al. (2001) [119]. The working fluids used are R22 in the topping cycle and R141b in the ejector cycle. The COP can be improved by 24% but further improvement in *COP* is possible since the prototype was not designed and operated at an optimal condition.

In order to replace the prohibited R114 widely used in the past, Arbel and Sokolov (2004) [125] presented a theoretical study on the same system proposed by [90], but using R142b as working fluid. The result of the analysis and simulation introduces not only an environmentally compatible but also a more efficient system. According to the authors, a combined CERS, in which solar space-heating, air-conditioning, and hot water are produced, with moderate condensing temperatures, could be a very feasible and economical system.

Hernandez et al. (2004) [126] tested R142b and R134a on the same systems in which the operating temperatures were selected considering ice production application, driven by solar energy: working with R134a had the best performance at a moderate condenser temperature of 30°C, while if higher condenser temperature are imposed R142b can give best performance.

Vidal and Colle (2010) [120] carried out an hourly simulation and a thermo-economical optimization of a solar CERS with a thermal storage tank. They chose R141b and R134a as working fluid for ejector cycle and compressor cycle respectively. The final optimized system for a 10.5 kW cooling capacity consists of 105 m^2 of flat plate collector and an inter-cooler temperature of 19°C resulting in a solar fraction of the system equal to 82% and a *COP* of the combined ejector cycle equal to 0.89. The authors discussed the importance of the proper selection of system components to obtain adequate payback periods and suggested the use of hybrid systems instead of conventional ERS.

Worall et al. (2010) [149] designed a hybrid jet-pump CO_2 compression system for transport refrigeration. The hybrid system has been simulated and its performance determined for different operating conditions and optimized using entropy generation minimization. The jet-pump circuit working fluid is methanol and it was proposed to extract heat from the discharge gases and vehicle exhaust and subcool the CO_2 transcritical sub-system. Sub-cooling increased the refrigeration effect, reduced the gas cooler outlet temperature below the critical point, and so improved heat transfer. The refrigerated transport presents an opportunity to exploit the exhaust gases from an independent diesel engine. The temperature of the exhaust gases from these engines range between 300°C and 500°C and the heat available can vary depending on the cooling capacity and hence the engine power output.

Petrenko et al. (2011) [135] proposed an innovative micro-trigeneration system composed of a cogeneration system and a cascade refrigeration cycle. The cogeneration system is a combined heat and power system for electricity generation and heat production. The cascade refrigeration cycle is the combination of a CO_2 mechanical compression refrigerating machine, powered by generated electricity, and an ejector cooling machine, driven by waste heat and using refrigerant R600. The

cooling system was developed for a capacity of 10 kW and reached a total *COP* = 1.4 when operating under design conditions.

Fixed evaporation, condensation and boiling temperatures, Mansour et al. (2014) [105] compered a conventional vapour-compression refrigeration system, a boosted assisted ERS and a combined CERS. The nominal conditions of the analysis were set for 5 kW cooling capacity. The boosted ERS and the cascade CERS show very interesting performance features: the compression ratio decreased substantially, so that compressor work is decreased nearly by 24% and 35% respectively. Consequently, the coefficient of performance for this system is improved by 21% and 40% over the reference for the same capacity (value shown in the following table).

Zhu and Jiang (2012) [86] proposed a hybrid vapour compression refrigeration system which combined with an ejector cooling cycle. The ejector cooling cycle was driven by waste heat from the condenser in the vapour compression refrigeration cycle. The additional cooling capacity from the ejector cycle in directly input to the evaporator of the main cycle. Simulation results showed that *COP* increased by 5.5% with R152a and 8.8% with R22 compared with the basic system. As with the basic vapour compression refrigeration system, the *COP* of the hybrid system increases with the evaporating temperature and decreases with the condensing temperature.

However, the cascade cycle may turn out to be easier to control since the ejector and compressor loops are physically separate. Another advantage is the possibility to use two different refrigerants, which provide more flexibility for performance and operational improvements.

Table 1-11: State of art of CERS operating conditions and performance. (T) Theoretical study, (E) Experimental study.

Ref.	Working Fluid	Generator temperature [°C]	Evaporator temperature [°C]	Condenser temperature [°C]	*COP* [-]	COP_{mec} [-]	*CC* [kW]
[89] E	R114	86	-8	30	0.77	8.1	2.9
[90] T	R114	76	4	50	0.85	5	3.5
[72] T	H_2O-R134a	120 – 140	5 – 10	35 – 45	0.3 – 0.4	5 – 7	5
[73] T	R11 R142b R12 R134a R21 R152a R113 R123 RC318 H_2O R500	70 – 100	5	35 – 45	0.5 – 0.8	-	na
[119] E	R141b-R22	68	-5 – 5	35 – 40	0.5 – 0.8	1.9 – 2.6	3.9
[125] T	R142b	100	4	50	1.52	5	3.5
[126] T	R142b R134a	85	-10	20 – 40	0.2 – 0.5 0.3 – 0.6	-	1
[120] T	R141b-R134a	80	8	32 – 34	0.8 – 0.9	-	10.5
[149] T	CH_3OH-R744	90 – 140	-15	35	0.8 – 1.3	1.3 – 3	3

[135] T	R600-R744	80 – 140	-20	28 – 40	0.4 – 0.9	2.5	10
[105] T	R134a	90	0	40	-	4.49 5.21	5
[86] T	R134a	90	-8 – 8	45 – 55	0.6 – 0.7	2.2 – 2.4	7
	R152a						7
	R22						12

1.4.8.2 Ejector expansion refrigeration system (EERS)

Using an ejector as expansion device is another alternative way of improving vapour compression refrigeration cycle performance. Typical vapour compression refrigeration cycle uses expansion valve and other throttling devices to reduce refrigerant pressure from condenser to evaporator. The pressure drop is considered isenthalpic process and causes a decrease in the evaporator cooling capacity because of energy loss in the throttling process [26, 186]. Use of ejector as an expansion device by replacing the throttling valve seems to be one of the efficient ways to reduce expansion irreversibility in the refrigeration cycle. Ejector also reduces the compression work by raising the suction pressure to a level higher than that in the evaporator leading to the improvement of *COP*. With the standard cycle, both expansion valve losses and compressor superheat losses have important effects on cycle *COP*. With the ejector expansion cycle, expansion valve losses are reduced. Thus, potential refrigerants which are unacceptable due to large expansion valve losses in a standard vapour-compression cycle, may be much more attractive when used in an ejector expansion cycle [186]. Because the phase of the working fluid in the diffuser is a two-phase, an ejector as an expansion device is usually named as two-phase ejector.

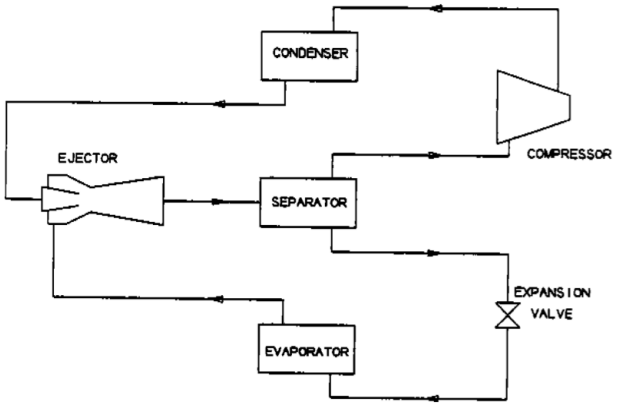

Figure 1-25: Vapour compression refrigeration system with two-phase ejector proposed by Kornhauser (1990) – taken from [83].

The idea of two-phase ejector as an expansion device dating back to 1931, when Gay (1931) [187] patented two-phase ejector to minimize throttling losses by replacing conventional expansion valve with ejector. However, Kornhauser (1990) [83] first analysed the ejector expansion refrigeration cycle. The principal modifications from the standard refrigeration system are the addition of a two-phase ejector and a liquid–vapour separator. In order to compare the performance of the ejector expansion refrigeration cycle with the standard vapour-compression cycle, simulations of the two cycles were carried out for the same evaporator temperatures, condenser temperatures, compressor

efficiencies, and heat loads. The improvement in *COP* with the ejector expansion system varies from refrigerant to refrigerant because the sources of loss in the standard vapour-compression cycle vary (+12÷30%). For some refrigerants, such as R717 (*COP* = 5.33), a large part of the loss is due to heat transfer from the superheated vapour: the potential increase in *COP* by reducing the loss in the expansion process is limited. For others refrigerants, such as R502 (*COP* = 5.67), there are little discharge superheat and almost all the loss is in the expansion process. For these refrigerants, the potential increase in *COP* with the ejector expansion cycle is much greater and in fact, R502 had the highest *COP* improvement than any other refrigerant. It was also found that the *COP* improvement decreases when the evaporator temperature increases. In other words, an increment in the *COP* is higher in freezers compared to the air conditioners.

Four years later, Kornhauser and Menegay (1994) [188] received a patent on how to increase velocity of flow at the motive nozzle in order to improve performance of the system. When the liquid refrigerant flows through the motive nozzle, part of it will change to vapour. Since the density of the vapour is much lower than the liquid, so the volume of the gas will reduce the amount of liquid in the nozzle. This condition causes a decrease in flow rate of refrigerant in the motive nozzle. The vapour entering the motive nozzle is in form of large bubbles, thus a breaker bubbles device is installed before converging–diverging nozzle in order to breaks up them into smaller bubbles.

Nakagawa and Takeuchi (1998) [189] showed that the longer the length of the divergent part of the motive nozzle, the higher the motive nozzle efficiency could be achieved leading performance improvement. This was likely caused because the longer divergent part provided a longer period of time for the two-phase flow to achieve equilibrium. With the increase in primary nozzle throat diameter, the recirculation ratio was found to be increased and both cooling capacity and *COP* were found to be increased whereas effect on compressor pressure ratio was found to be negligible.

Disawas and Wongwises (2004) [112] carried out the experiment to investigate the effect of heat source and heat sink temperature on the performance of refrigeration cycle using ejector as an expansion device. The experiment used a constant-pressure mixing chamber and convergent–divergent motive nozzle, with nozzle throat diameter of 0.9 mm. On testing with R134a, they found that the motive mass flow rate in the ejector was strongly dependent on the heat sink temperature and independent of the heat source temperature. This is due to the fact that choked flow occurs at the motive nozzle, and the upstream condition has a significant effect on the mass flow rate. The cooling capacity and *COP* increase with the rise of the heat source temperature due to increase in entrainment ratio, and decrease with increase in heat sink temperature due to decrease in entrainment ratio.

The performance improvement by using ejector as an expansion device is strongly dependent on nature of working fluids also. Nehdi et al. (2007) [113] compared several synthetic refrigerants and best performance of 22% *COP* improvement was obtained with R141b. They showed that for the different operating temperatures there are different optimum values of pressure drop in the suction chamber, ejector area ratio, ejector outlet pressure and corresponding maximum *COP*. As the difference between condenser and evaporator temperatures increases, the optimum ejector area ratio drops. Also the study showed that for a given evaporator temperature, the COP of the standard cycle decreases much more than that of the improved cycle, when the condenser temperature increases, and conversely.

Sarkar (2010) [133] compared three natural refrigerants and showed maximum performance improvement by using ejector can be achieved in case of R600a, whereas minimum performance

improvement can be achieved for ammonia. Further the values of optimum area ratio and corresponding entrainment ratio and pressure lift ratio are also dependent on refrigerant used. By using both constant pressure and constant area mixing ejectors, he also showed that optimum area ratio increases with increase in evaporator temperature and decrease in condenser temperature, whereas the *COP* improvement over basic expansion cycle increases with the increase in condenser temperature and decrease in evaporator temperature.

The performance of the refrigeration cycle using a two-phase ejector as an expansion device was experimentally investigated by Chaiwongsa and Wongwises (2007-2008) [110, 114]. Refrigerant R-134a is used as working fluid and motive nozzles having three different outlet diameters are tested. Variables affecting performance and varying directly with the heat sink temperature include the primary mass flow rate, secondary mass flow rate, recirculation ratio, compressor pressure ratio, and discharge temperature. On the other hand, the cooling capacity varies inversely with the heat sink temperature while the average evaporator pressure varies only a little and tends to vary directly. The primary mass flow rate and the secondary mass flow rate tend to be slightly increased as the heat source temperature increases. The use of motive nozzles having different outlet diameters in the range of 2.0–3.0 mm yields insignificant effects on the system performance. However, although the ejector cycle has higher performance over the standard cycle, some disadvantage should be considered, i.e. high refrigerant charge, high refrigerant flow, piping insulation and installation cost.

Bilir and Ersoy (2009-2010) [111, 190] performed a computational analysis, similar to that of Kornhauser [83], on the performance improvement of ejector expansion cycle over standard cycle. Using R134a refrigerant, the *COP* improvement of the expansion cycle over standard cycle is 10.1–22.34%. They also found that the *COP* improvement increases when the condenser temperature increases. This means that the use of ejector instead of an expansion valve is more advantageous in the air-cooled condensers than that of water-cooled condensers. Moreover, they have done the second law analysis on the system. They found that the exergy destruction of each component of the system is always lower than that of standard cycle: there is reduction in exergy destruction by 58.7%. They also found that the optimum ejector area ratio increases with decrease in ejector component efficiencies.

The study presented by Dokandari et al. (2014) [145], thermodynamically evaluated the ejector utilization's impact on the performance of the cascade cycle that uses CO_2 and NH_3 as refrigerants. The theoretical analysis on the functional features based on the first and second laws of the thermodynamics illustrated the facts that the maximum *COP* and the maximum second law efficiency are on average 7% and 5% higher than the conventional cycle. However, the exergy destruction rates roughly 8% lower as compared to the conventional cycle. Therefore, the novel ejector-expansion cascade cycle is a promising refrigeration cycle from the thermodynamically and practical points of view. The authors acknowledge that further investigations about the novel ejector-expansion CO_2/NH_3 cascade cycle are needed to verify experimentally these results.

Table 1-12: State of art of EERS operating conditions and performance. (T) Theoretical study, (E) Experimental study.

Ref.	Working Fluid	Evaporator temperature [°C]	Condenser temperature [°C]	COP_{mec} [-]	CC [kW]
[83] T	R11 R12 R22 R113 R114 R500 R502 R717	-15	30	5.3 – 5.7	na
[112] E	R134a	8 – 16	27 – 37	4.5 – 6	3
[113] T	R134a R141b R142b R404A	-15	30	4 – 4.7	na
[133] T	R290 R600a R717	-15 – -5	35 – 55	6.1 – 6.2	na
[114] E	R134a	8 – 16	27 – 37	2.5 – 6	3
[110] E	R134a	8 – 16	27 – 37	3 – 6	3
[111] T	R134a	-25 – 5	35 – 50	3 – 5.5	na
[145] T	R744-R717	-55 – -45	30 – 40	2.5 – 6.5	na

1.4.9 Multi-components ejector refrigeration system (MERS)

In order to maintain the highest possible performance at varying the working conditions (i.e. lower generator temperature), it is possible to introduce multi-components ejectors. The main muti-components ERS analysed over the years by researchers are:

[i] ERS with an additional jet pump;

[ii] Multi-stage ERS;

[iii] Multi-evaporator ERS.

ERS with an additional jet pump. Yu et al. (2006) [106] propose the addition to a second ejector in series to the main one: the jet-pump (liquid jet ejector) receives the mixing flow of the first ejector as secondary flow and the liquid condensate as primary flow. As a result, the backpressure of the ejector can be reduced by the jet-pump, increasing ω (ω = 0.6 maximum value) and *COP* (*COP* = 0.3). Simulation results showed that, compared with conventional ERS at same working conditions, the *COP* could increase by 57.1% and 45.9%, with R152a and R134a respectively.

Yu and Li (2007) [121] suggested another system with similar configuration: a regenerative ejector refrigeration cycle with an additional jet pump, used to produce preheating for the working flow. In fact, the exhaust flow of the ejector is divided in two parts: one is discharged at the condenser pressure; the other one at higher pressure is redirected to the jet pump and thus this part with higher temperature was rejected as heat for refrigeration. The cycle with R141b gets an advantage over the conventional cycle and shows its promise in using low-grade thermal energy for the ejector refrigeration system.

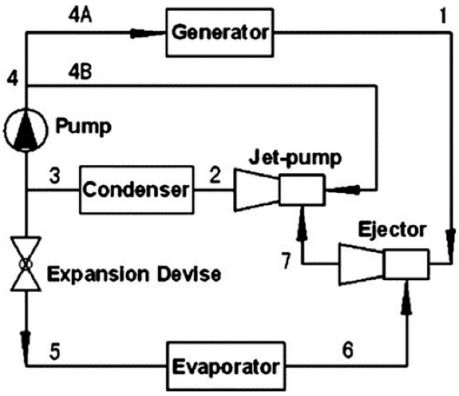

Figure 1-26: Bi-ejector refrigeration system proposed by Yu et al. (2006) – taken from [106].

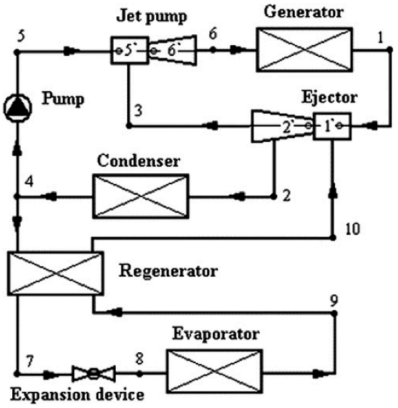

Figure 1-27: Bi-ejector refrigeration system with regenerator proposed by Yu and Li (2007) – taken from [121].

The same group has proposed some other solution, like [127], a mechanical sub-cooling ejector refrigeration cycle with R142b, and also in this case *COP* improves: the study concluded that the performance may be improved up to 10% with respect to another simple jet compression refrigeration cycles. However, a significant increase of performance occurs, but the possible technical difficulties due to the control of the system are not mentioned [36].

Multi-stage ERS. Multi-stage ejector refrigeration systems are another kind of multi-components ERS, in which some ejectors are place in parallels before the condenser. Sokolov and Hershgal (1990) [89] propounded this arrangement: each ejector works in a different operative range of condenser pressure.

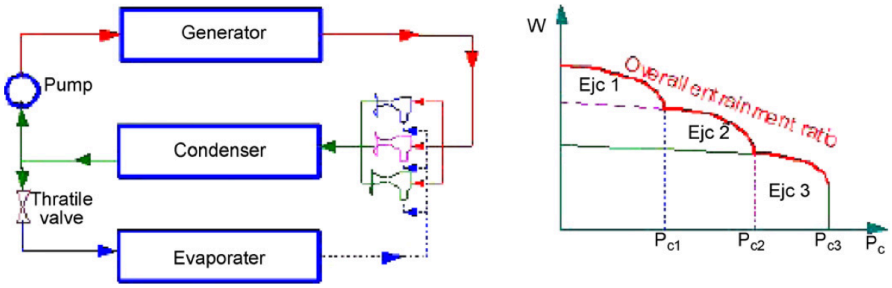

Figure 1-28: Multi-stage ejector refrigeration system proposed by Sokolov and Hershgal (1990) – taken from [89].

Multi-stage ejectors try to solve the main problem afflicting ERS, namely the difficulty to keep the system running at optimum conditions due to the variation of working conditions. This is especially true for the solar-driven ejectors, highly dependent upon environmental factors such as solar radiation. However, practical works are not available for refrigeration field.

Multi-evaporator ERS. More studied are the multi-evaporator compression systems. Elakdhar et al. (2007) [96] proposed a theoretical analysis of a compression/ejector hybrid cycle for domestic refrigeration. In this cycle, an ejector is employed to reduce the loss of available energy due to the large temperature difference between the fresh food section and the freezer section. Substantially the system employs ejector for vapour pre-compression. According to the results of simulation of the cycle using several refrigerants (R123, R124, R134a, R141b, R290, R152a, R717 and R600a), the ejection cycle can reach a higher coefficient of performance compared with the standard

vapour-compression cycle, an improvement of 32%. R141b gives the best performances. Note that the system makes use of a compressor: it needs less mechanical work but does not eliminate the compressor and then electricity consumptions are not negligible.

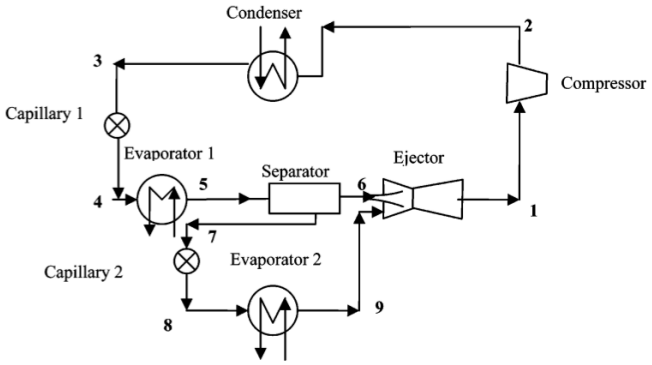

Figure 1-29: Multi-evaporator ejector refrigeration system proposed by Elakdhar et al. (2007) – taken from [96].

Kairouani et al. (2009) [109] suggested a similar solution with three evaporators and two ejectors. Also in this case, the ejectors are positioned at the outlets of the evaporators, which can increase the suction pressure. Consequently, the compressor specific work decreases and the *COP* of the system is improved. As previously, R141b proved to give the most advantageous *COP* among all tested working fluids.

A similar study was presented by Li et al. (2012-2014) [191, 192] who analyzed experimentally and numerically a multi-evaporator refrigeration system.

Liu et al. (2010) [139] presented three different connection methods in the hybrid two-evaporator refrigeration cycle: (i) the series hybrid circulatory system, (ii) the parallel hybrid circulatory system and (iii) the hybrid circulatory cross-regenerative thermal system. For the first two systems, the power consumption reduction compared to a system without ejector is negligible. With the third method, power consumption can be reduced to 0.655 kWh/day by using the heat loss in the system and ensuring that the refrigerant entering the refrigeration ejector maintains its gaseous state. This level of power consumption is lower than the original prototype by 7.75%, representing a great energy-saving effect.

Another kind of refrigeration plant is the autocascade refrigeration system that can use only one compressor to obtain lower refrigerating temperature between -40°C and -20°C. In order to reduce the throttling loss generated by throttling devices, an ejector is introduced to the system to recover the kinetic energy in the expansion process. Practically, the ejector is used to recover some available work to increase the compressor suction pressure. Yu et al. (2008) [107] applied an ejector in autocascade refrigerator with refrigerant mixture of R23/R134a. The ejector is set between the evaporative, condenser and the evaporator. Thermodynamic analysis showed that the system employed with an ejector had merits in decreasing the pressure ratio of the compressor as well as increasing *COP* that was improved by 19.1% over the conventional autocascade refrigeration cycle.

All the different MERS solutions ensure a performance improvement. However, it is necessary to carefully evaluate the impact on complication of equipment and its management.

Table 1-13: State of art of MERS operating conditions and performance. (T) Theoretical study, (E) Experimental study.

Ref.	Working Fluid	Generator temperature [°C]	Evaporator temperature [°C]	Condenser temperature [°C]	*COP* [-]	*CC* [kW]
[106] T	R134a R152a	80 – 100 80 – 98	5	35	0,20 – 0,30	1
[121] T	R141b	80 – 160	10	35 – 45	0,20 – 0,40	1
[127] T	R142b	80 – 120	5	35	0,30	1
[96] T	R123 R124 R141b R134a R152a R290 R600a R717	-5 – 10	-40 – -20	28 – 44	1,20 – 2,20	0,5+0,5
[139] E	R600a	4 – 20	-23	54	1,48 – 2,16	na
[107] T	mix R23/R134a	0 – 25	-35 – -20	40	0,6 – 0,9	na

1.4.10 Transcritical ejector refrigeration system (TERS)

Different from other ejector refrigeration systems which working in subcritical region, the transcritical ejectors involve refrigerant working over the critical conditions. TERS have a higher potential in making use of low-grade thermal energy [35]. The Figure 1-30 shows TERS scheme and cycle process, proposed by Yu et al. (2010) [193]:

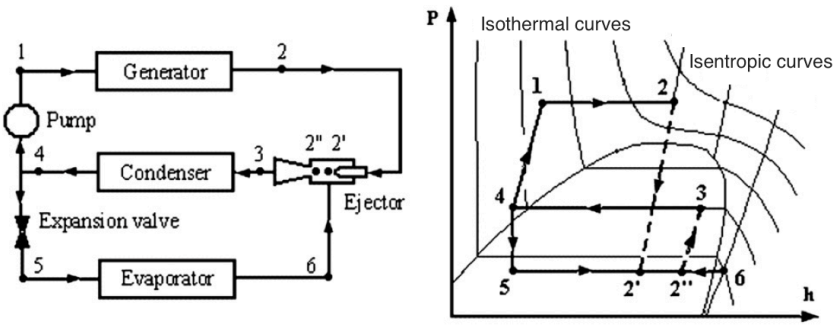

Figure 1-30: Transcritical ejector refrigeration system – taken from [193].

In the generation process (*1→2*) at supercritical pressure, the heat from low-grade heat source is transferred isobarically to the primary working fluid, undergoes a continuously decrease in density, from a liquid-like dense-gas state to a vapour state. This supercritical vapour (*2*) expands through the ejector nozzle and entrains the vaporized fluid from the evaporator (*6*).

It should be note that the operation of the transcritical process introduces the need to control the high-side pressure in order to obtain the required performance. In the transcritical cycle, the temperature at heat addition is no longer given by the high pressure. Therefore, pump discharge pressure (p_1) and generator outlet temperature (T_2) should be considered as operation parameters (are not linked with each other). In addition, the ejector may involve two-phase flows at the nozzle exit and in the diffuser, depending on the high-side pressure and the generation temperature.

Yu et al. (2010) [193] compared the above cycle with a subcritical one under the same operating conditions, using R143a as working fluid. The first one showed considerable advantages, in fact it presented a maximum *COP* of 0.75, while the subcritical one has a *COP* equal to 0.45. The problem in these cases is the high pressure to be handled, having to be carefully designed and operated. However, the higher working pressure resulted in a more compact system.

The most common TERS, however, are the ejector expansion refrigeration system and they mostly used the carbon dioxide (R744) as working fluid.

Liu et al. (2002) [194] first analysed the transcritical refrigeration cycle with CO_2. They performed a thermodynamic analysis of the transcritical hybrid vapour compression-ejection refrigeration cycle, based on the idea proposed by Kornhauser (1990) [83]. Compared to a traditional vapour-compression cycle, in this configuration an ejector is used instead of a throttling valve to recover some of the kinetic energy of the expansion process. Through the action of the ejector, the compressor suction pressure is higher than it would be in a standard cycle, resulting in less compression work and improved system efficiency.

However, their layout creates some difficulties to control the operating conditions of a real system, due to the close link among the entrainment ratio and the quality of the ejector outlet stream [186]. To relax this constraint, a new CO_2 TERS was proposed by Li and Groll (2005) [150]:

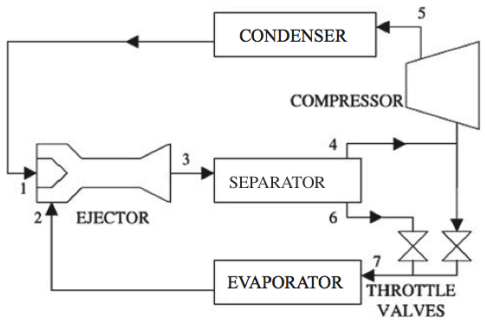

Figure 1-31: Transcritical ejector expansion refrigeration system proposed by Li and Groll (2005) – taken from [150].

Part of the vapour in the separator is feed back to the evaporator inlet through a throttle valve, which regulates the quality at the evaporator inlet. The results demonstrate that, for given conditions, the ejector expansion cycle could improve the *COP* by more than 18% compared with the basic transcritical cycle.

Deng et al. (2007) [151] presented an energy and exergy analysis of a transcritical CO_2 ejector expansion refrigeration cycle, which uses an ejector as the main expansion device instead of an expansion valve. They found that the improvement of *COP* achieved 22% over standard cycle. The exergy analysis showed that the sum of the throttling and ejector losses of the TERS is lower than that of standard vapour compression cycle and there is also a reduction in exergy loss in the compressor. The results indicated that the ejector entrainment ratio influenced significantly the refrigeration effect.

An experimental investigation on a similar refrigeration system was carried out by Elbel and Hrnjak (2008) [195]. The results were compared to that of a conventional system with an expansion valve. For the test conditions considered, the cooling capacity and COP simultaneously improved by up to 8% and 7%, respectively. Experiments were analysed to quantitatively estimate

the effects of changes in basic ejector dimensions on system performance. Ejector performed with a higher efficiency when the high-side pressure was relatively low, but it was also found that, despite lower ejector efficiencies, the *COP* increased as the high-side pressure increased, as a result of using the integrated needle to reduce the motive nozzle throat area in the ejector.

Yari and Sirousazar (2008) [152] presented a theoretical analysis on transcritical CO_2 refrigeration cycle with an internal heat exchanger and an intercooler to improve the performance significantly. It was found that the *COP* and the second law efficiency of the new cycle increased respectively by about 55.5% and 26% compared to conventional ejector-expansion TERS.

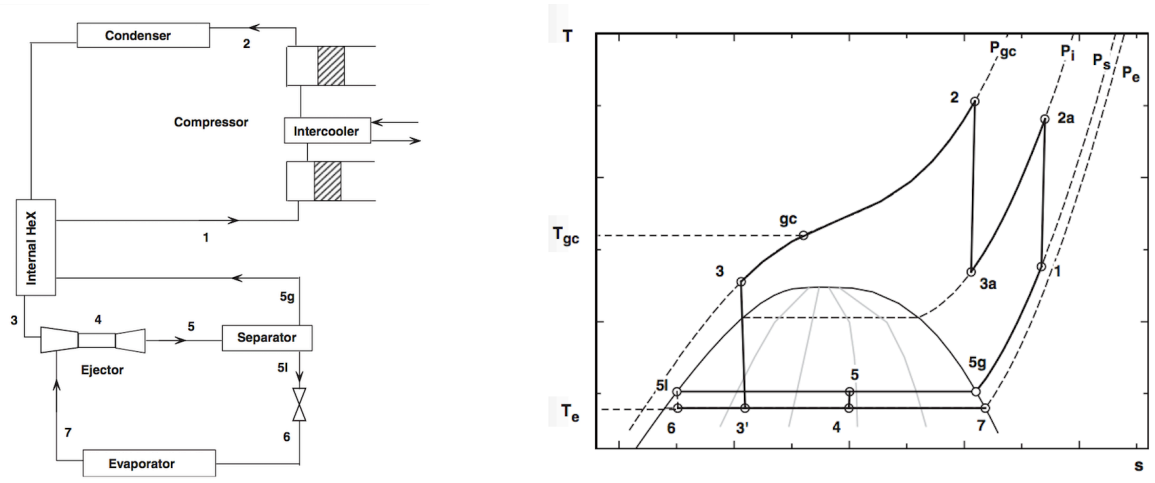

Figure 1-32: Trancritical ejector expansion refrigeration system proposed by Yari and Sirousazar (2008) – taken from [152].

Yari (2009) [153] continued the analysis and, performing a regression analysis on the data, determined correlations to predict estimates of the optimum design parameters (optimum discharge pressure, maximum *COP*, optimum inter-stage pressure and optimum entrainment ratio) valid for the ranges of evaporator temperature from -30 to 0°C and the gas cooler outlet temperature from 35 to 55°C. These correlations offer useful guidelines for optimal system design and for selecting appropriate operating conditions.

Fangtian and Yitai (2011) [156] presented a comparative study on transcritical carbon dioxide refrigeration cycle with ejector and with throttling valve by the first and second laws of thermodynamics. It was found that ejector instead of throttling valve can reduce more 25% exergy loss and increase *COP* more 30%. In addition, critical entrainment ratio of the ejector, optimal heat rejection pressure and critical outlet temperature of gas cooler affects *COP* greatly for the transcritical carbon dioxide refrigerating cycle with ejector. Therefore, the transcritical carbon dioxide refrigerating cycle with ejector can be applied to a place with a stable condition.

In transcritical ejector system, the mixing of high-speed two-phase primary flow and suction vapour is crucial in designing an efficient ejector. In the study conducted by Nakagawa et al. (2011) [154], the effect of mixing length on ejector system performance was analysed experimentally. The experiments were performed for both ejector and conventional expansion systems with and without internal heat exchanger at different operating conditions. Based on the experimental results, mixing length had significant effect on entrainment ratio and on magnitude and profile of pressure recovery. The 15 mm types yielded the highest ejector efficiency and *COP* in all of the conditions used in this research. However, a much longer mixing length would have minor change in pressure recovery but it yields significant penalty in entrainment ratio. Moreover,

the use of internal heat exchanger had net positive effect on system performance. A *COP* improvement of up to 26% over conventional system was obtained but improper sizing of mixing length lowered the *COP* by as much as 10%.

Behaviour of refrigeration system with ejector at different operating parameters is investigated by Ahammed et al. (2014) [155]. Parametric variation exhibited that at lower heat sink temperatures, performance is slightly better towards low gas cooler pressure, but cooling capacity significantly decreases; whereas at higher ambient temperature high gas cooler pressure leads to notable improvement in performance. Moreover, it is inferred that motive inlet is the deciding factor of performance and applicability. Additionally, a comprehensive exergy analysis was implemented to identify component level deficiencies and it establishes the justification of replacement of throttle valve by an ejector as an expansion device in a CO_2 based transcritical vapour compression refrigeration system: the resulting second law efficiencies obtained are 6.6% and 7.52% for conventional and systems with ejector, respectively, under the given conditions.

Table 1-14: State of art of TERS performance and operating conditions. (T) Theoretical study, (E) Experimental study.

Ref.	Working Fluid	Primary flow conditions [°C] / [MPa]	Secondary flow temperature [°C]	Outlet mixing flow temperature [°C]	COP [-]	CC [kW]
[193] T	R143a	60 – 100 6 – 10	10	30 – 40	0.3 – 0.75	1
[150] T	R744	36 – 48 8 – 12	5	15	+ 7 – 18%	na
[151] T	R744	36 – 40 8 – 12	0 – 10	4 – 20	1.5 – 3.5	na
[152] T	R744	40 – 50 8 – 12	-20 – 10	13	1 – 4	na
[153] T	R744	35 – 55 7.5 – 12	-30 – 0	-	1 – 3.5	na
[156] T	R744	40 – 45 8 – 9	-5 – 17	-	2.5 – 2.9	na
[154] E	R744	41 – 44 9 – 10.5	2 – 8	-	1 – 2	1 – 2.5
[155] T	R744	30 – 45 8 – 12	0 – 10	35	2 – 3.6	3.5

1.5 Ejector refrigeration market

In the previous paragraphs we have provide data, information and explanations about the ejector refrigeration systems and their energy, economic and environmental advantages. We have also talked about their critical aspects and the ways in which the authors have tried to overcome or mitigate them. In this section we want to give some brief evidence concerning the ERS market potential and the main world manufacturers of ejectors.

In the field of thermal energy refrigeration, the main competitors of the traditional vapour compression refrigeration system are the absorption and the ejector refrigeration system. However, these two systems have different characteristics also in terms of market potential. The absorption refrigerators (both single-effect and multiple-effect) are generally a good solution for the direct conversion of low-grade heat into cold with a *COP* in the range of 0.6÷1.0. However, they are rather expensive and marketed only in the multi-kilowatt power range. The smaller units, when available for niche applications, are rather inefficient [3]. Even if the ERS may have a lower *COP*, they could compete with absorption coolers (both systems being characterized by an almost static operation) because they have a wide range of system capacity and a much lower potential costs [3].

As already pointed out, the ejector is applied in many sectors as aeronautic, maritime, energy and process industry (i.e. chemical, petrochemical, food and drugs...).

The ejector systems are employed in the aircraft industry as cabin ventilators and for purposes of jet thrust augmentation (for further information, please refer to [196, 197]).

Concerning the maritime field, the ejector can be used for many different purposes, wherever there is a need for reliable and efficient pumping from ships. For example, it can be used to discharge the water from the anchor wells or as bilge pumps. The Maritime Diesel Electric, Inc. (Florida, U.S.A.) is currently a big distributor of equipment and supplies for the maritime and industrial market [198]. Their ejectors supplier is Ellehammer, a Danish company that is one of the world leading producers of ejectors for maritime applications: there are more than 75000 Ellehammer ejectors in service in the marine sector all over the world [199].

The process industry field employs ejectors in many applications very different each other. For example, the chemical industry uses routinely steam ejectors for vacuum production or several applications are reported in which ejectors were used for cold generation [3]. The SAMHWA Mixing Tech. Co. is a South Korean manufacturing company that supplies various items, including the ejectors, to more countries all over the world (mainly in China, India and U.S.A). Their products include the air ejectors and the steam jet liquid ejectors. For example, the air ejector is offered to their costumers for prevent cavitation in a water sealed vacuum pump, installing it in suction line of the pump and using atmospheric air as motive fluid. The steam ejector is, instead, applicable for transporting, discharging or heating liquid with high-speed steam as primary fluid. However, many other solutions are offered to their costumers. Among the most recent projects there is the “SFC ECH/CA Expansion Project”, which consists in design, manufacturing and testing static mixers and ejectors for the Samsung Fine Chemicals Co. [200].

The GD NASH company has been designing, manufacturing and troubleshooting steam jet ejector systems since 1986, mainly for chemical, electrical power, oil&gas and other process industries. For example, they suggest to their clients to remove corrosive gas from the condenser of a geothermal plant by means of an ejector. The use of a steam ejector in the distillation process in refineries is another interesting proposal. This application involves applying a vacuum to a crude oil distillation column and its purpose is to enhance the recovery of the lighter components, such as

gasoline. The vacuum distillation is more energy efficient than atmospheric distillation. The Nash Division of Gardner Denver has manufacturing facilities in China, Germany and Brazil and Engineered To Order (ETO) centers in the main world countries [201].

The Körting Hannover AG is specialized in the production of ejectors. The German company can count on around 340 employees and its sales volume exceed 65 M€, mainly due to the exports. The Körting ejectors are multi-purpose and can be used in many different application fields. They provide different process industries, like power plants, petrol refineries, fertilizer production, water treatment and many others. Recently, in collaboration with Chinese Engineering Company, Körting planned, constructed and put into operation a new steam jet chilling plant for the Sichuan Refinery of their customer, the largest Chinese oil concern, PetroChina. The evaporation tower and the downstream condenser in connection with the steam jet ejectors form the core of the plant. The cold water generated by this plant is urgently required in the newly constructed Sichuan Refinery to cool diverse petro-chemical processes. This new steam jet chilling plant with a cooling capacity of 24 MW, following a further Körting plant in Egypt (28 MW), is the second largest steam jet chilling plant in the world [202].

As regard the refrigeration field for air-conditioning and refrigerator purpose, there does not seem to be many companies that design the ERS plants. Nevertheless, an example is constituted by the Global DENSO, a leading supplier of advanced automotive technology, systems and components for all the world's major automakers. DENSO operates in more than 35 countries and regions and with approximately 140000 employees. In 2003, DENSO introduced the world's first refrigeration unit with an ejector cycle for mid and large-sized trucks. The proposed configuration is the EERS for car air conditioners, using the ejector instead of the conventional expansion valve. Compared to the expansion valve cycle with similar refrigeration capacity, the overall weight of the ejector cycle is reduced by 40% thanks to the remarkable minimization of the compressor, condenser and evaporator. The weight reduction also increases fuel efficiency by 60% [203].

The main barrier to uptake of the ERS market is the lack of performance data from commercial applications to provide confidence in the application of the technology. To increase the attractiveness and application of the ERS, research and development are required to extend the use of new refrigerants (i.e. hydrocarbons and carbon dioxide) and new plant configurations (i.e. EERS and TERS), increasing the efficiencies. This is encouraged by the fact that the benefits of the technology in applications where there is sufficient solar energy, waste heat or in tri-generation systems are successfully demonstrate [204].

1.6 Ejector Refrigeration Systems: summary

Ejector refrigeration system is a promising alternative to produce cooling effect due to its structural simplicity, low capital cost, little maintenance and long lifespan. It is able to be driven by solar energy, as for example in Ref. [87, 94, 100, 115, 134], with an interesting feature for air-conditioning applications since solar radiation is generally in phase with cooling demands in the buildings. It can also be used to recover the waste heat from industrial processes or other sources, like in Ref. [80, 86, 88, 119, 135], which helps to mitigate the problems related to CO_2 emission and to reduce the cost. Moreover, this system has an ability of using various refrigerants, particularly the environmentally-friendly refrigerants, making it even more attractive [50].

Studies in ejector refrigeration systems that have been carried out involved system modelling, design fundamentals, refrigerants selection and system optimization. The research and development was broad based and productive, concentrating on performance enhancement

methodology and feasibility of combining ERS with other systems. However, the ejector is the critical component of a jet refrigeration system and the understanding in ejector fluid dynamic theory has not been completely cleared [16].

ERS have the possibility of using a wide range of refrigerants [10] and this is a considerable advantage over the competitors, such as the absorption refrigeration systems. In particular, halocarbon and hydrocarbon compounds with low GWP and ODP were considered as new alternatives, and were widely studied and compared as working fluids in different ERS. Among these, R143a and R142b were proved to yield better performance than other working fluids. As the most environmentally friendly and economically available refrigerant, water has been widely used and tested as refrigerant for ERS [35].

The ability of making use of renewable energy and the other advantages make ERS more cost-effectively competitive compared with other refrigeration system. The system performance for ERS, however, is relatively low. Hence, the engineers and researchers are making effort to improve system efficiency for ERS. A number of studies have focused on system performance enhancement, including utilization of the special refrigerants, utilization and storage of available renewable energy, reduction of the mechanical pump work in ERS, multi-components ERS and other type of refrigeration systems (vapour compression, absorption system, etc.).

1.6.1 Summary of the different ejector refrigeration technologies

With the concept of energy conservation and environment protection, the utilization of low-grade energy, especially solar energy with ERS has been widely studied. It is demonstrated that the solar energy can be utilized and drive the system: according to the characteristic of an ejector and the initial investment cost, the solar jet refrigeration system is suitable for the application of air-conditioning system [16]. However, the major technical drawback of solar-driven ejector refrigeration system is that the system is strongly reliant on ambient conditions but the combination of energy storage partially solved the problem [35]. Thus, dynamic simulations are required for the dimensioning of the equipment in the system.

The use of combined systems (ejector-absorption, ejector-adsorption or ejector-compression) allows extending the jet compressor application range. Another competitive advantage is that the hybrid cycles make possible the use of one working fluid at a time for each subsystem increasing the improving cycle performance opportunity: it is in this configuration where an important improvement opportunity for these system exists, as the most adequate refrigerant thermo-physical properties for each subsystem can be selected. As for simple as well as for hybrid ERS, the most suitable application is air-conditioning because of the relatively higher evaporator temperatures required than for refrigeration applications [36].

The combined systems most powerful are the combined compression-ejector systems. From the economical point of view, these cycles require a high initial investment. Nevertheless, large-scale systems can result profitable because of the electrical energy consumption decrease, in which the cost presents a clear growth trend. In environmental terms, the energy diversification through combined cycles can help reduce the greenhouse effect gasses production by handling them with solar energy or waste heat from some thermal devices [36].

Numerical analysis and experiment results show that using ejector as an expansion device (EERS) to recover expansion work causes the improvement of COP on the vapour compression refrigeration cycle. The use of variable two-phase ejector will accelerate the implementation of this device to replace a conventional expansion device. However, to accomplish this, more intensive

study on the characteristics of two-phase ejector as an expansion device is still required. In fact, the majority of the available literature concerned with ejectors used in air-conditioning and refrigeration describes numerical simulations of vapour jet ejectors. A number of established ejector flow theories point out the importance of flow choking and shock wave phenomena. However, significantly less literature is available on the topic of two-phase ejectors.

Always with the aim of improving the ejector system's performance, the transcritical ERS have been proposed and it was shown that they could provide higher potential in utilizing low-grade heat. However, most of those studies are limited to numerical analysis, with few experimental results available [35]. In the particular case of TERS with R744, some numerical work on two-phase ejectors has been published in the open literature, but the availability of experimental R744 ejector data appears to be extremely limited. Moreover, even if many of the flow theories and design guidelines developed for single-phase ejectors should be transferable to two-phase ejectors, a number of significant differences exist. For example, the metastability effects caused by delayed flashing of the primary nozzle flow as well as supersonic two-phase flow are believed to add more complexity to the task of designing efficient two-phase ejectors [42]. At the time, almost all theoretical studies on ejector are based on one-dimensional homogeneous equilibrium model with fixed isentropic efficiencies of nozzle and diffuser. However, a more realistic analysis of vapour compression cycle with the two-phase ejector can be done by using multi-dimensional non-homogeneous flow, including the friction factor and shock calculations [186].

Regarding the numerical simulation of the ERS, as the limitations of analytical modelling were reached, CFD-based models attempted to provide clearer insight and increased accuracy with better turbulence models and more advanced meshes. A more detailed analysis of these and other aspects will be presented in the subsequent chapters.

In general terms, more large-scale works are needed in order to provide better understanding for the real industrial application of all the ejector refrigeration systems [35], especially for the most promising systems.

1.6.2 Ejector refrigeration systems: graphical presentation of data

In the previous paragraphs we have been examined the ERS literature studies published by many research groups. In this section we have grouped all the performance data, organized by technology, in order to provide summary charts able to put in evidence the remarkable COP improvements achieved over the years and thanks to the introduction of new system solutions and plant configurations.

The Figure 1-33 shows the historical evolution of *COP* for all the ejector technologies. A first evaluation of the graph confirms that the development of new technological solutions has resulted in an increase of the system performance. In fact, the growth of *COP* that is obtained with the combined systems, especially with the compression-ejector systems, is evident and not lower than that obtainable with the other refrigeration systems, such as absorption or vapour compression systems. However, the data are quite dispersed. Thus, in order to refine our analysis, we have divided the data into two graphs, gathering together the technologies with similar performance. As a result, in the Figure 1-34 there are the simpler layout systems, while the Figure 1-35 collects the hybrid systems and the more complex technologies. By means of the charts, it is now possible to note the progress, in terms of performance, that has taken place over the years for each technology. This evolution was made possible thanks to the great efforts of researchers to develop and improve the ejector refrigeration systems. Their work has contributed to raise the knowledge about the

ejector and their operation. In light of this, it is reasonable to expect for the future a further improvement of the ERS performance, as well as the development of new plant configurations.

A striking example of the above-mentioned is constituted by the ejector expansion refrigeration systems (Figure 1-35). The first EERS was proposed in 1990 and its coefficient of performance was equal to 5. The *COP* has continued to grow and fourteen years later it has reached the value of 6.5. Even the SERS (Figure 1-34) have had a similar growth, passing from a *COP* = 0.12 in the 1964 to a *COP* = 0.75 achieved in more recent years. Not to be outdone the SoERS (Figure 1-34): starting from a coefficient of performance equal to 0.34 obtained in the 1996, they have managed to stabilize around *COP* = 0.6, reaching the peak of *COP* = 1.5 in the 2011.

The Figure 1-36 reports the performance trend of all the ERS technologies with a value of *COP* less than 3, clarifying the relationship between *COP* and time in this operating range. The above considerations are still well founded, with the "value added" of having eliminate the out-of-range data, providing a great clarity.

However, the increasing trend of the coefficient of performance is not always so clear because in some cases the data are still scattered. This is because also other variables are involved in the ERS operation. As already mentioned, in fact, the generator temperature and the working fluid play a key role in the functioning of the system.

With regard to the influence of the generator temperature, the Figure 1-37 and the Figure 1-38 illustrate very well the correlation between *COP* and T_g. In particular, there are two interesting points to be highlighted. First, each technology has its own field of operation. The EERS and the TERS, in addition to being characterized by a high coefficient of performance, have the further advantage of being able to work with low T_g, less than 60°C. The SERS, SoERS and CERS operate with intermediate temperatures, around between 60°C and 140°C. The EAbRS requires, instead, high generator temperature, grater than 120°C. Secondly, the two graphs show that the coefficient of performance increases with the generator temperature for each technology. Many authors also find this general trend in their academic works (that we have presented in the previous paragraphs) through experimental or numerical analysis of their ERS. Instead, we have obtained the same result by means of a statistical study.

The effect of the working fluid is shown in Figure 1-39, Figure 1-40 and Figure 1-41. It reflects the directives of the various literature studies concerning this topic. In fact, the best halocarbon compound is the R134a (HFC compound) that is capable of providing excellent performance with all the kind of ERS technology and, in particular, with the EERS (the *COP* is around the value of 6). By using transcritical cycles, instead, the carbon dioxide can supply good performance (*COP* = 3÷6). Also the hydrocarbon compounds are versatile enough, but seems to give the best results when used in simple systems.

Even if the ammonia and the methanol have good properties as refrigerants, they do not adapt well with the best-performing systems (EERS and TERS above all).

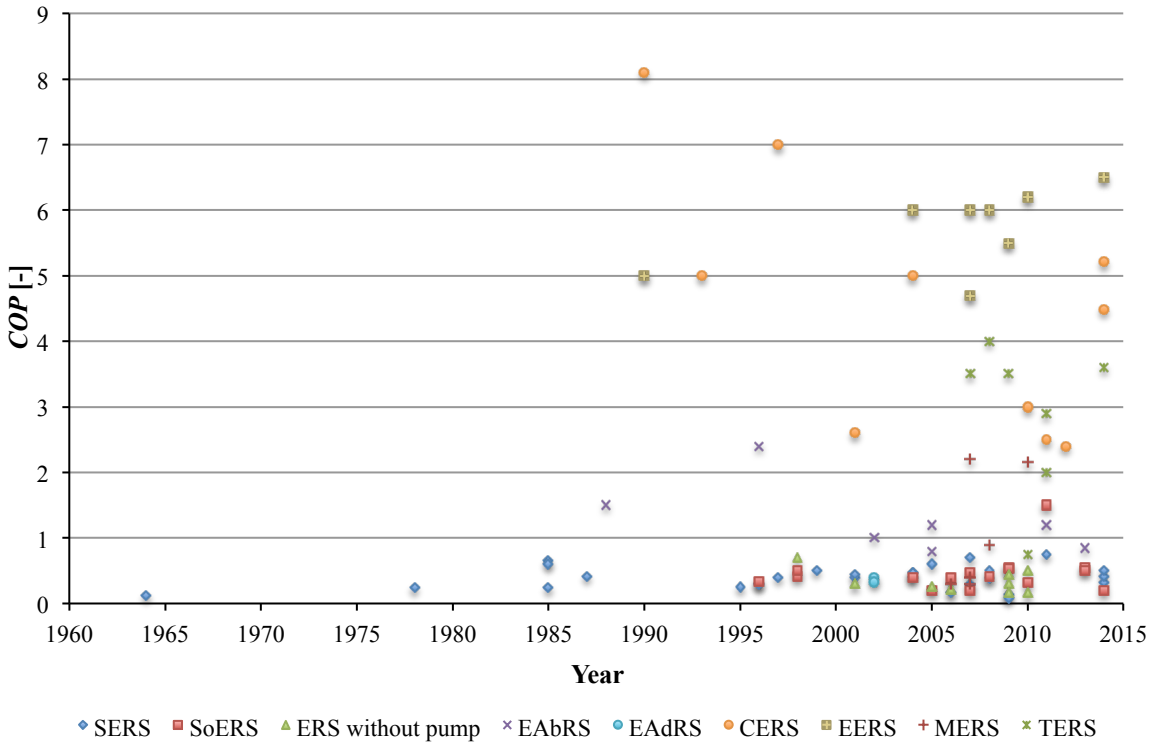

Figure 1-33: Performance trend of ERS technologies over the years.

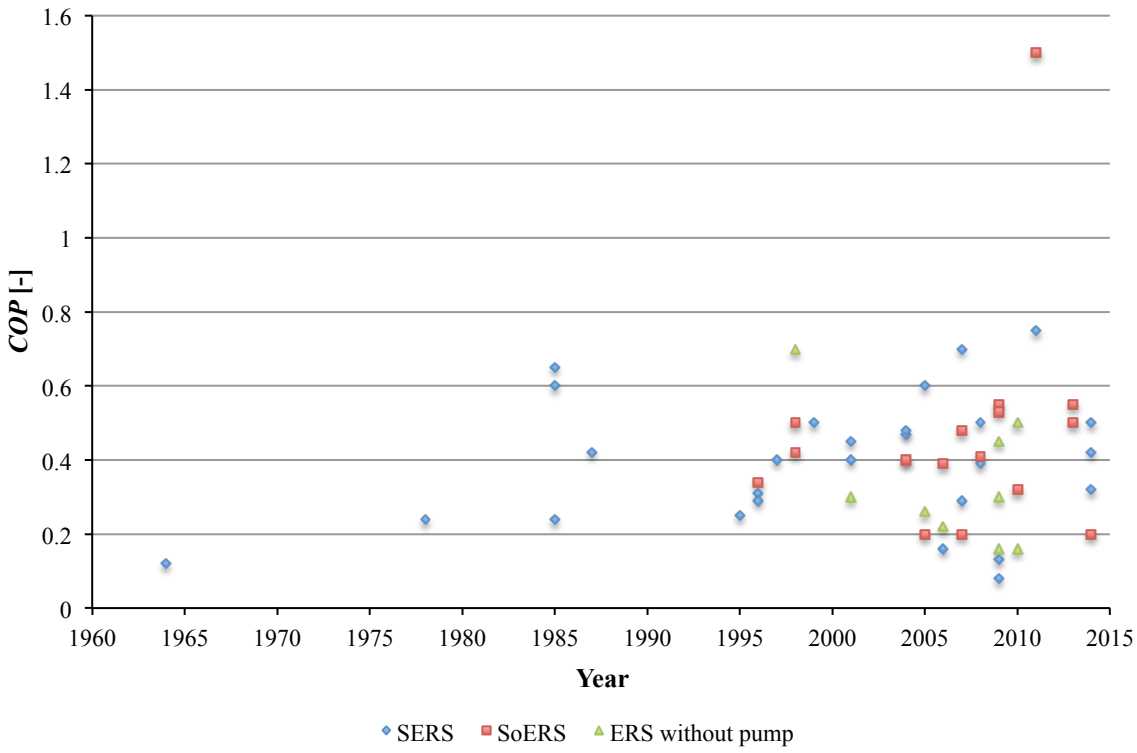

Figure 1-34: Performance trend of SERS, SoERS and ERS without pump over the years.

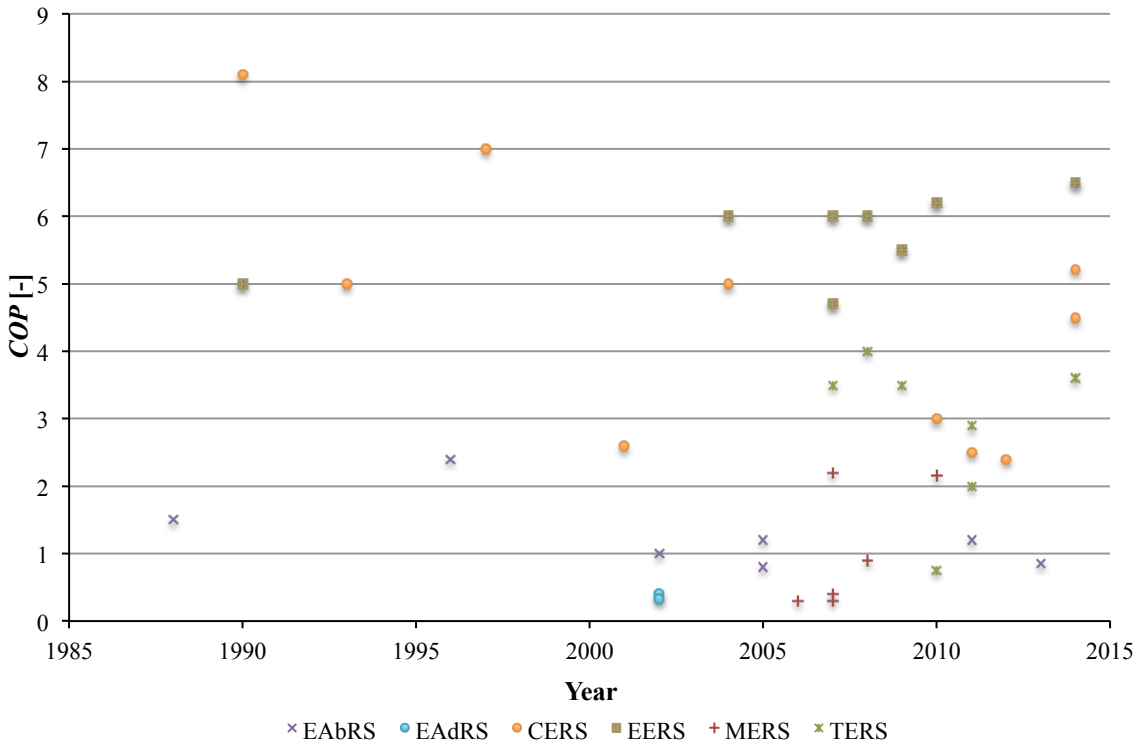

Figure 1-35: Performance trend of EAbRS, EAdRS, CERS, EERS, MERS and TERS over the years.

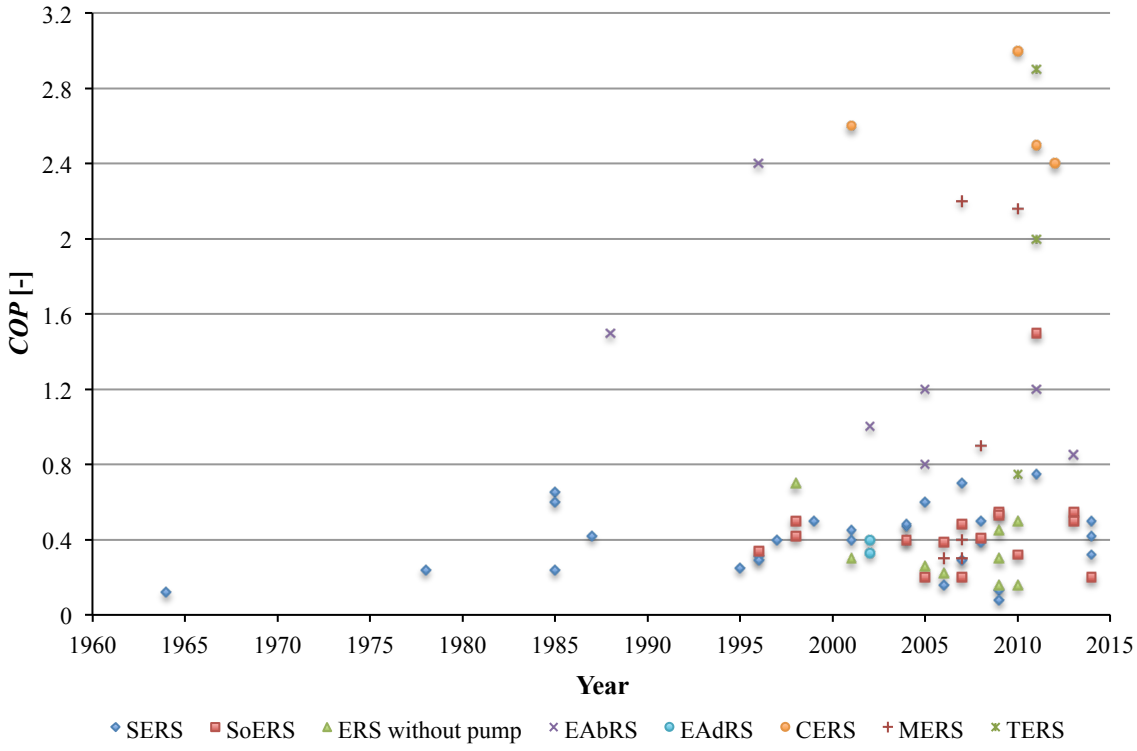

Figure 1-36: Performance trend of ERS technologies over the year with COP < 3.

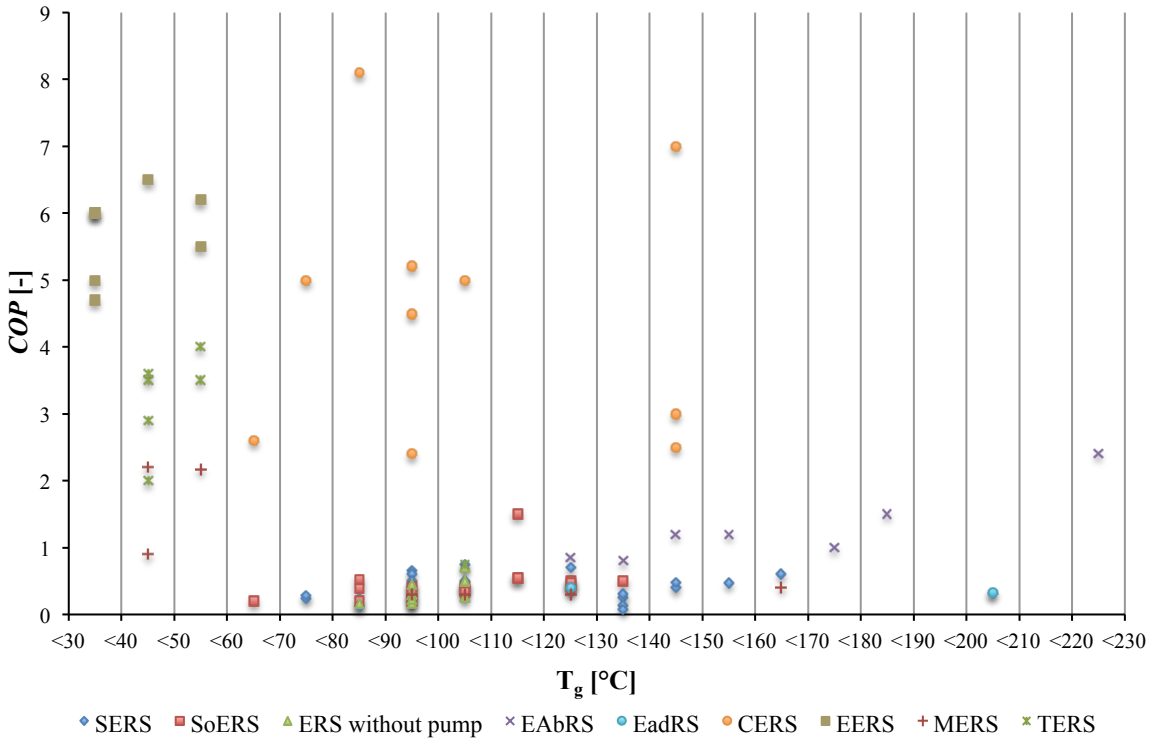

Figure 1-37: Performance trend of ERS technologies as a function of the generator temperature.

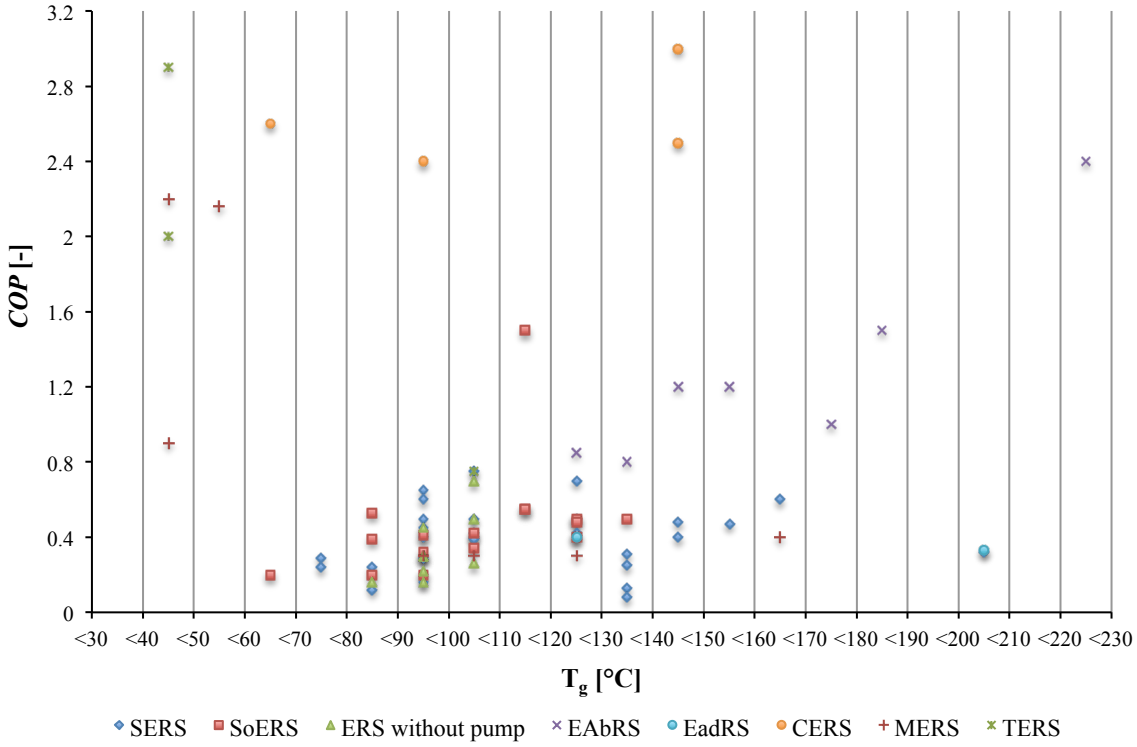

Figure 1-38: Performance trend of ERS technologies with COP < 3 as a function of the generator temperature.

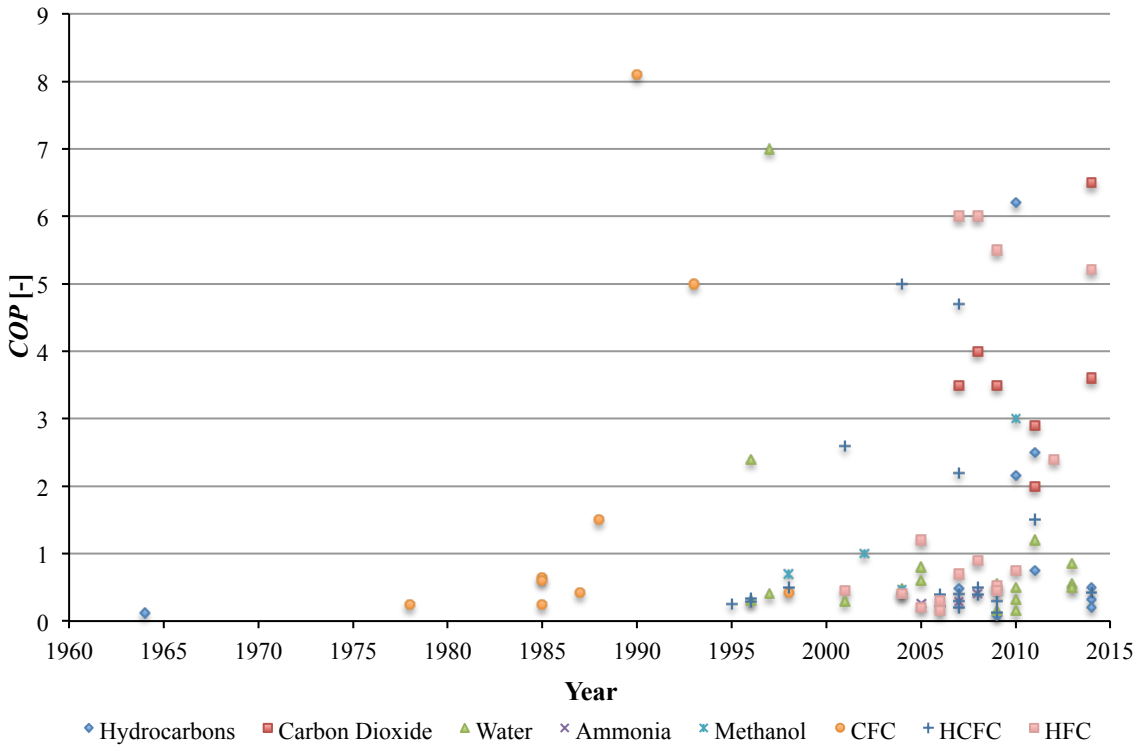

Figure 1-39: Performance trend of ERS organized by working fluid.

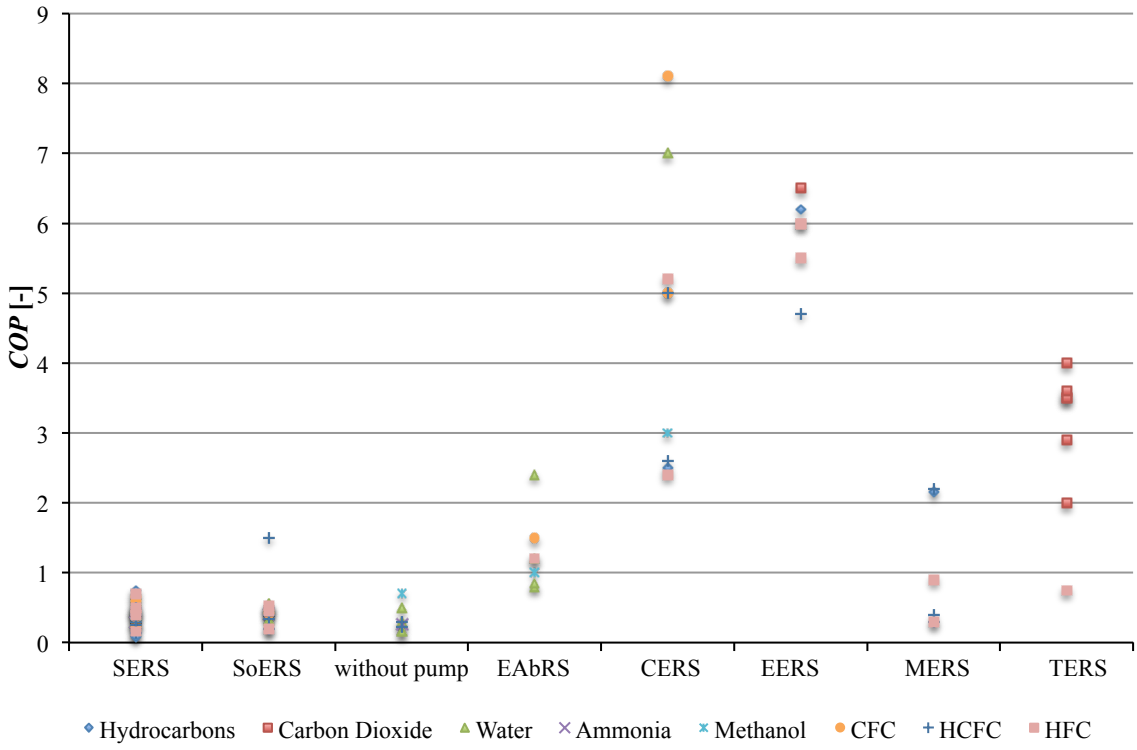

Figure 1-40: Performance trend of ERS technologies organized by working fluid.

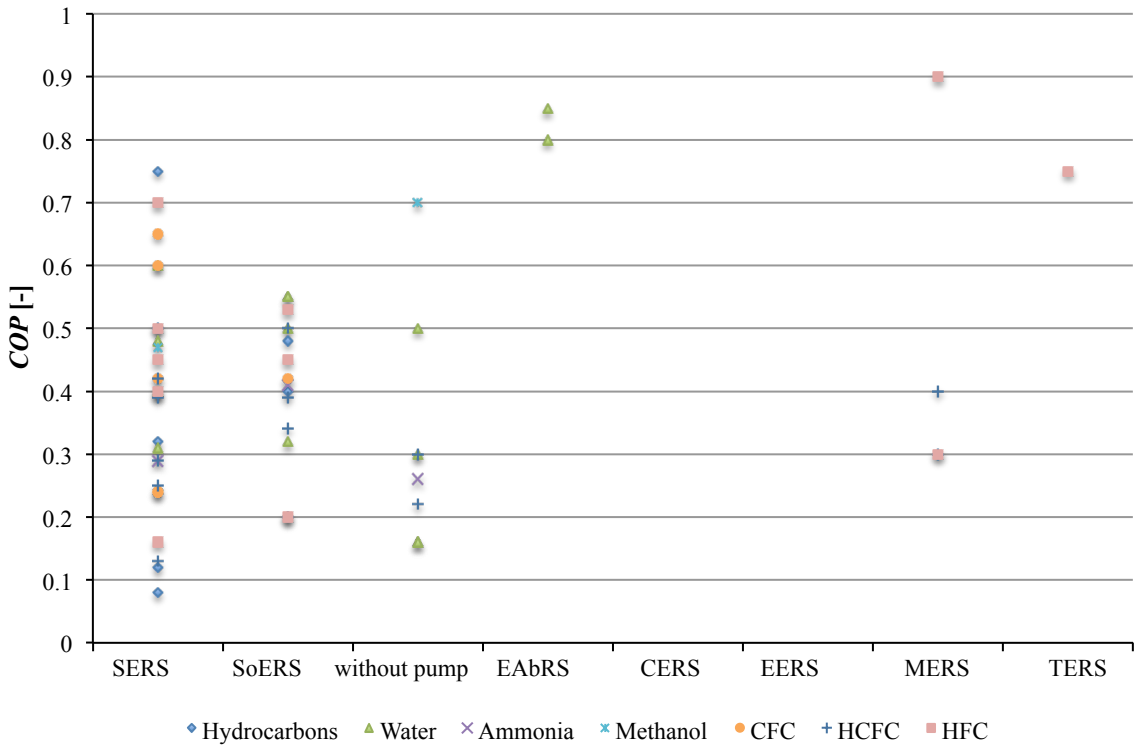

Figure 1-41: Performance trend of ERS technologies organized by working fluid with COP < 1.

Chapter 2

Ejector analysis and modelling

This chapter talks about the numerical modelling of the ejectors and their application in the ERS analysis. It is structured in three sections. After a brief introduction concerning the mathematical methods that allow the resolution of complex physical problems, in the first part a description of the lumped parameter models is given. The second part, instead, concerns the CFD models and their great usefulness in the ejectors modelling. In the third part the mainly mono-dimensional models provided by the literature and the CFD simulations carried out by some authors are reported: starting from the literature reviews presented in the theses of Besagni (2011-2012) [1] and Maddiotto (2012-2013) [2], we will proceed with these analyses, describing the academic works published in the last years.

2.1 Ejector modelling: introduction

The governing equations of fluid flow represent mathematical statements of the conservation laws of mass, momentum and energy [3]. These laws can be expressed by equations in integral (or global) form, applicable to an extended region, or in differential (or local) form, applicable at a point in the flow field. Both forms are equally valid and may be derived from each other [4].

Integral form. The integral forms of the equations of motion are stated in terms of the evolution of a control volume and the fluxes of mass M, momentum $\vec{\pi}$, and energy E that cross its control surface. Considering a generic control volume Ω, enclosed by the surface S, the conservation equations are [3, 5]:

- Mass conservation equation, for which the mass of a fluid is conserved on the control volume Ω.

$$\frac{dM}{dt} = 0 \qquad \Rightarrow \quad \frac{d}{dt}\int_{\Omega} \rho \, d\Omega + \int_{S} \rho \vec{V} \cdot \vec{n} \, dS = 0 \tag{2.1}$$

- Momentum conservation equation, for which the rate of change of momentum is equal to the sum of the forces $\vec{F}$ on the control volume Ω.

$$\frac{d\vec{\pi}}{dt} = \vec{F} \qquad \Rightarrow \quad \frac{d}{dt}\int_{\Omega} \rho \vec{V} \, d\Omega + \int_{S} \rho \vec{V} \left(\vec{V} \cdot \vec{n} \right) dS = \int_{\Omega} \vec{f} \, d\Omega + \int_{S} \vec{\sigma} \, dS \tag{2.2}$$

- Energy conservation equation, for which the rate of change of energy is equal to the sum of the rate of heat $\dot{Q}$ and the rate of work $\dot{W}$ done on the control volume Ω.

$$\frac{dE}{dt} = \dot{W} + \dot{Q} \quad \Rightarrow \quad \frac{d}{dt}\int_{\Omega} \rho e \, d\Omega + \int_{S} \rho h_t \left(\vec{V} \cdot \vec{n}\right) dS = \int_{S} -\vec{q} \cdot \vec{n} \, dS + \int_{S} \vec{\sigma} \cdot \vec{n} \, dS \tag{2.3}$$

Thus, the global conservation equations express the balance of the considered physical quantities in a finite control volume. They are typically useful when an average or integral flow property, such as a mass flux, a surface pressure force, or an overall velocity or acceleration, is sought [4].

Differential form. The differential forms of the equations of motion are stated in terms balance for a fluid element. Considering an infinitesimal control volume, the conservation equations of mass, momentum and energy are respectively [3, 5, 6]:

$$\frac{\partial \rho}{\partial t} + div\left(\rho \vec{V}\right) = 0 \tag{2.4}$$

$$\frac{\partial\left(\rho \vec{V}\right)}{\partial t} + div\left(\rho \vec{V}\vec{V}\right) = -grad\left(p\right) + div\left(\bar{\bar{\tau}}\right) + \vec{f} \tag{2.5}$$

$$\frac{\partial\left(\rho e\right)}{\partial t} + div\left(\rho h_t \vec{V}\right) = -div\left(\vec{q}\right) + div\left(\bar{\bar{\tau}}\vec{V}\right) \tag{2.6}$$

The differential forms of the equations are coupled nonlinear partial differential equations for the dependent flow-field variables of density, velocity, pressure, etc. Thus, they are often more appropriate for detailed analysis when field information is needed instead of average or integrated quantities [4].

According to [1, 7], the fundamental steps used to arrange mathematical models include:

[i] choose an approach to solve the physic problem. The main methods employ for ejector modelling are:

- Lumped Parameter Models (LPM) method;
- Computational Fluid Dynamics (CFD) method.

[ii] simplify the problem by making reasonable assumptions and hypothesis;

[iii] get the governing equations based on the mass, energy and momentum balances, simplifying or neglecting the terms that are not needed according to the assumptions made;

[iv] provide boundary conditions, initial conditions and auxiliary relations to close the governing equations.

Hence, the hydrodynamic and thermodynamic performance of the ejector can be formulated with complex mathematical feature as governing equations and auxiliary relations.

This is the main and universal method for constructing mathematical model, but it should not escape notice that there are also some simplified models for ease of computation such as semi-empirical model [8, 9]. The empirical/semi-empirical models consist on using large amounts of experimental results to derive correlations and implement them in a mathematical model. Its application is restricted in the specific range of experimental working conditions and it cannot be used in a large variety of situations [7].

The construction of mathematical models has been used as an effective method for analyzing the performance of the ejector and they can be used to predict system operation, interpret experimental results and assist in system design and optimization. There are many advantages of the LPM and

CFD methods. First, they are less onerous than experimental method in terms of time and cost for predicting the performance of an ejector. The second point is that the mathematical models can produce large volumes of results and this is very convenient to perform parametric research and optimization analysis. The third reason is that some parameters are difficult to be obtained by experimental measures. Moreover, a validated numerical model, tested on some systems, can be used to predict the ejector performance of many other installations, because of the fundamental physics of ejector used in various fields are similar [7].

2.1.1 Lumped parameter models

The most common way to evaluate the ejector performance is the use of lumped parameter models that, as we shall see, consist in one-dimensional fluid dynamics and thermodynamic models. This is the main method through which the ejectors have been modelled in the past and this is the simplest way and less time-consuming technique to predict ejector performance and general behaviour.

2.1.1.1 Assumptions

The straightforwardness of the LPM is mainly due to the assumptions that simplify the fluid-flow behaviour (chocking conditions, shock waves, mixing process) and allow to neglect some factors that do not influence the flow significantly. The typical analytical study makes many assumptions that are universal across authors, some of which are as follows [7, 10]:

[i] the flow is steady and one dimensional;

[ii] the inner walls of the ejector are adiabatic;

[iii] the primary fluid and secondary fluid are supplied to the ejector at stagnation pressure and zero velocity;

[iv] the velocity of the mixed flow leaving the ejector is negligible.

According to the assumptions (i)-(ii), the heat transfer between the ejector and the environment can be neglected. Thus, the steady one-dimensional equations for adiabatic process and the isentropic expressions can be used.

Other common assumptions can include either constant-pressure or constant-area mixing sections, normal shocks, start of mixing at the aerodynamic throat formed by the motive stream, use of isentropic efficiencies and loss coefficients for each subcomponent to account for various losses and nature of the working fluids (single-phase or two-phase, ideal gas or real gas).

Constant-pressure mixing model (CPM ejectors). It was assumed that the mixing of the primary and entrained flows occurs in the suctions chamber with a uniform pressure: $dp = 0$. This is achieved by placing a converging throat at the exit plane of the nozzle.

Constant-area mixing model (CAM ejectors). It was assumed that the mixing of the primary and secondary flows occurs inside the constant-area section: $dA = 0$. The exit plane of the nozzle is assumed to coincide with the constant area section of the mixing chamber.

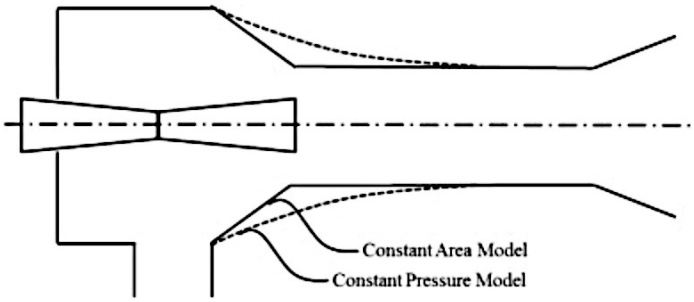

Figure 2-1: Comparison between CPM and CAM model – taken from [11].

Normal shocks. A normal compression shock is induced and it was assumed that it remains fixed in the constant area section (inside or at the end of the constant area), contributing to a compression effect and a sudden drop in velocity from supersonic to subsonic. However, experimental and CFD observations [12-14] have confirmed that a series of oblique shockwaves (shock train) rather than a normal shock were formed in the mixing chamber, but the assumption of normal shocks in the LPM has been widely validated in many studies [15-17].

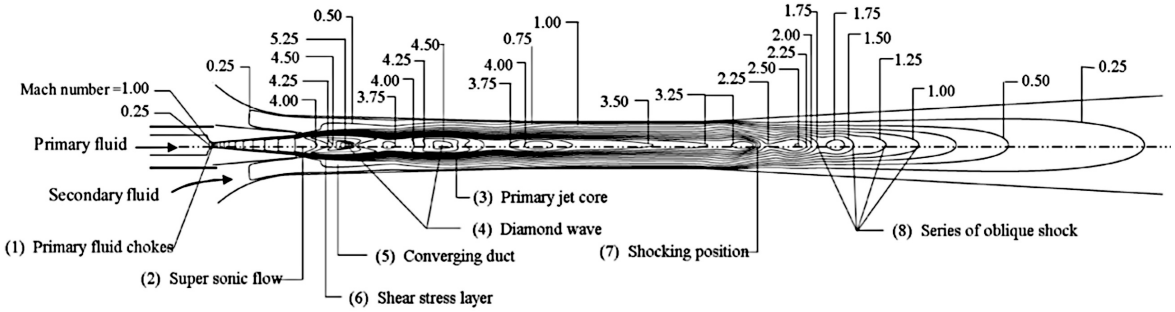

Figure 2-2: Contours lines of Mach number in a steam ejector – taken from [18].

Aerodynamic throat. In the first proposed models, like Keenan et al. (1950) [19], it was assumed that the mixing process between the primary and secondary flow begins at the entrance of the mixing chamber. However, after some experimental studies [20], it was observed that this hypothesis does not correspond to the real physical behaviour of the ejectors and in the 1977 Munday and Bagster (1977) [21] introduced the concept of the so called "Aerodynamic throat". The "Aerodynamic throat" concept assumes that the primary flow accelerates and expands through the nozzle, fans out forming oblique shocks, forming a converging duct for the induced flow. Therefore, the mixing cannot take place directly at the entrance of the mixing chamber, but only in a downstream section (section y-y in the Figure 2-3).

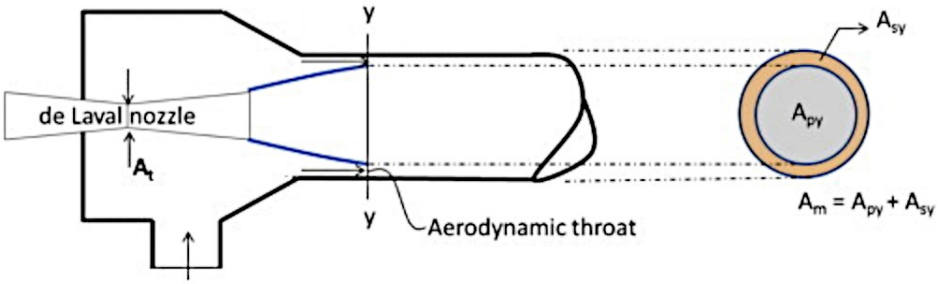

Figure 2-3: Aerodynamic throat in the mixing chamber of the ejector – modified from [11].

Ejector operational modes. Most of the developed lumped parameter models focus on the prediction of the maximum entrainment ratio at critical mode operation [11, 22-24]. However, during transient or off-design conditions, sub-critical mode operation can occur. Some models have as purpose the evaluation of the ejector performance also in these conditions [25].

Isentropic efficiencies and loss coefficients. As already remarked, the LPM employs isentropic expressions to modelling the ejector's behaviour. In order to take into account the flow losses, isentropic efficiencies and loss coefficients are used. Indeed, due to the great complexity of the flow behaviour, the losses have been aggregated into empirical coefficients [10]. Their values are assumed constants and in accordance with the literature information (usually in the range of 0.65÷1.0 [26, 27]). However, these coefficients highly influence the validity of the ejector models and depend on the working fluid, the operating conditions and the geometry [28, 29]. Therefore, these values can be much lower at certain conditions, such as demonstrated by experimental and CFD studies [26].

Working fluid: single-phase or two-phase. In order to simplify the analysis, most of the models assume that the inlet fluids are superheated and no phase change occurring inside the ejector. These models are developed based on single-phase flow. However, the experimental results indicate that phase transition can occur inside the ejector in several situations (please refer to Section 1.2.2.3). In these conditions, the two-phase flow models are needed [7].

Working fluid: ideal gas or real gas. The low pressures that occur inside the ejector enable some fluids (as water vapour) to exhibit ideal gas properties. Therefore, over the years, the mathematical models of the ejectors have been based on the ideal gas assumption. To mitigate the errors introduced by the ideal gas assumption, some researchers [16, 30] applied the properties of the real gas model. However, some studies [31, 32] concluded that the results produced by the real gas model are similar to those predicted by the ideal gas model [11].

2.1.1.2 Governing equations

Starting from the global conservation equations (Eqns. 2.1, 2.2, 2.3) and applying the hypotheses of steady, one-dimensional and adiabatic flow, we arrive at the following equations [7]:

$$\sum \rho_i u_i A_i = \sum \rho_e u_e A_e \tag{2.7}$$

$$p_i A_i + \sum m_i u_i = p_e A_e + \sum m_e u_e \tag{2.8}$$

$$\sum m_i \left(h_i + \frac{u_i^2}{2} \right) = \sum m_e \left(h_e + \frac{u_e^2}{2} \right) \tag{2.9}$$

Under ideal conditions, the governing equations express the mass, momentum and energy balance in the nozzle, mixing chamber and diffuser sections.

2.1.1.3 Boundary conditions

The boundary conditions are a set of additional restraints that describe the behaviour at the edges of the simulated region. The thermodynamic models usually fix the pressure values at the inlets and outlet of the ejector [11, 22, 23, 25, 33]. In some literature studies [34], also the mass flow rates or the velocities of the primary and secondary fluids have been used as boundary conditions [7].

2.1.1.4 Initial conditions

In order to initialize the simulation and start up the iterative cycles, the thermodynamic models need initial conditions, such as the entrainment ratio [23, 35] or the expansion ratio [34].

2.1.1.5 Auxiliary equations

In the lumped parameter models, the isentropic relations and some gas dynamic equations are used to assist in the description of the relationship among the physical quantities, such as the temperature, pressure, density and Mach number and/or velocity [5]:

$$\frac{p_T}{p} = \left(\frac{T_T}{T}\right)^{\frac{\gamma}{\gamma-1}} = \left(1 + \frac{\gamma-1}{2} M^2\right)^{\frac{\gamma}{\gamma-1}} \tag{2.10}$$

$$\frac{\rho_T}{\rho} = \left(\frac{T_T}{T}\right)^{\frac{1}{\gamma-1}} = \left(1 + \frac{\gamma-1}{2} M^2\right)^{\frac{1}{\gamma-1}} \tag{2.11}$$

$$\frac{S^*}{S} = \frac{M}{\sqrt{\left[\frac{2}{\gamma+1}\left(1 + \frac{\gamma-1}{2} M^2\right)\right]^{\frac{\gamma+1}{\gamma-1}}}} \tag{2.12}$$

Moreover, the state equation $h = h(p,\rho)$, the definition of the Mach number and the definition of the sonic velocity can be used to solve the problem.

The one-dimensional steady-state equations, with the help of the auxiliary equations, reduce the complexity of the problem and they are used to obtain state and parameters along the ejector in a simple and time-saving way. However, these models cannot obtain some detailed information, such as shock interactions or turbulent mixing of two streams. The dissipations are implemented by the use of the frictional and mixing coefficients.

2.1.2 Computational Fluid Dynamics models

Despite the usefulness and the remarkable progress provided by the thermodynamic models, this kind of models was unable to correctly reproduce the local flow phenomena along the ejector. It is the understanding of the local interactions between shock waves and boundary layers, and their influence on ejector behaviour, that will allow a more reliable and accurate design, in terms of geometry, refrigerant type and operating conditions in order to improve the ejector performance [7, 36]. Using the CFD modelling approach, it is possible to achieve a better understanding of the fluid dynamics of the ejector and reach more accurate results at a reasonable cost. With the development of computer science and mathematical method, the researchers have focused on this method with attempt to obtain more accurate information in the ejector [7].

2.1.2.1 Assumptions

One of the main purposes of the CFD approach is to reduce the number of assumptions that were previously needed in the analytical models [10]. In fact, the hypotheses on which they are based are [7]:

[i] the flow is steady;

[ii] the inner walls of the ejector are adiabatic;

[iii] the primary fluid and secondary fluid are supplied to the ejector at stagnation pressure and zero velocity;

[iv] the velocity of the mixed flow leaving the ejector is negligible.

Thus, the one-dimensional assumption is not necessary. The CFD models are usually created in a 2D domain and, thanks to the axisymmetric solver, the 3D effect was taken into account in the simulations [12]. Moreover, no hypotheses about the shock waves, the mixing process or other fluid dynamics phenomena are required.

Working fluid: single-phase or two-phase. Also the CFD models can be classified in two categories: single-phase model and two-phase model. In particular, the two-phase models can help to interpret the experiment results and understand the real physical happenings that occur inside the ejectors [37]. In a two-phase ejector, the motive nozzle flow is complicated by the non-equilibrium phase change affecting local sonic velocity and leading to various types of shockwaves, pseudo shocks, and expansion waves inside or outside the exit of the nozzle. The 1D models cannot simulate these occurrences, while the CFD approach shows clear potential for be used as a powerful design tool of ejectors [37]. Further information are discussed in the Section 2.1.2.6.

Working fluid: ideal gas or real gas. In many studies [12, 38, 39] the working fluid is treaded as an ideal gas because, also in this case, the real gas not significantly increase the prediction accuracy [31]. However, the choice depends on the working fluids and the operating conditions of the ejector (i.e. temperature, pressure) as well.

2.1.2.2 Governing equations

The CFD codes are structured around the numerical algorithms that can tackle fluid flow problems. The solution technique on which they are based is the "finite volume method" and in outline the numerical algorithms consists of the following steps [3]:

- integration of the differential governing equations of fluid flow (Eqn. 2.4, 2.5, 2.6) over all the control volumes of the domain;
- discretization and conversion of the resulting integro-differential equations into a system of algebraic equations;
- solutions of the algebraic equations by numerical (iterative) method.

For ejector modelling, the equations to be solved have to take into consideration both turbulence and compressibility, due to the presence of transonic and supersonic flows (high Reynolds and Mach numbers). Thus, the compressible steady-state axisymmetric form of the conservation equations governs the flow in the ejectors. For variable density flows, the Favre averaged Navier–Stokes equations are more suitable and are usually used. The total energy equation containing viscous dissipation is also included and coupled to the set with the equation of state (i.e. perfect gas law).

2.1.2.3 Boundary conditions

In order to solve the governing equations proper boundary conditions must be applied. The CFD models of ejectors commonly use thermodynamics boundary conditions (pressures and temperatures) at inlets according to the generator and evaporator states. On the outlet, pressure boundary condition is chosen according to the condenser pressure of the ejector cooling cycle. Moreover, no slip condition is set at walls and symmetric boundary condition is supplied to take

advantage of the axisymmetric feature of the solution region [3]. According to the hypotheses, the heat transfer through the walls is neglected (zero heat flux) [12, 40].

2.1.2.4 Initial conditions

The CFD models need to be initialized in the entire domain. A hybrid or a multi-grid initialization is suggested due to the presence of multiple inlets (primary and secondary flow) [41].

2.1.2.5 Auxiliary equations

The most important auxiliary relations in the CFD studies are the turbulence models, which are essential to close the system of equations and compute turbulent flow. The numerical procedure used is based on the Raynolds-averaged Navier-Stokes (RANS) equations and, generally, the Boussinesq hypothesis is adopted (Equation 2.13). This means that the turbulence models are based on an eddy viscosity assumption, for which there exists an analogy between the action of the viscous stresses and the Reynolds stress on the mean flow [3, 7]:

$$\tau_{ij} = \mu_t \cdot \left(\frac{\partial U_i}{\partial x_j} + \frac{\partial U_j}{\partial x_i} \right) - \frac{2}{3} \rho k \delta_{ij} \tag{2.13}$$

Thus, the Reynolds stresses are assumed proportional to the mean rates of deformation.

The most common RANS turbulence models, based on the Boussinesq hypothesis, are classified according to the number of additional transport equations that need to be solved coupled with the flow equations [3, 6]:

- zero extra transport equations (*mixing length* model);
- one extra transport equations (*Spalart-Allmaras* model);
- two extra transport equations (k-ε model, k-ω model).

These models are the basis of the standard turbulence calculation procedures in the CFD codes.

The equations modelling the turbulent flows near solid walls may require also the so-called “law of the wall”, which described the boundary layer near the walls [3, 6]. A more detailed description of the turbulence models and the respective wall treatments is presented in the Chapter 4.

2.1.2.6 Multi-phase models

For the multi-phase flow, the number of dependent variables exceeds that of the field equations. Consequently, it is necessary to supplement constitutive equations that close the problem. There are two main approaches for the numerical calculation of multi-phase flows: the Euler–Lagrange approach and the Euler–Euler approach. In the first approach, also called Discrete Phase Model (DPM), the trajectories of particles/droplets (disperse phase) are computed in a Lagrange frame, while the fluid phase is treated as a continuous by solving the Navier-Stokes equations [6]. The dispersed phase can exchange momentum, mass, and energy with the fluid phase. In the second approach, instead, different phases are treated as interpenetrating continua. This latter approach has been widely adopted in ejector modelling and there are two Euler–Euler multiphase models: the algebraic slip mixture model (ASM) and the two fluids Eulerian-Eulerian model (EEM) [7].

Algebraic Slip Mixture Model (ASM). This model solves the momentum, continuity, and energy equations for the mixture while the volume fraction equations are solved only for the dispersed phases. The model uses algebraic expressions for the relative velocities and the equations for multiphase flows are derived by mass-weighted averaging or Favre-averaging method [6, 7].

Eulerian-Eulerian Model (EEM). This model solves the momentum and continuity equations for each phase separately. The coupling of the equations is achieved through the pressure and inter-phase exchange coefficients. Momentum exchange between the phases is also dependent upon the type of mixture under consideration. Note that the transport equations for the modelling of the interface may be added [6, 7].

2.2 Ejector modelling: review

In this section, we provide a review about the most recent literature works that have proposed ejector models. The studies will be grouped by the modelling approach adopted. Moreover, each type of studies is divided according to the state of the working fluid (i.e. one-phase models and two-phase models).

2.2.1 Lumped parameter models

2.2.1.1 One-phase models

Chen, Liu et al. (2013) [25]. They proposed a 1D model to predict performance at critical and sub-critical operational modes, assuming a constant pressure mixing process inside the constant area section of the ejector. They supposed that there always exists the "aerodynamic throat" (section y-y) both in critical and sub-critical conditions. For critical mode operation the mixing process begins when the induced flow chokes (Eqn. 2.14); instead, for the case of sub-critical mode operation, it is assumed that there also exist an effective area where the velocity of the induced flow is the highest (Eqn. 2.15). Either way, the mixed fluid (Eqn. 2.16) undergoes a normal shock (Eqn. 2.17) and finally it passes through the diffuser.

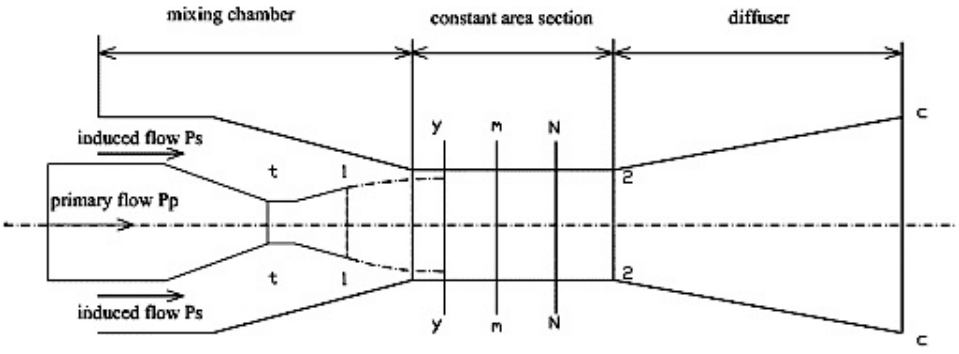

Figure 2-4: Schematic diagram of ejector – taken from [25].

Critical mode operation (isentropic flow relation):

$$\dot{m}_s = \frac{p_s A_{sy}}{\sqrt{T_s}} \cdot \sqrt{\frac{k}{R}\left(\frac{2}{k+1}\right)^{\frac{k+1}{k-1}}} \cdot \sqrt{\eta_s} \tag{2.14}$$

Sub-critical mode operation (from mass and energy balance):

$$\dot{m}_s = \frac{V_{sy} A_{sy}}{v_{sy}} \cdot \sqrt{\eta_s} \tag{2.15}$$

Mixed flow (momentum and energy balance):

$$\begin{cases} \psi_m \left(\dot{m}_p V_{py} + \dot{m}_s V_{sy} \right) = \left(\dot{m}_p + \dot{m}_s \right) V_m \\ \dot{m}_p \left(C_p T_{py} + \frac{V_{py}^2}{2} \right) + \dot{m}_s \left(C_p T_{sy} + \frac{V_{sy}^2}{2} \right) = \left(\dot{m}_p + \dot{m}_s \right) \left(C_p T_m + \frac{V_m^2}{2} \right) \end{cases} \tag{2.16}$$

Normal shock:

$$M_2^2 = \frac{1 + \frac{k-1}{2} M_m^2}{k M_m^2 - \frac{k-1}{2}} \tag{2.17}$$

According to the authors, the capacity to predict the ejector performance at also sub-critical mode makes the model ideal for integration into overall system models to accurately predict ERS performance, especially for start-up transient conditions.

Chen, Havtun and Palm (2014) [23]. The aim of the model proposed by the authors is to determine the optimum performance and the design area ratio of an ejector in a refrigeration system. They make use of the "aerodynamic throat" assumption: the primary and secondary flow begin to mix in the mixing chamber, leading the primary flow to be decelerated whilst the secondary flow continues accelerating, until they are completely mixed. They supposed also that the normal compression shock is induced at the end of the constant area. Starting from the isentropic relations and the mass, momentum and energy balances, the entrainment ratio can be found through the Equation 2.18:

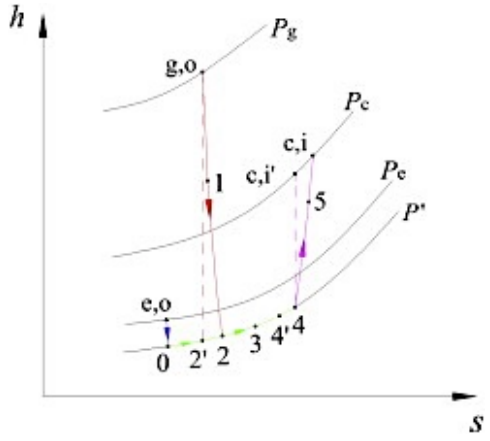

Figure 2-5: h-s diagram of ejector working processes – taken from [23].

$$\omega = \frac{\sqrt{2\eta_n \left(h_{g,o} - h_{2'} \right)} - \sqrt{2 \left(h_{c,i'} - h_4 \right) / \left(\eta_m \eta_d \right)}}{\sqrt{2 \left(h_{c,i'} - h_4 \right) / \left(\eta_m \eta_d \right)} - \sqrt{2 \left(h_{e,o} - h_0 \right)}} \tag{2.18}$$

The design area ratio is expressed by the Equation 2.19:

$$\phi = \frac{A_3}{A_t} = \frac{p_g \sqrt{1+\omega} \sqrt{1 + \omega T_e / T_g} \sqrt{1 - 2/(k+1)} \cdot \left[2/(k-1) \right]^{1/(k-1)}}{p_c \left(p_5 / p_c \right)^{1/k} \sqrt{1 - \left(p_5 / p_c \right)^{(k-1)/k}}} \tag{2.19}$$

The model helps to show that a variable-geometry ejector seems a very promising alternative to ensure that the ejector refrigeration system operates at its optimum conditions.

Kumar and Ooi (2014) [11]. The main characteristic of the model is the employment of the "Fanno flow" concept [42, 43] in order to capture frictional compressible flow occurring in the mixing chamber of the ejector (Eqn. 2.20). Moreover, the accuracy of the model is enhanced by averaging the heat capacity ratio k of the flow between each segment of the ejector, instead of keeping it constant. The model is a combination of both CPM and CAM. Indeed, they assumed that the mixing process takes place at constant pressure and the "aerodynamic throat" occurs inside the constant area section of the mixing chamber.

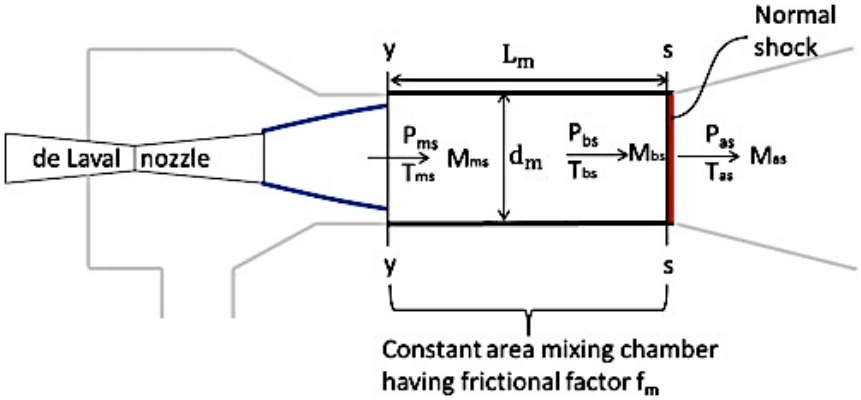

Figure 2-6: Schematic diagram of the mixing chamber – taken from [11].

$$\frac{f_m L_m}{d_m} = \frac{k_h + 1}{2k_h} ln \frac{1 + \left[\left(k_h - 1\right)/2\right] M_{bs}^2}{1 + \left[\left(k_h - 1\right)/2\right] M_{ms}^2} - \frac{1}{k_h}\left(\frac{1}{M_{bs}^2} - \frac{1}{M_{ms}^2}\right) - \frac{k_h + 1}{2k_h} ln \frac{M_{bs}^2}{M_{ms}^2} \tag{2.20}$$

where $k_h = (k_{ms} + k_{bs})/2$

The authors noted that the discrepancy between the measured condenser operating temperature and predictions from the model are mostly due to the superheating phenomenon of the secondary fluid due to heat transfer from the primary fluid, which was not accounted for.

In the Table 2-1 are reported the one-phase lumped parameter models presented in [2] and in the present work.

Table 2-1: Review of one-phase lumped parameter models.

Year	Ref.	Mixing mechanism			Fluid	Validation	
		Section y-y	CPM	CAM		Ref.	Error [%]
1995	[34]		√		H_2O (ideal gas)	[34]	$COP = \pm 30\%$
1998	[44]		√	√	H_2O (real gas)	[34]	qualitative
1999	[35]		√		H_2O (ideal gas)	[45]	$\Delta p = \pm 30\%$
1999	[24]	√	√		R141b (ideal gas)	[24]	$\omega = \pm 30\%$
2000	[46]	√	√		R717 (real gas)	No data	
2003	[47]	√	√		R142b (real gas)	[24]	$\omega = \pm 13\%$ (off-design), $\omega = \pm$

							8% (on-design)
2004	[48]	√	√		R134a (real gas)	[24]	$T_c = \pm 15\%$
2005	[49]	√	√	√	R123	No data	
2006	[50]			√	R134a, R152a (real gas)	No data	
2007	[22]	√	√		R11 (ideal gas)	[51]	$\omega = \pm 12.4\%$
					R141b (ideal gas)	[24]	$\omega = \pm 10.8\%$
2013	[25]	√	√		R141b (ideal gas)	[24]	$\omega = \pm 14.2\%$
					air (ideal gas)	[52]	$\omega = \pm 19.8\%$
					R290 (ideal gas)	[25]	$\omega = \pm 20\%$
2014	[23]	√	√		R123 (ideal gas)	[53]	*n.a.*
					R141b (ideal gas)	[24]	$\omega = \pm 29\%$
2014	[11]	√	√	√	R141b (ideal gas)	[24]	$T_c = \pm 11\%$

2.2.1.2 Two-phase models

Cardemil and Colle (2012) [33]. The proposed model takes into account both ideal and real gases. The use of real gas equations of state enables analyzing chocking phenomenon in two-phase ejectors. In fact, in two-phase mixtures, the compression and rarefaction effects due to the sonic wave are accompanied by a mass transfer from one phase to the other. Thus, the fluid state and the shockwaves are strictly linked. In these conditions, the evaluation of the speed of sound is a complicated task, because the pressure and temperature are not independent but are related through the equation of equilibrium of the phases. The model makes use of conservation equations based on mass, momentum and energy balance for each ejector segment. The calculation of the speed of sound was implemented using the phase transfer relaxation model developed by Lund and Flatten [54].

Banasiak and Hafner (2013) [55]. The main objective of this study was to analyse the effects of different phase transition models on the results of numerical simulations of transcritical CO_2 expansion in the ejector motive nozzle. Two distinct nucleation approaches using the delayed equilibrium model (DEM) were considered: solely homogenous nucleation and a superposition of homogeneous and heterogeneous nucleation. A correlation for the nucleation work reduction factor φ was developed and validated:

$$\varphi = \left(\frac{p}{p_c} \right)^{1.959} \left(0.3458 - \frac{\dot{m}/A_t}{\beta} \right)^{1.017} \tag{2.21}$$

with $\beta = 350 \cdot 10^3$ kg s^{-1} m^{-2}

The values of φ indicated dependence on the pressure of the metastable phase transition as well as on the critical mass flux.

The Table 2-2 summarizes the main characteristics of the two-phase lumped parameter models presented in [2] and in this work.

Table 2-2: Review of two-phase lumped parameter models.

Year	Ref.	Fluid	Primary fluid	Secondary fluid	Validation	
					Ref.	Error [%]
1999	[56]	H_2O	vapour	liquid	[56]	$\omega = \pm 15\%$
2000	[57]	R134a	two-phase	liquid	No data	
2000	[58]	H_2O	vapour	liquid	[59]	qualitative
2001	[9]	NH_3	wet	wet	No data	
2005	[60]	CO_2	transcritical	vapour	No data	
2008	[61]	CO_2	transcritical	vapour	[61]	$COP = \pm 8\%$
		R141b	dry	dry	[24]	$\omega = \pm 13.8\%$
2009	[62]	R11	wet	wet	[51]	$COP = \pm 5.5\%$
		H_2O	wet	wet	[16]	$\omega_{cr} = \pm 8\%$
2011	[63]	CO_2	transcritical	vapour	[63]	$\omega = \pm 5\%$
2012	[33]	CO_2	transcritical	vapour	[64]	$\omega = \pm 2.5\%$
2013	[55]	CO_2	transcritical	vapour	[55]	$\omega_{cr} = \pm 3\%$

2.2.2 Computational Fluid Dynamics models

2.2.2.1 One-phase models

Mazzelli and Milazzo (2014) [65]. They developed and experimentally tested an ejector for industrial refrigeration or air conditioning application. An extensive numerical campaign was performed to analyze its internal dynamics. For this purpose, the commercial CFD code Fluent 14.5 was used. The convergence of the solution is defined by an error in the mass flow imbalance of less than 10^{-5} kg/s and calculations are stopped when all residuals are stable. The boundary conditions were equal to experimental data and were provided as total pressure and static temperatures at inlets, static pressure at outlet. The analysis showed that in order to achieve an accurate matching with the experimental data, it is necessary to correctly account for the surface roughness of the ejector. This is especially true for off-design operating conditions. In fact, in this study three different sets of calculations were carried out with "sand-grain" roughness heights of 2, 20 and 60 micron, respectively. When the ejector is in choked conditions, the differences in the predicted entrainment ratios are rather small for different roughness heights (less than 4.5%). As the condenser pressure increases, higher values of friction cause the critical state to appear in advance. This result is indeed expected, as greater friction translates into larger amounts of total pressure losses, thus reducing the capability of the mixed flow to withstand high values of backpressure. Moreover, it can be noted that the presence of friction also influences the steepness and extension of the off-design regime. A higher level of roughness causes a slower reduction of the secondary mass flow with respect to backpressure increases. Consequently, the range of "non-choked" operations becomes larger.

Table 2-3: Review of one-phase CFD models – validation and purpose.

Year	Ref.	CPM	CAM	Ref. Validation	Purpose
2001	[66]	√	√	No data	*Influence of NXP on ejector performance*
2003	[67]	√		[67-69]	*Evaluation of the performance of six turbulence models for the study of a supersonic ejector*
2003	[70]		√	[67]	*Evaluation of the fluid flow behaviour*
2005	[71]	√		[24]	*Study of the flow field at different operating conditions and geometrical parameters (NXP and area ratio)*
2005	[72]		√	[71]	*Study of the transonic instability in the entrance part of the mixing chamber*
2005	[73]	√		[68, 69, 72]	*Evaluation of the performance of six turbulence models for the study of a supersonic ejector*
2006	[74]	√		No data	*Local CFD modelling that takes into account the interaction between shockwaves and boundary layer*
2007	[12, 18]	√		[12]	*CFD performance prediction of a steam ejector for refrigeration applications*
2007	[75]	√	√	[39]	*Comparison between 3D and 2D mesh of both CPM and CAM ejectors*
2008	[76]	√		[24, 71, 77]	*Parametric study in order to identify key features that may impact on ejector performance*
2009	[52]	√		[78]	*Compare the performance of two different turbulent models at on-design and off-design operating conditions*
2009	[79]	√		[79]	*Effect of geometrical parameters (NXP and converging angle of the mixing chamber)*
2009	[40]	√		No data	*Study of three geometrical parameters (area ratio, NXP and constant area section length)*
2010	[80]	√		[80]	*Study of the effect of operating conditions and geometrical parameters*
2011	[81]	√		[81]	*Experimental and CFD results of an ejector with variable primary nozzle geometry*
2012	[82]	√		[82]	*Influence of geometrical parameters on ejector performance*
2012	[83]	√		[12]	*Investigation of the influence of different nozzles on the mixing process*
2013	[84]	√		[66]	*Investigation of geometrical parameters*
2014	[65]	√		[65]	*Experimental and CFD analyses of a supersonic ejector*

Table 2-4: Review of one-phase CFD models – model settings.

Year	Ref.	Mesh	Code	Fluid	Turbulence model	Wall treatment
2001	[66]	3D structured non uniform	Fluent 4.3.2	CH_3OH (ideal)	k-ε RNG	Standard
2003	[67]	2D unstructured	Fluent	air (ideal)	k-ε, k-ε RNG, k-ε Realizable, k-ω, k-ω SST, RSM	Standard
2003	[70]	2D unstructured 500000 cells	Fluent 6	air (ideal)	k-ε RNG	Standard
2005	[71]	2D unstructured 40000 cells	Fluent	R141b (real)	k-ε Realizable	No info
2005	[72]	2D unstructured 300000 cells	Fluent 6	air (ideal)	k-ε RNG	No info
2005	[73]	2D unstructured	Fluent	air (ideal)	k-ε, k-ε RNG, k-ε Realizable, k-ω, k-ω SST, RSM	Standard
2006	[74]	2D unstructured	Fluent	R142b (real)	k-ε, k-ε RNG, k-ω SST	Standard
2007	[12, 18]	2D structured 43000 cells	Fluent 6	H_2O (ideal)	k-ε Realizable	Standard
2007	[75]	2D 48000 nodes, 3D 500000 nodes	Fluent 6	H_2O (ideal)	k-ε Realizable	No info
2008	[76]	No data	Phoenics 3.5.1	R141b (real) R245fa (real)	No info	No info
2009	[52]	2D structured 25800 cells	Fluent 6.2	air (ideal)	k-ε, k-ω SST	Enhanced
2009	[79]	77050 cells	Fluent 6.3	H_2O (ideal)	k-ε Realizable	No info
2010	[80]	2D structured 54000 cells	Fluent 6.2	R141b (ideal)	k-ε RNG	Standard
2012	[82]	No info	Phoenics 3.4	Natural gas (real)	k-ε RNG	No info
2014	[65]	2D structured 80000 cells	Fluent 14.5	R245fa (real)	k-ω SST	Enhanced

2.2.2.2 Two-phase models

Smolka et al. (2013) [85]. They proposed a mathematical model developed to predict the transcritical compressible flow of a real fluid occurring in an ejector for CO_2. The model is implemented in commercial CFD software but using subroutines developed in-house. In the proposed approach, the temperature-based energy equation is replaced with the enthalpy-based formulation, in which the specific enthalpy, instead of the temperature, is an independent variable. The real fluid properties, such as the density, the dynamic viscosity and the diffusion coefficient, are defined as functions of the pressure and the specific enthalpy. In modelling the considered two-phase turbulent flow, it is assumed that both phases are in thermodynamic and mechanical equilibrium. This means that both phases have the same pressure, temperature, velocity, turbulence kinetic energy and turbulence dissipation rate. The main advantage of the methodology proposed is its numerical robustness as compared to well-known multi-phase models, such as the Euler–Euler or the mixture models. In addition, the developed model can also be successfully used in different practical applications to predict the one-phase and two-phase flows of working fluids, especially when real gas properties are essential.

Yazdani et al. (2014) [37]. Since the characteristics of the jet leaving the motive nozzle greatly affect the performance of the ejector, this work focuses on the details of flow development and shockwave interaction within and just outside the nozzle. The approach developed in this study combines multiple separately validated sub-models for mass and energy transfer between phases, two-phase sonic velocity and real-fluid properties of CO_2 in the presence of finite-rate phase change and embedding them into a high-fidelity commercial CFD model. Unlike single-phase expanding flows where the flow chokes at the minimum-area throat, the numerical results show that the choke occurred further downstream of the throat, where void generation promoted flow acceleration while leading to a sufficient drop in the sound speed. In addition, the void generation rate and how the two-phase jet emits from the nozzle was found to be, in large part, dependent on the nozzle configuration and the upstream operating conditions. However, the model helps to interpret the experiment results and shows clear potential for use as an ejector design tool.

Lucas et al. (2014) [86]. In this work, a numerical model based on a homogeneous equilibrium approach, which is implemented in OpenFOAM, is used to simulate the CO_2 ejector. The numerical investigation of the ejector operated with and without a suction mass flow. If the ejector is operated without a suction flow, no mixing losses occur and the friction losses are one of the main losses affecting the flow. Thus, this operating condition is suitable to validate if the friction losses are determined correctly by the numerical model. Afterwards, an ejector which is operated with a suction flow is simulated in order to validate the accurate prediction of the mixing losses by the numerical model. The results show that the mixing losses are predicted less accurately.

Table 2-5: Review of two-phase CFD models – validation and model settings.

Year	Ref.	Code	Two-phase model	Primary fluid	Secondary fluid	Phase change	Turbulence model	Ref. Validation
2005	[87]	Fluent 6.1	ASM	H_2O	air (ideal)		k-ε	[88]
2007	[89]	Fluent 6.2	ASM	H_2O	air (ideal)		No info	[87]
2008	[90]	Fluent 6.2	ASM	H_2O	air (ideal)		k-ε	[88]
2008	[91]	Fluent 6.2	ASM	air (ideal)	H_2O		k-ε	[88]
2009	[52]	Fluent 6.2	DPM	air + H_2O droplets	air		k-ε, k-ω	[78]
2011	[92]	Fluent 6.3	ASM	N_2/He (ideal)	H_2O/CO_2 (liq.)		k-ε	[91]
2012	[93]	Open-Foam	EEM	CO_2	CO_2	√	k-ε	[94]
2012	[95]	Fluent 12	ASM	CO_2	CO_2	√	k-ω SST	[94]
2013	[85]	Fluent 12	In-house	CO_2	CO_2	√	k-ε RNG	[85]
2014	[37]	Fluent 12	Non-homogeneous mixture	CO_2	CO_2	√	k-ω SST	[96]
2014	[86]	Open-Foam	Homogeneous mixture	CO_2	CO_2	√	k-ω SST	[97]

2.3 Summary

The flow phenomena occur inside an ejector are very complex and an understanding of these phenomena is very important for modelling ejector flow. With the development of computer hardware and numerical methodology, lots of mathematical models have been constructed and employed to analyze, develop and design ejectors [7]. In this way, they have helped to provide a better understanding of the compression process, system design and performance evaluation considering the fluid dynamics performance. The validation of the model is an important step in model development since it offers the possibility of comparing simulation results with actual system behaviour. Experiments are mostly used to validate the mathematical model. Besides, comparing with previous numerical results is also a good validation method [10]. The validation of model with local parameters (for CFD models) is preferable.

The majority of studies that explore the ejector operation have developed lumped parameter models. The typical thermodynamic analysis makes many simplifying assumptions, such as 1D problem, ideal gas, steady-state operation, isentropic flow and adiabatic subcomponents [10]. Hence, most of them are steady-state models and work at design conditions. Moreover, in order to simplify modelling, most of the models [23, 24] assume that no phase change occurring in the

ejector [7]: these models are developed based on single-phase flow and they supposed that a normal shock way occur inside the mixing chamber.

However, under many real applications, phase change can occur and a condensation shock may develop. In vapour ejectors, the additional rise in pressure caused by the shockwaves can facilitate the mixture condensation. Moreover, the sub-cooled or saturated secondary flow accelerates and expands until the "aerodynamic throat" and thus it can flash into vapour and form either a two-phase mixture or pure vapour. On the other hand, in condensing ejector (high-pressure vapour entrains liquid) and two-phase ejector (high-pressure liquid entrains gas), phase transition occurs (please refer to Section 1.2.2.3). These flow phenomena affect the ejector behaviour. Therefore, some researchers [33] are engaged in ejector simulation with two-phase flow [36].

Anyway, due to the mixing of two different streams, high-velocity flows and changing cross-sectional area, the flow phenomena inside ejectors are very complicated and difficult to capture analytically, especially for wide range of operating conditions [10]. Although recent thermodynamic models are able to predict global properties more accurately, compared to older ones, by accounting for additional flow phenomena (such as suction flow chocking from the formation of the "aerodynamic throat") or losses (due to shocks, mixing or friction) the precise flow behaviour inside the ejector still remained unresolved. In fact, a large degree of uncertainly and error remain [10]. The main reason lies in the fact that the actual mechanisms of most sources of loss have been aggregated into constant coefficients [10]. These values are actually specific to the working fluid, operating conditions, geometry and local phenomena [26].

It is the understanding of local interactions between shockwaves and boundary layers, their influence on mixing and re-compression rate that will produce a more reliable and accurate design, in terms of geometry, refrigerant type and operating conditions [36]. Therefore, many studies have turned to the use of CFD to better understand ejector fluid flow phenomena. The CFD models accounts the turbulence interaction between the primary and secondary stream, the shock reflection and chocking. It is more related to the actual process occurred in the ejector and the effect of the geometrical parameters and operation parameters can be well explained. Therefore, CFD modelling can provide more accurate simulations in accordance with the experiment results and the precision of the CFD models is greatly improved. However, the choice of the turbulence model is very important. The literature studies show that for compressible flowing model, the k-ε RNG and k-ω SST are the best suited to predict the shock phase, strength, and the mean line of pressure recovery [73]. Nevertheless, the standard k-ε model and realizable k-ε model are sometimes used for time saving. With regard to the two-phase flowing model, the mixture model can give reasonable results [7].

Despite the improvement made to ejector modelling, aided by the increasing sophistication and accuracy of CFD software and the use of finer, adaptive grids, a few major question about ejector flow phenomena remain [10]. Though a large amount of works have been conducted on modelling and analyzing ejector, further efforts are still needed [7, 10]:

- to study the influence of variable isentropic coefficients which are taken as constant in almost all existing thermodynamic models;
- to construct a simulation package of the whole ejector-based system by combining the model of the ejector and other components in the system;

- to improve the accuracy of the model based on turbulence model, since by now, there still no uniform model being used and simulations have been shown to be sensitive to the choice of model;
- to take into account the effects of nucleation, growth of condensation droplets and metastable states present in two-phase flow.

Chapter 3

Lumped parameter model evaluation and performance analysis

In this chapter, we focus on the lumped parameter modelling for ejector performance evaluation. We have selected five lumped parameter models from the previous reviews and we have evaluated their effectiveness by comparing the predicted results with experimental data available in the literature. The models have been chosen among the most recent 1D analytical studies published by different research groups in order to obtain an assorted set of simulations. The experimental data have been selected from different studies for considering different working conditions, working fluid and geometries. Afterwards, on the basis of the comparison results, we have selected one lumped parameter model for a sensitivity analysis to examine the influence of some key parameters, like the isentropic efficiencies of the ejector. Finally, taking as reference a recent academic work presented by Kasperski and Gil (2014) [1], we want also evaluate the behaviour of the ejector using several working fluids, with the purpose of verifying the great importance that the refrigerants have on ejector operation. The working fluids have been selected from the review presented in the Section 1.3.

3.1 Lumped parameter models (1D thermodynamic models)

The flow dynamics equations include the mass conservation equations, momentum conservation equations and energy conservation equations. All these equations are coupled and the overall problem is very complex to solve. Therefore, the typical analytical study makes many assumptions in order to simplify the problem without loss of generality. The hypotheses on which these studies are based will be presented in detail for each model on their own section. However, the main assumptions, common to all the models are:

- the flow is steady and one dimensional;
- the walls of the ejector are adiabatic.

Thus, the system can be described by the steady one-dimensional equations for adiabatic process (please refer to Chapter 2).

In this section we have considered five models from the literature to predict ejector performance:

[i] Chen, Havtun and Palm (2014) [2]. They presented an ejector model to determine the optimum performance as well as the design area ratio of an ejector in a refrigeration system;

[ii] Chen, Liu et al. (2013) [3]. They proposed a 1D model to predict ejector performance at critical and sub-critical operational modes;

[iii] Zhu, Cai et al. (2007) [4]. They developed a "shock circle" analysis in order to simplify the calculation compared to others 1D modelling methods;

[iv] Kumar and Ooi (2014) [5]. They applied the Fanno flow concept (for further information please refer to [6, 7]) to capture frictional compressible flow occurring in the mixing chamber of the ejector;

[v] Cardemil and Colle (2012) [8]. They presented a model which takes into account both ideal and real gasses and for wet vapour ejector the chocking phenomenon is analysed considering a relaxation model for the calculation of the speed of sound in two-phase mixture.

All these models have been implemented in the MATLAB® R2013a [9] framework and have been validated using the following experimental data:

[i] Huang, Chang et al. (1999) [10] examined 11 different ejectors using R141b as working fluid, obtaining 39 sets of data under various operating conditions;

[ii] Ablwaifa (2006) [11] ran his experiment at different operating conditions using R236fa and R245fa as working fluid.

The two-phase model proposed by Cardemil and Colle (2012) [8] have been also tested by means of the experimental study on a transcritical CO_2 ejector system prepared by Xu et al. (2011) [12], just to verify its performance with a two-phase ejector.

With regard to the calculation of the thermodynamic properties of the working fluids, the open-source thermophysical property library name CoolProp [13] was used. In the original models are instead used the NIST database [14, 15] (in Ref. [2-5]) or the EES software [16] (in Ref. [8]).

The effectiveness of the model is evaluated in terms of the relative error E_R defines as:

$$E_R(X) = \left| \frac{X_{mod} - X_{exp}}{X_{exp}} \right| \cdot 100 \tag{3.1}$$

where X_{exp} and X_{mod} are the measurement and the model estimates, respectively.

Our results have been also compared with the original model results. Please notice that [10] have been widely used for validating the model performance in the original references. We have also used this benchmark in order to evaluate the influence of the model implementation on the results (i.e. the thermodynamic libraries for working fluid properties).

The Figure 3-1 shows a schematic view of an ejector structure, indicating the typical cross sections of the ejector that identify specific fluid dynamics situations that occur during its operation. In the following, we will use the notation of this figure to refer to certain section of the ejector.

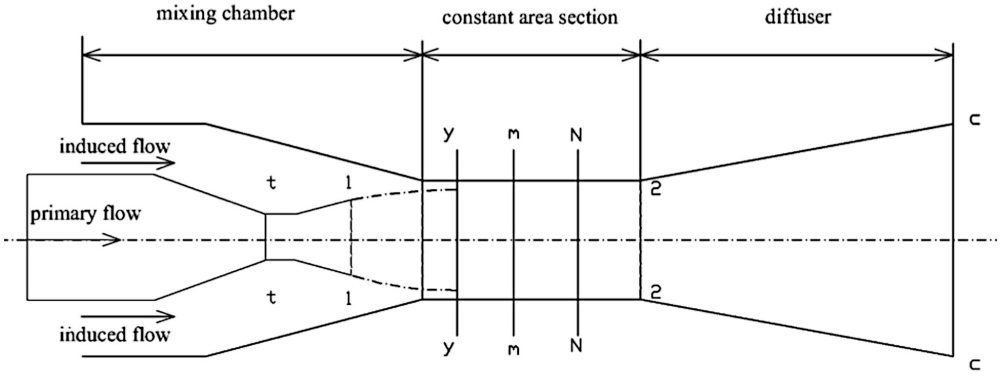

Figure 3-1: Schematic view of an ejector structure – modified from [3].

3.1.1 Single-phase models

3.1.1.1 Chen, Havtun and Palm (2014) [2]

The model is based on the following assumptions:

- the primary and secondary flow are saturated vapour;
- the velocity at the primary and secondary flow inlets are negligible;
- the velocity of the mixed flow leaving the ejector is negligible;
- the losses in the nozzle, in the mixing chamber and in the diffuser are taken into account by using isentropic efficiencies η_n, η_m and η_d, respectively;
- the expansion of the secondary flow from inlet to nozzle exit is considered isentropic (low velocity gives small losses);
- in this range of operation conditions the working fluid is an ideal gas with constant heat capacity ratio k.

To determine the entrainment ratio ω and the calculated pressure at the ejector outlet, a computational procedure with two iteration processes is needed.

Selected the working fluid, the variables that must be assigned are: one variable to fix the thermodynamic state of the primary flow (generator) and secondary flow (evaporator) at the inlet and the condenser conditions at the outlet. The heat capacity ratio and the ejector efficiencies are known.

Assuming a value for the mixing pressure, the velocity of the primary flow and secondary flow at the nozzle exit can be calculated through the energy conservation equation. An initial value for the entrainment ratio ω is estimated and, using an iterative cycle, its real value can be evaluated: the calculated ω is compared to the initial value and the process ends when the difference between the two values is acceptable. The outlet pressure is calculated by means of isentropic flow equation and energy conservation, and this calculated value is compared to the input condenser pressure. A new value for the mixing pressure is estimated and the previous steps are repeated until convergence. The ejector area ratio ϕ (A_2/A_t) and the *COP* are finally calculated.

To validate the accuracy of the model, the authors used experimental results from literature by Yapici et al. (2008) [17] and Huang et al. (1999) [10].

In particular, in the first case efficiencies η_n and η_d were set to 0.9 (as in Ref. [17]) while $\eta_m = 0.85$ was selected to approach the experimental data. They obtained very good agreement with the experimental results, obtaining errors less than 3.5% and 6.5% in *COP* and ϕ, respectively. In the second one, the nozzle efficiency was fixed to 0.95 for all the ejectors, while the mixing chamber efficiency and the diffuser efficiency, that have different definitions in Ref. [10], are calculated from the first experimental data point of each ejector using a trial-and-error method. Then the same values are employed to the rest of data of each ejector. In these conditions, area ratios were well predicted (errors less than 6%), while almost half of the calculated entrainment ratios had relatively large deviation from the test data (over 20%). The agreement with the model at optimum operating conditions was very good, while the deviation between the model and the experimental data for a fixed-geometry under wide ranges of operating conditions was slightly larger. For the same authors, the main reason lies in the selection of the efficiencies value and for this they will present in a future work empirical correlations to determine η_n, η_m and η_d varying operating conditions.

Our simulations lead to similar results. With R141b benchmark [10] we get a prediction of the area ratios ϕ with an error under 6%, while more than half of the entrainment ratios ω values have an error greater than 20%. These errors are generally a bit higher, especially when generator temperatures decrease.

The second benchmark [11] implies better results especially in entrainment ratio prediction: using the R245fa benchmark most of the error values are under 20%, but with a greater maximum error. Using the R236fa benchmark, instead, the errors are much smaller. In both cases, the greater errors occur for low evaporator temperature.

Table 3-1: Efficiencies assumed and errors of the simulations.

	Chen, Havtun and Palm [2]		Our simulation		
Benchmark	[17]	[10]	[10]	[11]	[11]
Fluid	R123	R141b	R141b	R236fa	R245fa
η_n	0.90	0.95	0.95	0.95	0.95
η_m	0.85	G.D.	G.D.	0.9	0.9
η_d	0.90	G.D.	G.D.	0.85	0.85
$E_R(\phi)$ [%]					
Min	n.a.	0.12	0.05	2.59	0.02
Max	6.50	5.87	5.54	6.83	1.81
Mean	n.a.	1.67	1.75	4.90	0.55
Variance	n.a.	2.14	2.25	1.73	0.28
$E_R(\omega)$ [%]					
Min		0.07	1.25	0.40	0.36
Max	n.a.	29.03	38.98	28.67	47.76
Mean		11.84	17.53	12.01	17.39
Variance		80.97	129.97	110.26	279.85

Most of the models developed [3-5, 8, 10] need either predefined entrainment ratio for ejector design or predefined ejector geometry for performance evaluation. The present model, instead,

allows to calculate simultaneously the optimum entrainment ratio and the corresponding area ratio, known the operating conditions, the properties of the working fluid and the ejector efficiencies. This represents a considerable advantage.

However, as already pointed out, the accuracy of the model is adequate only in a restricted range of operating conditions.

3.1.1.2 Chen, Liu et al. (2013) [3]

The hypothesises on which the model was grounded are:

- the velocity at the primary and secondary flow inlets are negligible;
- the velocity of the mixed flow leaving the ejector is negligible;
- the losses of the primary flow in the nozzle and in the first part of the mixing chamber, the losses of the secondary flow and the frictional loss in the mixing chamber are taken into account by using the coefficients η_p, η_{py}, η_s and ψ_m respectively;
- in this range of operation conditions the working fluid is an ideal gas with constant C_p and heat capacity ratio k;
- the primary flow fans out from the nozzle and it does not mixing with the secondary flow up to at a certain cross section inside the constant area section (section y-y).

The last assumption is a peculiarity of this model.

The 1D model intends to predict the ejector performance over the entire range of operations for fixed geometrical parameters. For a given inlet thermodynamics condition, the mass flow rate through the nozzle is obtained using the isentropic flow relation. If the ejector works in critical condition, the mass flow rate of secondary flow is given by the same formula, using the respective isentropic efficiency. Otherwise, the ejector works in sub-critical mode and it is necessary an iterative process to calculate the secondary mass flow, using the conservation of mass and energy, as well as isentropic relations. In both the situations, the mixed flow is calculated applying a momentum and energy balance, taking into account the statement of the last hypothesis. Afterwards, we can evaluate the pressure drop through the shock wave and the pressure recovery through the subsonic diffuser thanks to the gas dynamic relations.

An essential step is to determine the critical backpressure p_c^*, then gives a backpressure value p_c. If p_c is lower than p_c^*, the ejector is at critical operation, otherwise the ejector is at sub-critical operation.

In the present model, all of the equations are similar with the model proposed by Huang et al. (1999) [10] but the method of resolution is different: in Huang's model, the critical backpressure p_c^* is an independent parameter obtained from experimental data; in this model p_c^* is an output variable.

The isentropic efficiencies are taken as $\eta_p = 0.95$, $\eta_{py} = 0.88$ and $\eta_s = 0.85$. The frictional loss in the mixing section ψ_m is sensitive to the area ratio and an empirical relation is used:

$$\psi_m = \begin{cases} 0.8 & for\ A_2/A_t > 8.3 \\ 0.82 & for\ 6.9 \le A_2/A_t \le 8.3 \\ 8.84 & for\ A_2/A_t < 6.9 \end{cases} \tag{3.2}$$

According with the data collected by Huang et al. (1999) [10], the present model quite accurately predict the entrainment ratio at critical mode operation: the largest error is less than 15%.

In order to validate the ability of the present model to predict entrainment ratio at also sub-critical mode operation, experimental data with air from Hemidi et al. (2009) [18] was used. The largest error of the theoretical results is close to 20%.

Moreover, a comparison with the performance of an in-house test ejector embedded in a refrigeration cycle with propane was carried out. The properties of propane deviate more from the ideal gas law, thus the coefficients in the model are different compared to those taken in the previous simulations. In critical and sub-critical mode operation, the relative errors are all within 20%.

Even our results are into line with this trend. The comparison with the experimental data by Huang et al. (1999) [10] led in a maximum error of the order of 20%, while with both the benchmark in Ref. [11] the errors are even smaller.

Table 3-2: Efficiencies assumed and errors of the simulations.

	Chen, Liu et al. [3]			Our simulations		
Benchmark	[10]	[18]	[3]	[10]	[11]	[11]
Fluid	R141b	Air	R290	R141b	R236fa	R245fa
η_p	0.95	0.95	0.98	0.95	0.95	0.95
η_{py}	0.88	0.88	0.95	0.88	0.88	0.9
η_s	0.85	0.85	0.85	0.85	0.85	0.85
ψ_m	G.D.	0.84	0.84	G.D.	0.82	0.80
$E_R(\omega)$ **[%]**						
Min	0.06	n.a.	n.a.	0.04	0.03	1.47
Max	14.20	19.8	20	23.90	8.42	16.81
Mean	4.56	n.a.	n.a.	6.11	3.37	10.31
Variance	12.66	n.a.	n.a.	28.88	5.37	14.44

The present model predicts the ejector performance over the entire range of operation conditions with errors less than about 20%. The way to reduce the errors is to adjust the isentropic efficiencies.

3.1.1.3 Zhu, Cai et al. (2007) [4]

The following assumptions are made to simplify the analysis:

- the ejector operates at critical mode;
- the primary flow inside the ejector is uniformly distributed in the radius *r* direction;
- the pressure and temperature of the secondary flow are uniformly distributed in the *r* direction;
- the pressure of the secondary flow in the suction chamber is equal to its inlet pressure;

- the friction losses are taken into account by using the coefficient relating to the isentropic efficiency of the compressible flow in the nozzle ψ_p and of the secondary flow ψ_s;
- in this range of operation conditions the working fluid is an ideal gas with constant heat capacity ratio k;
- the primary flow can expand and accelerate the secondary flow in the suction chamber, and afterwards the secondary flow reaches the chocking condition at the cross section y-y.

The main characteristic of the shock circle models consists in using the velocity distribution in the r direction, together with the isentropic flow relations. In this way, the calculation of the ejector performance is independent of the flows in the constant area chamber and in the diffuser. However, the model can only predict the ejector performance of the critical mode operation field.

The governing equations are non-linear and closely coupled. Thus, an iterative procedure must be use to solve the set of equations and the following data are required: the ejector geometry (nozzle throat and nozzle exit diameters), the inlet conditions (T_g, p_g and p_e) and the coefficients relating to the isentropic efficiency of the primary flow and secondary flow (ψ_p and ψ_s). The mass flow rate of the primary flow at chocking conditions can be calculated using the isentropic flow relations. Involving the conservation equations, it is possible to determine the Mach number and the velocity of the primary flow at the exit of the nozzle and, subsequently, at the entrance of the constant area chamber (section y-y). By introducing the "shock circle" at the section y-y, a 2D exponential expression for the velocity distribution in the r direction is adopted to approximate the viscosity flow near the ejector inner wall. In fact, inside the operational ejector, the velocity is non-uniformly distributed due to the velocity boundary layer near the walls. In addition, there is also a zero thickness layer between the primary flow (with a near uniform velocity distribution) and the secondary flow (with a quite non-uniform velocity distribution). Only this layer is in the chocking condition (M = 1) and it is defined as the "shock circle". Finally, the secondary mass flow rate is determined from the energy balance relation for an ideal gas in the section y-y.

In order to validate the accuracy of this model, the experimental results by Huang et al. (1999) [10] are used. In the shock circle analysis, the friction losses coefficients are taken ψ_p = 0.95 and ψ_s = 0.85. According to the model assumptions, the specific heat ratio is constant (for R141b it is equal to 1.135), while the specific heat C_p is evaluated through a polynomial function of degree 3 in the temperature (NIST database [15]). The relative errors committed in the prediction of the entrainment ratio are, according to the authors, less than 11%.

The model is also tested with the experimental data with refrigerant R11 provided by Aphornratana et al. (2001) [19]. For this simulation the friction losses coefficients are taken ψ_p = 0.9 and ψ_s = 0.85. As previously, the specific heat ratio is constant and equal to 1.13 and the C_p is computed by the NIST relation for the R11. Excluding the sub-critical data from the simulation, the authors have obtained relative errors less than 13%.

Using the Huang et al. (1999) [10] dataset, our calculations have led to relative errors less than 11%, in line with those obtained by the authors with the same reference. With regard to the second benchmark [11], the model's performance has been below expectations, according to what is claimed by the authors. However, with refrigerant R236fa the results are very good, but worsen considerably at low evaporator temperatures. With R245fa benchmark, the results are quite good: the relative errors are all less than 23% and mostly less than 18÷19%.

Table 3-3: Efficiencies assumed and errors of the simulations.

	Zhu, Cai et al. [4]		Our simulation		
Benchmark	[10]	[19]	[10]	[11]	[11]
Fluid	R141b	R11	R141b	R236fa	R245fa
ψ_p	0.95	0.9	0.95	0.95	0.95
ψ_s	0.85	0.85	0.85	0.85	0.85
$E_R(\omega)$ [%]					
Min	0.18	n.a.	0.01	0.12	9.59
Max	10.78	12.39	10.70	16.08	22.31
Mean	4.52	n.a.	4.61	5.40	17.00
Variance	9.65	n.a.	9.62	40.98	11.33

The shock circle model is easy to run: there are fewer equations than the other models and only two basic isentropic coefficients ψ_p and ψ_s are needed. Moreover, the modelling of the complicated mixing process is not required. However, this model generally leads to good results, but only for critical mode operation ejectors.

3.1.1.4 Kumar and Ooi (2014) [5]

The novelty of this model is that the "Fanno flow" concept has been applied to capture the frictional compressible flow occurring in the mixing chamber of the ejector. It is based on the following assumptions:

- the ejector operate at critical mode;
- the velocity at the primary and secondary flow inlets are negligible;
- the velocity of the mixed flow leaving the ejector is negligible;
- the various losses occurring in the ejector are taken into account by using the coefficients η_p, φ_p, η_s and η_d;
- the friction factor f_m remains constant throughout the mixing chamber;
- in this range of operation conditions the working fluid is an ideal gas;
- after exiting the nozzle, the primary flow fans out without mixing with the secondary flow up to at a certain cross section inside the constant area section (section *y-y*);
- leaving from the nozzle, the primary flow creates an aerodynamic throat and chocked conditions for the secondary flow;
- the normal shock remains fixed at the end of the mixing chamber.

The model uses the ideal gases compressible flow assumptions. To maximize the accuracy, variations in heat capacity ratio, due to temperature and pressure changes, will be accounted for. This involves an iterative method, as heat capacity ratio has to be evaluated repeatedly until convergence occurs in the predicted temperature.

By means of the isentropic flow relations, the primary flow is studied in three sections: the nozzle throat section, the nozzle outlet plane and the section *y-y* of the mixing chamber. The losses are

taken into account by the isentropic efficiency of the primary nozzle η_p and the isentropic expansion efficiency from the nozzle to the section *y-y* φ_p. The secondary flow can be determined using the isentropic flow equations as well and the isentropic efficiency of the suction chamber is accounted for by the coefficient η_s. The mixing process commences after the section *y-y* and occurs at constant pressure. Then, the Fanno flow equation can be used to model the compressible frictional flow occurring in the mixing chamber. The equation depends on a characteristic geometric parameter L_m/d_m (assumed equal to 10). For the calculation of the friction factor f_m, the Schlichting equation is used (please refer to [20]). Finally, equations similar to the previous are employed for determining the flow until the outlet plane of the diffuser, characterized by the isentropic efficiency η_d.

The model was verified by comparing the numerical values obtained from the model against the experimental data by Huang et al. (1999) [10]. The predicted entrainment ratio agrees well with the measured data with an average error less than 4%. Moreover, a sensitivity analysis about some assumed parameters (L_m/d_m = 5÷15, η_d = 0.8÷0.9) has been performed by the authors. It shown that the diffuser efficiency has a marginal impact on the model's results, but the L_m/d_m ratio has a sensible effect.

The predicted entrainment ratios agree well with the R141b benchmark [10]. The maximum error is quite high (27.49%) but the average error is less than 7% and the 75% of the relative errors are lower than 10%. With the other benchmarks [11] we have obtained average errors greater but the maximum errors are less compared to the previous reference.

With regard to the prediction of the condenser temperature, the authors and we have come to the same conclusions. In general, in fact, the model over-predicts the T_c and the discrepancies between the predictions and the measurement grow with increasing of the generator temperature. This is mainly due to the superheating phenomenon of the secondary flow caused by the heat transfer from the primary flow, which was not accounted for.

Table 3-4: Efficiencies assumed and errors of the simulations.

	Kumar and Ooi [5]	Our simulation		
Benchmark	[10]	[10]	[11]	[11]
Fluid	R141b	R141b	R236fa	R245fa
η_p	0.95	0.95	0.95	0.95
φ_p	0.88	0.88	0.88	0.88
η_s	0.85	0.85	0.85	0.85
η_d	0.9	0.9	0.9	0.9
$E_R(\omega)$ [%]				
Min	n.a.	0.09	2.96	1.91
Max	n.a.	27.49	15.23	18.65
Mean	4.00	6.95	8.64	10.67
Variance	n.a.	39.70	15.43	16.73
$E_R(T_c)$ [%]	n.a.	7.39	5.35	10.42
Min	11.00	12.58	6.89	17.84

Max	5.00	10.18	6.23	13.83
Mean	n.a.	1.92	0.25	3.83
Variance				

This model aims to improve the accuracy of the performance predictions by including Fanno flow effects in the mixing chamber of the ejector and by accounting for variations in heat capacity ratio. Even though the number of the equations needed is quite high, the model is not onerous from the computational point of view. In addition, the results highlight the importance of using variables heat capacity ratio rather than taking them as constant.

3.1.1.5 Cardemil and Colle (2012) [8]

This model is characterized by an approach that takes into account the real gas effects. Ejector modelling is commonly based on ideal gas dynamics models. However, depending on the characteristics of the working fluid these models may not be acceptable. As already mentioned, the working fluids can be classified as wet fluid, isentropic fluid and dry fluid according to the shape of the saturation curve in the *T-s* diagram. For dry and isentropic fluids there is no phase change during the expansion process in the ejector's nozzle. Nevertheless, for a wet fluid a partial phase transition can occur. For further information, please refer to the Section 1.3.2.

In this section the first kind of fluids (single-phase flow) will be treated, while the two-phase flow model will be analyzed in the next one.

The hypotheses of the model are:

- the velocity at the primary and secondary flow inlets are negligible;
- the velocity of the mixed flow leaving the ejector is negligible;
- the losses in the nozzle, in the mixing chamber and in the diffuser are taken into account by using isentropic efficiencies η_n, η_m and η_d, respectively;
- the mixing loss factor ϕ_m remains constant throughout the mixing chamber;
- after exiting the nozzle, the primary flow fans out without mixing with the secondary flow up to at a certain cross section inside the constant area section (section *y-y*);
- the actual area occupied by the primary flow in correspondence of the section *y-y* is obtained by correcting the effective area occupied by the primary flow at the hypothetical pressure (equal to the secondary pressure inlet) according to the parameter ψ;
- the mixing process begins after the chocking of the secondary flow.

For each section of the ejector (nozzle throat, nozzle exit, start and end mixing section, shock wave section and diffuser exit), the model requires the iterative resolution of a system of equations based on mass, momentum and energy conservation. In addition, the thermodynamic properties are evaluated by the equation of state of the working fluid. The speed of sound *a*, reached in the ejector when the primary flow and secondary flow are chocked, can be obtained from its thermodynamic definition, without resorting to particular models:

$$a = \sqrt{\left(\frac{\partial p}{\partial \rho}\right)_s} \tag{3.3}$$

This is because the flow is everywhere single-phase. At the end of the calculation process, the ejector performance is measured in terms of the entrainment ratio ω and *COP*.

To validate the accuracy of the predictions by this model, experimental results by Huang et al. (1999) [10] with R141b are used. The working fluid is classified as isentropic vapour fluid. A value of 0.95 was considered for the isentropic efficiencies of the nozzle, suction chamber and diffuser, while the mixture loss coefficient is obtained from a relation as a function of the ejector area ratio. The model fits the experimental results committing relative error for the entrainment ratio within 9%.

Using the same benchmark [10], our results are practically the same. With the other dataset [11] the errors are higher, but still acceptable for a 1D model.

Table 3-5: Efficiencies assumed and errors of the simulations.

	Cardemil and Colle [8]	Our simulation		
Benchmark	[10]	[10]	[11]	[11]
Fluid	R141b	R141b	R236fa	R245fa
η_n	0.95	0.95	0.95	0.95
η_m	0.95	0.95	0.95	0.88
η_d	0.95	0.95	0.95	0.85
ϕ_m	G.D.	G.D.	0.92	0.9
$E_R(\omega)$ [%]				
Min	0.21	0.32	0.52	7.78
Max	8.88	8.85	10.64	17.78
Mean	3.06	3.17	6.87	13.66
Variance	4.87	4.94	14.57	8.21

The effectiveness of this model demonstrates the importance of considering the real gas effects in the evaluation of the ejector performance by means of numerical simulations. This has a beneficial effect also in the single-phase flow case.

3.1.1.6 Sensitivity analysis

The sensitivity analysis has been performed to access the variability of the predictions due to changes in the assumed parameters. Therefore, we have chosen the model proposed by Cardemil and Colle (2012) [8] because it has the major findings comparing to the Huang et al. (1999) [10] benchmark. For this evaluation, the isentropic efficiencies (η_n and η_m) and the expansion coefficient (ψ) have been selected and the ranges of variation are ±5 percentage points for the isentropic efficiencies and ±5% for the expansion coefficient. The results are shown in the Figure 3-2: the x-axis expresses the average absolute changes of the entrainment ratio ω compared to the reference (calculated) values.

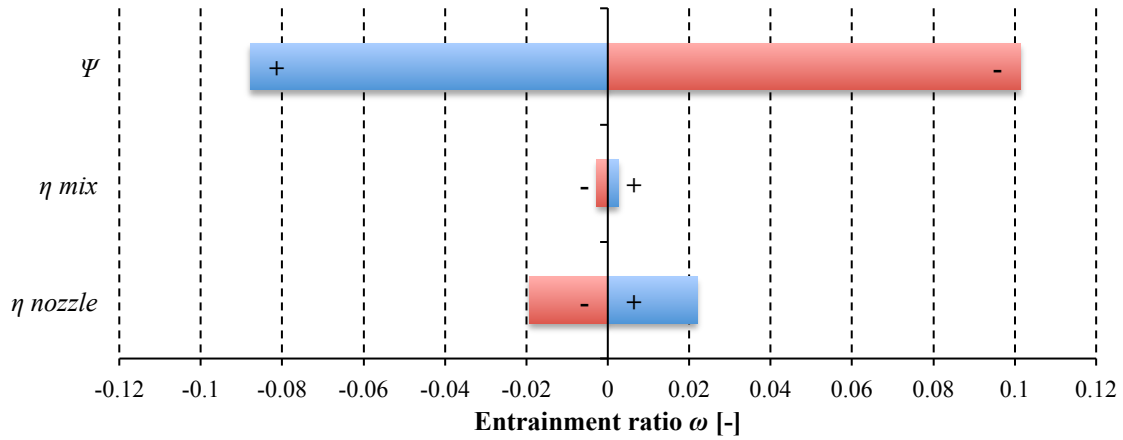

Figure 3-2: Sensitivity analysis on the assumed parameters.

The study shows that the model has a high sensitivity to the expansion coefficient ψ (-8.8÷10.1%) and a moderate sensitivity to the nozzle efficiency η_n (-1.9÷2.2%). The isentropic efficiency of the mixing chamber η_m, instead, has practically no effect on the prediction of the entrainment ratio (-0.3÷0.3%).

3.1.1.7 Results of the numerical simulations

To conclude the first part of the analysis about the single-phase 1D models, all the graphs concerning the comparison between the results of the models and those experimentally obtained are reported in the Figure 3-3. In this way, it is possible to obtain an immediate comparison among the different simulations.

The best performances are achieved with the models [3, 4, 8]. In particular, the model [8] is able to keep relative errors within 17.8% with all the experimental data, while the model [4] worsens its good performance with the R245fa benchmark, for which the mean relative error is equal to 17% and the maximum error exceeds the 22%. The model [3], instead, is somewhat penalized by some less satisfactory results obtained with R141b; however, around the 85% of the relative errors are less than 10%.

The model [5], which involves the use of variable heat capacity ratio, gets quite good results but the maximum error with R141b is very high (equal to 27.5%). However, the 75% of the relative errors are less than 10%. Its performance improves with R236fa.

It is also quite clear that the model [2] results in higher errors compared to the other implemented models. Moreover, its results are spread out and this is evidenced by a very high variance with all the benchmarks.

The comparison among the histograms of the models highlights that the models [4, 8] get the best results with the R141b benchmark, while R245fa provides the worst performance with all the models, especially with [2, 4, 8].

Single-phase model: Chen, Havtun and Palm (2014) [2]

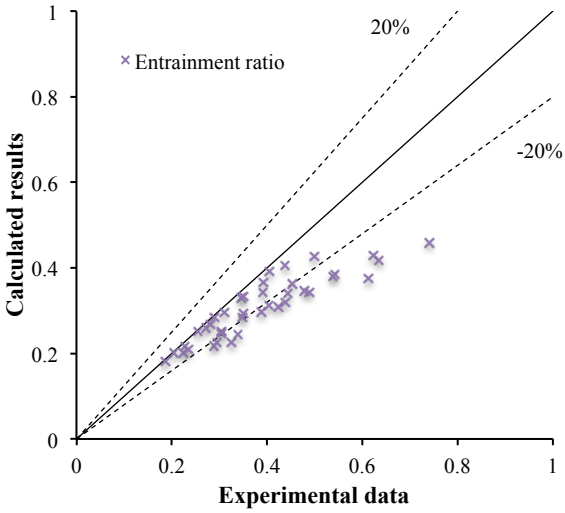

Experimental data from Huang et al. [10].

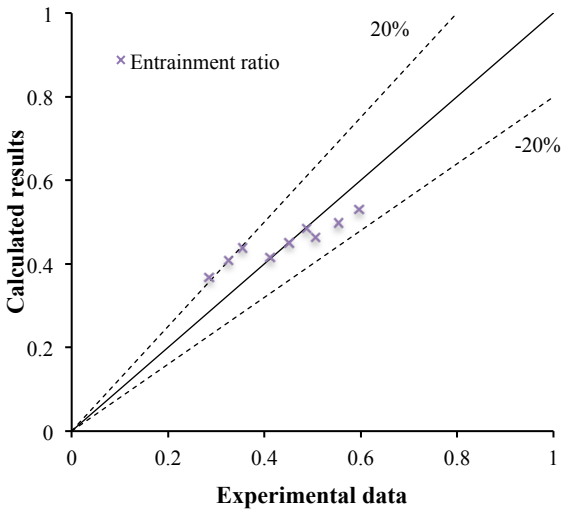

Experimental data from Ablwaifa with R236fa [11].

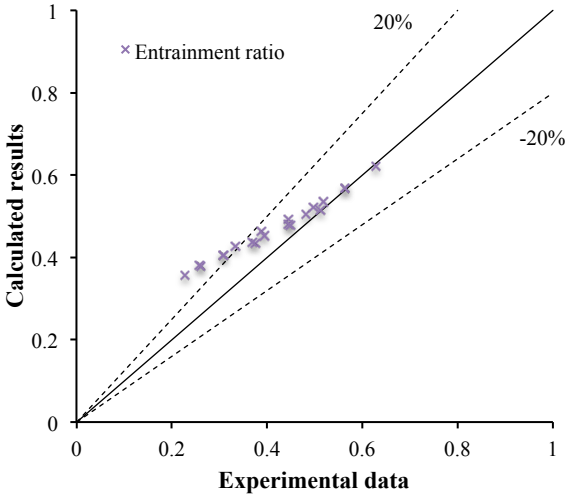

Experimental data from Ablwaifa with R245fa [11].

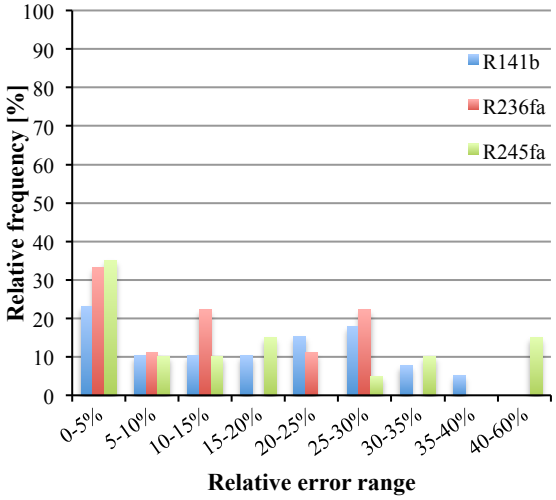

Relative frequency distribution of the errors.

Single-phase model: Chen, Liu et al. (2013) [3]

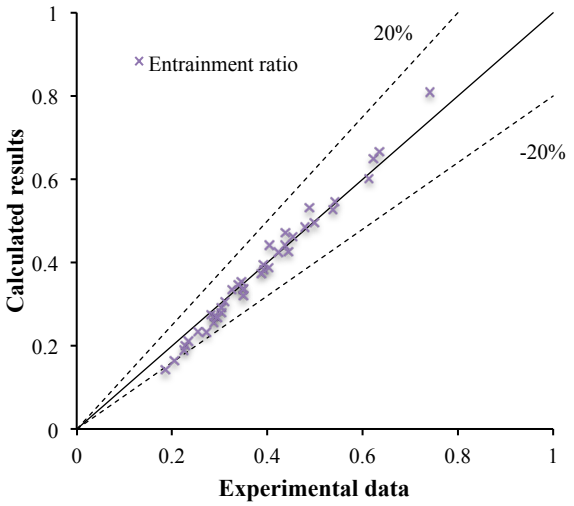

Experimental data form Huang et al. [10].

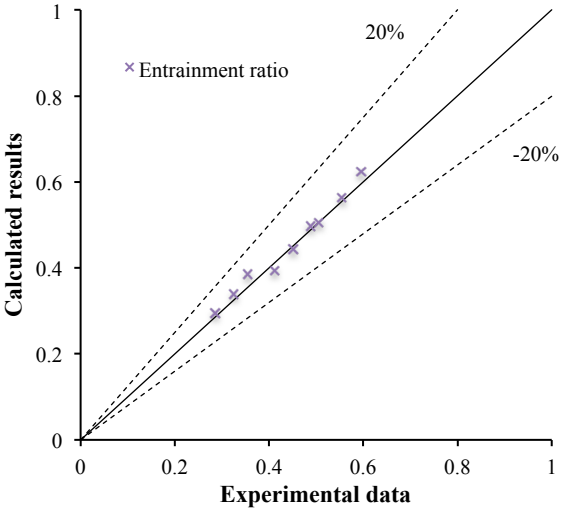

Experimental data from Ablwaifa with R236fa [11].

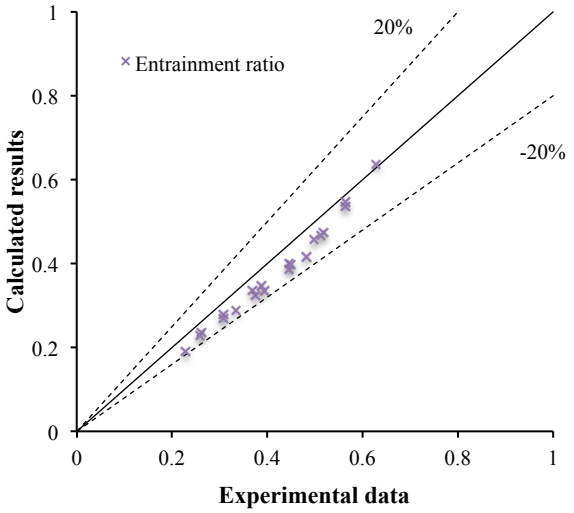

Experimental data from Ablwaifa with R245fa [11].

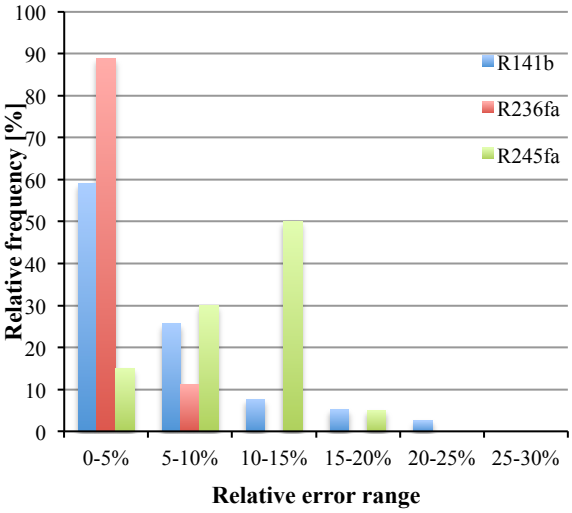

Relative frequency distribution of the errors.

Single-phase model: Zhu, Cai et al. (2007) [4]

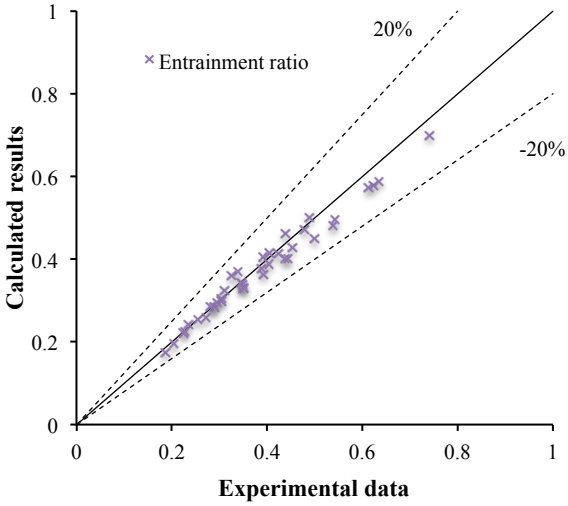

Experimental data form Huang et al. [10].

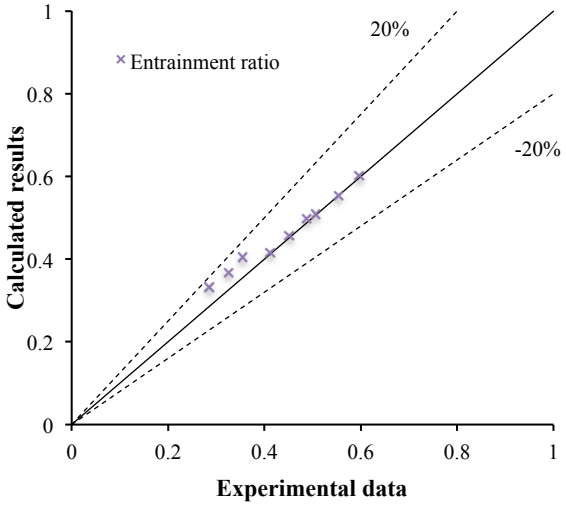

Experimental data from Ablwaifa with R236fa [11].

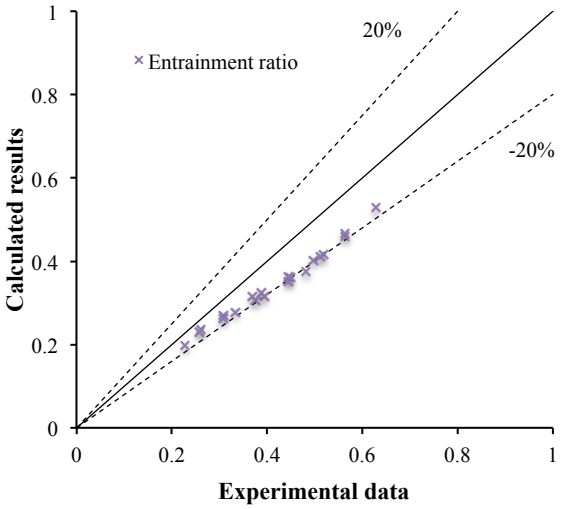

Experimental data from Ablwaifa with R245fa [11].

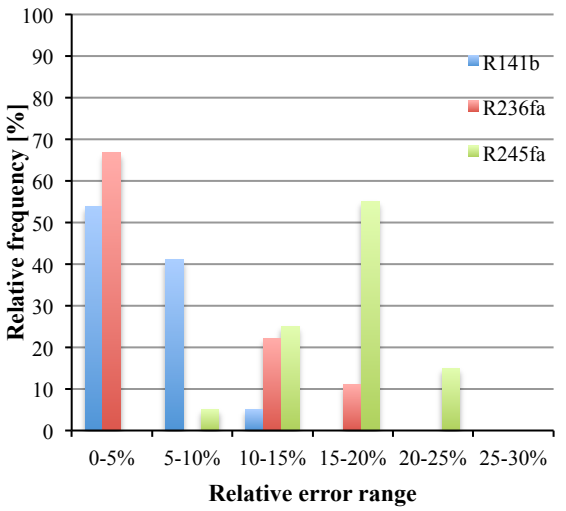

Relative frequency distribution of the errors.

Single-phase model: Kumar and Ooi (2014) [5]

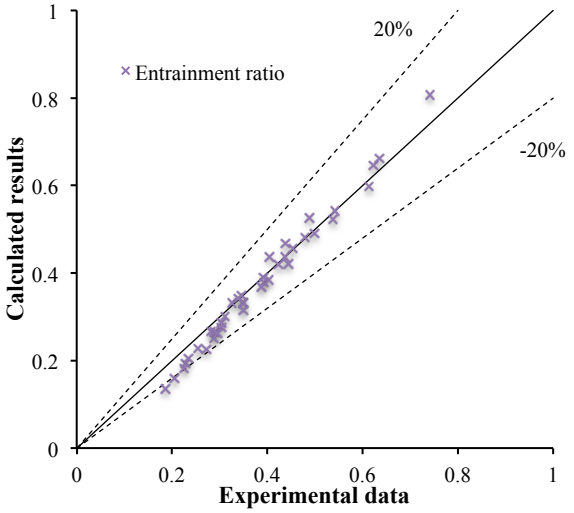

Experimental data form Huang et al. [10].

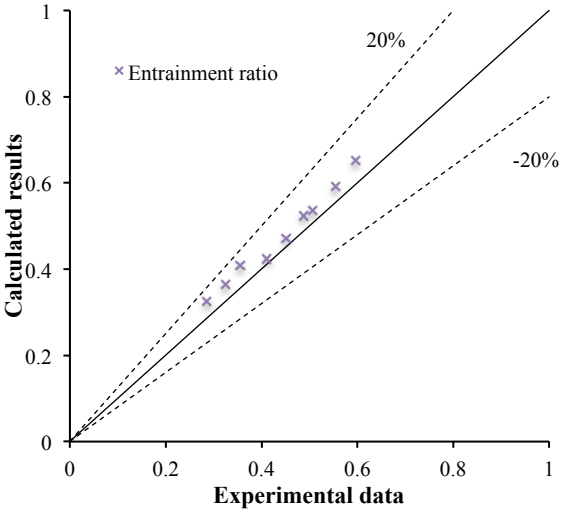

Experimental data from Ablwaifa with R236fa [11].

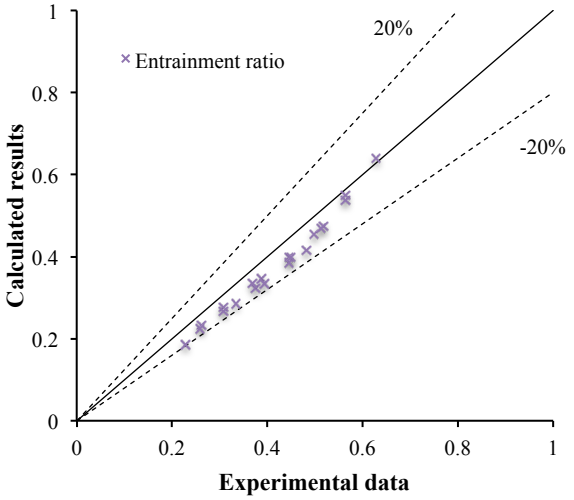

Experimental data from Ablwaifa with R245fa [11].

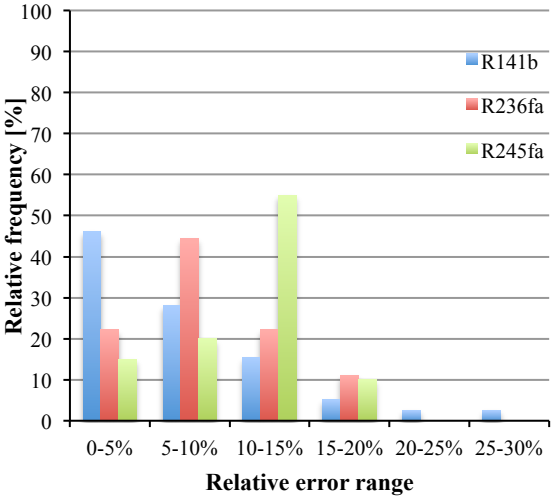

Relative frequency distribution of the errors.

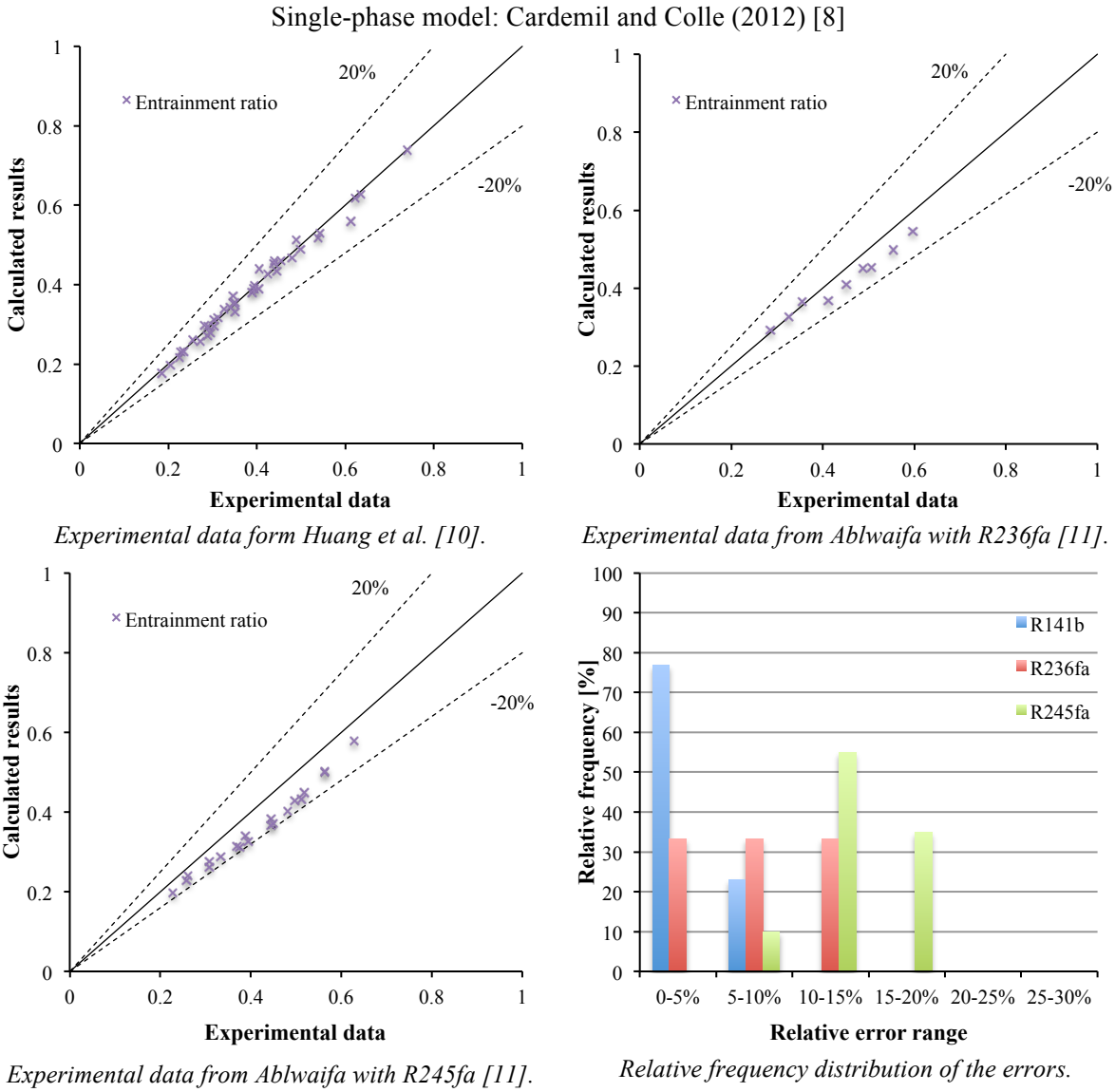

Experimental data form Huang et al. [10].

Experimental data from Ablwaifa with R236fa [11].

Experimental data from Ablwaifa with R245fa [11].

Relative frequency distribution of the errors.

Figure 3-3: Comparison of calculated results to experimental data and distribution of the relative errors.

3.1.1.8 Summary

In the Table 3-6 are summarized the main characteristics of the implemented single-phase models. Indeed, it collects the main assumptions on which the models are grounded, the required input parameters, the output results and the computational effort of each model. In particular, the computational effort is calculated on the basis of the time spent for the calculation, in relative terms, taking as reference the model [3].

Table 3-6: Summary of the main characteristics of the single-phase models.

Model	Main hypotheses	Input parameters	Output parameters	Computational effort
[2]	Isentropic expansion of the secondary flow from inlet to nozzle exit; Ideal gas with k=cost.	T_g , T_e , p_c k η_n , η_m , η_d	ω , ϕ , COP	11.6
[3]	Primary flow does not mixing with the secondary flow up to at y-y section; Ideal gas with k=cost. and C_p=cost.	T_g , p_g , T_e , p_e , p_c A_t , A_1 , A_2 k , C_p η_p , η_{py} , η_s , ψ_m	ω	1
[4]	Parameters uniformly distributed in the radius r direction; Secondary flow reaches chocking condition at cross section y-y; Ideal gas with k=cost.	T_g , p_g , T_e , p_e , p_c A_t , A_1 , A_2 k ψ_p , ψ_s	ω , COP	3.8
[5]	Secondary flow reaches chocking condition at cross section y-y; Normal shock fixed at the end of the mixing chamber; Ideal gas with $k=f(T)$.	T_g , p_g , T_e , p_e A_t , A_1 , A_2 η_p , φ_p , η_s , η_d	ω , T_c	1.4
[8]	Primary flow does not mixing with the secondary flow up to at y-y section; Mixing process start after the chocking of the secondary flow; Real gas effect.	T_g , p_g , T_e , p_e , p_c A_t , A_1 , A_2 η_n , η_m , η_d , ϕ_m	ω , COP	9.6

The results concerning the computational burden require some comment. First, we have chosen for all the models the same operating condition, corresponding to the critical mode operation. Thus, in these conditions, the model [3] is the fastest to run, followed by the model [5] although it requires an iterative cycle for each part of the ejector. The most onerous model is [2], penalized by the fact that requires a computational procedure with two iteration processes, one inside the other. It is important to remember, however, that it does not require geometrical parameters in input.

3.1.2 Two-phase models

3.1.2.1 Cardemil and Colle (2012) [8]

The purpose of this model is to present a new approach that allows to considering either dry or wet vapour working fluids. The main difference from the single-phase case resides within the calculation of the speed of the flow in specific section. For wet vapour ejectors, in fact, the chocking phenomenon that occurs in the two-phase flow is analyzed considering a model for the calculation of the speed of sound.

For the two-phase mixtures, the evaluation of the speed of sound is a complicated task. Indeed, the pressure and the temperature are not independent, but are related by means of the equation of equilibrium between the phases. There are several equilibrium models in literature. The authors suggested the use of the phase transfer relaxation model, developed by Lund and Flatten (2010) [21]. This model considers a hierarchy of hyperbolic relaxation models describing two-phase flows in pipelines. The hierarchy is characterized by the number of equilibrium assumptions imposed:

1. pressure equilibrium (p equil.);
2. temperature equilibrium (p, T equil.);
3. phase transfer equilibrium (p, T, μ equil.).

The relaxation two-phase flow model consists of six equations: the momentum conservation equation, the volume advection equation and the mass and energy conservation equations for each phase. It is possible to derive the wave velocity applying the eigenvalues analysis on this system of equations (for further information, please refer to [21, 22]). In the final analysis, thanks to this study, for each new level n of equilibrium condition added, the mixture sound velocity can be expressed as:

$$\hat{c}_{n+1}^{-2} = \hat{c}_{n}^{-2} + S_n \tag{3.4}$$

where S_n can be written as a positive sum of squares.

In order to verify the effectiveness of the 1D model applied to steam ejectors and to transcritical CO_2 ejectors, the results predicted were compared to the experimental data given in Eames et al. (1995) [23] and Xu et al. (2011) [12], respectively. The relative error for the *COP* of the steam jet refrigerator (wet vapour) [23] is within ±8%. No information was provided about the entrainment ratio prediction.

With regard to the transcritical CO_2 ejectors [12], in which a two-phase mixture with low vapour quality flows through the ejector, a fixed geometry ejector under a wide range of operating conditions was tested. The relative error for the entrainment ratio is within ±2.5%.

We have tested the model with the same CO_2 benchmark [12]. The results, in terms of prediction of the entrainment ratio ω, are a little different than those of the authors. The relative errors are higher, but quite good compared with the other examined models.

The Figure 3-4 shows the results of the numerical analysis and the distribution of the relative errors:

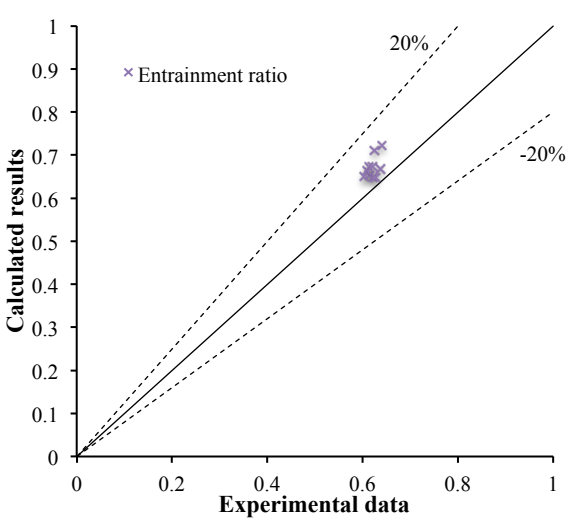

Experimental data from Xu et al. [12].

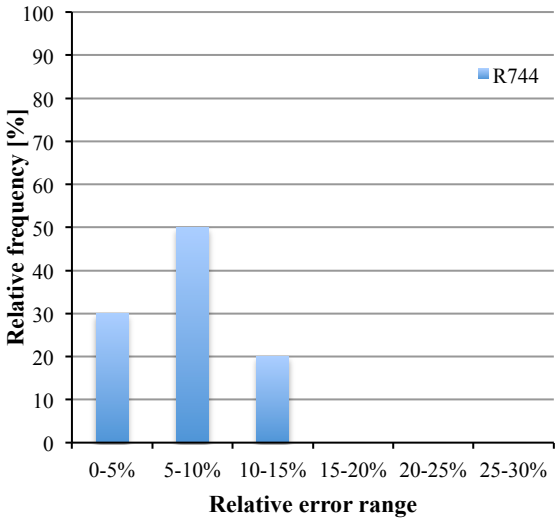

Relative frequency distribution of the errors.

Figure 3-4: Comparison of calculated results to experimental data and distribution of the relative errors.

Table 3-7: Efficiencies assumed and errors of the simulations.

	Cardemil and Colle [8]		Our simulation
Benchmark	[23]	[12]	[12]
Fluid	H_2O	CO_2	CO_2
η_n	0.85	0.95	0.95
η_m	0.95	0.95	0.95
η_d	0.95	0.95	0.95
ϕ_m	0.77	1	1
$E_R(\omega)$ [%]			
Min		0.60	3.38
Max	n.a.	2.48	13.78
Mean		1.42	8.04
Variance		0.40	10.98

The range of applications of this model even covers two-phase flow regimes and thus it appears to represent an improvement in ejector modelling. However, as the authors themselves recognize, the interaction between the primary and secondary flows is not completely describable because the oblique shock and other phenomena are impossible to model through a one-dimensional analysis. Further fluid dynamics information can only be obtained through CFD simulations [8]. Anyhow, a numeric solver is required, due to the non-linear system of equations of which the model is constituted.

A separate discussion deserves the problem concerning the relaxation two-phase model and its equilibrium assumptions. This analysis will be addressed in the next section.

3.1.2.2 Two-phase flow model: equilibrium assumptions and calculation of the speed of sound

As already mentioned, the relaxation two-phase flow model [21], on which the 1D model relies, is based on three equilibrium conditions. The model proposed by Cardemil and Colle (2012) [8] considers that both the pressure and the temperature are at equilibrium, but not the chemical potential of the phases. Hence, the two-phase speed of sound calculation takes on a simplified form.

According to the authors, we also have relied on the same assumption. Thereby, several problems have been encountered. Indeed, the integration of the simplified two-phase model flow and the thermodynamic model has not led to convergence. The reason seems to lie in the fact that the speed of sound is underestimated and this causes problems in the resolution of the non-linear system of equations of the 1D model.

Therefore, we have implemented the two-phase model assuming the temperature, pressure and chemical potential equilibrium of the phases. Please note that the choice was dictated by numerical reasons and not for physical considerations. In this way, we were able to carry out our simulations. However, it was still necessary resort to numerical techniques, like the under relaxation method, to ensure numerical stability, but penalizing the rate of convergence. In particular, the use of under relaxation factor has been necessary in the calculation of the speed of sound at the nozzle throat, as in the following formula:

$$c_t = c_{t,old} + \alpha \cdot \left(c_{t,calc} - c_{t,old} \right) \tag{3.5}$$

The relaxation factor α is assumed equal to 0.8.

The Figure 3-5 shows an example of the relative error and speed of sound trends during the simulation for a determined operating condition. In particular, the Figure 3-5a illustrates the case of the single-phase model with R141b: it has not convergence or stability problem. The Figure 3-5b show the result of the implementation of the two-phase model using the under relaxation factor. It may be note that in the latter case the function trends are however more discontinuous.

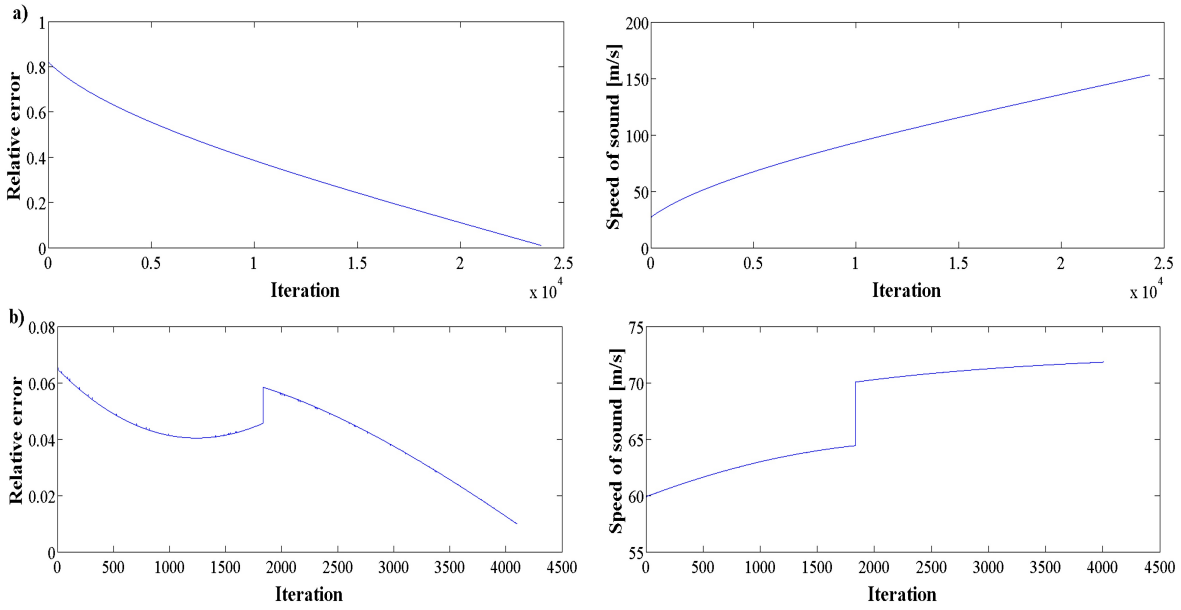

Figure 3-5: Relative error and speed of sound trends during the numerical simulation. a) single-phase model; b) two-phase model with under relaxation factor.

These numerical problems have not been mentioned in the paper. Moreover, it would be interesting to enquire if the use of the p, T, μ equilibrium assumption has also a physical meaning.

3.2 Effect of the working fluids on the ejector performance

As reported by the previous review (please refer to the Chapter 1), the refrigerants used in the ejector refrigeration systems seem to have a great impact on the ejector operation. In this section, we want evaluate the influence that the different working fluids have on the performance of the ejector, testing some of the most common refrigerants employed in the ERS. For this purpose, we have taken as reference the academic papers published by Kasperski and Gil (2014) [1], in which some hydrocarbons were selected and their performance were compared with those of the halocarbons R141b and R134a.

3.2.1 Numerical simulation: assumptions

Our analysis is conducted through the Chen, Havtun and Palm (2014) [2] model and, according to [1], the operating conditions assumed are: T_e = 10°C, T_c = 40°C and T_g = 70÷180°C (if available, based on the critical temperature of the fluid). The efficiency coefficients are assumed as η_n = 0.95, η_m = 0.85 and η_d = 0.9. The Table 3-8 summarizes the assumptions made for the numerical simulations in terms of operating conditions and isentropic efficiencies.

Table 3-8: Operating conditions and isentropic efficiencies assumptions.

Generator temperature [°C]	Evaporator temperature [°C]	Condenser temperature [°C]	Nozzle efficiency [-]	Mixing chamber efficiency [-]	Diffuser efficiency [-]
70÷180	10	40	0.95	0.85	0.9

3.2.2 Numerical simulation: working fluids

The tested refrigerants have been selected from those described in the Section 1.3: propane (R290), butane (R600), iso-butane (R600a), pentane (R601), iso-pentane (R601a), R134a, R141b and R152a.

Each refrigerant has a unique saturated vapour temperature-entropy line: R134a, R152a and R290 have negative *T-s* slopes (wet vapour), while the other refrigerants R141b, R600, R600a, R601 and R601a have positive *T-s* slopes (dry vapour). As already remarked in the Section 1.3.2, the refrigerants with large positive *T–s* slopes are more desired working fluids due to the absence of phase transition during the expansion process. This property is particularly important for the hydrocarbon compounds. In fact, in negative slope case, the refrigerant is more probably to stay at metastable states initially [24]. The domain of existence of a metastable fluid is between the saturated vapour line and the spinodal line corresponding to the limit of intrinsic phase stability for superheated vapour. In the metastable supersaturated vapour zone, the tendency of the small droplets to evaporate overcomes the thermodynamic driving force for vapour to condense: the small droplet would shrink and the vapour phase remains. However, in the case that the droplet reaches the critical radius, the droplet grows instantaneously and triggers the homogeneous nucleation of droplets. One possible consequence is an extremely rapid rate of liquid generation and thus explosive condensation into a stable two-phase state (for further information, please refer to [25, 26]). This would cause significant performance deterioration and potentially even hurt the life of equipment and people nearby [26] and the flammability of HC compounds may worsen the situation.

Among the tested refrigerants, the pentane R601 is the one with the largest positive *T-s* slopes. In addition, it has a relatively high critical temperature (T_{cr} = 196.7°C), which provides a wide operating temperature range above the ambient temperature. Thus, it has great potential of harnessing low-grade thermal energy also in hot climates [26].

3.2.3 Numerical simulation: results

The numerical results of our simulations are reported in the Figure 3-6 and a detailed analysis is provided, but first a brief explanation is needed. As is well-known from the literature, the performance of an ejector refrigeration system significantly depends on its working fluid [1], working conditions [17] and ejector geometrical configurations [27, 28]. It should be noted that the effects described in this discussion refer to optimum performance evaluation with a corresponding suitable ejector area ratio ϕ (A_2/A_t), which are different from a fixed-geometry ejector working under different conditions [2]. These assessments have been widely presented in the Chapter 1 and they will be explained in detail through the application study of the Chapter 4.

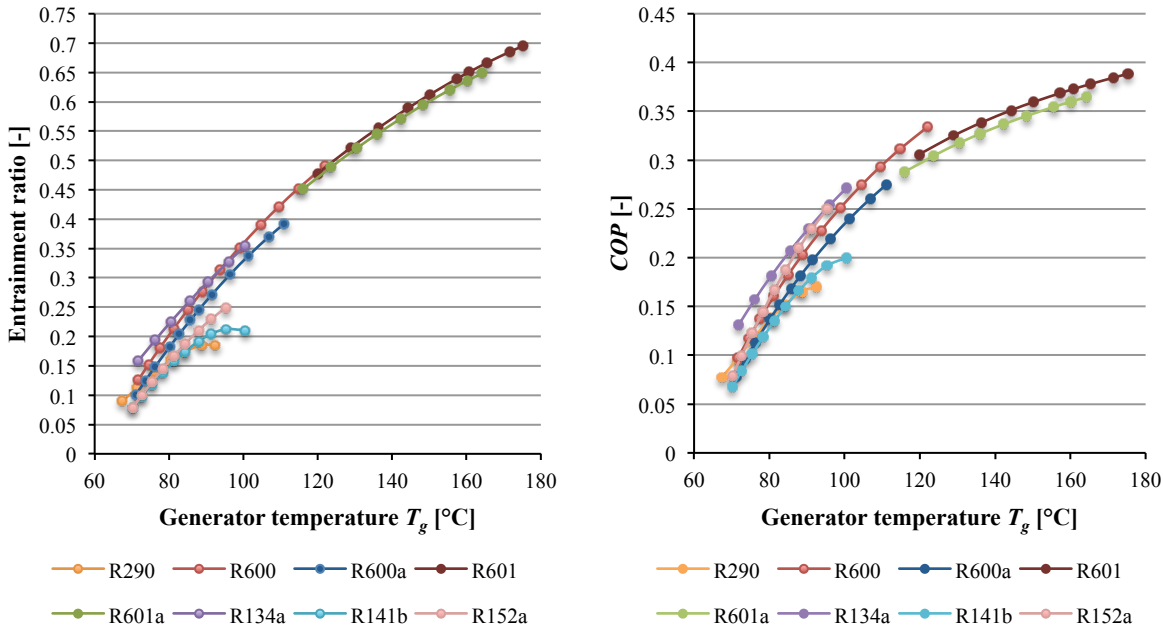

Figure 3-6: Entrainment ratio and COP trends for halocarbon and hydrocarbon compounds.

The Figure 3-6 shows the entrainment ratio ω and the *COP* trends in function of the generator temperature T_g, with the evaporator and condenser conditions fixed at T_e = 10°C and T_c = 40°C. The calculated *COP* from the model increase nearly linearly with increasing of T_g, which are the same trends determined from experiments carried out by Yapici (2008) [17] with R123. It is clear that the entrainment ratio ω and the *COP* increase with a rise in T_g. In fact, the pressure and enthalpy of the primary flow increase with the T_g, and a higher T_g causes a better entrainment effect at a given T_c and T_e. More secondary flow could therefore be entrained into the ejector, resulting in a higher ω. This is obtained through an adjustment of the area ratio to provide sufficient flow area for the flow [29]. For a fixed-geometry ejector, instead, each ejector with a specific area ratio ϕ (A_2/A_t) has its own optimum T_g, at where the maximum *COP* could be obtained [27].

However, the analysis shows that the halocarbon refrigerant R134a is the best choice for ERS that work at low generator temperature (T_g = 70÷100°C), both in terms of entrainment ratio (ω = 0.16÷0.35) and coefficient of performance (*COP* = 0.13÷0.27). With regard to the *COP*, the more

environmentally friendly refrigerant R152a can be a good solution for medium temperatures (T_g = 90 ÷ 100 °C). However, the halocarbon compounds tested have a limited range of operating conditions due to the low critical temperature.

Thus, in order to work in a higher range of generator temperature, the hydrocarbons represent a valid alternative. The graphs show that each hydrocarbon has its own operating range related to the molecular mass of the compound, as pointed out by [1] too. In fact, the generator temperature range increase with the hydrocarbon heaviness, from the propane (R290) to the pentane (R601). In particular, the working fluid R290, able to work with T_g = 70÷95°C, loses the competition in terms of performance with the halocarbon compounds, but the heavier hydrocarbons achieve better performance at high generator temperature (T_g = 100÷180°C). In these operating conditions, the best working fluids are R600 at medium temperatures (T_g = 100÷130°C) with COP = 0.23÷0.34 and R601 at high generator temperatures (T_g = 130÷180°C) with COP = 0.30÷0.39.

In this range of generator temperature, the heat source for the vapour production could be provided by waste heat and solar energy. Considering a solar drive, several types of collectors can be applied according to the temperature demand [30, 31]:

Table 3-9: Available solar collectors according to the generator temperature.

Generator temperature [°C]	70 ÷ 100	100 ÷ 150	150 ÷ 180
Solar collectors	Flat-plate solar collector	Evacuated tube solar collector	Parabolic-trough concentrating collector

In Table 3-10 are reported the plant applications related to these operating conditions. The ejector systems can be mainly used in air conditioning applications (motor vehicle, office, building), but also in domestic, commercial and industrial (chemical, pharmaceutical,…) fields for refrigeration purpose [32].

Table 3-10: ERS applications according to the generator temperature.

Generator temperature [°C]	70 ÷ 100	100 ÷ 150	150 ÷ 180
Application	Air conditioning (motor vehicle, office) Refrigeration (domestic)	Air conditioning (office, building) Refrigeration (commercial, industrial)	Air conditioning (building) Refrigeration (commercial, industrial)
Best refrigerant	R134a, R152a	R600	R601

However, the operating conditions and the working fluid selection for a specific application is affected by several factors, such as the economic feasibility (in order to justify the temperature level), the heat source availability, the environment (that influence the condition to which release heat) and the evaporator conditions (that determine the cooling effect and thus the potential application).

3.2.4 Numerical simulation: sensitivity analysis

The sensitivity analysis has been performed in order to determine the influence of the isentropic efficiency coefficients (η_n, η_m and η_d) on the numerical results. For this evaluation, the range of variation of the isentropic efficiencies is ±2.5 percentage points. The results are shown in the Figure 3-7 and **Errore. L'origine riferimento non è stata trovata.**Figure 3-8, in which the x-axis expresses the average absolute changes of the entrainment ratio ω and *COP* compared to the reference values, respectively.

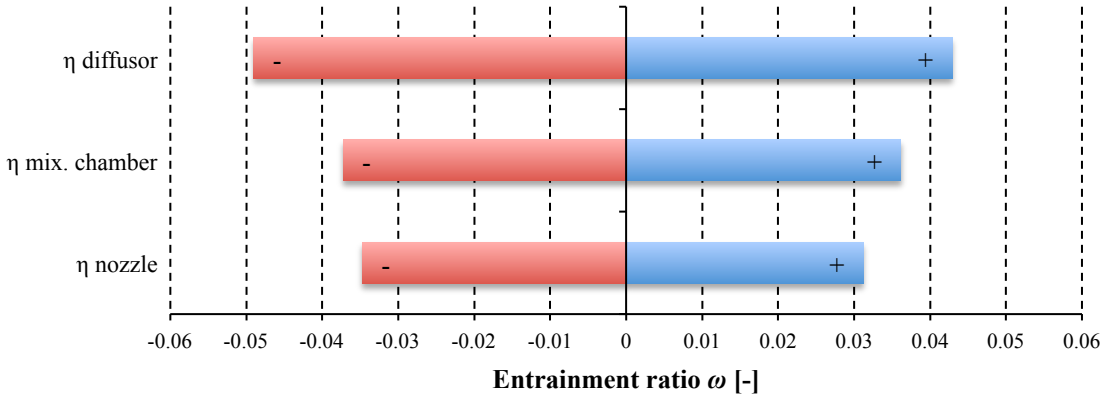

Figure 3-7: Sensitivity analysis on the assumed parameters of the entrainment ratio.

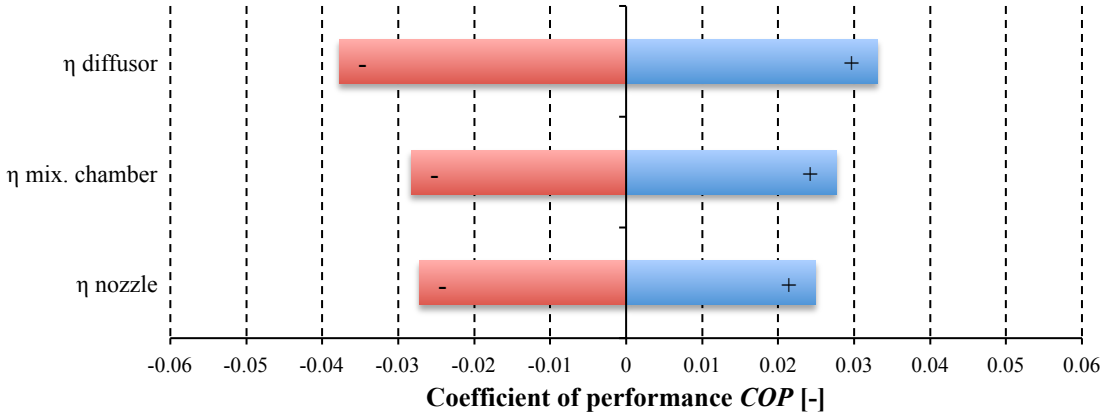

Figure 3-8: Sensitivity analysis on the assumed parameters of the coefficient of performance.

The study shows that the model has a quite high sensitivity to the isentropic efficiencies, especially to the diffuser efficiency η_d, both for ω and *COP*. In fact, varying the isentropic coefficient by only ±2.5 percentage points, the predicted value of the entrainment ratio undergoes a variation in the range of -4.90÷4.29% while those of the *COP* is equal to -3.78÷3.31%. The isentropic efficiency of the mixing chamber η_m and of the nozzle η_n have a slightly lower effect on the prediction of the entrainment ratio (-3.72÷3.62% and -3.47÷3.12%, respectively) and of the *COP* (-2.83÷2.77% and -2.72÷2.49%, respectively).

3.2.5 Numerical simulation: effect of the operating conditions

We have also evaluated the effect of the other operating conditions on the ERS performance, in terms of the entrainment ratio and *COP*. The generator temperature is now assigned and equal to 90°C. This value was chosen so that it was feasible by all the tested fluid. The ranges considered for the evaporator and condenser temperature are T_e = 5÷15°C and T_c = 30÷50°C, according to

several literature works [33, 34]. The numerical simulation assumptions are summarized in the Table 3-11:

Table 3-11: Operating conditions and isentropic efficiencies assumptions.

Case	Generator temperature [°C]	Evaporator temperature [°C]	Condenser temperature [°C]	Nozzle efficiency [-]	Mixing chamber efficiency [-]	Diffuser efficiency [-]
1	90	5÷15	40	0.95	0.85	0.9
2	90	10	30÷50	0.95	0.85	0.9

The results are shown in the Figure 3-9:

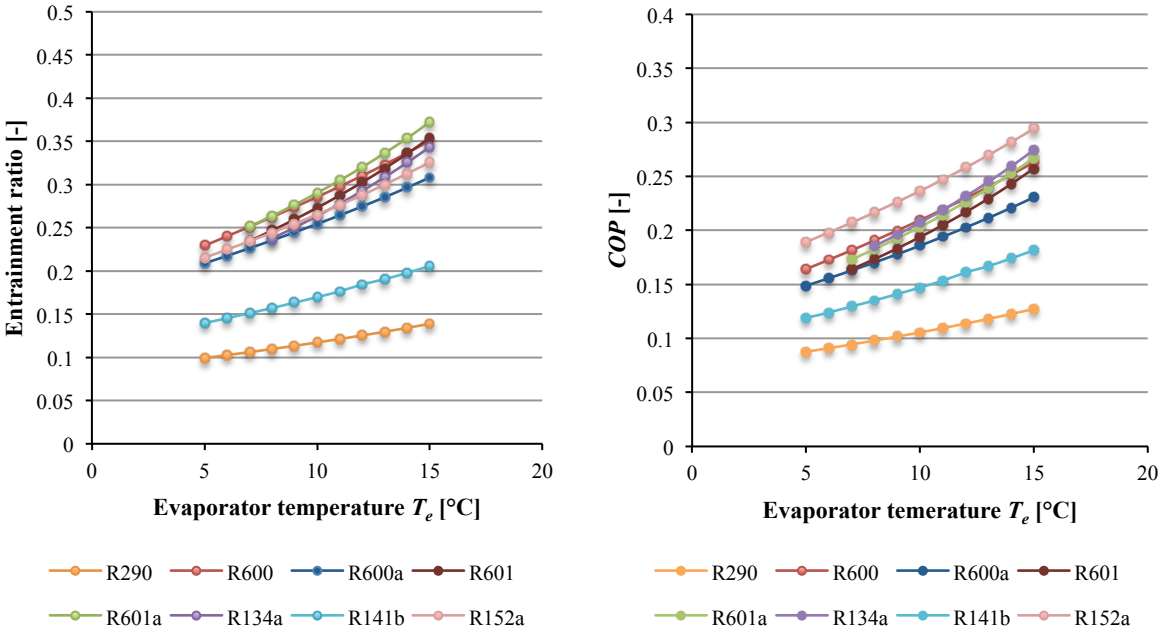

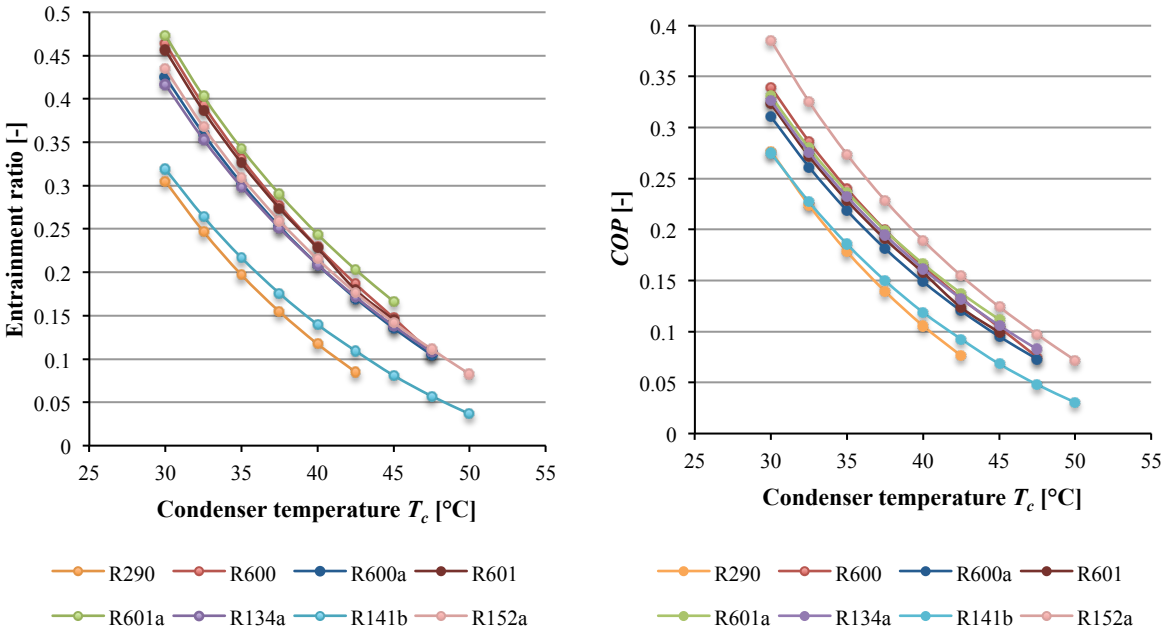

Figure 3-9: Entrainment ratio and COP trends in function of the evaporator and condenser temperature.

According to the results, an increase in T_e leads to a rise in the entrainment ratio ω and *COP*.

However, the condenser temperature has more influence than the evaporator temperatures on the ejector performance. For a fixed-geometry ejector, it is known that there exists a critical condenser pressure p_c*: the entrainment ratio is independent of the condenser temperature T_c when p_c is lower than the critical value; a slightly further increase of p_c beyond p_c* will cause ω to drop sharply (as described in the Section 1.2.2). With a variable-geometry ejector, instead, an increase in T_c leads to a gradual decrease in ω and *COP*. This is because less secondary flow can be entrained into the ejector if the backpressure increases [2]. Another reason might be that an increase in the p_c will force the shock to pass through the mixing section and move towards the nozzle exit, which limits the entrainment effect [35].

As a result, a high T_e and a low T_c will always be good for the ejector operation and the whole system performance. However, the evaporator and the condenser temperature should be chosen according to the desirable and feasible cooling effect and on the basis of the environmental conditions, respectively.

3.3 Lumped parameter models: summary

In this section, a detailed analysis on the LPM of ejector is carried out. First, we have selected five thermodynamic models that have been implemented and validated with several benchmarks from the literature. With the tested models, quite good results have been achieved. Indeed, the mean values of the relative errors of the models are about between 3% and 17%. These results are obtained through quite easy modelling technique with a low computational effort, thanks to their simplified approach.

Whereupon, the model proposed by Chen, Havtun and Palm (2014) [2] is selected in order to carry out a numerical analysis, testing several working fluids at different operating conditions. It was found that the entrainment ratio and the *COP* increase with increasing of generator temperature and evaporator temperature, while an increasing condenser temperature leads a decrease in the ejector performance. For this occurrence, the ejector area ratio needs to be adjusted to maintain optimum

performance of an ERS under different working conditions. The variable-geometry ejectors play an important role in achieving optimum performance and widen the operating conditions. Indeed, a variable-geometry ejector seems a very promising solution to ensure that the ERS operates at its optimum conditions [2, 27].

For each fluid is then found an application field according to the performance reached in specific ranges of operating conditions. The hydrocarbon compounds R600 and R601 are good solutions for the ERS that operated at high generator temperature (T_g = 100÷150°C), reaching COP = 0.3÷0.4. While, for T_g less than 100°C, the environmental friendly halocarbon compounds R134a and R152a achieved the best performance (COP = 0.15÷0.25).

As a result of our analysis, it was observed that the ejector efficiencies are crucial parameters in the LPM model. Indeed, the sensitivity analysis has shown that the model has high sensitivity to the isentropic efficiencies, leading remarkable variations for the entrainment ratio and COP. The loss coefficients are supposed constant but it is known form literature [36, 37] that they depend upon the working fluid, the operating conditions, the geometry and the local phenomena. Thus, the performance prediction of the LPM can be improved using variable efficiencies. For example, a validated CFD ejector model can be used to determine the efficiencies of the ejector components and the resulting efficiency maps can be used to take into account the local flow behaviour in lumped parameter models [38]. In this way, CFD approach represents a useful tool for ejector performance analysis and optimization and as a supporting tool for thermodynamic models improvement. This integrated LPM/CFD approach (ILPM-CFD) will be presented in the Chapter 5.

Chapter 4

Computational Fluid Dynamics model

This chapter discusses the CFD modelling approach. The applications of CFD analyses are numerous and used in many industrial sectors. In fact, it is a powerful investigative tool for supporting product and process development, prototyping, verification, optimisation and innovation [1]. Like all other research and design tools, the CFD is affected by errors and uncertainties. Thus, appropriate standards and protocols for increasing confidence and reliability need to be applied. In the introductory part of this chapter, we present a methodological approach to qualify CFD, named Q^3 approach, proposed by Colombo et al. [1]. According to this modus operandi, we will make use of some global and local experimental measures, taken from literature, in order to validate the results obtained through the CFD simulations. Thus, the validated CFD model will be employed with knowledge for analyze and investigate some aspects of the fluid dynamics behaviour of the ejectors. Therefore, the chapter is structured as follow. The first part concerns the quality assurance in CFD approach, the second part reports and explains the validation process of the CFD model and in the last section an applicative case is studied through the validated CFD model.

4.1 Quality assurance in CFD: the Q^3 approach

4.1.1 Introduction

The Quality Assurance (Q.A.), understood as methodological approach, is a monitoring tool, consists of protocol procedures and management method, able to ensure the achievement of excellent standard and reproducible results [2, 3].

The CFD, as Research and Development (R&D) instrument, requires proper standard since it is associated to errors and uncertainties, in order to enhance the reliability of its results. In particular, Q.A. is mainly needed in CFD for increasing accuracy and reliability in three areas [3]:

- produce qualified results to support design and innovation;
- reduce cost and time in the design or verification process;
- produce acceptable results by governmental regulations.

Thus, the quality improvement in CFD requires application of best practices and software recommendations, based on theoretical considerations, practical experience and peer reviews.

The Quality Assurance in CFD is very important both for the basic and applied research [1]. At the international level, the Q.A. procedures are generally developed in a regional context. In Europe, there are two meaningful experiences, such as the European Research Community On Flow, Turbulence And Combustion (ERCOFTAC) [4] and the QNET-CFD [5]. In the United States, the

Idaho National Laboratory (INL) in collaboration with the American Society of Mechanical Engineers (ASME) have proposed a Q.A. approach focusing in the nuclear applications [3].

However, all these methodologies are not very generalizable. The new CFD demands, arising from the many industrial sectors and application fields in which it is employed, require a new approach able to ensure CFD reliability independently, as far as possible, of the different applications [2, 3]. This aspect is captured by the approach to quality in CFD proposed by Colombo et al. [1] named Q^3 approach.

4.1.2 Q^3 approach: description

The Q^3 approach is focus on considering three different dimensions of quality [2, 3]:

- quality of software, which is attributable to developers and/or software houses (commercial code, in-house and academic code, open source code). The commercial codes are the best from this point of view because their software development is based on quality assurance.
- quality of users, ranging from the basic-user, a technician with a poor fluid dynamic background, to the user-analyst, an analyst with high level of competence and knowledge.
- quality of process, which includes procedures and protocols in order to ensure reliable results.

The quality of the process is the core of the Q^3 approach and it is the most complex aspect because it would lead to the definition of a standard protocol for driven the process of analysis.

In the present work, the first dimension of the Q^3 approach is assured by the use of the commercial software ANSYS 15.0 Fluent® as the CFD solver, the second dimension is provided by the university background and the third dimension is guaranteed by the use of the standard protocol proposed in [1] as a process control tool.

4.1.3 Q^3 approach: protocol structure and CFD cycle

The protocol of analysis is an instrument through which the process quality may be achieved. This methodology is based on a cyclic process. The main steps of the CFD cycle of analysis may be detailed in the following four phases [1-3]:

i. Phase 1: problem analysis. The engineering problem and the main quantities of interest are clearly defined in order to facilitate the physical model's selection.

ii. Phase 2: conceptual model setting. The mathematical problem is identified and simplified according to the specific goals of the CFD project.

iii. Phase 3: model building and solving. The CFD approach is defined and implemented, reporting the details of the numerical model used for the analysis.

iv. Phase 4: problem evaluation, assessment and review. The analysis of the results, calculation validation and revision of the model are completed, accuracy and quality control are checked and geometrical, modelling and physical revision are discussed.

By introducing the critical revision of the overall steps, the process of analysis stops being linear and becomes a cyclic process.

The key passage of this process is the phase 4. The analysis of the results must be done with great care. It requires the awareness of all the uncertainly sources, the evaluation of the numerical convergence and the assessment of the model accuracy through the comparison between the

numerical results and other fount of information (literature data, experimental data, physical theories) [2]. If experimental or literature data are not available, a turnaround procedure needs to be introduced in order to guarantee the reliability of the CFD calculations [1]. At the end of the CFD cycle, the revision of the model is required. In particular, the review must focus three aspects [2]:

- the assumptions made in the transition process from the engineering problem to the mathematical problem (i.e. geometric simplification);
- the physical modelling (i.e. working fluid assumptions, boundary conditions);
- the numerical modelling (i.e. discretization schemes, mesh).

The Q^3 approach to quality in CFD increases the reliability of industrial CFD, promotes CFD application for supporting processes or product design and contributes to the conversion of research results into real innovation [1], reducing cost and design time.

4.2 CFD modelling: validation

4.2.1 Phase 1: problem analysis

4.2.1.1 Frame of action and general purposes

The CFD model is used for the fluid dynamics analysis of the ejector and as a supporting tool for the integrated lumped-parameter/CFD ejector model (ILPM-CFD) [6]. In the present chapter, a CFD modelling approach is presented and employed in an applicative case study. In the Chapter 5 the integrated model will be implemented, using the validated CFD model to generate efficiency maps and correlations for the LPM models presented in the Chapter 3.

4.2.1.2 Problem identification

The objects of study of the present thesis are the ejector used in refrigeration systems. In this section, the CFD model focuses on the supersonic single-phase ejectors (the physical aspects of the flow have been described in the Chapter 1). Therefore, a turbulent compressible flow is expected inside the ejector. The energy equation and the turbulent model are needed to the resolution of the problem, but the multi-phase modelling is not required.

From this study, we expect a better understanding in the flow and mixing processes within the ejector and in the effects of operating conditions and geometry on its performance. However, we also presume that the goodness of the solution depends on simulation settings, such as turbulent models [7, 8] and boundary conditions. Thus, a validation process is required to ensure the reliability of the results.

4.2.2 Phase 2: conceptual model setting

4.2.2.1 Specific goals of the CFD analysis

The main goals of the analysis are:

- validate the CFD model, providing guidelines on CFD simulations about, in particular, turbulent models, boundary conditions and mesh settings;
- apply the validated model on a case-study of interest in order to analyze the fluid dynamics behaviour under varying operating conditions and geometry (Section 4.3);
- evaluate ejector efficiencies for different operating conditions in order to understand how local flow structures affect ejector performance and provide efficiency maps for the ILPM-CFD model [9] (Chapter 5).

In the follow-up of this section, we will focus on the first goal. The features of the other aims will be described in their own section.

4.2.2.2 State-of-art of CFD in the field

The state-of-art of CFD modelling of ejectors has been presented in the Chapter 2.

4.2.2.3 Expected results and benchmark used

The validation of the CFD model is carried out by means of the experimental data set provided by Sriveerakul et al. (2007) [10]. The benchmark is composed of both global and local measures. In particular, the entrainment ratio and the measurements of the wall static pressure along the ejector are provided. The local parameters are essential in order to verify the correspondence between the experiments and the numerical simulations. In fact, a not validated CFD model is able to correctly determine the global parameters, but it might not accurately estimate the main internal effects (i.e. mixing losses and friction losses) [9].

The experimental investigation concerns a steam ejector that works under different working conditions (T_g = 120÷130°C, T_e = 5÷15°C and T_c = 24÷40°C) and with different geometry configurations. The ejector consisted of four parts (primary nozzle, mixing chamber, constant-area throat and subsonic diffuser) and designed with CPM scheme, as shown the Figure 4-1:

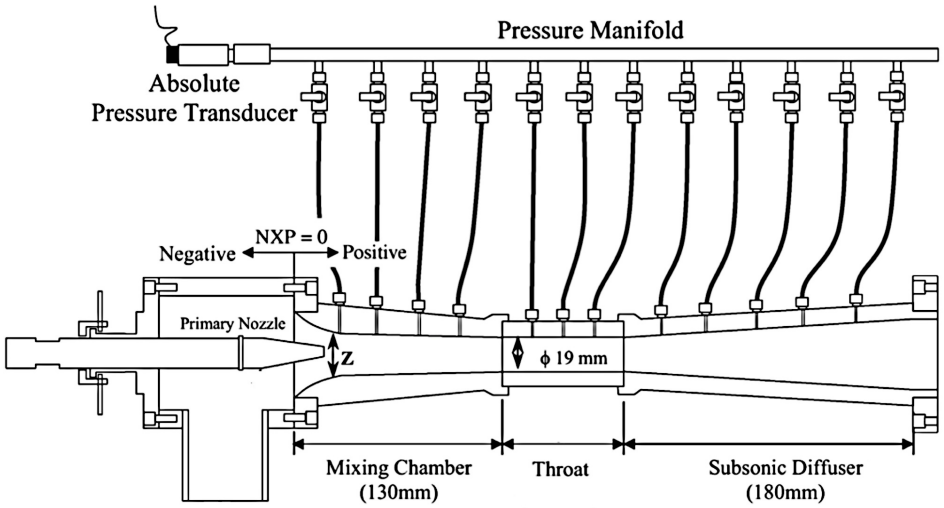

Figure 4-1: Schematic diagram of experimental ejector – taken from [10].

The nozzle was fixed at NXP = 35 mm and the diffuser was thought to have a very small influence on ejector performance. The significant geometries of the ejector and the operating conditions are listed in the Table 4-1 and Table 4-2, respectively:

Table 4-1: Ejector's geometry.

[mm]	G1	G2	G3
Nozzle throat diameter	2	2	2
Nozzle exit diameter	8	8	8
Mixing chamber inlet diameter (Z)	24	24	19
Throat length	95	57	95

Table 4-2: Operating conditions of numerical simulations.

Run	1	2	3	4	5	6	7	8
Geom.	G1	G1	G1	G1	G1	G1	G2	G3
$\mathbf{T_g}$ [°C]	130	130	130	130	130	120	130	130
$\mathbf{p_g}$ [Pa]	270280	270280	270280	270280	270280	198670	270280	270280
$\mathbf{T_e}$ [°C]	5	10	10	10	10	10	5	5
$\mathbf{p_e}$ [Pa]	872.5	1228.1	1228.1	1228.1	1228.1	1228.1	872.5	872.5
$\mathbf{T_c}$ [°C]	24.08	24.08	26.67	28.96	31.01	24.08	24.08	24.08
$\mathbf{p_c}$ [Pa]	3000	3000	3500	4000	4500	3000	3000	3000

The values of each boundary were assigned as the saturation properties (temperature and pressure). For each of these operations, the static pressure distribution along the ejector wall is available.

4.2.3 Phase 3: model building and solving

4.2.3.1 Pre-processing

The user activities at the pre-processing stage involve: (i) the definition of the computational domain; (ii) the generation of the grid.

Domain definition. The ejector consists of two inlets (primary and secondary flow) and one outlet (mixed flow). The axisymmetric geometry allows to solve the problem in two dimensions and to analyze only half of the real domain. This reduces the computational effort.

Grid generation. The generation of the grid has the task to subdivide the domain into a number of smaller and non-overlapping sub-domains (cells), creating a grid (mesh). The mesh generation requires particular attention. In fact, a poor quality grid will cause inaccurate solutions and/or slow convergence. The mesh quality can be evaluated through some parameters [3, 11]:

- *Aspect ratio*. For quadrilateral (n=2) and hexahedral (n=3) elements it is defined as

$$Asp = \frac{max\left(e_1, e_2, \ldots, e_n\right)}{min\left(e_1, e_2, \ldots, e_n\right)} \tag{4.1}$$

  where e_i is the average length of the edge in a coordinate direction i local to the element and n is the total number of coordinate directions associated with the element. Asp=1 describes an equilateral elements (best) and should not greatly exceed 10.

- *Size-change*. It represents how the size of a cell is different than that of the adjacent cells. It is always advisable that this value does not greatly exceed the unit.

- *Cell surface*. It helps to evaluate local mesh refinement and cells area gradient.

- *Equi-angle skew*. It is calculated from the largest (θ_{max}) and smallest (θ_{min}) angle of the cell. For quadrilateral cells, the skewness is given by

$$Skew = max\left[\frac{\theta_{max} - 90°}{90°}, \frac{90° - \theta_{min}}{90°}\right] \tag{4.2}$$

  It ranges between 0 (best) and 1 (worst).

Moreover, some guidelines should be taken into account in order to obtain a good mesh [3, 11]:

- tetraedral /triangular cells are not desirable near the walls;
- the quadrilateral/hexahedral elements permits a much larger aspect ratio compared with the triangular/tetrahedral cells;
- the numerical diffusion is minimized when the flow is aligned with the mesh. It is clear that with triangular/tetrahedral mesh the flow can never be aligned with the grid;
- the numerical diffusion is inversely related to the resolution of the mesh;
- the numerical diffusion increase with the aspect ratio and the skewness.

Considering these information and best practices, we have prepared the 2D structured grids using the software GAMBIT 2.4.6. The three meshes (one for each geometry) are composed of about 70000 quadrilateral elements and were refined on proximity of the wall. The dynamic solution-adaptive mesh refinement, performed during the simulations, ensures a good representation of the flow field (oblique shock-waves, boundary layer, mixing process). The grid independence of the calculated results, which is the main goal of the mesh technique [11], is verified through the grid analysis reported in the Section 4.2.4.2. In Table 4-3 are summarized the mesh quality parameters:

Table 4-3: Mesh quality parameters.

Mesh:		G1	G2	G3
Cells		71289	68129	71289
Aspect ratio	**worst value**	10.1	10.1	10.1
	> 8	0.06 %	0.06 %	0.06 %
Size-change	**worst value**	1.27	1.27	1.19
	> 1.1	0.37 %	0.39 %	0.27 %
Cell surface	**worst value**	0.22	0.22	0.22
	> 0.2	1.91 %	2.00 %	1.91 %
Equi-angle skew	**worst value**	0.86	0.86	0.86
	> 0.65	0.13 %	0.14 %	0.13 %

4.2.3.2 Processing

In this section, we have reported the setting adopted to run the CFD simulations using the solver ANSYS 15.0 Fluent®. The main parameters that must be configured relate to the following items: (i) solver; (ii) turbulence model; (iii) thermophysical properties; (iv) boundary conditions; (v) initialization; (vi) numerical setting; (vii) convergence control.

Solver. Because of the strong effect of compressibility of the flow (high Mach number), a coupled implicit density-based approach is used [12] to take into account the strong coupling among the mass, momentum and energy equations (due to the interdependence among density, velocity and temperature that characterizes the high-speed compressible flows). The desired steady-state solution is achieved through steady solver using the pseudo-transient method until convergence. In this way a fast convergence and stable solution without reversed flow problem at the outlet is obtained.

Table 4-4: Solver setups.

Solver	Geometry	Formulation	Time	Velocity formulation	Gradient option
Density-based	2D axisymmetric	Implicit	Steady	Absolute	Least Squares Cell Based

Turbulence model. In order to validate the CFD approach, the main turbulence models are used and their performances are compared each other. The RANS models [11, 12] that have been evaluated are:

- *Spalart-Allmaras* model. It involves one transport equation for kinematic eddy viscosity parameter (ν);
- *Standard k-ε* model. It is constituted by the turbulent kinetic energy (k) and the dissipation rate of k (ε) transport equations;
- *RNG k-ε* model. It is a *k-ε* model developed using Re-Normalization Group methods to account for the effects of smaller Kolmogorov turbulence scales of motion;
- *Realizable k-ε* model. It is a *k-ε* model with a different formulation of the ε transport equation;
- *Standard k-ω* model. It is composed of the turbulent kinetic energy (k) and the specific dissipation rate (ω) transport equations;
- *SST k-ω* model. It is a *k-ω* model with Shear Stress Transport formulation;
- v^2*-f* model. It is a four-equation model based on transport equations for the turbulent kinetic energy (k), its dissipation rate (ε), a velocity variance scale ($\overline{v^2}$) and an elliptic relaxation function (f). It is similar to the *Standard k-ε* model, but incorporates near-wall turbulence anisotropy and non-local pressure-strain effects.
- *Reynolds Stress Model* (*RSM*). It is a higher-level turbulence model using six transport equations for the Reynolds stress components and one transport equation for ε. Thus, the Boussinesq approximation is not adopted and the Reynolds stresses are directly computed.

The main aspects concerning the behaviour of the turbulence models are summarize in the Table 4-5:

Table 4-5: Turbulence models [3, 12].

Turbulence model	Benefits	Problems
Spalart-Allmaras	Economical (1 eqn.); Good track-record for mildly complex b.l. flow under high pressure gradient (airfoil, wing).	Perform poorly for 3D flow, free shear flow, flow with strong separation (jets, wakes, mixing layer).
Standard k-ε	Robust and economical; Widely used despite the known limitations.	Poor for complex flow involving strong pressure gradient, separation and vortices.
RNG k-ε	Enhances accuracy for shear flow involving rapid strain, swirl and vortices.	Worsen the plane round-jet anomaly.
Realizable k-ε	Same benefits of *RNG k-ε*, but possibly more accurate and easily to converge.	Poor for b.l. separation.

Standard k-ω	Ideal for b.l. flow under adverse pressure gradient and separation, free shear, low Re flow and transitional flow.	Separation is typically excessive and early predicted.
SST k-ω	Same benefits of *Standard k-ω*.	Dependency on wall distance makes this less suitable for free shear flow.
v^2-f	Developed for attached or mildly separated b.l.; Also accurate for flow dominated by separation.	Expensive (CPU time and memory); Very hard to converge.
RSM	Physically the most sound RANS model; Ideal for complex 3D flow with strong swirl/rotation and streamline curvature, flow in duct with secondary flow and flow over curved surface.	More expensive (CPU time and memory); Tougher to converge due to close coupling of equations.

Due to the difficult convergence properties of the v^2-f turbulence model, it was not possible to verify its performance. Moreover, the literature does not provide information about its use in ejector modelling.

Wall treatment. The walls are the main source of turbulence and it usually gives rise to turbulent momentum and thermal boundary layers. The flow velocity changes rapidly near to the wall and a very fine mesh would be required in order to determine the actual velocity gradient. This requirement is too expensive for many CFD simulations. However, a dimensionless velocity profile (universal law of the wall) can be identified for many turbulence flows. The model suggests the existence of two main flow regions according to the dimensionless distance from the wall (y^+): (i) viscous sub-layer ($y^+ < 5$) and (ii) log-law layer ($30 < y^+ < 500$). There are two different wall-modelling strategies [12]:

- resolving the viscous sub-layer, using low-Reynolds-number turbulence models (*Spalart-Allmaras*, v^2-f or k-ω models) or adopting the enhanced wall treatment with *RSM* or k-ε models. The first grid cell need to be at about $y^+ = 1$.
- using a wall function (Standard, Scalable, Non-Equilibrium) with *RSM* or k-ε models. The first grid cell need to be $30 < y^+ < 300$.

In this section, the Standard wall function is used when necessary. Moreover, an analysis about the wall treatment with the different turbulence models is reported in the Section 4.2.4.5.

Thermophysical properties. The working fluid of the model is water vapour and the ideal gas assumption is made because the operating pressure is relatively low. No phase transition is considered. The thermophysical properties of water vapour, provided by the Fluent database, are summarized in the **Errore. L'origine riferimento non è stata trovata.**Table 4-6:

Table 4-6: Water vapour properties.

Phase	ρ [kg/m^3]	***MM*** [kg/kmol]	C_p [J/(kg·K)]	k [W/(m·K)]	μ [kg/(m·s)]
Vapour	Ideal gas law	18.01534	2014.0	0.0261	$1.34 \cdot 10^{-5}$

Therefore, the density is evaluated using the ideal gas law during the simulations, while the other properties are defined as constant.

Boundary conditions. The boundary conditions of two face inlets are set as pressure-inlet, whilst the one leaving ejector was set as pressure-outlet. These parameters were varied with the same

operating condition as was reported in the previous section. The boundary conditions used in the simulations are summarized in Table 4-7:

Table 4-7: Boundary conditions.

	Primary flow	Secondary flow	Outlet flow	Wall
Condition	Total pressure Total temperature	Total pressure Total temperature	Static pressure Total temperature	Adiabatic No slip
Turbulence intensity	5%	2%	5%	-
Hydraulic diameter	0.003875 m	0.020 m	0.020 m	-

Note that there was no difference between an input of the stagnation pressure and static pressure because the velocity of the flow entering and leaving the domain was thought to be relatively small compared with the supersonic speed during the flow process of the ejector [10]. The turbulence intensity and hydraulic diameter have been chosen as turbulence boundary conditions. However, these values are arbitrary specified because no turbulence measurements have been performed.

Initialization. Due to the complex fluid dynamics and in order to achieve fast convergence, a full multi-grid (FMG) initialization scheme has been adopted. In order to ensure a stable solution, the value of the pressure-outlet boundary condition was discretely increased until convergence during the initialization process. In this way, there is no reversed flow problem at the outlet.

Numerical setting. The simulation is started with first-order discretization schemes and pseudo-transient formulation method. When the simulation is quite defined, discretization schemes are switched to second-order and a standard steady-state solution is pursued. In this way, fast convergence and low numerical diffusion are obtained.

Table 4-8: Numerical methods – Spalart-Allmaras turbulence model.

	Flow	Modified turbulent viscosity
Preliminary results (pseudo-transient)	1st order upwind	1st order upwind
Final results	2nd order upwind	2nd order upwind

Table 4-9: Numerical methods – two-equation turbulence models (k-ε, k-ω).

	Flow	Turbulent kinetic energy	Dissipation rate
Preliminary results (pseudo-transient)	1st order upwind	1st order upwind	1st order upwind
Final results	2nd order upwind	2nd order upwind	2nd order upwind

Table 4-10: Numerical methods – RSM turbulence model.

	Flow	Reynolds stresses	Dissipation rate
Preliminary results (pseudo-transient)	1st order upwind	1st order upwind	1st order upwind
Final results	2nd order upwind	2nd order upwind	2nd order upwind

In order to run stable simulations and aid convergence, low Courant-Friedrichs-Lewis number (*CFL* = 0.5) is set. Once flow behaviour is stabilized, the CFL number is increased up to 5. The under-relaxation factors are set as shown in the following tables.

Table 4-11: Control parameters – Spalart-Allmaras turbulence model.

	Modified turbulent viscosity	Turbulent viscosity	Solid
Preliminary results (pseudo-transient)	0.7	0.7	-
Final results	0.8	0.8	1

Table 4-12: Control parameters – two-equation turbulence models (k-ε, k-ω).

	Turbulent kinetic energy	Dissipation rate	Turbulent viscosity	Solid
Preliminary results (pseudo-transient)	0.7	0.7	0.7	-
Final results	0.8	0.8	0.8	1

Table 4-13: Control parameters – RSM turbulence model.

	Turbulent kinetic energy	Dissipation rate	Turbulent viscosity	Reynolds stresses	Solid
Preliminary results (pseudo-transient)	0.7	0.7	0.7	0.6	-
Final results	0.8	0.8	0.8	0.5	1

Convergence control. The solution is considered as converged according to the following criteria:

- *Residual control*. Every residual of the calculation must be stable and lower than the specified value 10^{-6}.
- *Parameters monitoring*. The calculated mass fluxes of every face are steady and the mass flow rate balance must be ensured with a tolerance of 10^{-7}.

The convergence will occur when each residual will be reduced to the set values. Sometimes the residuals may not fall below the convergence criterion set in the case setup. However, monitoring the variables through iterations may show that the residuals have stagnated and do not change with further iterations. This could also be considered as convergence.

4.2.3.3 Post-processing

The validation of the model is performed using both global and local experimental quantities. In particular, the entrainment ratio and the static pressure profile along the wall ejector are checked and compared with the experimental measures for each simulation. Moreover, a grid analysis and a comparison among the different wall treatment methods are carried out.

4.2.4 Phase 4: problem evaluation, assessment and review

In this section, CFD model results are presented and discussed after a brief review about the state of the art of the turbulence models employed in the CFD simulation of supersonic ejectors.

4.2.4.1 State of the art of the CFD turbulence models

In order to provide references and guidelines about the turbulence models for ejector application, a review of the main CFD studies is presented. The mostly used turbulence models are the *Realizable k-ε* [10, 13-19], which is able to predict more accurately the spreading rate of both planar and curved jets [12], and the *k-ω SST* [15, 20, 21], which has a better resolution of boundary layer under adverse pressure gradients [12]. However, some literature studies have carried out comparative analyses among different turbulence models in order to assess their performance.

Bartosiewicz, Aidoun et al. (2003-2005) [7, 22] evaluated the performance of six turbulence models (*Standard k-ε, RNG k-ε, Realizable k-ε, Standard k-ω, SST k-ω, RSM*) for the study of a supersonic ejector with air for refrigeration applications. When appropriate, standard wall functions are used as wall treatment. The results were compared with static pressure measurements along the ejector centerline. The *RNG k-ε* and the *SST k-ω* models performed well thanks to a better prediction of the shock phase. However, all the models seem to fail in predicting expansion strength due to the occurrence of fluid condensation observed in the experiments but not accounted in the numerical simulations.

Hemidi, Henry et al. (2009) [8] compared the *Standard k-ε* and *SST k-ω* models for supersonic ejector working with air. They demonstrated that the *k-ε* model provides better results for on-design conditions, with errors mostly less than 10%. The *SST k-ω* model, instead, yields errors often more than 20%, but with better prediction at off-design operation conditions. Thus, for the analysis of ejector performance in a wide range of operating conditions the *SST k-ω* or other models should be considered.

C. Li and Y.Z. Li (2011) [23] investigated the entrainment behaviour and performance of single-phase and two-phase ejectors. The fluid pairs considered are N_2-N_2, He-He, N_2-H_2O and He-LO_2. For their analysis, the *Standard k-ε,* the *Standard k-ω* and the *SST k-ω* models were considered. The *k-ε* model provides best results in entrainment ratio prediction: the relative errors are less then 25% in almost all cases. Moreover, it appears that the *SST k-ω* model significantly over-predicts the entrainment ratio for small pressure difference between the entrained pressure p_e and the discharge pressure p_e.

Ruangtrakoon, Thongtip et al. (2013) [15] used CFD technique to investigate the effect of the primary nozzle geometries on the performance of an ejector. In this study, the *Realizable k-ε* and *SST k-ω* models were used and compared with each other. It was found that the simulated results based on the *SST k-ω* model more closely corresponded to the experimental values than those based on the *Realizable k-ε* model. In particular, this was observed when the ejector was operated at a relatively high generator temperature (T_g > 140°C). According to the authors, a possible reason is that the *Realizable k-ε* model is unable to accurately predict the performance of the ejector under a strong adverse pressure gradient.

Zhu and Jiang (2014) [24] carried out a CFD study in order to investigate the entrainment performance and the shockwave structures in a 3D ejector. Four turbulence models are used: *Standard k-ε, RNG k-ε, Realizable k-ε* and *SST k-ω.* The results show that the *RNG k-ε* and *SST k-ω* models agree best with the experimental entrainment ratio and shockwave structures. Otherwise,

the *Standard k-ε* model fails in predicting shock location after the second shock and, for the critical working conditions, the *Standard k-ε* and *Realizable k-ε* models over-predict the first shock wavelength and fail in predicting the reflected shocks.

4.2.4.2 Analysis of the results: grid sensitivity analysis

In order to assess the grid sensitivity of the results, the simulations corresponding to the case "RUN 1" were performed with three different meshes: (i) coarse mesh (composed by about 40000 quadrilateral elements); (ii) medium mesh (70000 elements) and (iii) fine mesh (280000 elements).

In the Table 4-14 are reported the values of the entrainment ratio predicted with the seven turbulence models.

Table 4-14: Grid sensitivity analysis – Entrainment ratio prediction.

	Entrainment ratio ω [-]						
	Spalart-Allmaras	***Standard k-ε***	***RNG k-ε***	***Realizable k-ε***	***Standard k-ω***	***SST k-ω***	***RSM***
Coarse mesh	0.298	0.349	0.313	0.302	0.262	0.298	0.273
Medium mesh	0.303	0.351	0.312	0.302	0.273	0.303	0.273
Fine mesh	0.302	0.304	0.309	0.306	0.292	0.303	0.284

In order to confirm the grid independence of the results, the static pressure profiles along the ejector are compared each others. As shown in the Figure 4-2, the grid independency is practically reached for the medium grid, employed for the validation of the CFD model.

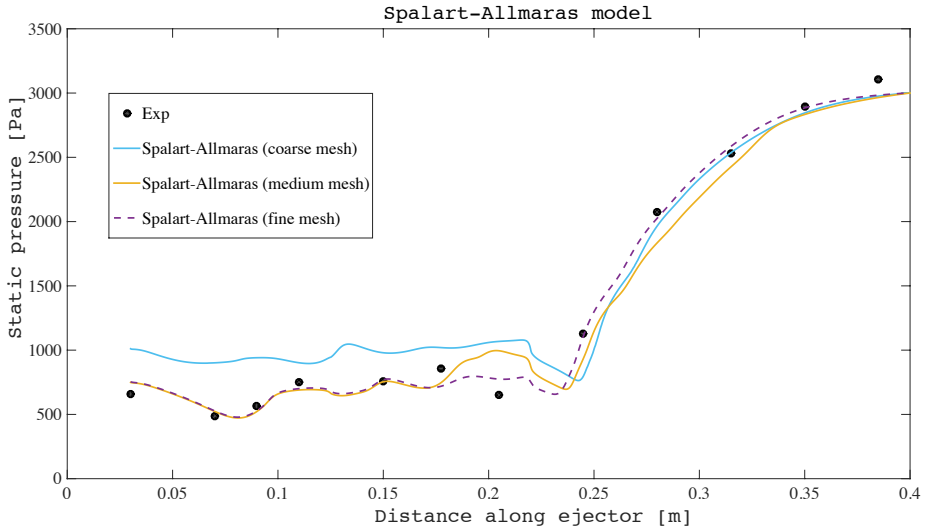

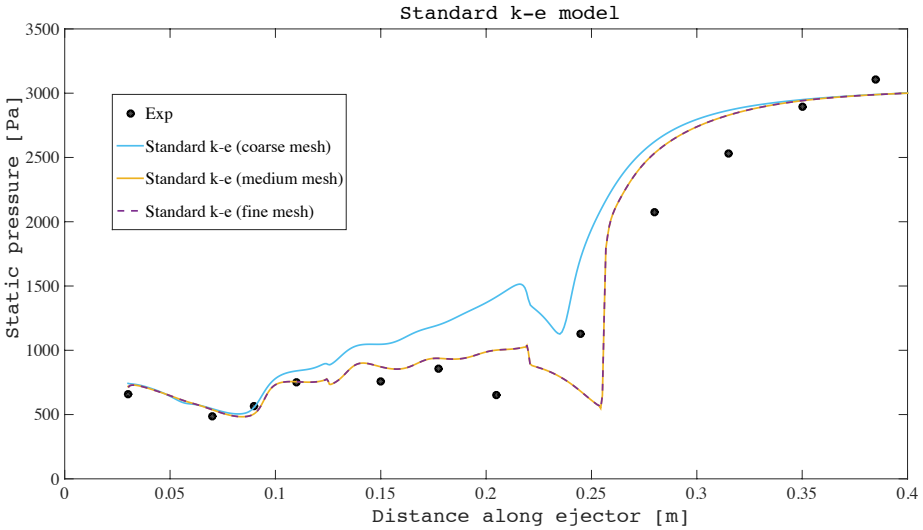
Standard k-e model
Static pressure [Pa]
Distance along ejector [m]
Exp
Standard k-e (coarse mesh)
Standard k-e (medium mesh)
Standard k-e (fine mesh)

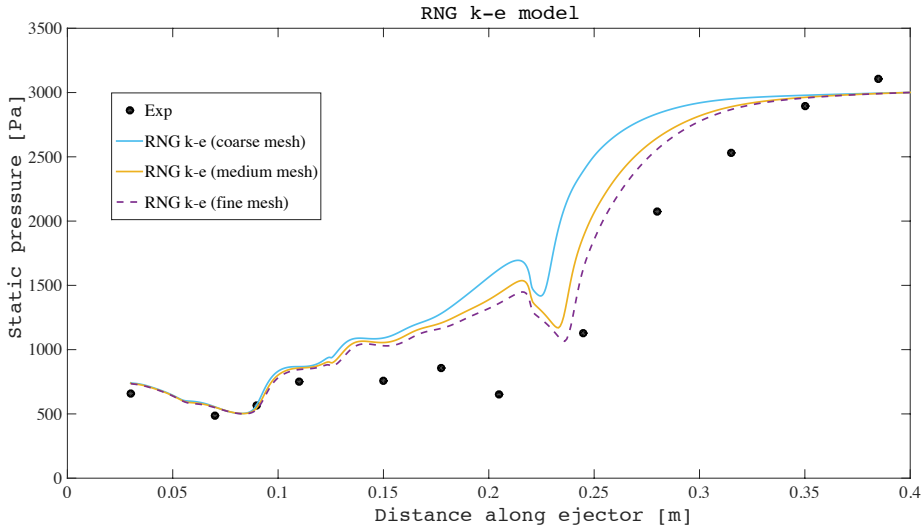
RNG k-e model
Static pressure [Pa]
Distance along ejector [m]
Exp
RNG k-e (coarse mesh)
RNG k-e (medium mesh)
RNG k-e (fine mesh)

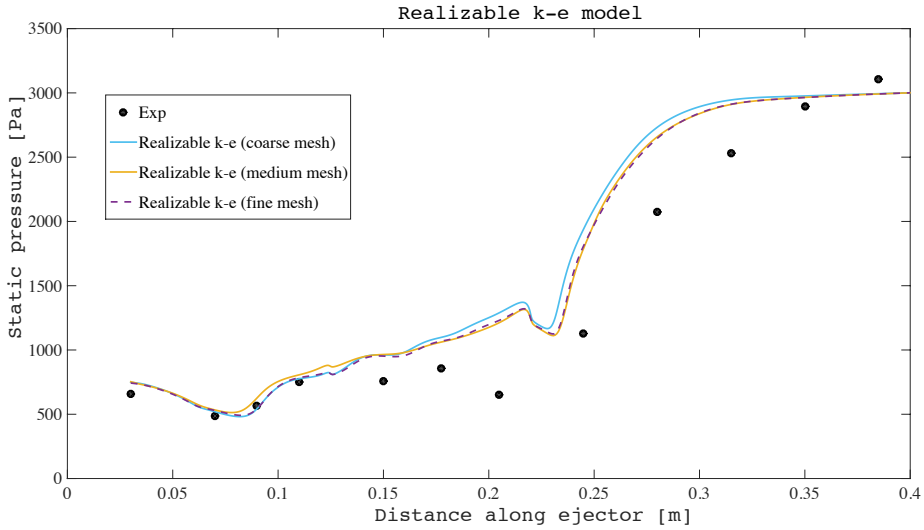
Realizable k-e model
Static pressure [Pa]
Distance along ejector [m]
Exp
Realizable k-e (coarse mesh)
Realizable k-e (medium mesh)
Realizable k-e (fine mesh)

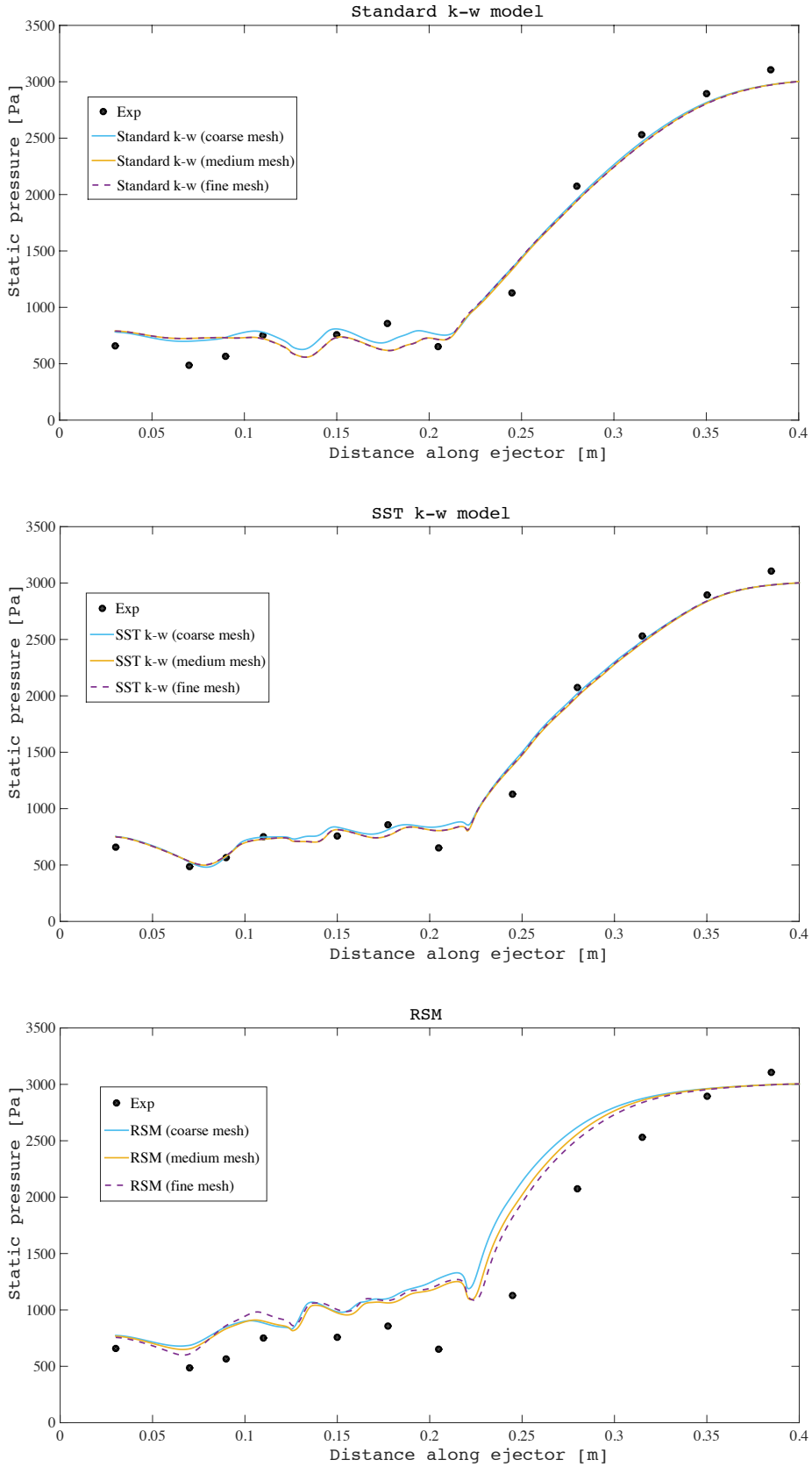

Figure 4-2: Wall static pressure distribution along the ejector – Grid sensitivity analysis.

4.2.4.3 Analysis of the results: global parameters

The first point of comparison concerns the performance prediction of the CFD models of the mass flow rates through the ejector. In particular, the experimental entrainment ratio is compared with the entrainment ratio calculated from the CFD simulations. The results are summarized in Table 4-15:

Table 4-15: CFD models prediction of the entrainment ratio.

	Entrainment ratio ω [-]							
	Run 1	**Run 2**	**Run 3**	**Run 4**	**Run 5**	**Run 6**	**Run 7**	**Run 8**
Exp.	0.309	0.397	0.400	0.400	0.403	0.527	0.301	0.172
Spalart-Allmaras	0.303	0.477	0.477	0.477	0.477	0.656	0.304	0.169
Standard k-ε	0.351	0.338	0.302	0.390	0.387	0.622	0.307	0.177
RNG k-ε	0.312	0.485	0.487	0.487	0.487	0.577	0.312	0.176
Realizable k-ε	0.302	0.470	0.469	0.469	0.469	0.574	0.304	0.172
Standard k-ω	0.273	0.394	0.394	0.394	0.394	0.531	0.252	0.158
SST k-ω	0.303	0.438	0.438	0.438	0.438	0.476	0.302	0.169
RSM	0.273	0.413	0.413	0.414	n.c.	0.550	0.274	0.158

The relative errors committed in the prediction of the entrainment ratio are reported in Table 4-16:

Table 4-16: Relative errors of the CFD models in the prediction of the entrainment ratio.

	Relative error E_R (ω) [%]							
	Run 1	**Run 2**	**Run 3**	**Run 4**	**Run 5**	**Run 6**	**Run 7**	**Run 8**
Spalart-Allmaras	1.94	20.15	19.25	19.25	18.36	24.48	1.00	1.74
Standard k-ε	13.59	14.86	24.50	2.50	3.97	18.03	1.99	2.91
RNG k-ε	0.97	22.17	21.75	21.75	20.84	9.49	3.65	2.33
Realizable k-ε	2.27	18.39	17.25	17.25	16.38	8.92	1.00	0.00
Standard k-ω	11.65	0.76	1.50	1.50	2.23	0.76	16.28	8.14
SST k-ω	1.94	10.33	9.50	9.50	8.68	9.68	0.33	1.74
RSM	11.65	4.03	3.25	3.50	n.c.	4.36	8.97	8.14

The Figure 4-3 shows the frequency distribution of the errors for the seven turbulence models employed:

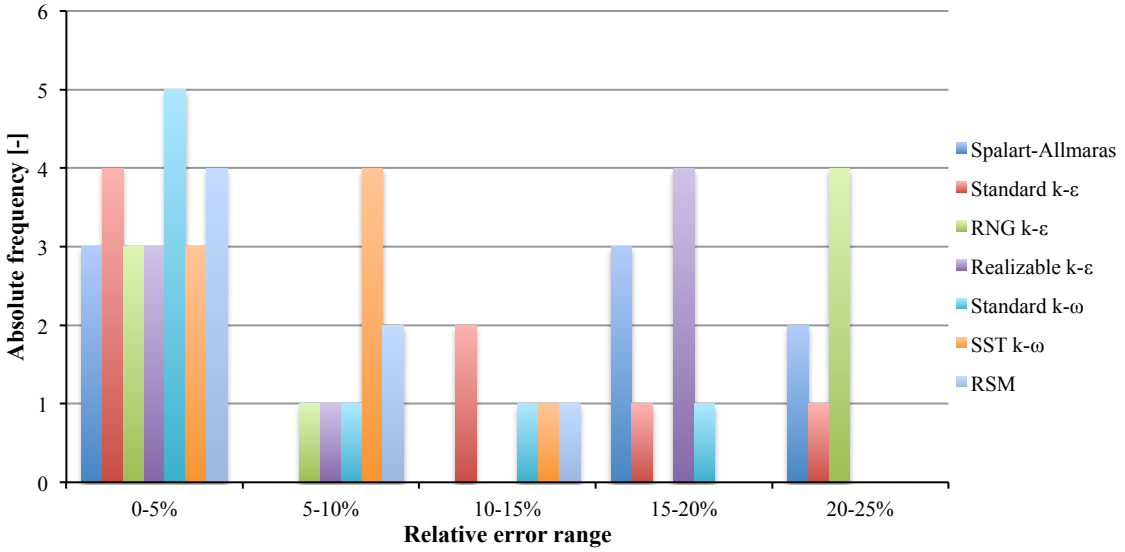

Figure 4-3: Absolute frequency distribution of the errors.

According to the results, all the turbulence models are able to predict the entrainment ratio with acceptable errors and in line with the literature [8, 23]. The maximum relative error was obtained with the *Standard k-ε* model (equal to 24.5%) and, in general, the *k-ε* models have lower performance than the other turbulence models. The *Standard k-ω* model has achieved a maximum error equal to 16.3%, but the half of the relative errors is less than 5%. The *SST k-ω* and *RSM* models, instead, attain errors less than 12%. However, the *SST k-ω* model is the best turbulence model in terms of prediction ability of the entrainment ratio of the ejector. Moreover, its computational cost is less than the *RSM* and it has better convergence properties.

4.2.4.4 Analysis of the results: local parameters and flow fields

However, as already remarked, the validation of CFD models with global parameters is not sufficient. Therefore, we have also performed a comparison between local measures and numerical results. The benchmark provides experimental measures of the wall static pressure along the ejector.

For each simulation, we have summarized the results in a table, compared the pressure profiles by means of a graph and reported the flow field, in terms of the Mach number, for all the turbulence models.

Run 1: G1, p_g = 270280 Pa, p_e = 872.5 Pa, p_c = 3000 Pa

Table 4-17: Run 1 – Experimental and numerical results of the wall static pressure.

	Wall static pressure p_w [Pa]											
x [mm] =	30	70	90	110	150	177.5	205	245	280	315	350	385
Exp.	661	488	564	752	755	854	653	1130	2076	2532	2892	3109
Spalart-Allmaras	1011	901	941	902	979	1019	1068	798	1979	2535	2846	2978
Standard k-ε	718	537	507	756	870	937	1001	673	2530	2828	2942	2989
RNG k-ε	738	552	550	857	1055	1209	1437	1899	2654	2889	2963	2992
Realizable k-ε	753	533	626	811	965	1062	1211	1806	2655	2910	2965	2993
Standard k-ω	791	724	731	723	734	618	716	1334	1946	2446	2807	2974
SST k-ω	751	531	580	729	813	761	805	1381	1998	2468	2836	2983
RSM	768	656	834	901	971	1061	1192	1889	2568	2858	2960	2998

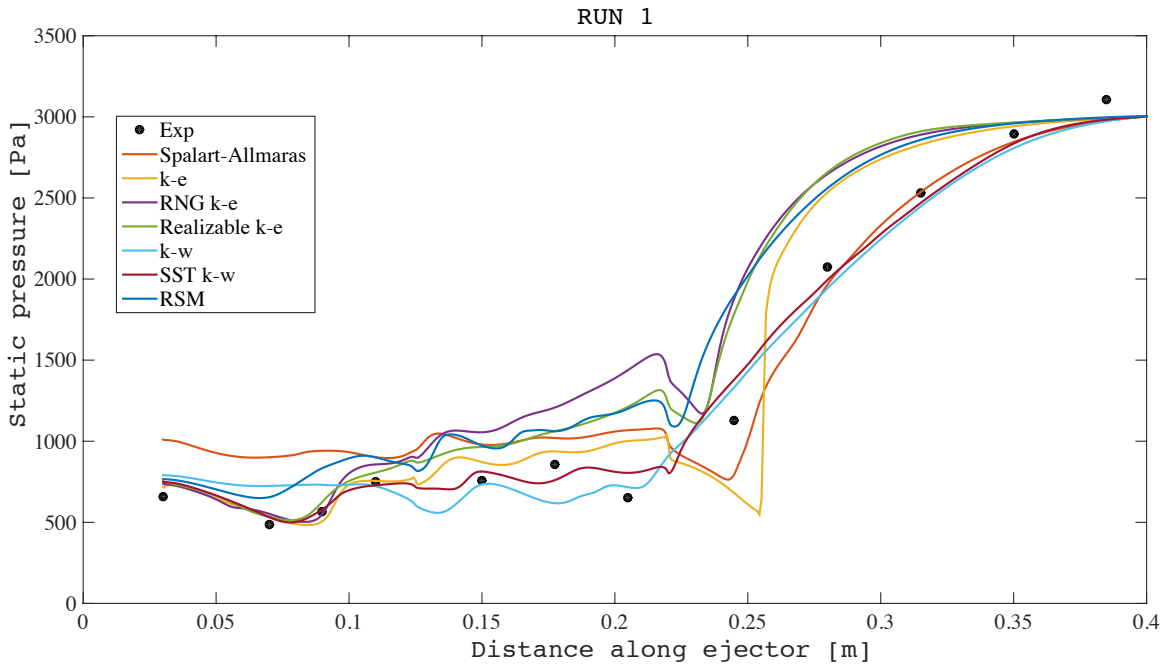

Figure 4-4: Wall static pressure distribution along the ejector (RUN 1).

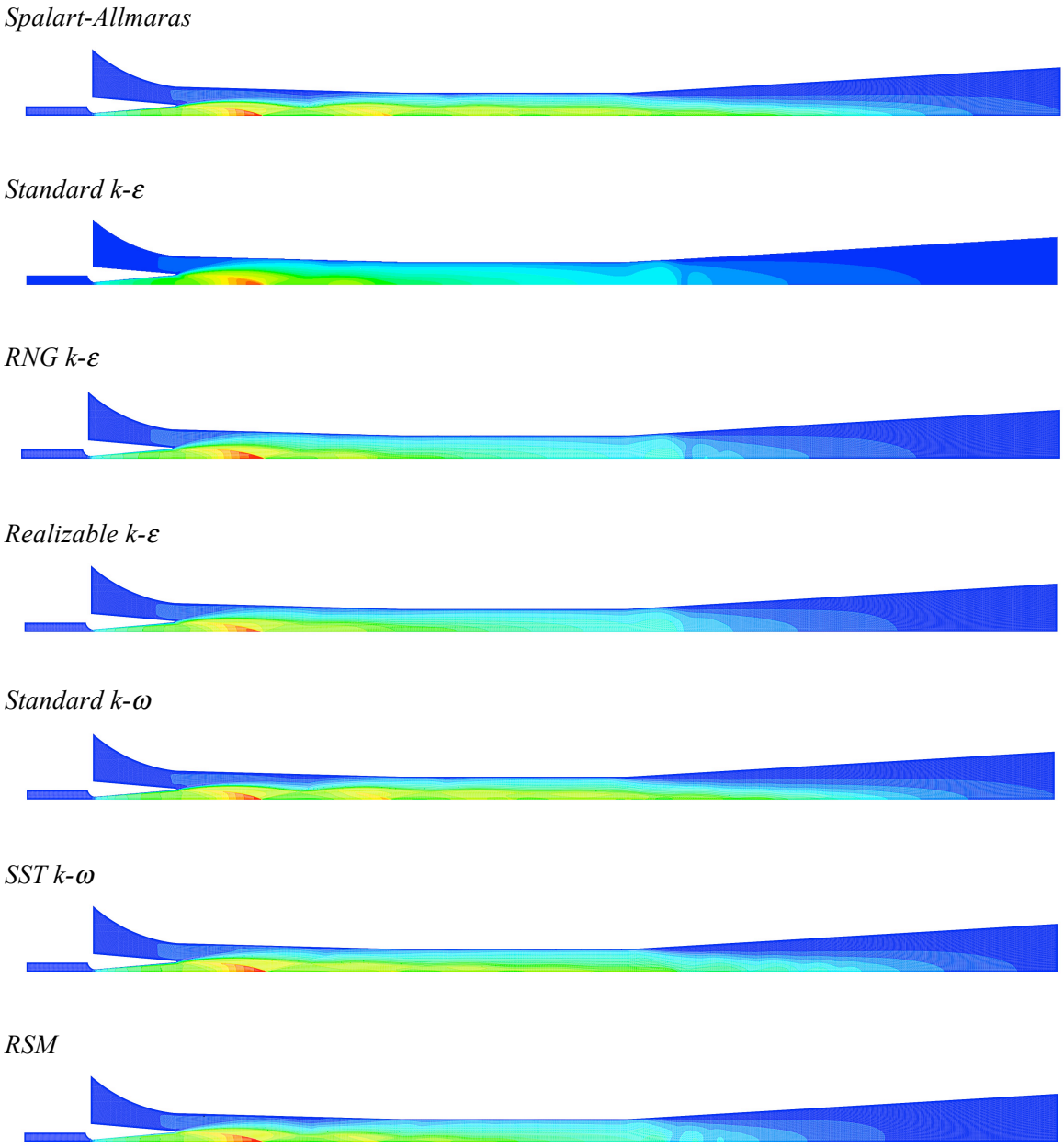

Figure 4-5: Mach contours of the ejector flow field (RUN 1).

Run 2: G1, p_g = 270280 Pa, p_e = 1228.1 Pa, p_c = 3000 Pa

Table 4-18: Run 2 – Experimental and numerical results of the wall static pressure.

	Wall static pressure p_w [Pa]											
x [mm] =	30	70	90	110	150	177.5	205	245	280	315	350	385
Exp.	884	877	864	792	849	993	840	1332	1867	2466	2840	3032
Spalart-Allmaras	1020	911	946	899	977	1020	1059	796	1989	2548	2852	2979
Standard k-ε	957	692	917	956	1177	1232	1321	831	2414	2786	2920	2984
RNG k-ε	738	552	550	857	1055	1209	1439	1865	2644	2889	2963	2992
Realizable k-ε	1015	842	963	982	1228	1455	1704	1424	2395	2837	2932	2984
Standard k-ω	1089	1034	973	861	882	889	867	1244	1851	2377	2767	2964
SST k-ω	1032	953	913	867	968	1024	1077	1306	1953	2431	2793	2970
RSM	1064	993	998	1170	1170	1328	1470	1714	2452	2796	2943	2997

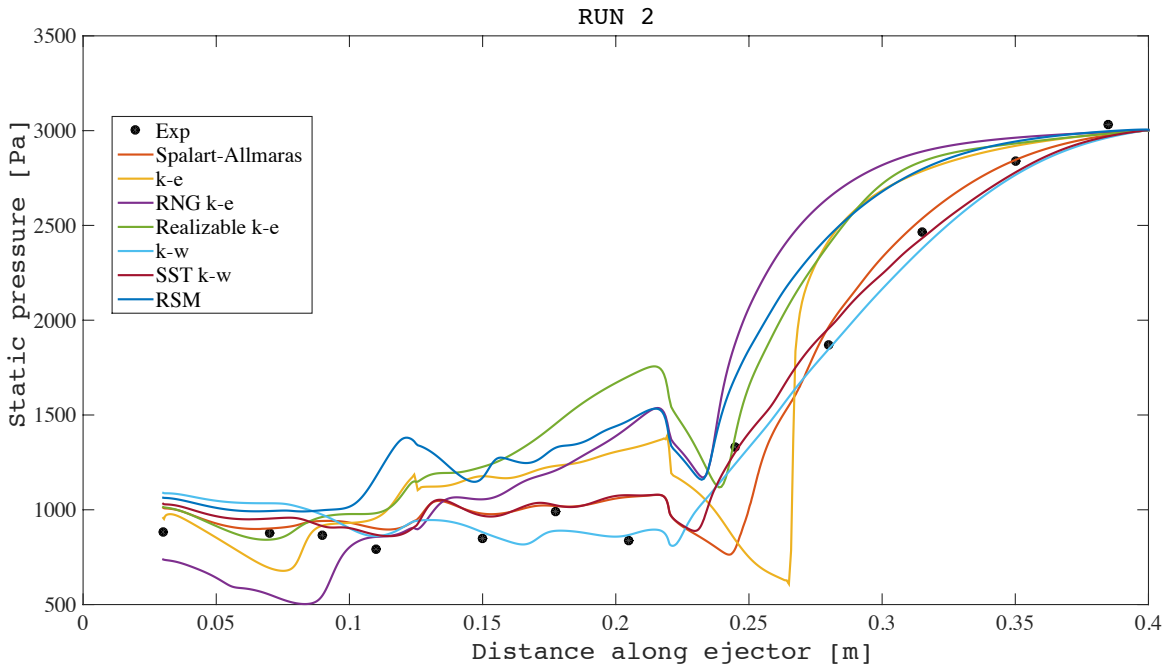

Figure 4-6: Wall static pressure distribution along the ejector (RUN 2).

Spalart-Allmaras

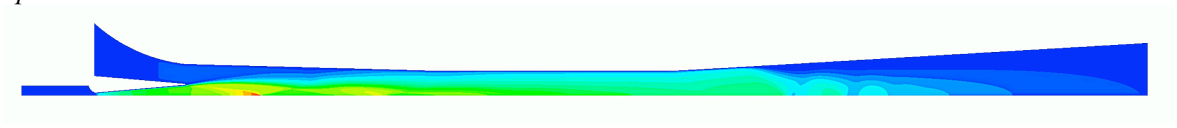

Standard k-ε

RNG k-ε

Realizable k-ε

Standard k-ω

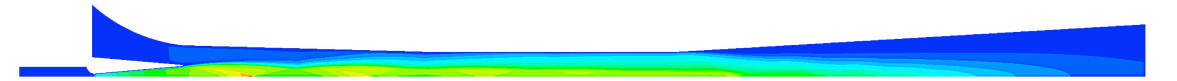

SST k-ω

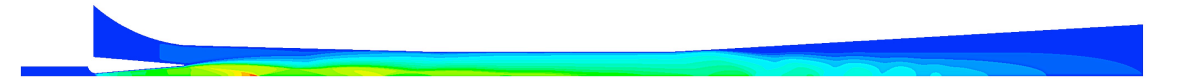

RSM

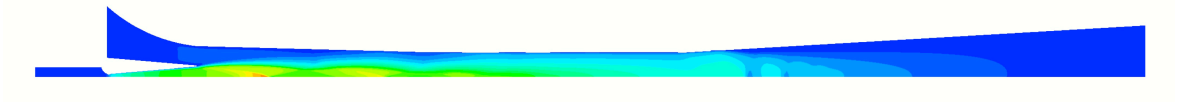

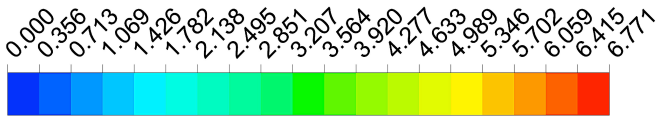

Figure 4-7: Mach contours of the ejector flow field (RUN 2).

Run 3: G1, p_g = 270280 Pa, p_e = 1228.1 Pa, p_c = 3500 Pa

Table 4-19: Run 3 – Experimental and numerical results of the wall static pressure.

	Wall static pressure p_w [Pa]											
x [mm] =	30	70	90	110	150	177.5	205	245	280	315	350	385
Exp.	820	869	811	781	846	959	720	1877	2545	3072	3375	3542
Spalart-Allmaras	1011	902	941	901	979	1019	1068	1720	2723	3199	3412	3486
Standard k-ε	780	749	841	918	1030	1059	1087	1307	3225	3413	3471	3493
RNG k-ε	996	697	955	1072	1371	1604	2397	2619	3186	3377	3455	3491
Realizable k-ε	1030	900	975	986	1282	1399	1582	2564	3220	3397	3460	3491
Standard k-ω	1089	1034	972	861	909	890	879	1764	2494	3347	3375	3483
SST k-ω	1032	953	914	868	968	1023	1077	1879	2599	3097	3397	3487
RSM	1064	993	997	1184	1175	1328	1470	2540	3149	3378	3461	3496

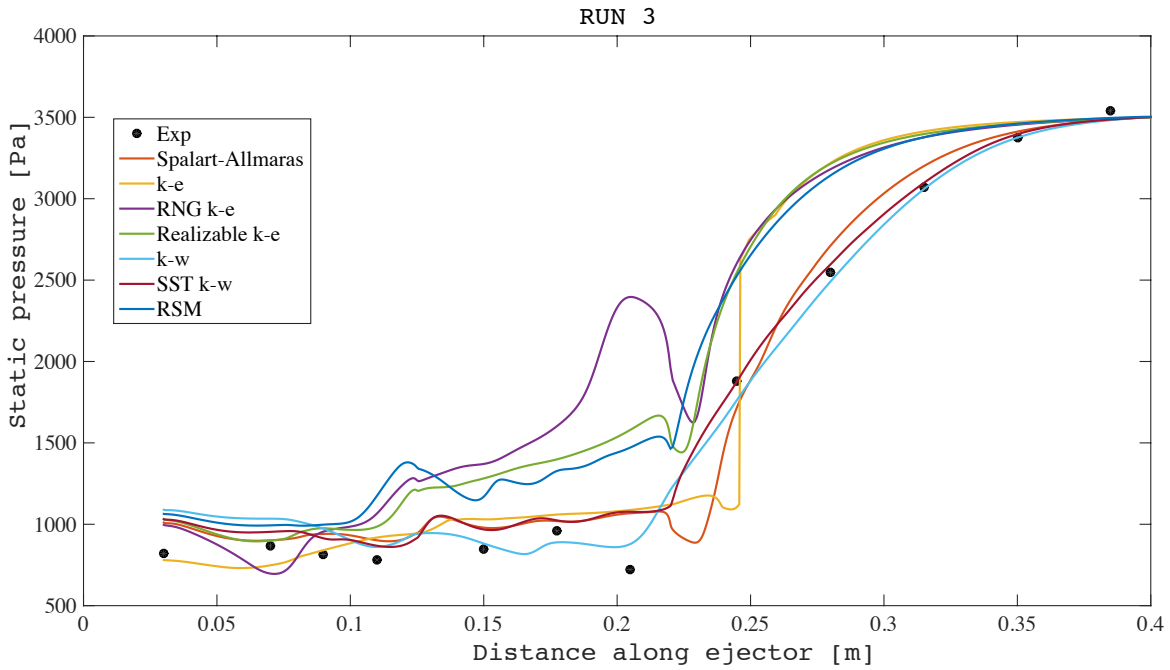

Figure 4-8: Wall static pressure distribution along the ejector (RUN 3).

Spalart-Allmaras

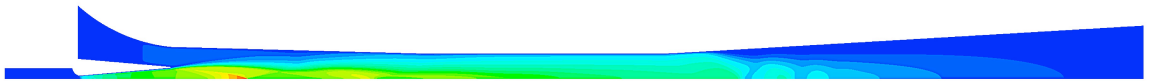

Standard k-ε

RNG k-ε

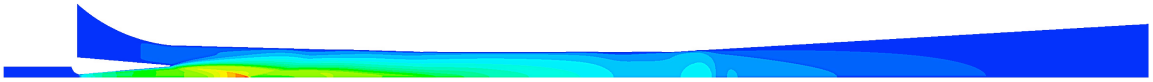

Realizable k-ε

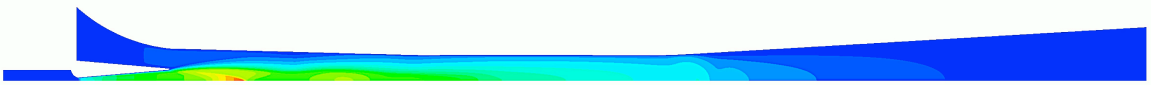

Standard k-ω

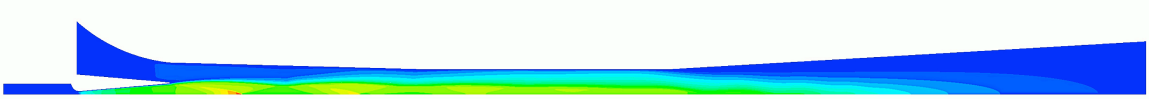

SST k-ω

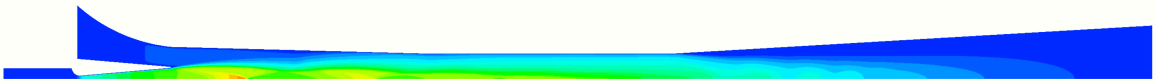

RSM

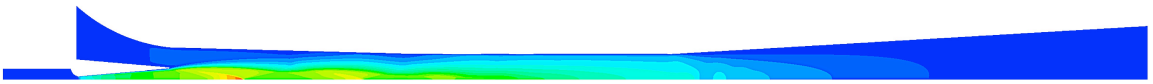

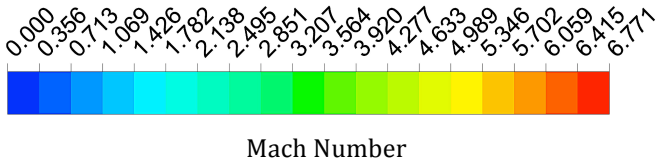

Figure 4-9: Mach contours of the ejector flow field (RUN 3).

Run 4: G1, p_g = 270280 Pa, p_e = 1228.1 Pa, p_c = 4000 Pa

Table 4-20: Run 4 – Experimental and numerical results of the wall static pressure.

	Wall static pressure p_w [Pa]											
x [mm] =	30	70	90	110	150	177.5	205	245	280	315	350	385
Exp.	870	871	866	942	1221	1664	2127	3192	3582	3828	4096	4244
Spalart-Allmaras	1011	901	941	901	980	1020	1068	2521	3410	3803	3940	3989
Standard k-ε	1090	1074	1033	897	921	932	1265	2476	3297	3767	3942	3991
RNG k-ε	1224	1083	1203	1257	1403	1514	1914	3578	3849	3940	3977	3995
Realizable k-ε	1029	902	983	1003	1229	1348	2198	3504	3808	3914	3966	3993
Standard k-ω	1089	1034	972	861	883	889	1283	2417	3235	3749	3938	3990
SST k-ω	1032	953	913	867	968	1024	1156	2588	3322	3789	3950	3991
RSM	1064	993	997	1181	1174	1377	2461	3419	3782	3913	3968	3996

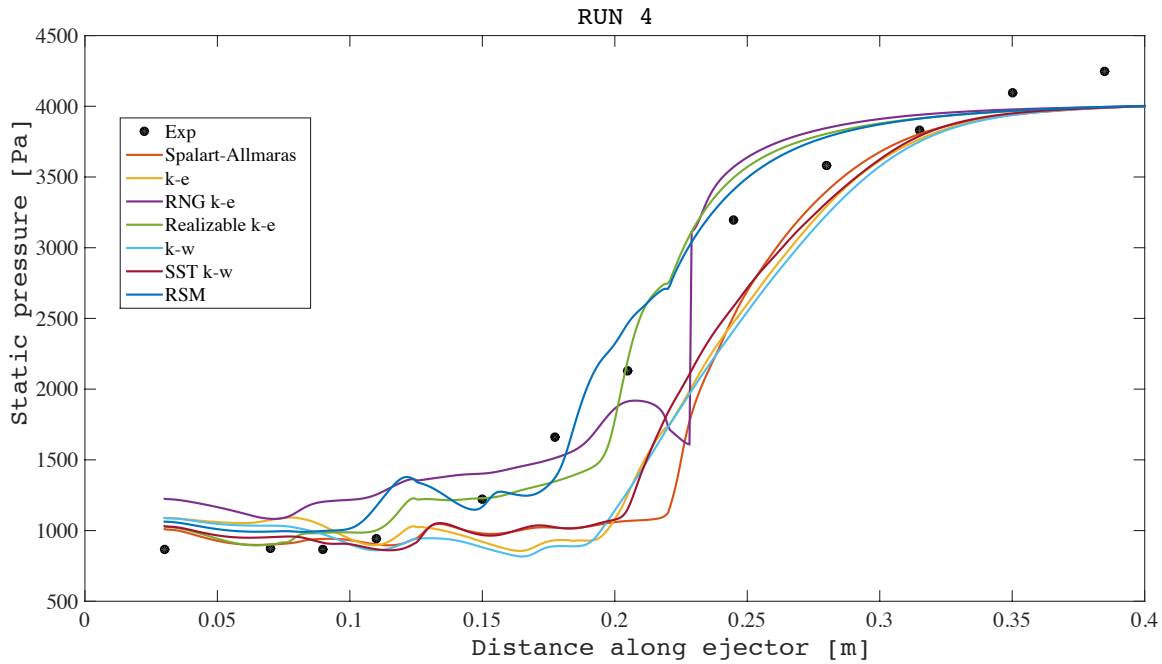

Figure 4-10: Wall static pressure distribution along the ejector (RUN 4).

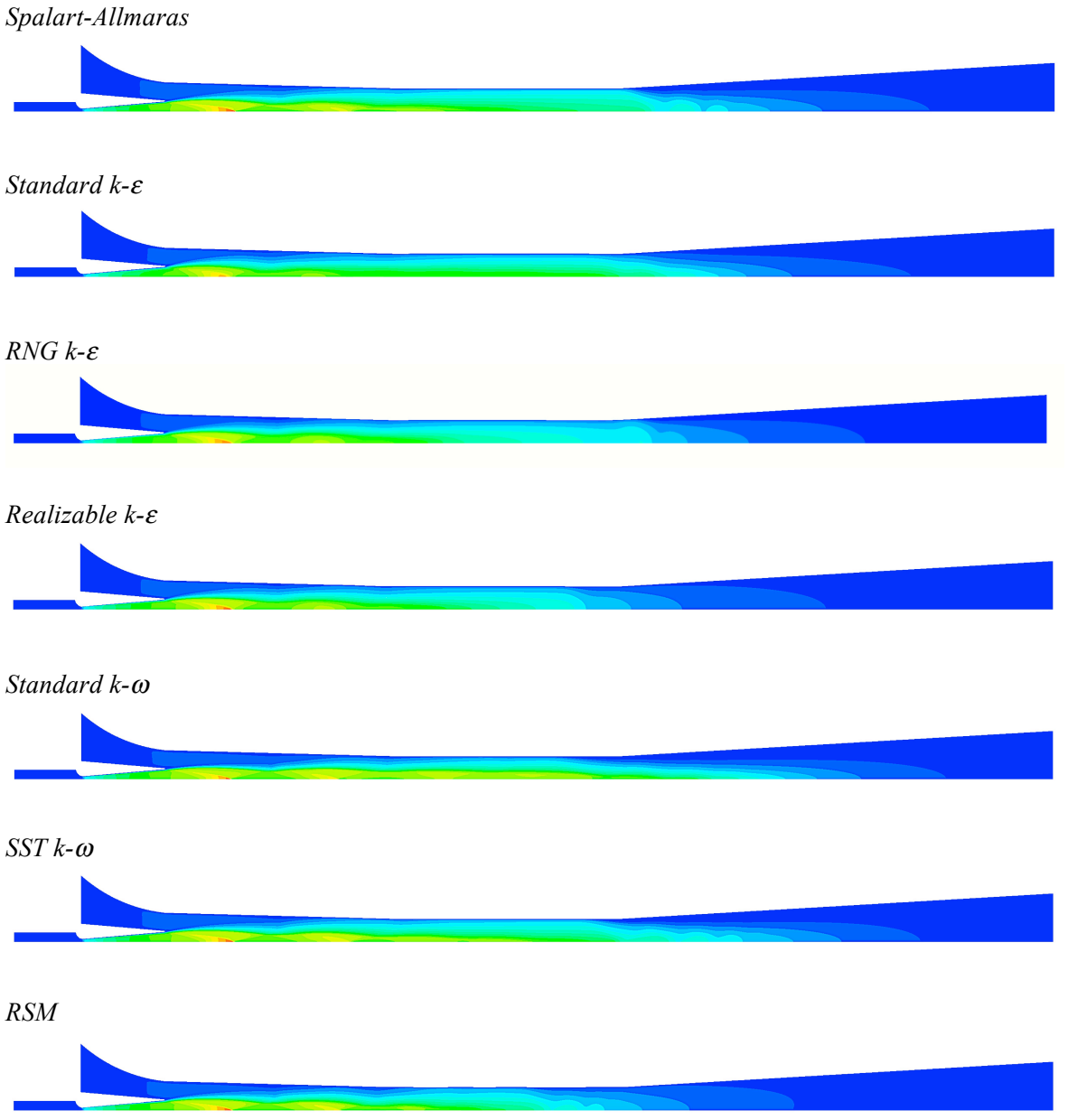

Figure 4-11: Mach contours of the ejector flow field (RUN 4).

Run 5: G1, p_g = 270280 Pa, p_e = 1228.1 Pa, p_c = 4500 Pa

Table 4-21: Run 5 – Experimental and numerical results of the wall static pressure.

	Wall static pressure p_w [Pa]											
x [mm] =	30	70	90	110	150	177.5	205	245	280	315	350	385
Exp.	879	1044	953	696	1689	2506	3231	4217	4655	4727	4860	4763
Spalart-Allmaras	1010	901	941	902	980	1020	1166	3397	4116	4369	4454	4491
Standard k-ε	1092	1046	973	874	892	1166	1964	3242	4051	4373	4462	4493
RNG k-ε	1224	1083	1204	1257	1403	1514	1913	4078	4349	4439	4477	4495
Realizable k-ε	1311	1244	1193	1130	1215	1389	1782	2917	3735	4249	4438	4490
Standard k-ω	1090	1034	973	860	882	1169	1951	3228	4045	4371	4461	4493
SST k-ω	1032	953	914	867	968	1026	2054	3393	4118	4394	4464	4490

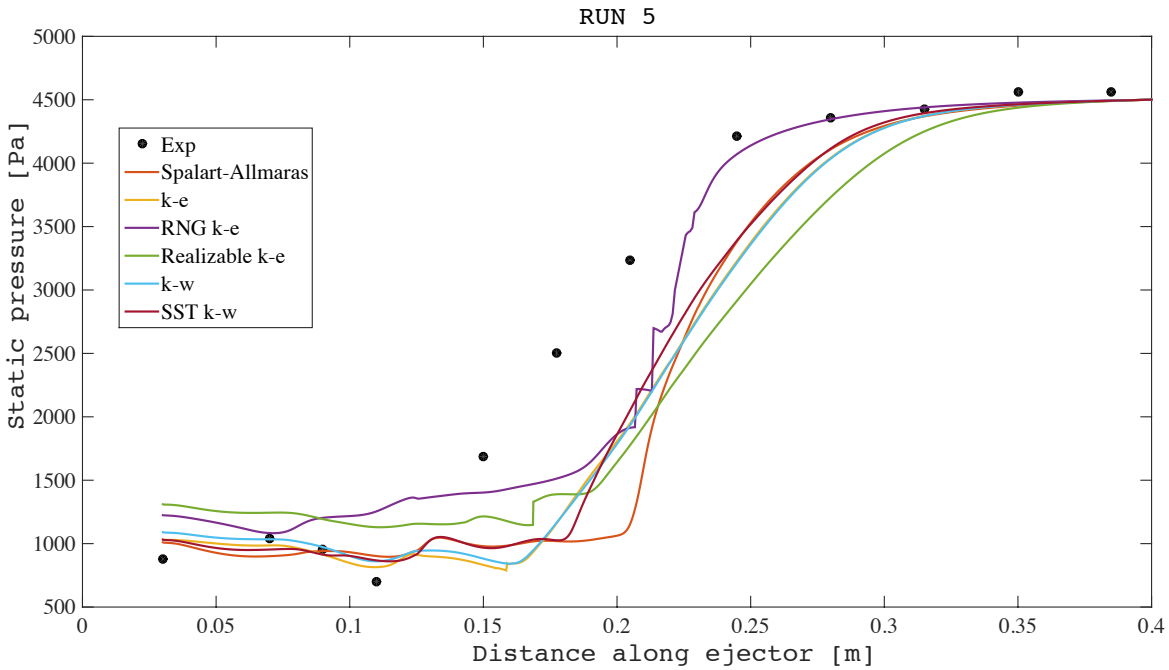

Figure 4-12: Wall static pressure distribution along the ejector (RUN 5).

Spalart-Allmaras

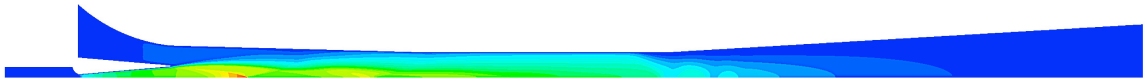

Standard k-ε

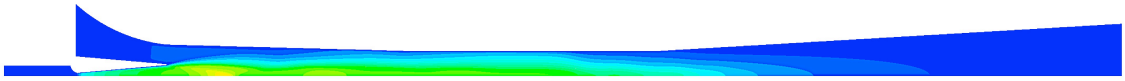

RNG k-ε

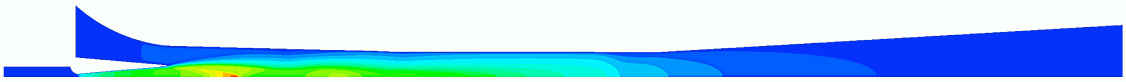

Realizable k-ε

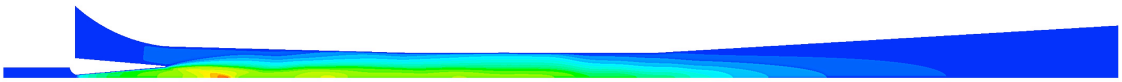

Standard k-ω

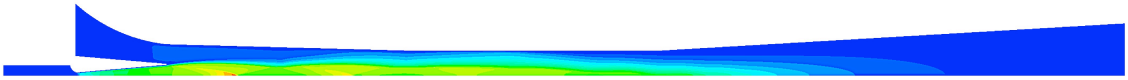

SST k-ω

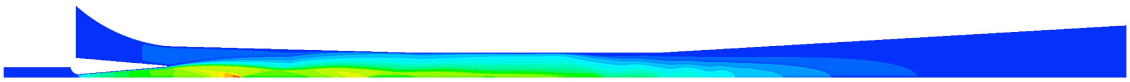

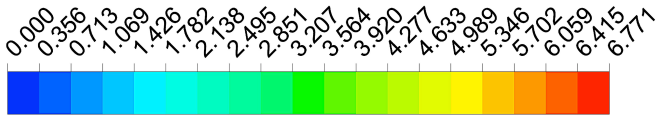

Figure 4-13: Mach contours of the ejector flow field (RUN 5).

Run 6: G1, p_g = 198670 Pa, p_e = 1228.1 Pa, p_c = 3000 Pa

Table 4-22: Run 6 – Experimental and numerical results of the wall static pressure.

	Wall static pressure p_w [Pa]											
x [mm] =	30	70	90	110	150	177.5	205	245	280	315	350	385
Exp.	981	921	942	948	931	925	879	1666	2302	2688	2893	2896
Spalart-Allmaras	1011	901	941	902	980	1020	1068	798	1978	2535	2846	2977
Standard k-ε	719	536	508	756	871	939	1003	670	2529	2832	2947	2988
RNG k-ε	738	552	550	857	1055	1209	1437	1900	2654	2889	2963	2992
Realizable k-ε	750	534	631	809	967	1061	1215	1803	2659	2921	2967	2992
Standard k-ω	1090	1044	998	965	829	801	933	1758	2360	2761	2937	2990
SST k-ω	751	533	580	728	813	761	808	1381	1997	2468	2836	2983
RSM	764	659	832	909	969	1066	1195	1893	2572	2852	2963	2997

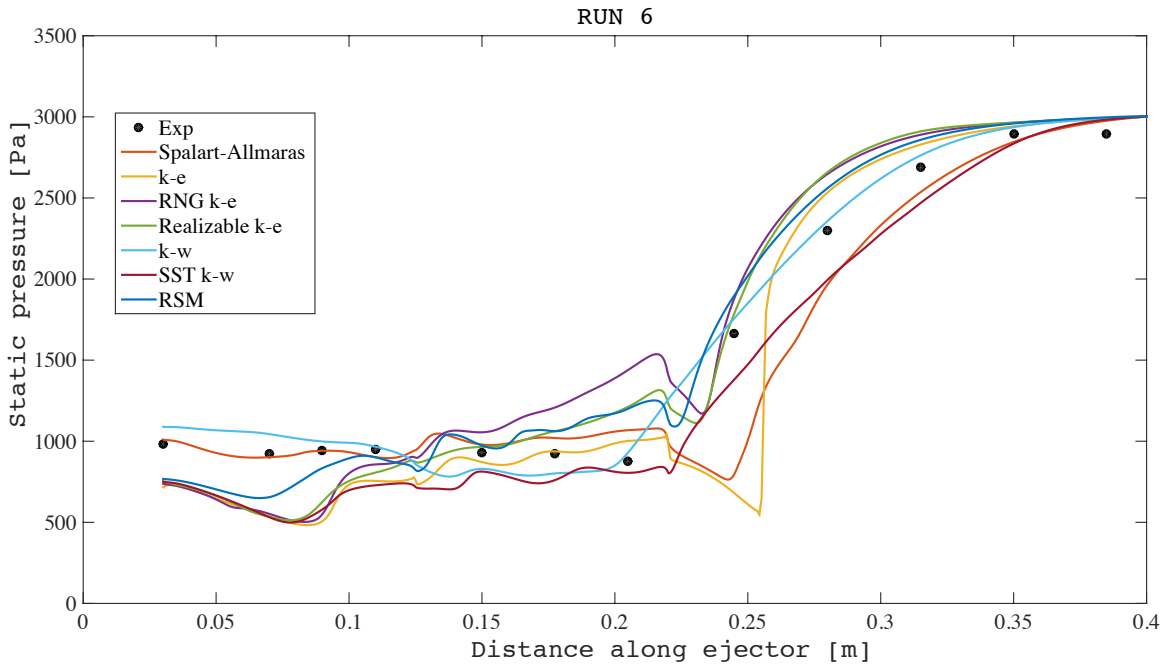

Figure 4-14: Wall static pressure distribution along the ejector (RUN 6).

Spalart-Allmaras

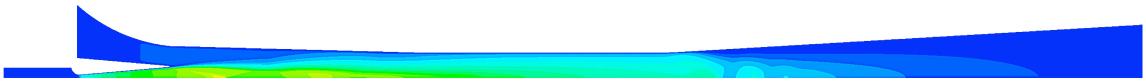

Standard k-ε

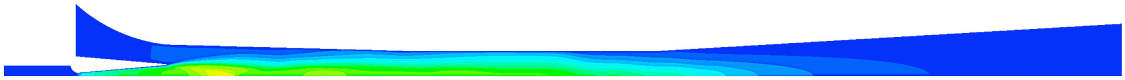

RNG k-ε

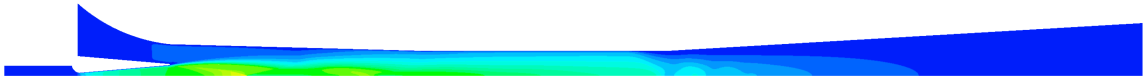

Realizable k-ε

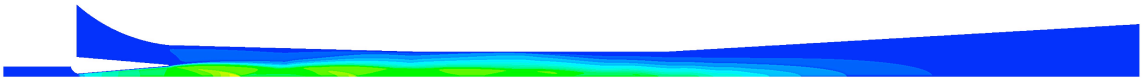

Standard k-ω

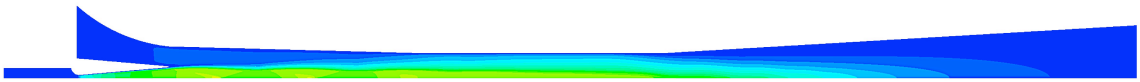

SST k-ω

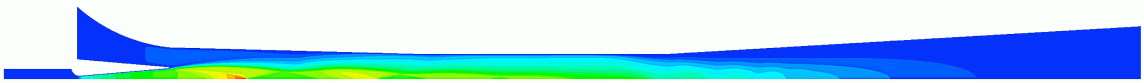

RSM

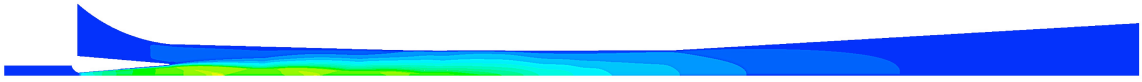

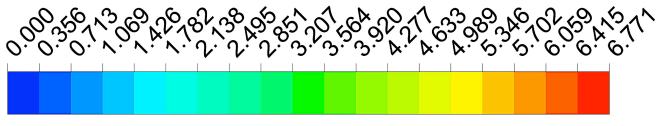

Figure 4-15: Mach contours of the ejector flow field (RUN 6).

Run 7: G2, p_g = 270280 Pa, p_e = 872.5 Pa, p_c = 3000 Pa

Table 4-23: Run 7 – Experimental and numerical results of the wall static pressure.

	Wall static pressure p_w [Pa]										
x [mm] =	70	90	110	150	177.5	205	245	280	315	350	385
Exp.	452	488	639	683	824	739	1679	2269	2602	2714	2893
Spalart-Allmaras	744	647	509	696	682	712	1078	1962	2544	2879	2984
Standard k-ε	742	632	536	859	1053	1156	1662	2622	2891	2964	2991
RNG k-ε	733	624	542	859	1065	1158	1157	2587	2893	2965	2993
Realizable k-ε	741	643	516	788	931	1035	1413	2627	2884	2941	2987
Standard k-ω	789	741	725	713	603	676	1347	1929	2405	2777	2967
SST k-ω	746	653	518	731	707	748	1315	1919	2417	2829	2983
RSM	765	694	663	891	1040	1064	1722	2457	2839	2958	2997

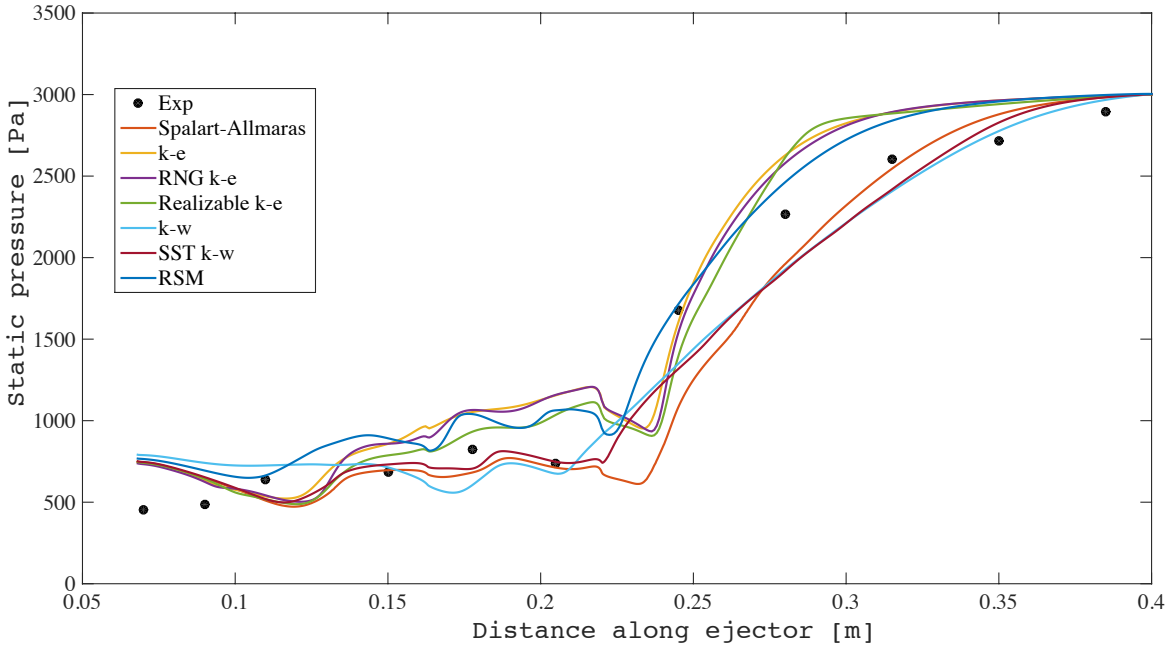

Figure 4-16: Wall static pressure distribution along the ejector (RUN 7).

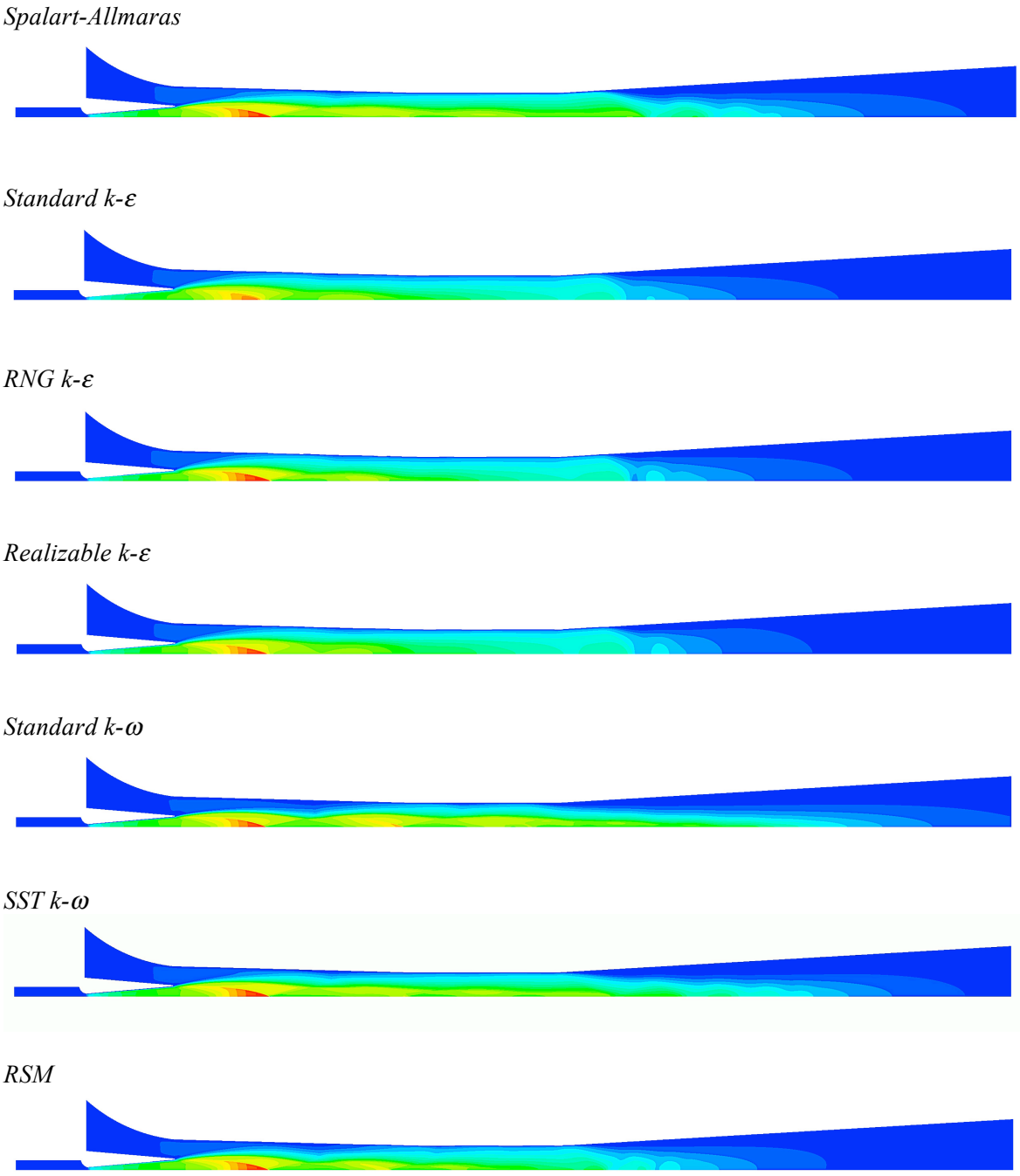

Figure 4-17: Mach contours of the ejector flow field (RUN 7).

Run 8: G3, p_g = 270280 Pa, p_e = 872.5 Pa, p_c = 3000 Pa

Table 4-24: Run 8 – Experimental and numerical results of the wall static pressure.

	Wall static pressure p_w [Pa]											
x [mm] =	30	70	90	110	150	177.5	205	245	280	315	350	385
Exp.	461	251	169	340	392	519	534	1222	1983	2273	2518	2893
Spalart-Allmaras	746	462	352	489	436	517	540	1237	1987	2575	2904	2988
Standard k-ε	729	547	463	681	784	905	1027	2015	2731	2917	2967	2993
RNG k-ε	729	546	472	675	782	910	1022	1909	2700	2922	2971	2994
Realizable k-ε	735	525	454	653	755	797	879	1796	2724	2936	2972	2994
Standard k-ω	763	465	428	481	428	497	627	1347	1947	2441	2814	2976
SST k-ω	745	468	363	512	479	539	620	1394	1952	2466	2879	2983
RSM	752	498	449	619	711	729	815	1819	2525	2868	2966	2998

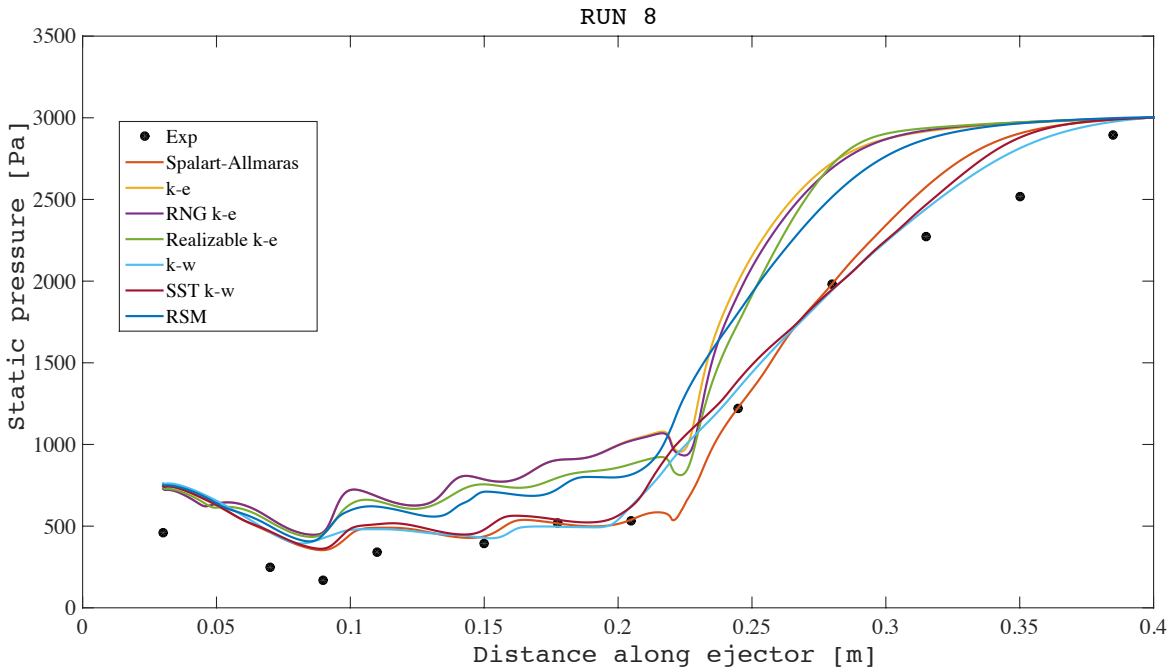

Figure 4-18: Wall static pressure distribution along the ejector (RUN 8).

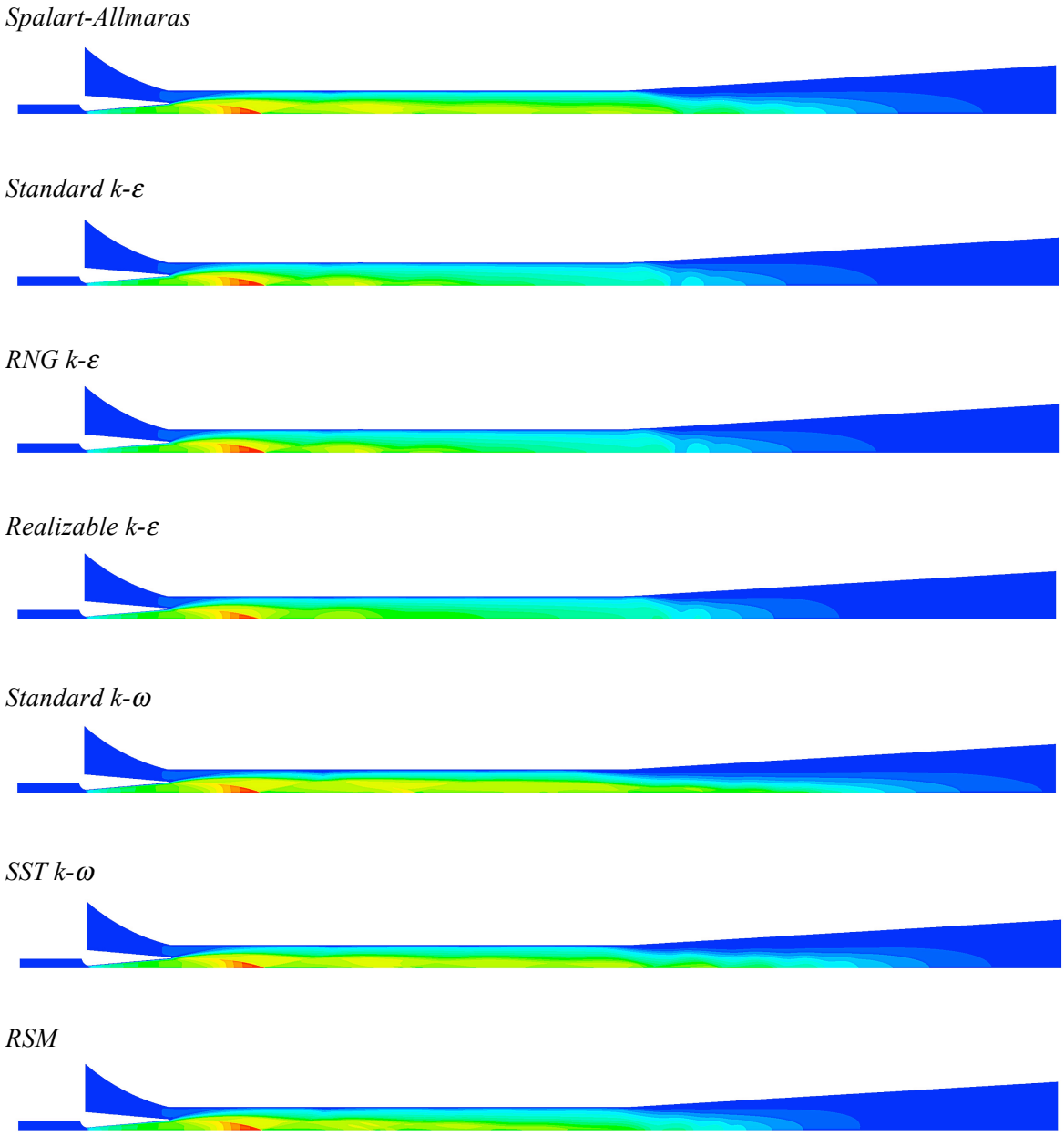

Figure 4-19: Mach contours of the ejector flow field (RUN 8).

At a glance, the wall static pressure distribution is quite well predicted by all the turbulence models and it is similar to those presented by Sriveerakul et al. (2007) [10] and other literature studies [25, 26]. However, at high discharge pressure (RUN 5) with all the turbulence models, the results are slightly worse and it is possible to observe that the 'shock starts', corresponding to the rapid increase in pressure, is predicted in a downstream position respect with the experimental measurements. In all other cases, generally, the *Standard k-ω* and *SST k-ω* models fit better the experimental results than the other turbulence models. The good performance prediction of the *SST k-ω* model also emerges from the literature [7, 15, 22]. It may be note also that the *Spalart-Allmaras* model, characterized by low computational costs, allows achieving satisfactory performance, especially in cases RUN 2 and RUN 8 with a low outlet pressure (p_c = 3000 Pa).

With regard to contours, the flow pattern shows a supersonic jet exited from the nozzle outlet and extended into the mixing chamber of the ejector. Thus, shockwaves occur in a determined position in the mixing chamber. According to the value of the discharge pressure, the shock is more or less close to the diffuser. The flow downstream of the shock wave is subsonic.

The under-expanded wave at the nozzle exit is well described by the turbulence models for all the simulated geometries and operating conditions. The comparison among the different cases shows that the expansion angle depends also on the secondary flow conditions. For example, the Figure 4-20 shows the Mach contour lines for the cases RUN 1 and RUN 2 calculated with the *SST k-ω* model. It can be observed that an increase of the secondary flow pressure determines a smaller shocks region (jet-flow core) and thus a greater secondary mass flow rate can be entrained in the mixing chamber.

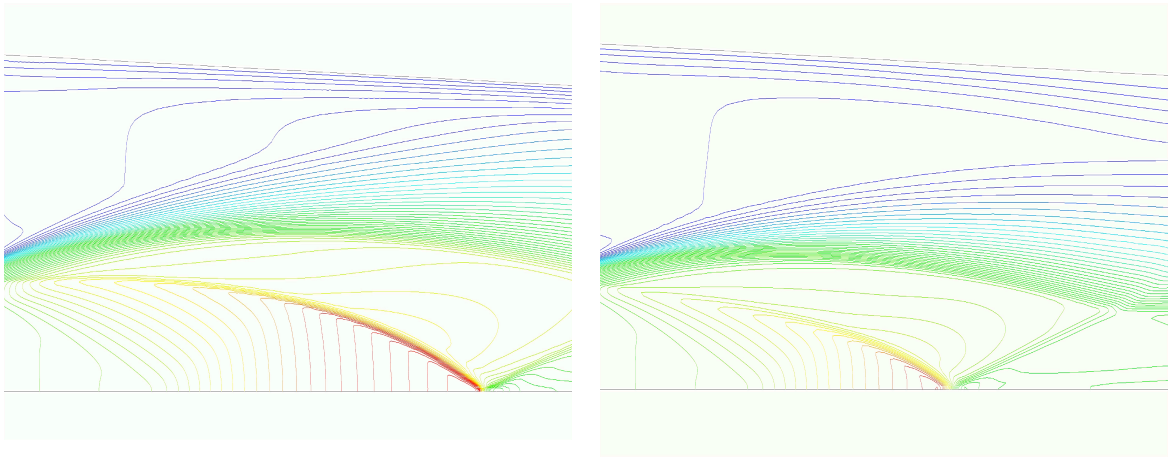

Run 1: p_g = 270280 Pa, p_e = 872.5 Pa, p_c = 3000 Pa

Run 2: p_g = 270280 Pa, p_e = 1228.1 Pa, p_c = 3000 Pa

Figure 4-20: Mach contour lines comparison.

The major difference among the turbulence models consists in the prediction of the flow behaviour in correspondence of the shocking position. It can be observed that the *k-ε* models predict the shock in advance position respect to the other turbulence models for all the simulated cases. Also in this aspect, the *SST k-ω* model seems to have a greater relevance to the actual physical behaviour and to several literature analyses [17, 19, 27]. According to [13], the investigation about the effect of the downstream pressure shows that the shock will not affect the mixing behaviour of the two streams because the discharge pressure is not exceed the critical backpressure. Indeed, the flow structures in front of the shocking position are shown unchanged and the size of the primary jet core remained constant and independent from downstream conditions. However, the shocking position change

with the value of the backpressure: an increase of the discharge pressure moves the shock position to the upstream of the ejector.

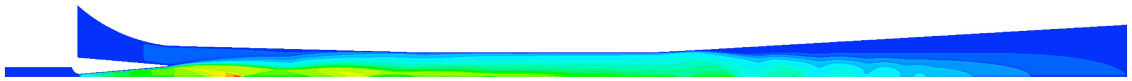

Run 2: p_g = 270280 Pa, p_e = 1228.1 Pa, p_c = 3000 Pa

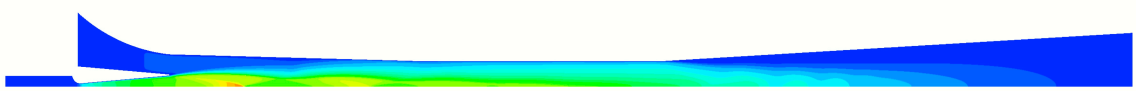

Run 3: p_g = 270280 Pa, p_e = 1228.1 Pa, p_c = 3500 Pa

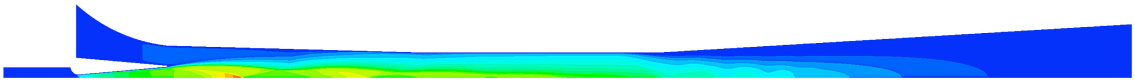

Run 4: p_g = 270280 Pa, p_e = 1228.1 Pa, p_c = 4000 Pa

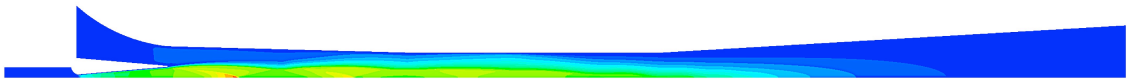

Run 5: p_g = 270280 Pa, p_e = 1228.1 Pa, p_c = 4500 Pa

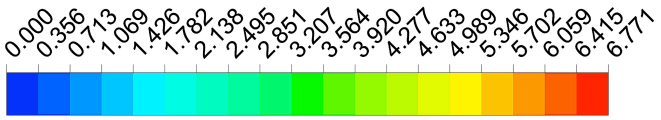

Figure 4-21: Mach contours of the ejector flow field – Effect of the discharge pressure.

Therefore, according to the results, the best agreement with both global and local parameters is achieved with the *SST k-ω* model.

4.2.4.5 Analysis of the results: effect of the wall treatment

As already remarked, there are two main approaches for the wall treatment in the CFD codes: (i) the Low-Reynolds turbulence models (i.e. *Spalart-Allmaras*, *Standard k-ω*, *SST k-ω*); (ii) the turbulence models with wall functions (i.e. *Standard k-ε*, *RNG k-ε*, *Realizable k-ε*, *RSM*).

According to the mesh refinement near the wall, the Low-Reynolds models are suitable both in the viscous sub-layer ($y^+ < 5$) and in the log-law layer ($30 < y^+ < 300$). Anyhow, they do not need wall functions because their mathematical structure already emphasizes on the flow close to the wall. The *Standard k-ω* and *SST k-ω* models can use the low-Reynolds correction if necessary.

Instead, the *RSM* and *k-ε* models are equipped with the so-called "wall functions" to model the flow behaviour near the walls. The main available wall functions are [12]:

- Standard wall function. The viscous sub-layer is not resolved and the first grid cell need to be in the region $30 < y^+ < 300$. It become less reliable when the local equilibrium assumption is not valid (i.e. strong pressure gradient, large curvature, highly 3D flow).
- Non-equilibrium wall function. It has the same validity range of the standard wall function, but relax the local equilibrium assumption in the turbulent region of the wall-neighbouring cells.

- Enhanced wall function. It generally requires a very fine near-wall mesh capable of resolving the viscous sub-layer ($y^+ < 1$). It is indicated for low-Reynolds flows or flows with complex near-wall phenomena.

In order to investigate the wall treatment effect on the numerical results, six turbulence models were tested under different near-wall modelling options. In particular, the *RSM* and *k-ε* models with the wall functions, the *SST k-ω* model with the low-Reynolds correction and the *Spalart-Allmaras* model with $y^+ \approx 1$ have been implemented and compared with each other. The results for the operating conditions "RUN 1", in terms of entrainment ratio ω, are summarized in the Table 4-25. The comparison is also performed in terms of performance prediction of the wall static pressure profile along the ejector for the different turbulence models (Figure 4-22).

Table 4-25: Run 1 – Turbulence models and wall treatments.

Turbulence model	Wall treatment	Entrainment ratio ω [-]
Exp.		0.309
Standard k-ε	Standard ($y^+ \approx 40$)	0.351 (E_R = 13.59%)
	Non-equilibrium ($y^+ \approx 40$)	0.320 (E_R = 3.56%)
	Enhanced ($y^+ < 1$)	0.322 (E_R = 4.21%)
RNG k-ε	Standard ($y^+ \approx 40$)	0.312 (E_R = 0.97%)
	Non-equilibrium ($y^+ \approx 40$)	n.c.
	Enhanced ($y^+ < 1$)	0.314 (E_R = 1.62%)
Realizable k-ε	Standard ($y^+ \approx 40$)	0.302 (E_R = 2.27%)
	Non-equilibrium ($y^+ \approx 40$)	0.302 (E_R = 2.27%)
	Enhanced ($y^+ < 1$)	0.319 (E_R = 3.24%)
RSM	Standard ($y^+ \approx 40$)	0.273 (E_R = 11.65%)
	Non-equilibrium ($y^+ \approx 40$)	n.c.
	Enhanced ($y^+ < 1$)	0.318 (E_R = 2.91%)
Spalart-Allmaras	- ($y^+ \approx 40$)	0.303 (E_R = 1.94%)
	- ($y^+ \approx 1$)	0.301 (E_R = 2.59%)
SST k-ω	- ($y^+ \approx 40$)	0.303 (E_R = 1.94%)
	Low-Re correction ($y^+ \approx 1$)	0.302 (E_R = 2.27%)

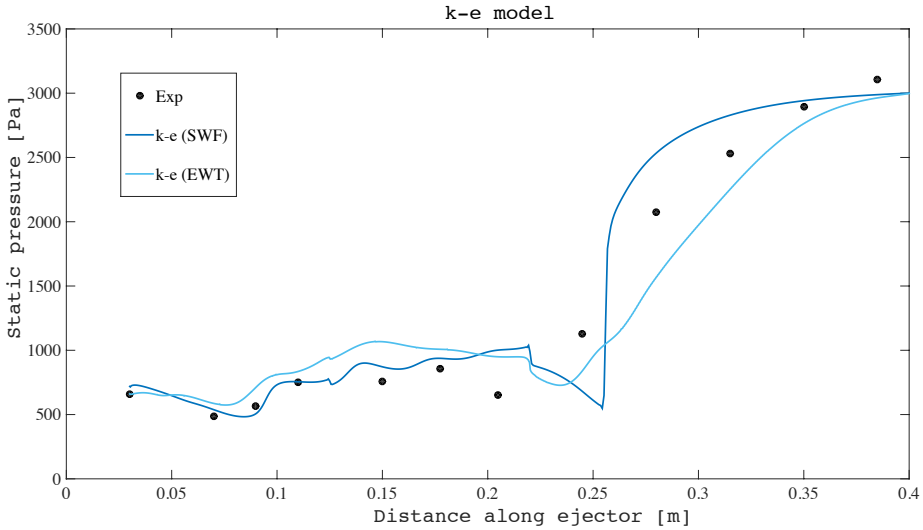
k-e model
Static pressure [Pa]
Distance along ejector [m]
Exp
k-e (SWF)
k-e (EWT)
0
500
1000
1500
2000
2500
3000
3500
0
0.05
0.1
0.15
0.2
0.25
0.3
0.35
0.4

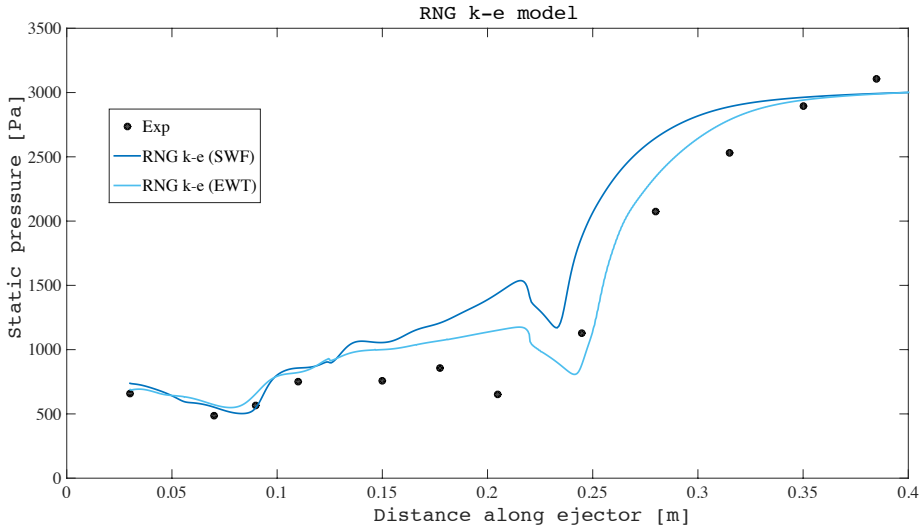
RNG k-e model
Static pressure [Pa]
Distance along ejector [m]
Exp
RNG k-e (SWF)
RNG k-e (EWT)
0
500
1000
1500
2000
2500
3000
3500
0
0.05
0.1
0.15
0.2
0.25
0.3
0.35
0.4

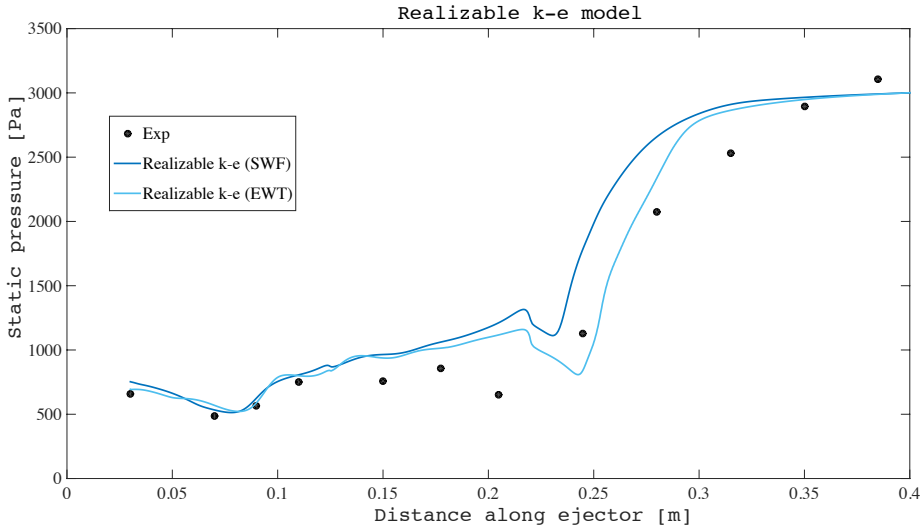
Realizable k-e model
Static pressure [Pa]
Distance along ejector [m]
Exp
Realizable k-e (SWF)
Realizable k-e (EWT)
0
500
1000
1500
2000
2500
3000
3500
0
0.05
0.1
0.15
0.2
0.25
0.3
0.35
0.4

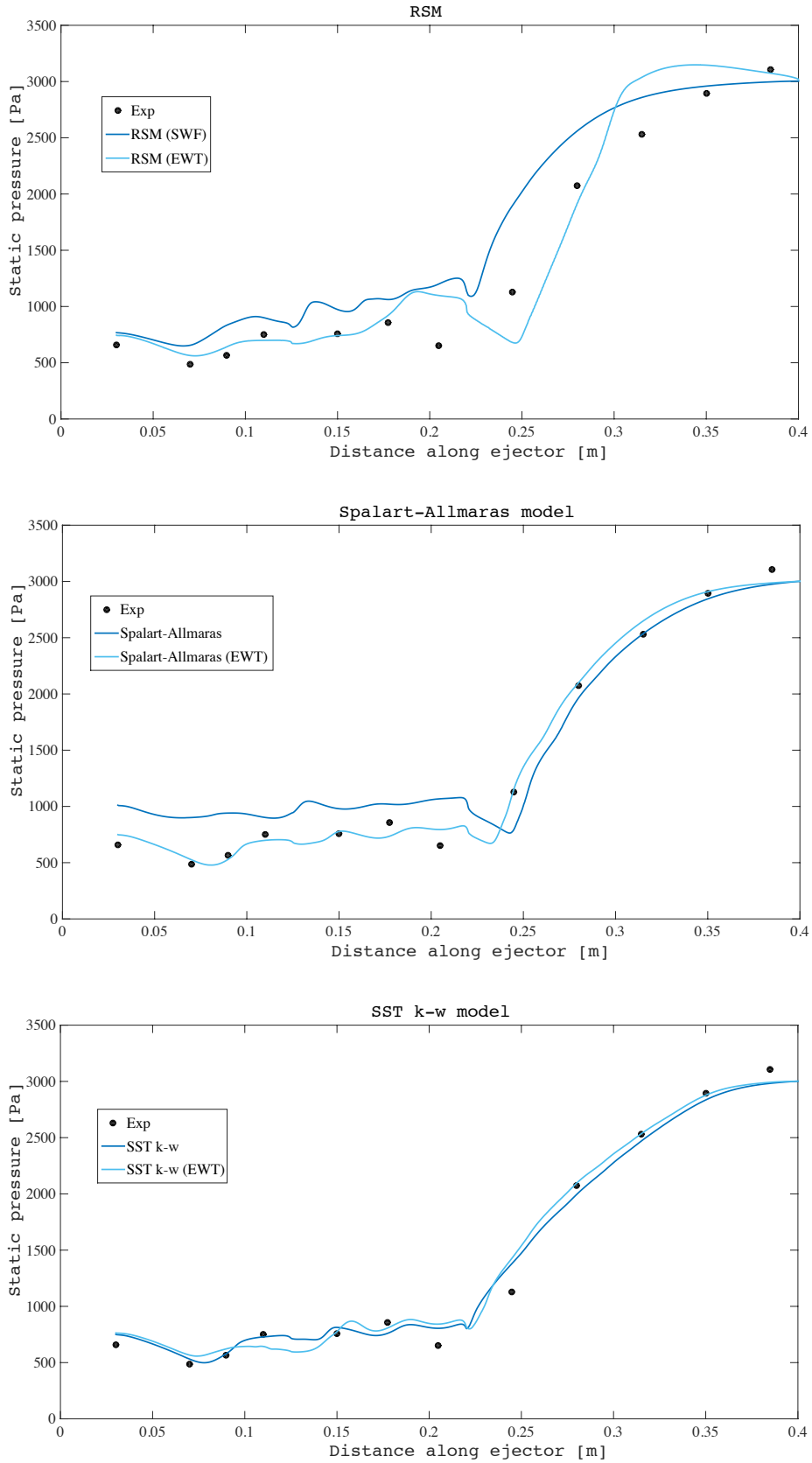

Figure 4-22: Wall static pressure distribution along the ejector – Enhanced wall treatment performance.

The modification of the wall treatment method resulted in a change of the results, especially for the wall pressure profile along the ejector.

The non-equilibrium wall function seems to have little effect on the results. Moreover, it worsens the convergence capability of the turbulence models.

The enhanced wall treatment allows achieving better results with all the turbulence models. This is especially true for the *RSM* and the *k-ε* models that involve wall function. The *Spalart-Allmaras* model, that do not need wall treatment because already implemented in its mathematical structure, has a slight benefit from the near-wall grid refinement, while the Low-Reynolds correction of the *SST k-ω* model not improve the results. The refinement of the grid near the wall involves an increase of the computational cost due to the growth of the cell number. The independence of the *SST k-ω* model from the wall treatment, in this range of y^+ ($y^+ < 40$), is thus a great advantage compared with the other turbulence models.

4.2.4.6 Analysis of the results: comparison of turbulence models

In this section, we summarize the salient aspects of the analysis. It mainly concerns the comparison among turbulence models, which is the critical step of the validation process. The RANS models are evaluated on the basis of the accordance with experimental data, the convergence capability and the computational effort.

Accordance with experimental data. The results show that the *SST k-ω* model performs better than the other employed models both in global and local parameters prediction. Indeed, the entrainment ratio is well predicted under different geometries and operating conditions with a maximum relative error equal to about 10%. Moreover, the predicted wall pressure distribution is quite well fitted with the experimental data.

Convergence capability and computational effort. According to the convergence criteria reported in the Section 4.2.3.2, we have carried out a convergence analysis in order to compare the models from this aspect. For this purpose, we have selected for all the turbulence models the fine mesh (280000 elements), used also for the grid sensitivity analysis. For a rigorous analysis, the main factors that influence the convergence capability and the computing time (i.e. grid resolution, discretization scheme, numerical methods, CFL and under-relaxation factor) must be the same for all the simulations [9]. Thus, we have tried to change these parameters (i.e. increase of the CFL number, first/second order method switch) in the same way for every turbulence model.

In all the simulated cases, the reduction of the mass and energy residuals has been the most difficult to achieve. In particular, these residuals have not fallen below 10^{-4} with the *RSM*. The convergence problems of this model are mainly due to the high degree of non-linearity [9]. However, the *Spalart-Allmaras*, *Standard k-ω* and *SST k-ω* models easily reach convergence.

From a computational point of view, the *Spalart-Allmaras* is the fastest model to converge, while the most onerous model is the *RSM*. This is due to the number of equations that must be resolved.

The results of the analysis are reported in the Table 4-26. The computational effort is calculated on the basis of the number of iterations needed to achieve convergence, in relative terms, taking as reference the *Spalart-Allmaras* model.

Table 4-26: Computational effort of CFD simulation with different turbulence models.

	Spalart-Allmaras	$k-\varepsilon$	$k-\varepsilon$ RNG	$k-\varepsilon$ Realizable	$k-\omega$	$k-\omega$ SST	RSM
Computational effort	1	1.33	1.53	1.45	1.42	1.84	3.73

4.2.4.7 Calculation validation and critical review of the model

According to the "best practice" recommended by [12], we have followed the solution procedure summarized in Figure 4-23:

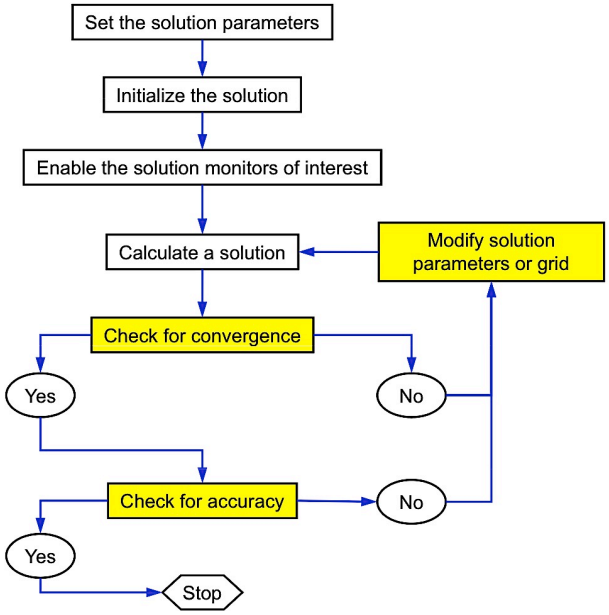

Figure 4-23: Solution procedure overview – taken from [12].

Our numerical method, reported previously, was the result of this solution scheme. In particular, the following issues have been subject to critical review:

- pressure-outlet boundary conditions. The best choice was to set this condition with strong enforcement of the average pressure as pressure specification method. Moreover, the static pressure was discretely increased until the desired value during the FMG initialization process. In this way a stable solution without reversed flow problem at the outlet was obtained.
- Courant-Friedrichs-Lewis number (CFL). The initial value of the CFL number was set equal to 0.5. When the solution was quite stable, the CFL was gradually increases to 5 in order to increase the rate of convergence.
- mesh adaptation. This solver setting, adopted for the case analysis, has proved essential to capture the mixing process and shockwaves. The dynamic refinement of mesh was defined on the Mach number gradient.

4.2.4.8 Strategy improvement

In this study, the calibration of turbulence model constants was not performed. According to [6], a model improvement can be reached by investigating the role of closure coefficients for ejector flow mixing.

Further improvements may results from the application of the real gas equations rather than using the perfect gas assumption as the properties of the working fluid [10].

4.3 Lumped parameter and CFD modelling: applicative case

4.3.1 Introduction

The validated CFD model is now employed in an applicative case concerning the experimental study carried out by J. G. del Valle et al. (2014) [28]. The results are also compared with that obtained with the lumped parameter models presented in the Chapter 3.

In this analysis, an ejector refrigeration system working with R134a was considered. The ejector critical conditions have been determined for three mixing chambers with the same nozzle, diffuser and constant-area diameter (4.8 mm) but different entrance geometry and for several stagnation conditions of primary and secondary fluid. The influence of the nozzle longitudinal position (NXP) has also been analyzed. The ejector design condition were: T_g = 85°C, T_e = 10°C and T_c = 30°C. The three mixing chambers, labelled as "A", "B" and "C", have the following features:

- the Chamber "A" is the classical shape with a 30° half-angle conical entry and a constant area zone with a length to diameter ratio equal to 8.6;
- the Chamber "B", as proposed by Munday and Bagster (1977) [29], has been tested to enhance the performance of the ejector by promoting a supersonic compression in a convergent region rather than a shock system in a constant area region. Thus, the present design has a convergent conical entrance and a short constant area region;
- the Chamber "C" corresponds to the description made by Ginoux (1972) [30], who proposed that the supersonic compression could also be produced through a sharp contraction. This geometry has two constant area regions with diameters of 5.5 and 4.8 mm, respectively.

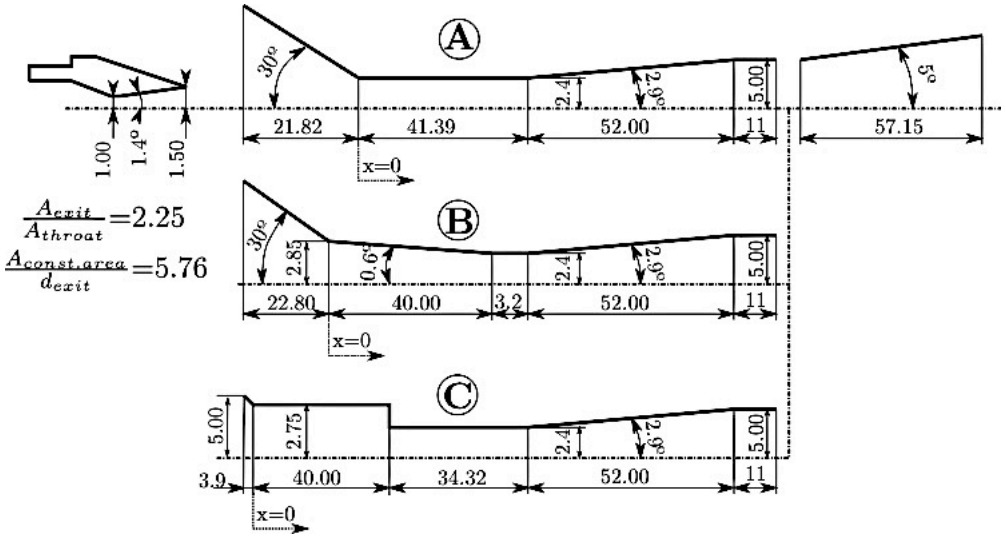

Figure 4-24: Geometry for the three mixing chamber – taken from [28].

The experimental analysis mainly concerns the determination of the critical condition for each of the mixing chambers under different primary and secondary flow stagnation conditions in the neighbourhood of the design ones. Moreover, the operating curves of the entrainment ratio as a function of discharge pressure are experimentally determined for T_g = 84.39°C and T_e = 10°C. The nozzle has been positioned at the location of the highest entrainment ratio, corresponding to -5.58 mm, -1.70 mm and -1.95 mm for the mixing chambers "A", "B" and "C", respectively.

4.3.2 Experimental determination of the critical conditions

In the Table 4-27 are reported the experimental results, where the "n.a." boxes correspond to cases for which the critical condition has not been attained for the range of discharge pressures of the study. The results show that the critical entrainment ratio diminishes whereas the critical backpressure increase with the primary flow pressure. Instead, the growth of the secondary flow pressure results in the increase of both the critical entrainment ratio and the corresponding discharge pressure. This trend is in accordance with the analyses presented in the Chapter 1, and it is independent on geometry and working fluid.

However, the experimental study reveals several other issues [28]:

- the mixing chamber "B" yields the higher critical entrainment ratio for all the operating conditions whereas the higher critical backpressure have been obtained with the mixing chamber "A";
- the mixing chamber "C" has not reached critical conditions for most of the tested conditions; however, for the few cases for which critical conditions has been attained, the critical entrainment ratio was very close to that of chamber "A";
- the geometries "B" and "C" were designed to improve the compression process that takes place along the mixing chamber. However, while the performance of geometry "B" is close to that of "A", a significant worsening of performance with respect to the other two has been observed for chamber "C".

These issues have not physical arguments or enough experimental data to obtain an adequate justification. The aim of our analysis is to provide plausible explanations by means of the validated CFD model.

Table 4-27: Entrainment ratio for the critical condition for the three mixing chambers – Experimental data.

		Chamber "A"		Chamber "B"		Chamber "C"	
T_g [°C]	T_e [°C]	T_c [°C]	ω_{exp} [-]	T_c [°C]	ω_{exp} [-]	T_c [°C]	ω_{exp} [-]
74.89	10	n.a.	n.a.	n.a.	n.a.	n.a.	n.a.
79.37	7	28.95	0.422	n.a.	n.a.	n.a.	n.a.
79.37	10	29.41	0.494	27.01	0.571	n.a.	n.a.
84.39	7	31.68	0.342	29.14	0.438	n.a.	n.a.
84.39	10	32.48	0.398	28.86	0.484	26.38	0.384
89.15	5	32.02	0.273	30.40	0.365	27.17	0.276
89.15	7	34.11	0.297	31.46	0.391	27.01	0.297
89.15	10	35.41	0.339	32.04	0.437	28.40	0.332

4.3.3 Determination of the critical conditions with lumped parameter models

In this section the lumped parameter models, presented in the Chapter 3, are implemented in order to predict the ejector performance and compared the results with the experimental measurements. The lumped parameter models used in this analysis are:

- Model 1 – Chen, Havtun and Palm (2014) [31];
- Model 2 – Chen, Liu et al. (2013) [32];
- Model 3 – Zhu, Cai et al. (2007) [33];
- Model 4 – Kumar and Ooi (2014) [34];
- Model 5 – Cardemil and Colle (2012) [35].

As already remarked, the three mixing chambers have the same nozzle, diffuser and the same value of the mixing chamber area. They differ only for the shape of the entrance geometry, but the lumped parameter models are not able to take into account this feature. Therefore, we have defined a different set of efficiencies for each geometry (Table 4-28). The values were chosen in agreement with the literature [36] and in order to fit the experimental data.

Table 4-28: Efficiencies assumed for the three mixing chambers.

	Model 1	Model 2	Model 3	Model 4	Model 5
Chamber "A"	$\eta_n = 0.9$ $\eta_m = 0.9$ $\eta_d = 0.9$	$\eta_p = 0.95$ $\eta_{py} = 0.7$ $\eta_s = 0.95$ $\psi_m = 0.75$	$\psi_p = 0.8$ $\psi_s = 0.7$	$\eta_p = 0.95$ $\varphi_p = 0.95$ $\eta_s = 0.75$ $\eta_d = 0.9$	$\eta_n = 0.85$ $\eta_m = 0.9$ $\eta_d = 0.85$
Chamber "B"	$\eta_n = 0.9$ $\eta_m = 0.92$ $\eta_d = 0.9$	$\eta_p = 0.95$ $\eta_{py} = 0.8$ $\eta_s = 0.95$ $\psi_m = 0.8$	$\psi_p = 0.8$ $\psi_s = 0.8$	$\eta_p = 0.95$ $\varphi_p = 0.9$ $\eta_s = 0.85$ $\eta_d = 0.9$	$\eta_n = 0.85$ $\eta_m = 0.75$ $\eta_d = 0.85$
Chamber "C"	$\eta_n = 0.9$ $\eta_m = 0.78$ $\eta_d = 0.9$	$\eta_p = 0.95$ $\eta_{py} = 0.9$ $\eta_s = 0.95$ $\psi_m = 0.65$	$\psi_p = 0.75$ $\psi_s = 0.7$	$\eta_p = 0.95$ $\varphi_p = 0.95$ $\eta_s = 0.7$ $\eta_d = 0.9$	$\eta_n = 0.85$ $\eta_m = 0.95$ $\eta_d = 0.85$

It can be observed that the primary nozzle and the diffuser efficiencies are the same for the Chamber "A", "B" and "C" for each model, according to the actual geometry of the three ejectors.

In the following sections, we have reported the obtained results, the relative errors committed and the errors distribution for each geometry.

4.3.3.1 Mixing chamber "A"

Table 4-29: Entrainment ratio for the critical condition for the mixing chamber "A" – Lumped parameter models prediction.

T_g	T_e	T_c	Entrainment ratio ω [-]					
[°C]	[°C]	[°C]	Exp.	Model 1	Model 2	Model 3	Model 4	Model 5
79.37	7	28.95	0.422	0.4349	0.4544	0.4678	0.4427	0.4354
79.37	10	29.41	0.494	0.4972	0.5404	0.5575	0.5185	0.4923
84.39	7	31.68	0.342	0.3784	0.3737	0.3824	0.3720	0.3673
84.39	10	32.48	0.398	0.4172	0.4513	0.4637	0.4406	0.4200
89.15	5	32.02	0.273	0.3533	0.2615	0.2619	0.2733	0.2767
89.15	7	34.11	0.297	0.3342	0.3057	0.3095	0.3124	0.3074
89.15	10	35.41	0.339	0.3523	0.3763	0.3843	0.3750	0.3559

Table 4-30: Relative errors of the lumped parameter models in the prediction of the entrainment ratio for the mixing chamber "A".

T_g	T_e	T_c	Relative error E_R (ω) [%]				
[°C]	[°C]	[°C]	Model 1	Model 2	Model 3	Model 4	Model 5
79.37	7	28.95	3.06	7.68	10.86	4.90	3.17
79.37	10	29.41	0.64	9.39	12.85	4.96	0.35
84.39	7	31.68	10.65	9.27	11.81	8.77	7.41
84.39	10	32.48	4.82	13.39	16.52	10.71	5.54
89.15	5	32.02	29.40	4.21	4.06	0.11	1.35
89.15	7	34.11	12.54	2.93	4.20	5.19	3.51
89.15	10	35.41	3.93	11.00	13.37	10.62	4.98

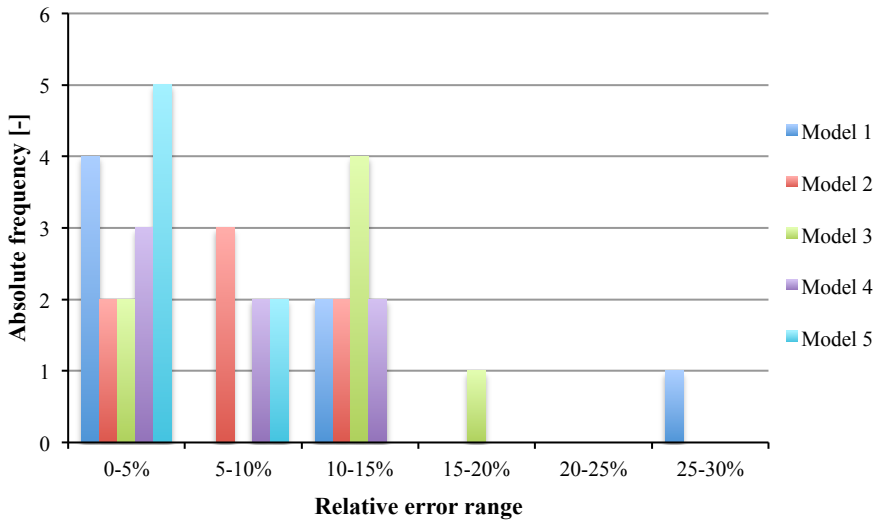

Figure 4-25: Absolute frequency distribution of the errors – Mixing chamber "A".

4.3.3.2 Mixing chamber "B"

Table 4-31: Entrainment ratio for the critical condition for the mixing chamber "B" – Lumped parameter models prediction.

T_g [°C]	T_e [°C]	T_c [°C]	Entrainment ratio ω [-]					
			Exp.	Model 1	Model 2	Model 3	Model 4	Model 5
79.37	10	27.01	0.571	0.6092	0.6170	0.6072	0.5752	0.5036
84.39	7	29.14	0.438	0.4613	0.4479	0.4377	0.4180	0.3787
84.39	10	28.86	0.484	0.5574	0.5268	0.5163	0.4917	0.4315
89.15	5	30.40	0.365	0.3984	0.3340	0.3220	0.3120	0.2873
89.15	7	31.46	0.391	0.4082	0.3789	0.3676	0.3541	0.3186
89.15	10	32.04	0.437	0.4589	0.4507	0.4396	0.4213	0.3676

Table 4-32: Relative errors of the lumped parameter models in the prediction of the entrainment ratio for the mixing chamber "B".

T_g [°C]	T_e [°C]	T_c [°C]	Relative error E_R (ω) [%]				
			Model 1	Model 2	Model 3	Model 4	Model 5
79.37	10	27.01	6.69	8.06	6.33	0.74	11.80
84.39	7	29.14	5.33	2.26	0.08	4.57	13.55
84.39	10	28.86	15.16	8.84	6.67	1.59	10.85
89.15	5	30.40	9.15	8.49	11.78	14.52	21.29
89.15	7	31.46	4.41	3.09	5.99	9.45	18.53
89.15	10	32.04	5.01	3.14	0.59	3.59	15.88

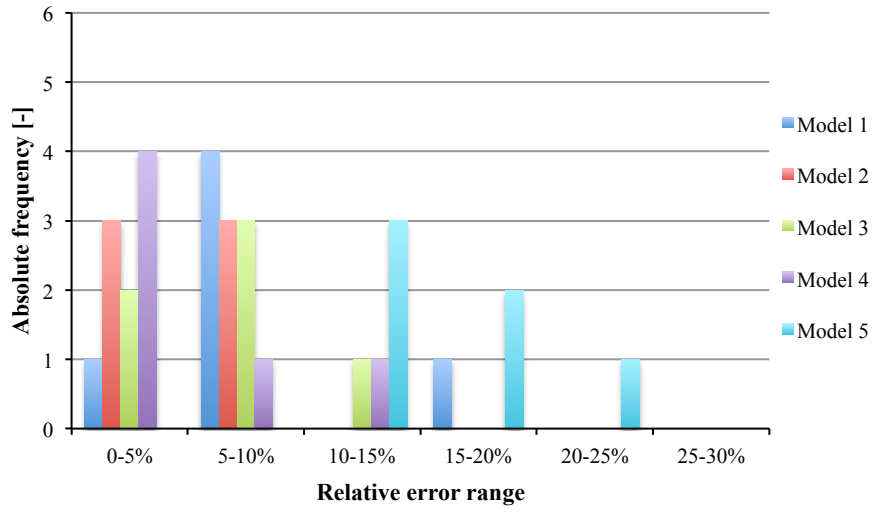

Figure 4-26: Absolute frequency distribution of the errors – Mixing chamber "B".

4.3.3.3 Mixing chamber "C"

Table 4-33: Entrainment ratio for the critical condition for the mixing chamber "C" – Lumped parameter models prediction.

T_g [°C]	T_e [°C]	T_c [°C]	Entrainment ratio ω [-]					
			Exp.	Model 1	Model 2	Model 3	Model 4	Model 5
84.39	10	26.38	0.384	0.3598	0.4765	0.4471	0.4253	0.4161
89.15	5	27.17	0.276	0.2599	0.2857	0.2352	0.2639	0.2731
89.15	7	27.01	0.297	0.2896	0.3301	0.2853	0.3016	0.3036
89.15	10	28.40	0.332	0.2992	0.4011	0.3639	0.3620	0.3519

Table 4-34: Relative errors of the lumped parameter models in the prediction of the entrainment ratio for the mixing chamber "C".

T_g [°C]	T_e [°C]	T_c [°C]	Relative error E_R (ω) [%]				
			Model 1	Model 2	Model 3	Model 4	Model 5
84.39	10	26.38	6.31	24.09	16.43	10.76	8.35
89.15	5	27.17	5.85	3.51	14.78	4.40	1.05
89.15	7	27.01	2.49	11.14	3.94	1.55	2.24
89.15	10	28.40	9.89	20.81	9.62	9.04	5.98

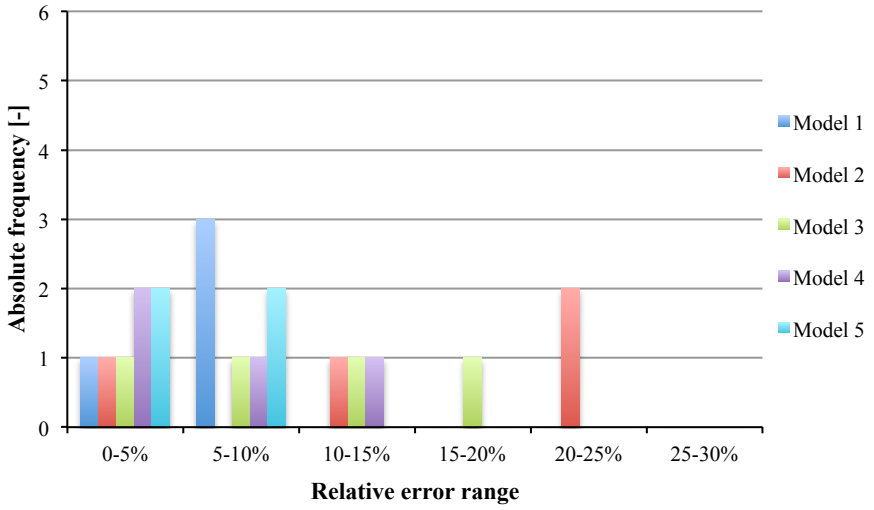

Figure 4-27: Absolute frequency distribution of the errors – Mixing chamber "C".

According to the results, the lumped parameter models well predict the ejector performance that works in critical conditions. However, it can be observed that the performance prediction of the different models rather varies depending on the geometry. This issue testified the impact of the efficiency values on the results obtained with LPM.

The model that has achieved the best results is the model 5, as in the validation analysis performed in the Chapter 3. The models 3 and 4 obtained good performance as well.

With regard to the model 5, the relative errors are less than 7.5% and 8.5% with the mixing chambers "A" and "C", respectively. However, the error is greater with the mixing chamber "B", for which it grows up to 20%.

The models 1 and 2 have performance similar to the previous one. The first model, with the geometries "B" and "C", has a maximum error less than 16% and 10% respectively, while with the mixing chamber "A" the maximum error is quite high (around 30%). The second model, instead, performs better with the geometries "A" and "B", for which the maximum error does not exceed the 14%. With the mixing chamber "C", the maximum error grows up to 24%.

The models 3 e 4 obtained, instead, fairly uniform performance with all the geometries and the maximum error is equal to 16.5% and 14.5%, respectively.

4.3.4 Determination of the critical conditions with CFD model

In this section, the validated CFD model is implemented in order to determine the ejector performance in critical condition.

In the Table 4-35 are summarized the main quality parameters of the meshes used in this study.

Table 4-35: Mesh quality parameters.

Mesh:		Chamber "A"	Chamber "B"	Chamber "C"
Cells		68375	66000	71400
Aspect ratio	**worst value**	8.1	8.3	9.2
	> 6	41.02%	47.97%	45.27%
Size-change	**worst value**	1.69	1.55	1.08
	> 1.1	0.07%	0.05%	-
Cell surface	**worst value**	0.10	0.09	0.08
	> 0.05	6.20%	9.14%	6.20%
Equi-angle skew	**worst value**	0.56	0.42	0.63
	> 0.5	0.12%	-	0.04%

The solver setups (Table 4-36) and the kind of boundary conditions (Table 4-37) are the same of the validation analysis. Moreover, the *SST k-ω* model was chosen due to its good performance prediction. For all the simulations of this case, the y^+ value range from 40 to 60.

Table 4-36: Solver and model setups.

Solver	Geometry	Formulation	Time	Velocity formulation	Gradient option	Viscous model
Density-based	2D axisymmetric	Implicit	Steady	Absolute	Least Squares Cell Based	*SST k-ω*

Table 4-37: Boundary conditions.

	Primary flow	Secondary flow	Outlet flow	Wall
Condition	Total pressure Total temperature	Total pressure Total temperature	Static pressure Total temperature	Adiabatic No slip
Turbulence intensity	5%	2%	5%	-
Hydraulic diameter	0.0025 m	0.013 m	0.010 m	-

The strategy solution adopted is the same of the validation analysis. The desired steady-state solution is achieved through steady solver using the pseudo-transient method until convergence with first-order discretization schemes. When the simulation is quite defined, discretization schemes are switched to second-order and a standard steady-state solution is pursued.

In this case, however, the working fluid is the refrigerant R134a. Thus, we have used the NIST real gas model included in the Fluent libraries. Due to the limited validity range of the database, the problem was initialized with the ideal gas assumption, switching in a later time to the real gas model.

The flow modelling of NIST real-gas flow is much more complex and challenging than simple ideal-gas flow [12]. Thus, in order to run stable simulations and aid convergence, a lower CFL number ($CFL = 0.1$) is set. Once flow behaviour is stabilized, the CFL number is increased up to 3. The numerical methods and the parameter controls are summarized in the Table 4-38 and Table 4-39.

Table 4-38: Numerical methods.

	Flow	Turbulent kinetic energy	Dissipation rate
Preliminary results (pseudo-transient)	1st order upwind	1st order upwind	1st order upwind
Final results	2nd order upwind	2nd order upwind	2nd order upwind

Table 4-39: Parameter controls.

	Turbulent kinetic energy	Dissipation rate	Turbulent viscosity	Solid
Preliminary results (pseudo-transient)	0.7	0.7	0.7	-
Final results	0.6	0.6	0.6	1

Adopting this solver setting and solution strategy, we have obtained the results reported in the Table 4-40.

Table 4-40: Entrainment ratio for the critical condition for the three mixing chambers – CFD prediction.

		Mixing chamber "A"			Mixing chamber "B"			Mixing chamber "C"		
T_g [°C]	T_e [°C]	T_c [°C]	ω [-]	E_R (ω) [%]	T_c [°C]	ω [-]	E_R (ω) [%]	T_c [°C]	ω [-]	E_R (ω) [%]
84.39	10	32.48	0.4165	4.64	28.86	0.4348	10.16	26.38	0.3879	0.75
89.15	5	32.02	0.2879	5.45	30.40	0.3877	6.22	27.17	0.2797	1.34
89.15	7	34.11	0.3145	5.90	31.46	0.4189	7.14	27.01	0.2995	0.84
89.15	10	35.41	0.3573	5.40	32.04	0.4721	8.03	28.40	0.3369	1.48

The critical entrainment ratio is well predicted by the CFD model. The maximum error is equal to around 10% with the mixing chamber "B". The simulations with the geometries "A" and "C" have even better performance, with relative errors less than 6% and 1.5%, respectively.

4.3.5 Determination of the operating curves

In this section, the behaviour of the ejector at different discharge pressure is analysed in order to determine the operating curves for the three mixing chambers under investigation.

As already remarked, according to the variation of the entrainment ratio ω with the backpressure p_c, fixed the primary and secondary flow conditions, the ejector operation can be divided into three operational modes (Figure 4-28).

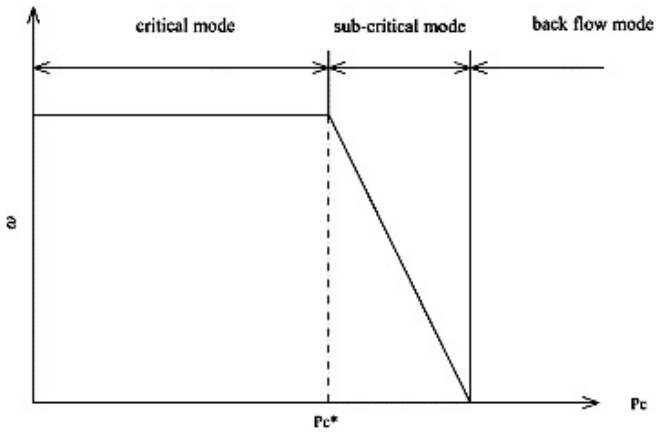

Figure 4-28: Ejector operational modes – taken from [32].

During critical mode operation, the primary and secondary flows are both chocked and the entrainment ratio remains constant. In the sub-critical mode operation, only the primary flow is chocked, while the induced flow, and thus the entrainment ratio, changes with the discharge pressure. For the back flow mode, the p_c is so high that the secondary flow is reversed and the entrainment ratio is less than zero. The critical backpressure p_c^* delimits the critical and the sub-critical region.

The ejector performance both in critical and sub-critical mode operations was then evaluated through the lumped parameter and CFD modelling techniques.

4.3.5.1 Lumped parameter model

Among the considered lumped parameter models, the only one able to predict the ejector performance in the entire operating range under analysis is the Model 2. It has been proposed by the authors precisely with the purpose of predict ejector performance at critical and sub-critical operational regimes.

Table 4-41: Entrainment ratio for the three mixing chambers – LPM prediction.

Mixing chamber "A"				Mixing chamber "B"				Mixing chamber "C"			
T_c [°C]	ω_{exp} [-]	ω_{lpm} [-]	$E_R(\omega)$ [%]	T_c [°C]	ω_{exp} [-]	ω_{lpm} [-]	$E_R(\omega)$ [%]	T_c [°C]	ω_{exp} [-]	ω_{lpm} [-]	$E_R(\omega)$ [%]
26.38	0.401	0.4513	12.54	**26.38**	0.484	0.5268	8.84	**26.38**	0.385	0.4765	23.8
27.25	0.395	0.4513	12.54	**27.25**	0.488	0.5268	7.95	**27.25**	0.371	0.4765	28.4
28.86	0.402	0.4513	12.54	**28.86**	0.484	0.1974	59.21	**28.12**	0.305	0.1486	51.3
30.83	0.402	0.4513	12.54	**30.83**	0.179	0.1643	8.21	**28.86**	0.267	0.1397	47.7
31.86	0.398	0.4513	12.54					**29.91**	0.080	0.1124	40.4
32.48	0.398	0.4513	12.54								
34.05	0.217	0.1687	22.26								
34.93	0.111	0.1533	38.1								

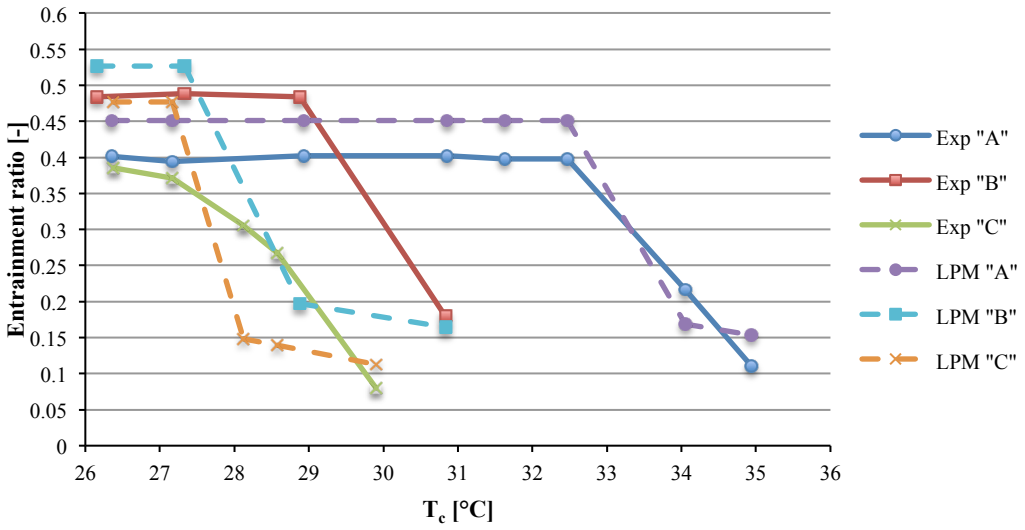

Figure 4-29: Experimental and LPM operating curves.

The relative errors are quite high throughout the operating range with the mixing chamber "C" and thus the LPM is not able to describe the ejector behaviour for this particular geometry shape. The model prediction improves with the mixing chamber "A" and "B". The results are in line with the validation analysis as regard the performance prediction in the critical mode operation. However, the results get worse in the sub-critical region. In particular, the LPM with the geometry "B" underpredicts the critical backpressure and this causes a worsening of its results. As already remarked, this issue mainly depends on the use of constant efficiency values also for off-design conditions.

4.3.5.2 CFD model

The same operating conditions were simulated with the CFD model and the results are summarized in the Table 4-42.

Table 4-42: Entrainment ratio for the three mixing chambers – CFD model prediction.

Mixing chamber "A"				Mixing chamber "B"				Mixing chamber "C"			
T_c [°C]	ω_{exp} [-]	ω_{cfd} [-]	E_R (ω) [%]	T_c [°C]	ω_{exp} [-]	ω_{cfd} [-]	E_R (ω) [%]	T_c [°C]	ω_{exp} [-]	ω_{cfd} [-]	E_R (ω) [%]
26.38	0.401	0.4167	3.91	**26.38**	0.484	0.5239	8.24	**26.38**	0.385	0.3879	0.75
27.25	0.395	0.4167	5.76	**27.25**	0.488	0.5239	7.36	**27.25**	0.371	0.3868	4.26
28.86	0.402	0.4166	3.63	**28.86**	0.484	0.4348	10.16	**28.12**	0.305	0.2753	9.74
30.83	0.402	0.4167	3.66	**30.83**	0.179	0.2108	17.76	**28.86**	0.267	0.2602	2.55
31.86	0.398	0.4165	4.65								
32.48	0.398	0.4165	4.64								
34.05	0.217	0.2412	11.15								
34.93	0.111	0.1282	15.49								

The Figure 4-30 shows the comparison among the experimental and CFD curves:

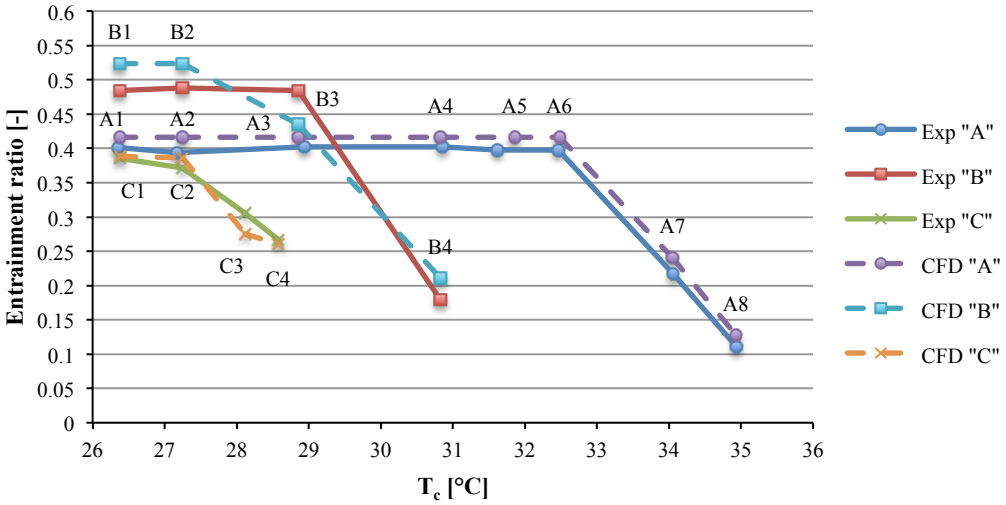

Figure 4-30: Experimental and CFD operating curves.

The CFD modelling allows achieving good performance prediction throughout the operating field with all the considered geometries. The relative errors are less than 18% also in sub-critical mode operations. Its performance prediction is, therefore, significantly higher than the LPM. However, it is possible to highlight two analogies between LPM and CFD models. Firstly, both the approaches get worse their performance in the sub-critical region. Secondly, the critical backpressure for the mixing chamber "B" is underpredicted.

In Figure 4-31 are represented the Mach flow fields of the three mixing chambers for each operating condition.

Mixing chamber "A"

A1

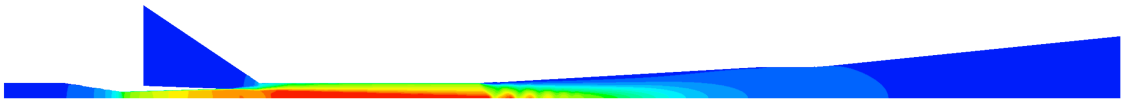

A2

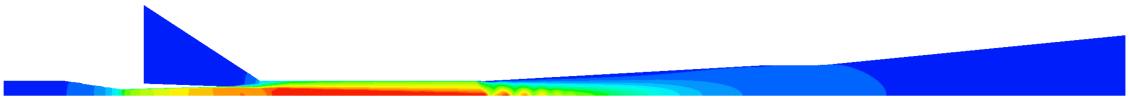

A3

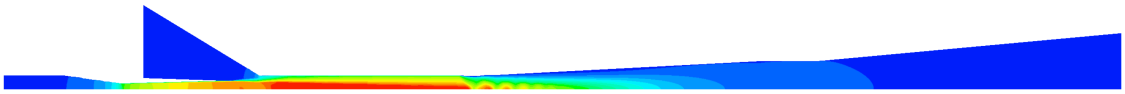

A4

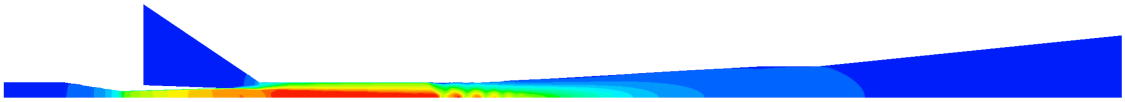

A5

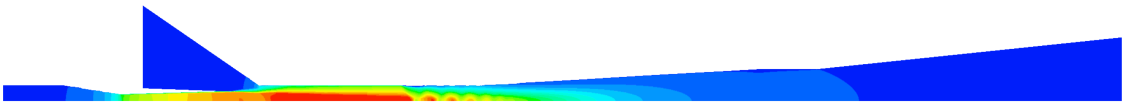

A6

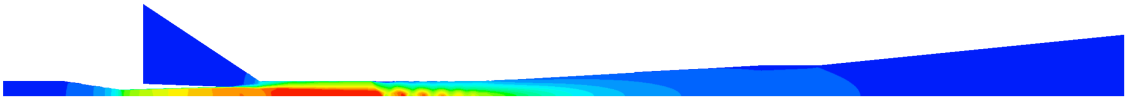

A7

A8

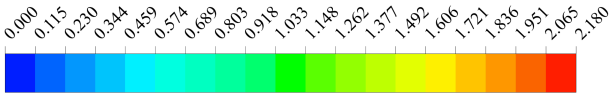

Mixing chamber “B”

B1

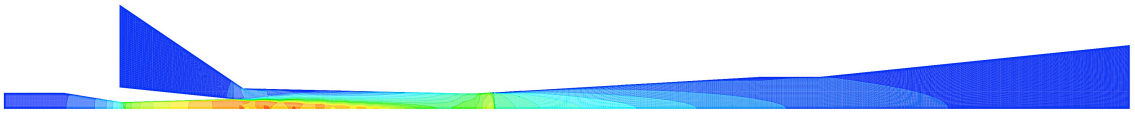

B2

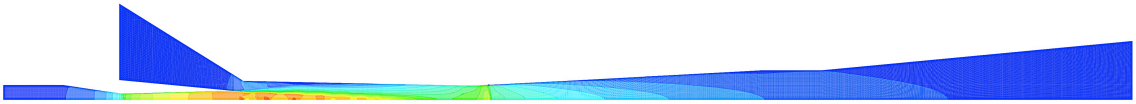

B3

B4

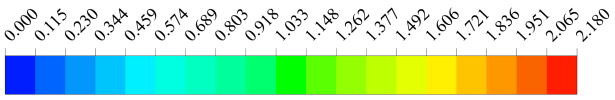

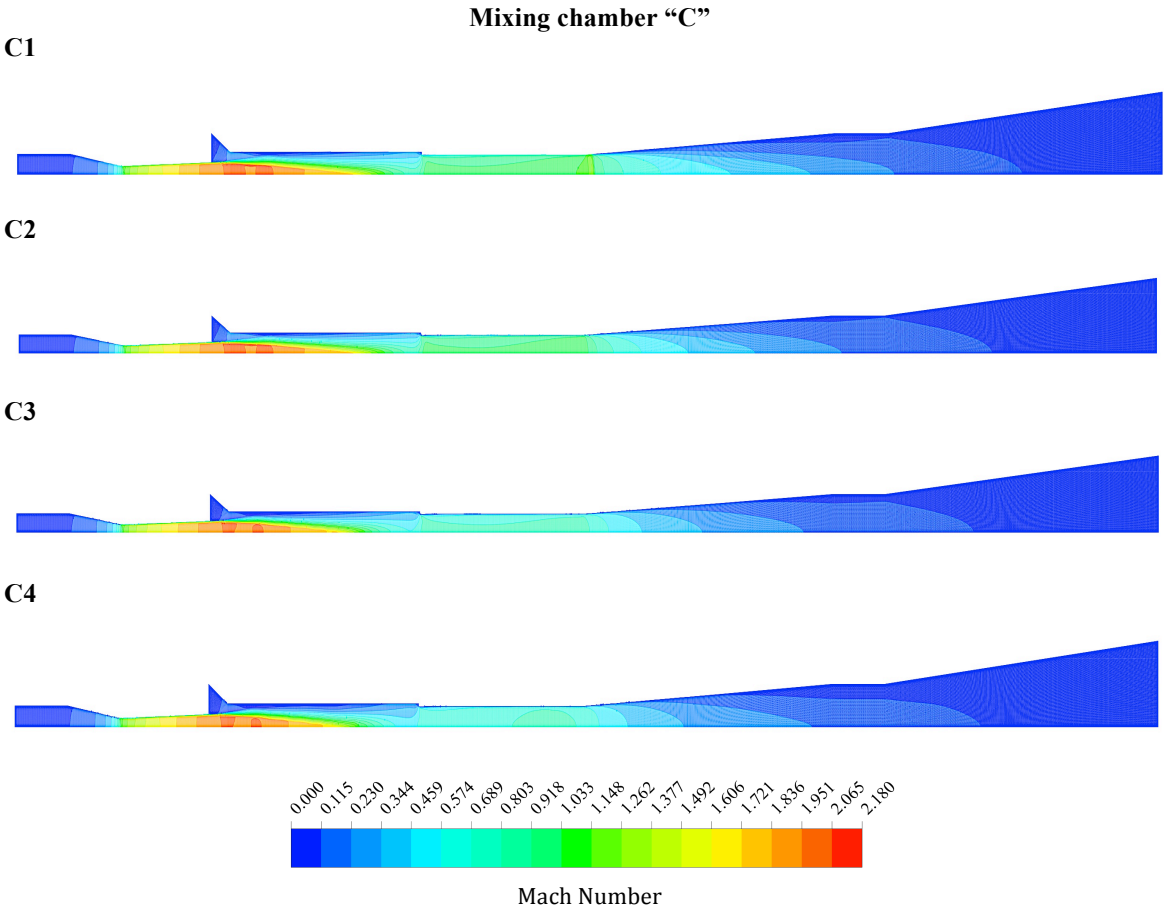

Figure 4-31: Mach contours of the ejector flow field – Effect of the discharge pressure.

4.3.6 CFD analysis: resolution of experimental issues

As already remarked, the experimental analysis has showed some issues that have not physical arguments or enough experimental data to obtain an adequate justification. Thanks to the CFD simulations, we are now able to give explanations about these matters.

4.3.6.1 Critical conditions of the mixing chambers "A" and "B"

"The mixing chamber B yields the higher critical entrainment ratio for all the operating conditions whereas the higher critical backpressure has been obtained with the mixing chamber A".

The first issue concerns the behaviour of the mixing chambers "A" and "B" in critical mode operations. The Figure 4-32 shows how the shockwave in the mixing chamber "A" is farthest from the nozzle exit section than the chamber "B". An increase of the discharge pressure moves the shock position to the upstream of the ejector and, therefore, the chamber "B" achieves before the critical condition. On the other hand, in critical condition, the mixing chamber "B" allows the entry of more secondary flow in the mixing chamber, as shown in the Figure 4-33. Thus, the critical entrainment ratio is higher than that of the mixing chamber "A" at equal generator and evaporator temperature.

Chamber "A"

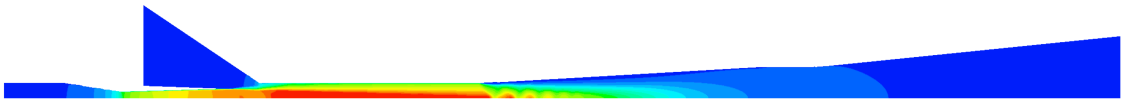

Chamber "B"

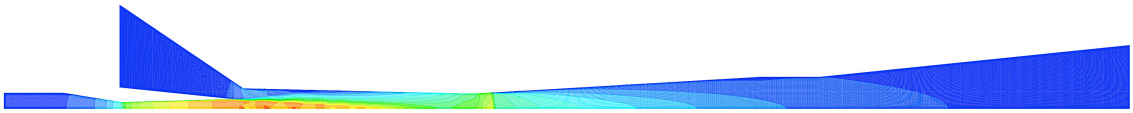

Figure 4-32: Mach contours of the ejector flow field – Comparison between mixing chambers "A" and "B" (T_g = 84.39°C, T_e = 10°C, T_c = 26.38°C).

Chamber "A": T_c = 32.48°C

Chamber "B": T_c = 28.86°C

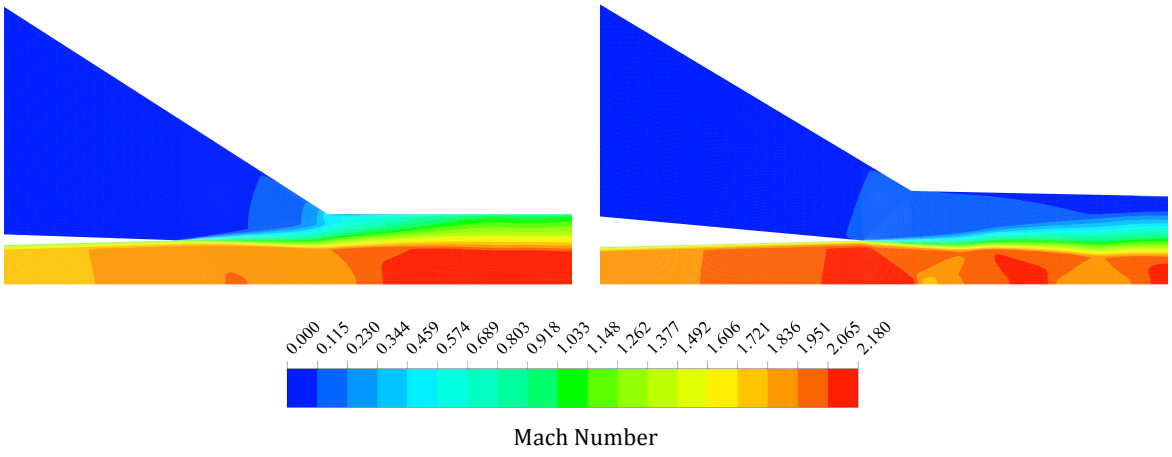

Figure 4-33: Mach contours of the ejector flow field – Comparison between mixing chambers "A" and "B" in critical conditions (T_g = 84.39°C, T_e = 10°C).

4.3.6.2 Critical conditions of the mixing chambers "A" and "C"

"The mixing chamber C has not reached critical conditions for most of the tested conditions; however, for the few cases for which critical conditions has been attained, the critical entrainment ratio was very close to that of chamber A".

The chamber "C" is characterized by an oversize of the initial constant area region (5.5 mm in diameter) and, therefore, the secondary flow fails to reach the chocking condition. The Figure 4-34 shows how the primary flow accelerates and expands but is not able to create a converging duct for the induced flow.

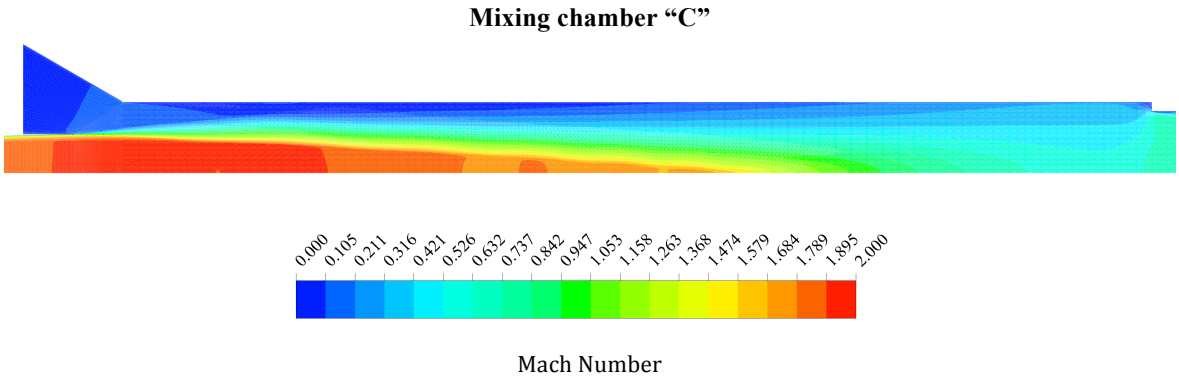

Figure 4-34: Mach contours of the ejector flow field of the mixing chambers "C" in sub-critical mode operation (T_g = 84.39°C, T_e = 10°C, T_c = 28.12°C).

When the mixing chamber "C" reaches the critical conditions, it can be observed (Figure 4-35) that, even if the mixing chamber diameter of "C" is greater than "A", the fluid dynamics behaviour of the two geometries is very similar. The ratio between the primary jet core section and the "aerodynamic throat" section of secondary flow is the same and this determines similar performance in terms of entrainment ratio for the two cases.

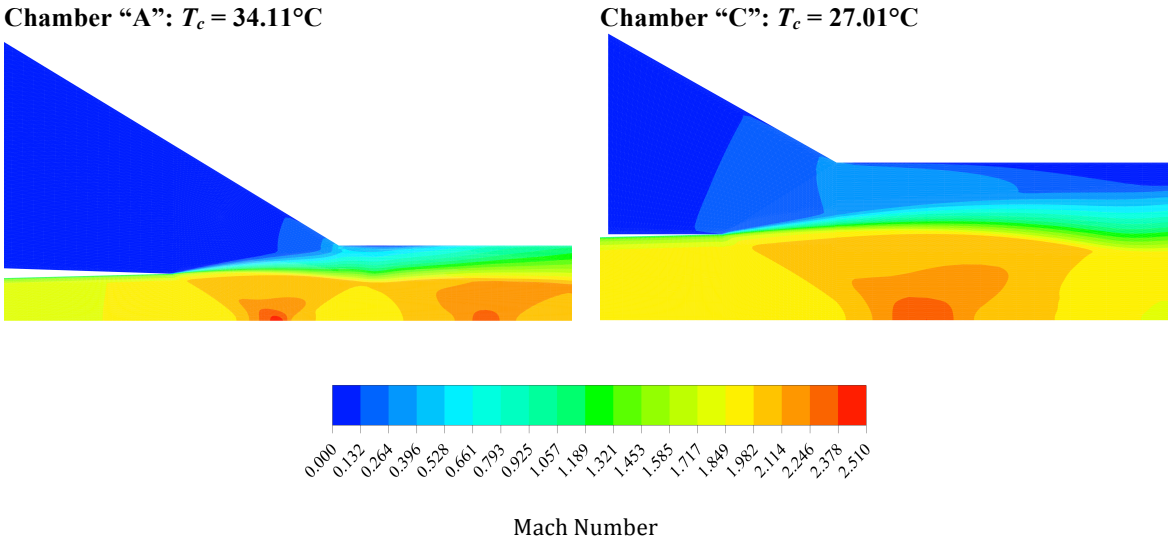

Figure 4-35: Mach contours of the ejector flow field – Comparison between mixing chambers "A" and "C" in critical conditions (T_g = 89.15°C, T_e = 7°C).

4.3.6.3 Critical conditions of the mixing chambers "A" and "C"

"The geometries B and C were designed to improve the compression process that takes place along the mixing chamber. However, while the performance of geometry B is close to that of A, a significant worsening of performance with respect to the other two has been observed for chamber C".

The main reason for which the mixing chamber "C" has a significant worsening of performance with respect to the chamber "A" and "B" seems to lie in the sharp contraction of the mixing chamber. In fact, as shown in the Figure 4-36, the detachment of the fluid flow from the wall surface occurs in this region. This causes a reduction of the entrainment effect and thus performance drop. The Figure 4-37 shows the mixing chamber wall shear stress, in order to assess this issue.

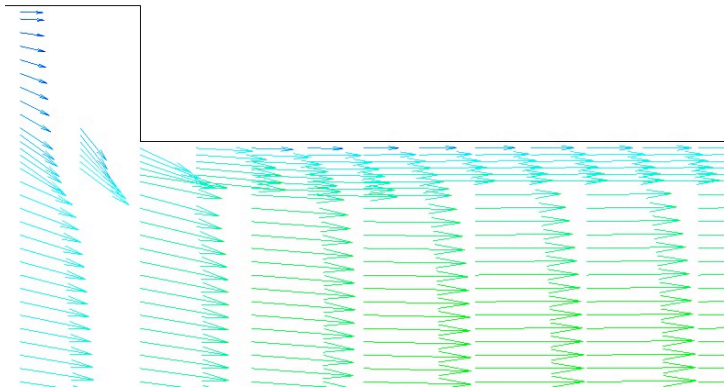

Figure 4-36: Sharp contraction of the mixing chamber "C" – Velocity vector plot (T_g = 84.39°C, T_e = 10°C, T_c = 26.38°C).

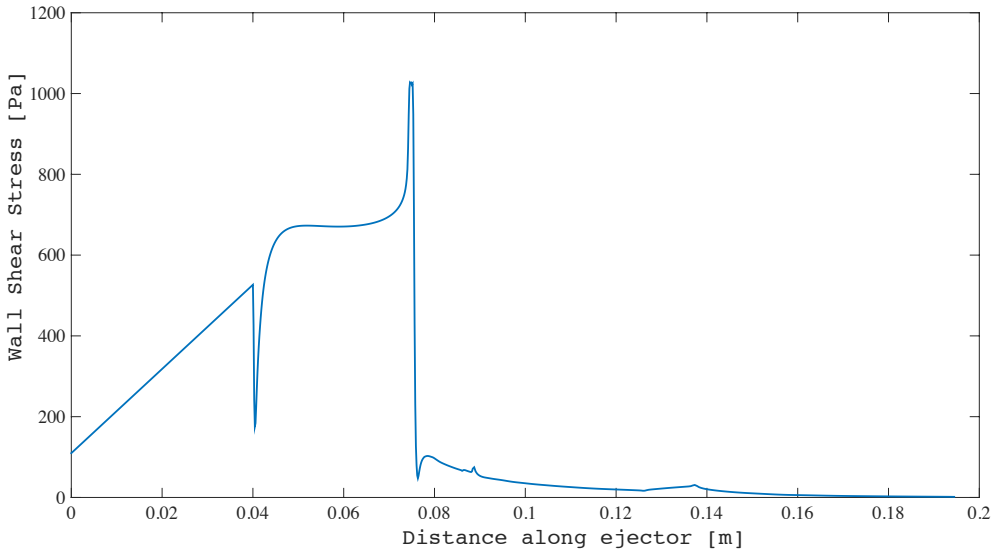

Figure 4-37: Wall shear stress distribution along the mixing chamber "C" plot (T_g = 84.39°C, T_e = 10°C, T_c = 26.38°C).

4.4 CFD modelling: summary

In this chapter a validation analysis of the CFD model was performed. In particular, seven turbulence models (*Spalart-Allmaras*, *Standard k-ε*, *RNG k-ε*, *Realizable k-ε*, *Standard k-ω*, *SST k-ω*, *RSM*) were used and compared with experimental data from the literature [10]. The experimental benchmark includes measurement of the entrainment ratio and the wall static pressure profile along the ejector at different operating conditions and geometries. The performance prediction of both global and local measurements is quite good with all the employed turbulence models. The results show that the *SST k-ω* model has the better performance in terms of prediction of the entrainment ratio, wall pressure profile and flow field of the ejector. In particular, the entrainment ratio is predicted with relative errors less than around 10%. However, the description of the wall static pressure distribution along the ejector gets worse at high discharge pressure (4500 Pa) because all the turbulence models predict in a downstream position the actual 'shock starts'.

In order to investigate the wall treatment effect on the numerical results, the turbulence models were tested under different near-wall modelling options. The low-Reynolds models (*Spalart-Allmaras*, *SST k-ω*), that do not need wall functions because already implemented in their mathematical structure, have a slight benefit from the near-wall grid refinement ($y^+ \approx 1$) and the Low-Reynolds correction of the *SST k-ω* model not improves the results. This allows to employ the *SST k-ω* model without a high wall grid refinement, reducing the computational costs. On the other hand, the *RSM* and *k-ε* models improve their performance predictions with the enhanced wall function ($y^+ < 1$) and thus the wall grid refinement is a good choice in order to improve the results.

From the point of view of the convergence capability the *Spalart-Allmaras*, *Standard k-ω* and *SST k-ω* models easily reach convergence. Moreover, the *Spalart-Allmaras* is also the least onerous turbulence model due to its less number of equations involved. Whereas, the *RSM* is the slowest model to converge and it has also some convergence problems.

In the second part of this chapter, we have employed the validated CFD model for the analysis of an applicative case [28], with the purpose of explain some issues detected by the authors that have not physical arguments or adequate justifications. The experimental measurements were compared with both lumped parameter and CFD models predictions. While the critical mode operation performances are well predicted with both the approaches (the CFD model achieved, however, better results), the sub-critical mode operation performances are predicted with greater relative errors and only the CFD approach can ensure satisfactory results (E_R (ω) < 18%). However, the CFD technique proved to be a powerful tool in order to analyze and assess the flow behaviour and the local phenomena occurring inside the ejector.

Chapter 5

Integrated lumped parameter-CFD model

In this chapter, the integrated lumped parameter-CFD model (ILPM-CFD model) [1] is presented for a supersonic ejector suitable for refrigeration applications. The method involves the assessment of the ejector efficiencies and their implementation in a numerical method. The chapter is divided in four parts. In the first part, a description of the ILPM-CFD model is provided. In the second part, a thermodynamic model is proposed and descripted, reporting the constitutive equations and the numerical procedure. In the third part, the efficiency definitions are provided and in the fourth part, the proceeding to determine the efficiency maps related to the ejector components is presented. The proposed ILPM-CFD model for supersonic ejector may be employed for future applications.

5.1 Introduction

As remarked in the Chapter 2, there exist two approaches to modelling the ejectors: (i) the lumped parameter models, which require low computational efforts in terms of time and cost; (ii) the CFD models, which provide a deep understanding of the global and local flow behaviour inside the ejector. The aim of the integrated model is to put together the advantages of the two approaches.

The ILPM-CFD model consists in a lumped parameter model with variable efficiencies. The ejector efficiencies are obtained from efficiency maps and correlations provided by the CFD analysis. Therefore, the integrated model is composed of two steps:

- investigation of the local flow phenomena and their influence on ejector component efficiencies;
- implementation of the efficiency functions in a 1D thermodynamic model in order to take into account the effect of the internal flow field.

In this way, the thermodynamic model limitations, in terms of operating conditions field and representation of the local behaviour, are overcome. To improve the performance prediction of the models, and thus the ejector design process, the understanding of the internal fluid behaviour is very important. The CFD modelling is a valuable tool for the evaluation of the local flow phenomena and, in the integrated model, it is used for the assessment of the ejector efficiencies, expressed as a function of local flow parameters.

However, in order to ensure well founded results, the employed CFD model must be widely validated, like that presented and discussed in the Chapter 4.

5.2 Theoretical lumped parameter model

5.2.1 Presentation

In accordance with the purpose of our analysis, we have developed an ejector lumped parameter model. The assumptions made have been taken in accordance with the 1D models available in the literature and presented in the Chapter 2 [2, 3]. The main hypotheses are:

- the flow is steady and one dimensional;
- the walls of the ejector are adiabatic;
- the velocity at the primary and secondary flow inlets are negligible;
- the velocity of the mixed flow leaving the ejector is negligible;
- the losses in the nozzle (primary fluid), in the suction chamber (secondary flow), in the mixing chamber and in the diffuser are taken into account by using isentropic efficiencies η_g, η_e, η_m and η_d, respectively;
- in this range of operation conditions the working fluid is an ideal gas with constant heat capacity ratio k.

5.2.2 Constitutive equations and numerical procedure

The Figure 5-1 shows a schematic view of the ejector structure:

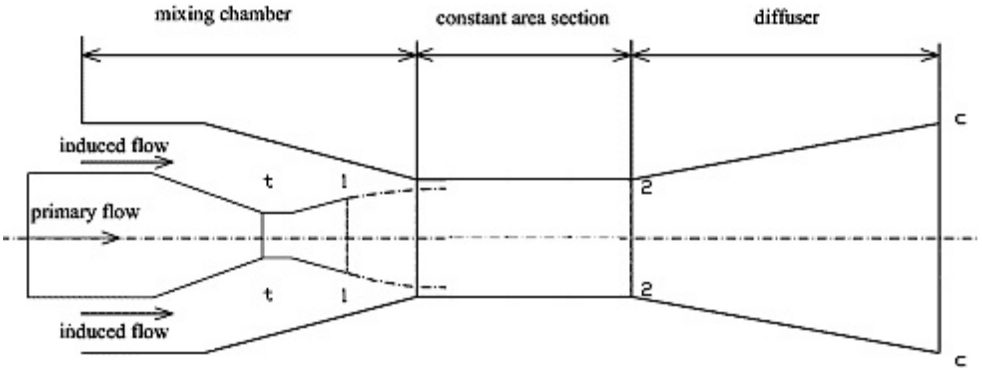

Figure 5-1: Schematic view of an ejector structure – modified from [3].

Some typical ejector cross sections can be pointed out:

- section *t-t* – primary nozzle throat;
- section *1-1* – primary nozzle exit;
- section *2-2* – constant area section exit;
- section *c-c* – diffuser exit.

The constitutive equations of the model involve conservation equations (mass, momentum and energy) and isentropic flow relations between these representative sections.

The variables of the problem are:

- input parameters – operating conditions (p_g, T_g, p_e, T_e, p_c), geometric parameters (A_t, A_{p1}, A_2), ejector efficiencies (η_g, η_e, η_m, η_d) and fluid properties (k);
- output parameter – entrainment ratio (ω).

5.2.2.1 Primary flow from inlet to nozzle exit (section *1-1*)

For a given inlet total pressure p_g and temperature T_g, the mass flow rate of the primary flow $\dot{m}_g$ is obtained from the isentropic relation:

$$\dot{m}_g = \frac{p_g A_t}{\sqrt{T_g}} \cdot \sqrt{\frac{k}{R}\left(\frac{2}{k+1}\right)^{\frac{k+1}{k-1}}} \cdot \sqrt{\eta_g} \tag{5.1}$$

where η_g is the efficiency coefficient for the nozzle.

According to [3], the isentropic flow relations between the primary flow inlet and the section *1-1*, applying conservation equations of mass and energy, are given by:

$$\left(\frac{A_{p1}}{A_t}\right)^2 = \frac{1}{M_{p1}^2}\left[\frac{2}{k+1}\left(1+\frac{k-1}{2}M_{p1}^2\right)\right]^{\frac{k+1}{k-1}} \tag{5.2}$$

$$\left(\frac{p_g}{p_{p1}}\right) = \left(1+\frac{k-1}{2}M_{p1}^2\right)^{\frac{k}{k-1}} \tag{5.3}$$

$$\left(\frac{T_g}{T_{p1}}\right) = 1+\frac{k-1}{2}M_{p1}^2 \tag{5.4}$$

where M_{p1}, p_{p1} and T_{p1} are unknown.

The primary flow velocity at section *1-1* can be derived by the Mach number definition:

$$V_{p1} = M_{p1}\sqrt{kRT_{p1}} \tag{5.5}$$

where $a_{p1} = \sqrt{kRT_{p1}}$ is the sonic velocity for an ideal gas.

5.2.2.2 Secondary flow from inlet to entrance section (section *1-1*)

For a given inlet total pressure p_e and temperature T_e, the mass flow rate of the secondary flow $\dot{m}_e$ is obtained from the isentropic relation:

$$\dot{m}_e = \frac{p_e A_{s1}}{\sqrt{T_e}} \cdot \sqrt{\frac{k}{R}\left(\frac{2}{k+1}\right)^{\frac{k+1}{k-1}}} \cdot \sqrt{\eta_e} \tag{5.6}$$

where $A_{s1} = A_2 - A_{p1}$ and η_e is the efficiency coefficient for the induced flow.

Using conservation mass and energy equation, as well as isentropic relations, the following equations are obtained:

$$\frac{T_{s1}}{T_e} = \left(\frac{p_{s1}}{p_e}\right)^{\frac{k-1}{k}} \tag{5.7}$$

$$V_{s1} = \sqrt{2C_p\left(T_e - T_{s1}\right)} \tag{5.8}$$

The pressure of the secondary flow at section *1-1* p_{s1} is unknown and thus an iterative cycle is required. Assuming an initial value for p_{s1}, the T_{s1} and V_{s1} can be determined.

5.2.2.3 Mixed flow in the mixing chamber from section *1-1* to section *2-2*

Applying a mass, momentum and energy balance between section *1-1* and *2-2*, the equations include:

$$\begin{cases} \dot{m}_g + \dot{m}_e = \dfrac{p_2 V_2 A_2}{R T_2} \\ \eta_m \left[\left(\dot{m}_g V_{p1} + p_{p1} A_{p1} \right) + \left(\dot{m}_e V_{s1} + p_{s1} A_{s1} \right) \right] = \left(\dot{m}_g + \dot{m}_e \right) V_2 + p_2 A_2 \\ \dot{m}_g \left(C_p T_{p1} + \dfrac{V_{p1}^2}{2} \right) + \dot{m}_e \left(C_p T_{s1} + \dfrac{V_{s1}^2}{2} \right) = \left(\dot{m}_g + \dot{m}_e \right) \left(C_p T_2 + \dfrac{V_2^2}{2} \right) \end{cases} \tag{5.9}$$

where V_2, p_2 and T_2 are the velocity, pressure and temperature of the mixed flow at section *2-2* and η_m is the mixing chamber efficiency coefficient.

5.2.2.4 Mixed flow through the diffuser from section *2-2* to section *c-c*

The Mach number of the mixed flow at section *2-2* is given by:

$$M_2 = \frac{V_2}{\sqrt{k R T_2}} \tag{5.10}$$

Using the gas dynamic relation for the isentropic flow, the calculated backpressure $p_{c,calc}$ can be determined as follow:

$$\frac{p_{c,calc}}{p_2} = \left(1 + \eta_d \frac{k-1}{2} M_2^2 \right)^{\frac{k}{k-1}} \tag{5.11}$$

The pressure of the secondary flow at section p_{s1} must be updated until the condition expressed by the Equation 5.12 is not met:

$$\frac{\left| p_c - p_{c,calc} \right|}{p_c} \leq \varepsilon \tag{5.12}$$

where ε is the admitted tolerance.

The entrainment ratio ω can be calculated by the Equation 5.13:

$$\omega = \frac{\dot{m}_e}{\dot{m}_g} \tag{5.13}$$

The numerical procedure is summarized in the Figure 5-2:

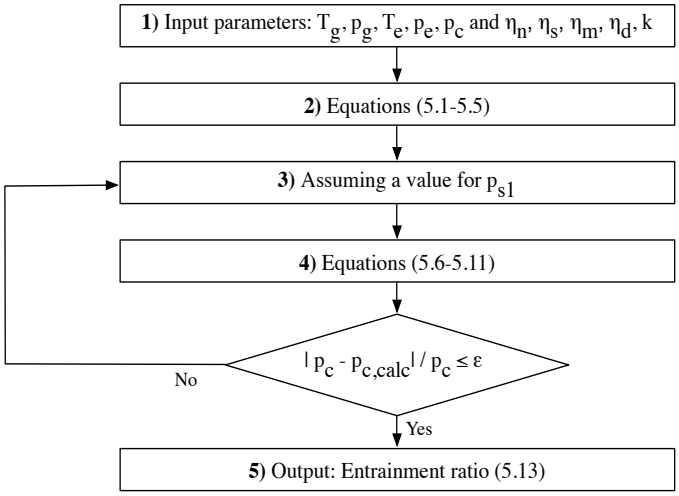

Figure 5-2: Flow diagram of the computational procedure.

The lumped parameter model is the base of the ILPM-CFD model proposed in this chapter. Unlike the traditional LPM model, the integrated model employs variable efficiencies, determined by efficiency maps and regression equations. The theoretical procedure required for the calculation of the efficiency values and their involvement in the integrated model will be explained in the following sections.

5.3 Evaluation of the ejector efficiencies

In a lumped parameter model, the ejector efficiencies are usually assumed constant. In order to take into account local phenomena effects on ejector model validity, the integrated model employs variable efficiencies as a function of the operating conditions. For this purpose, the efficiencies coefficients are defined through the relations show in this section.

5.3.1 Primary nozzle efficiency η_g

It is a coefficient accounting for the fluid dynamics loss of the primary flow in the nozzle. It measures as the flow expansion deviates from an isentropic process. Thus, it can be defined as follow [4]:

$$\eta_g = \frac{h_g - h_{p1}}{h_g - h_{p1,is}} \tag{5.14}$$

where h_g is the stagnation enthalpy of primary flow at inlet section, h_{p1} is the actual enthalpy at exit section and $h_{p1,is}$ is the exit enthalpy under isentropic conditions for the same exit pressure.

5.3.2 Secondary flow efficiency η_e

The secondary flow efficiency η_e takes into account the entrained flow losses from inlet to section *1-1*. Similar to the primary nozzle efficiency, it is defined as:

$$\eta_e = \frac{h_{e,in} - h_{sy}}{h_{e,in} - h_{sy,is}} \tag{5.15}$$

5.3.3 Mixing chamber efficiency η_m

The coefficient η_m is a comprehensive parameter that takes into account all the dissipative phenomena occurring in the mixing chamber (primary jet core and shock train, mixing and frictional loss, shockwave). It can be defined as the efficiency of the momentum transfer between the primary and secondary flows:

$$\eta_m = \frac{\left(\dot{m}_g + \dot{m}_e\right)V_2 + p_2 A_2}{\left(\dot{m}_g V_{p1} + p_{p1} A_{p1}\right) + \left(\dot{m}_e V_{s1} + p_{s1} A_{s1}\right)} \tag{5.16}$$

5.3.4 Diffuser efficiency η_d

The coefficient η_d is the isentropic efficiency of the diffuser, defined as the ratio of the ideal enthalpy change to the actual total enthalpy change for the same exit stagnation pressure [5]:

$$\eta_d = \frac{h_{c,is} - h_2}{V_2^2 / 2} \tag{5.17}$$

It can be note that the diffuser efficiency was defined like a total to static efficiency because the outlet kinetic energy is not recovered.

5.4 Integrated lumped parameter-CFD model

The CFD model has the task of determine the efficiency coefficients η_g, η_e, η_m and η_d to vary with appropriate quantities, in order to define suitable correlations for each parameter:

$$\eta_g = \tilde{f}\left(PR, \dot{m}_{e,ad}\right) \tag{5.18}$$

$$\eta_e = \tilde{f}\left(PR, \dot{m}_{e,ad}\right) \tag{5.19}$$

$$\eta_m = \tilde{f}\left(PR, \dot{m}_{e,ad}\right) \tag{5.20}$$

$$\eta_d = \tilde{f}\left(PR, \dot{m}_{e,ad}\right) \tag{5.21}$$

The independent variables must be defined in order to ensure a good description of the dissipative phenomena by the efficiencies. They are defined as follow:

$$PR = \frac{p_g}{p_e} \tag{5.22}$$

$$\dot{m}_{e,ad} = \frac{\dot{m}_e \sqrt{R T_{s1}}}{p_{s1} A_{s1}} \tag{5.23}$$

The pressure ratio PR is strictly linked to the pressure drop of the primary flow, while the dimensionless secondary mass flow rate $\dot{m}_{e,ad}$ involves geometry and operating parameters and can be associated to the working mode operation (critical or sub-critical) of the ejector.

The CFD cases must cover a wide range of operating conditions to guarantee a good description of the ejector behaviour. Thus, a number of simulations are run varying the operating parameters involve in the dimensionless variables. Then, the four efficiencies are calculated for each case and

plotted in order to define the efficiency maps. The resulting correlations can be included in the integrated model.

5.5 Integrated lumped parameter-CFD model: summary

The integrated model purpose is to exploit and combine the advantages of the LPM and CFD approaches. On the one hand, the lumped parameter modelling allows obtaining low computational cost and easy implementation. On the other hand, the CFD technique provides a good description of the local phenomena occurring in the ejector and it is then used for link local quantities to global performance parameters through the generation of the efficiency maps [6].

The Figure 5-3 shows the computational procedure of the integrated lumped parameter-CFD model:

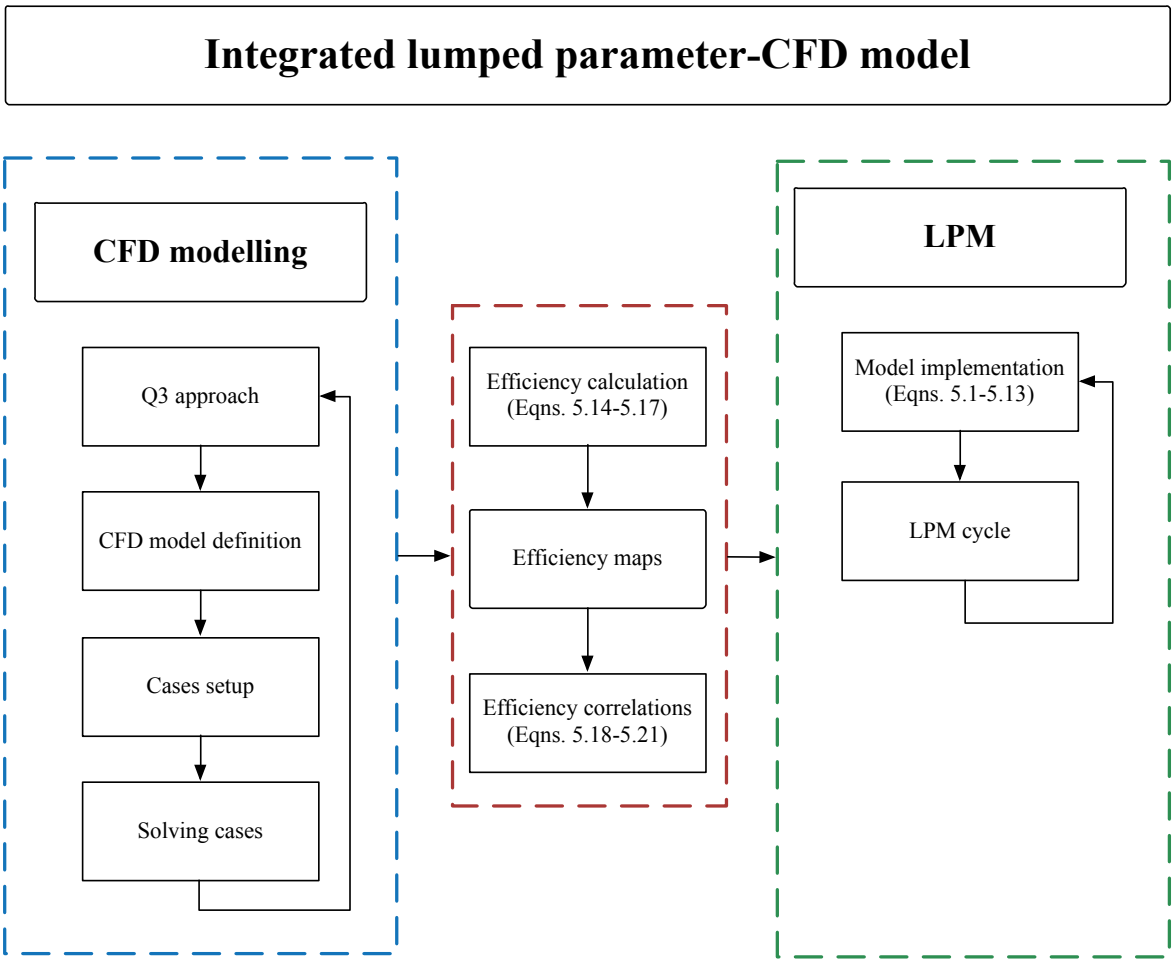

Figure 5-3: Integrated lumped parameter-CFD model – Computational procedure.

Conclusions

The topic of the present thesis concerns the numerical modelling of ejectors for refrigeration applications. These systems can be a good solution for refrigeration purpose in order to reduce the electricity consumptions and are taken into account for a future replacement of the traditional technologies used in this field.

The future tendency of electricity consumptions predicts a "demand's electrification", consequent widening of electricity application in many sectors, like refrigeration and air-conditioning systems. This involves a high load on the power transmission grid and, on the other hand, air pollution and greenhouse gases emissions. To moderate these issues, significant rearrangements of the entire electrical system will need in terms of new power plants but also strong measures in the matter of energy demand. One of these interventions will certainly affect the refrigeration field. The thermal energy refrigeration would allow a significant reduction of these drawbacks (i.e. electricity consumption and environmental impact) and the use of low-grade heat or solar energy for cooling purposes can provide cheap and clean energy for refrigeration. Their involvement in the refrigeration field is also in line with the European directive 2009/28/EC that promote the introduction of renewable energy in many sectors.

The heat-driven ejector refrigeration system (ERS) is one of the most promising technologies of thermal refrigeration due to its low capital cost, simplicity of operation, reliability and low maintenance cost. The ejector systems can be mainly employed in:

- air conditioning applications (motor vehicle, office, building) in which solar-driven ejectors may be used for heating and cooling purpose or in distributed tri-generation systems;
- refrigeration applications (domestic, commercial, industrial), that represent an attractive solution for waste heat upgrading and new opportunities for their integration in innovative cycle based on the combinations of ejectors with vapour compression or absorption systems.

Nevertheless, ERS have not yet been able to penetrate the market because of their low coefficient of performance *COP*, compared to the traditional vapour-compression refrigeration cycles, mainly due to fluid dynamic losses occurring inside the ejector. Thus, many researchers have been engaged in improving it and combining ERS with other refrigeration systems in order to enhance the overall system performance. In the Chapter 1 a detailed review concerning the ejector refrigeration systems was carried out. Our analysis of the experimental and numerical literature studies has showed that over the years there was an increase of the performance, thanks to the great efforts of researchers to improve ERS and develop new technological solutions, like combined or hybrid systems, ejector expansion refrigeration systems and transcritical ejector refrigeration systems. In light of this, it is reasonable to expect for the future a further improvement of the ERS performance, as well as the development of new plant configurations.

For these reasons, the ejector modelling techniques play a very important role in performance improvement of the ejector systems. In the Chapter 2, the main modelling approaches were presented and discussed. The research mainly focuses on:

- lumped parameter approach that essentially consists in one-dimensional thermodynamic models;
- computational fluid dynamics (CFD) that uses finite volume methods to solve numerically the fluid dynamics problems.

In the Chapter 3, we have implemented five lumped parameter models and evaluated their effectiveness by comparing the predicted results with experimental data available in the literature for different geometries, operating conditions and working fluids. The models have been chosen among the most recent 1D analytical studies published by different research groups in order to obtain an assorted set of simulations. Then, one of these validated models was selected in order to evaluate the ejector behaviour using several working fluids, with the purpose of verifying the great importance that the refrigerants have on ejector operation. For each fluid was found an application field according to the performance reached in specific ranges of operating conditions.

The CFD approach was proposed in the Chapter 4, following the methodological procedure to qualify CFD, named Q^3 approach. The CFD model was validated and seven turbulence models (*Spalart-Allmaras*, *Standard k-ε*, *RNG k-ε*, *Realizable k-ε*, *Standard k-ω*, *SST k-ω*, *RSM*) were compared each other. The *SST k-ω* has showed the best agreement with the experimental measurements. Moreover, the turbulence models were tested under different near-wall modelling options in order to investigate the wall treatment effect on the numerical results. Then, the validated CFD model will be employed with knowledge for analyze and investigate some aspects of the fluid dynamics behaviour of the ejectors, taking as reference a recent experimental study. The CFD technique proved to be a powerful tool in order to analyze and assess the flow behaviour and the local phenomena occurring inside the ejector. However, the results were also compared with those obtained with a LPM presented in the Chapter 3. The analysis shows that the use of constant efficiency values is a major limitation for the LPM, mainly because they depend upon the working fluid, the operating conditions, the geometry and the local phenomena occurring in the ejector.

Thus, the performance prediction of the LPM can be improved using variable efficiencies. In the Chapter 5 was proposed an integrated approach (ILPM-CFD) for supersonic ejectors with the purpose to exploit and combine the advantages of the LPM and CFD approaches. On the one hand, the lumped parameter modelling allows obtaining low computational cost and easy implementation. On the other hand, the CFD technique provides a good description of the local phenomena occurring in the ejector and it can be used for determine the efficiencies of the ejector components.

Future developments may concern the following matters:

- the implementation and validation of the proposed ILPM-CFD model for supersonic ejectors;
- the development of a simulation package of the whole ejector-based system by combining the model of the ejector and other components in the system;
- take into account the effects of nucleation, growth of condensation droplets and metastable states present in two-phase flow that can occur in the ejector.

References

Introduction

[1] Terna, Previsioni della domanda elettrica in Italia e del fabbisogno di potenza necessario (2013-2023), (2013).

[2] M.A. Produttive, Scenario tendenziale dei consumi e del fabbisogno al 2020, (2005).

[3] International Energy Agency, Energy Policies of IEA Countries (Italy), (2009).

[4] M.d.S. Economico, Bilancio Energetico Nazionale (1995-2012), (1995).

[5] Eni, Lo scenario energetico in Italia.

[6] Terna, Dati Statistici sull'Energia Elettrica in Italia, (2013).

[7] X. Chen, S. Omer, M. Worall, S. Riffat, Recent developments in ejector refrigeration technologies, Renewable and sustainable energy reviews, 19 (2013) 629-651.

[8] K. Chunnanond, S. Aphornratana, Ejectors: applications in refrigeration technology, Renewable and sustainable energy reviews, 8 (2004) 129-155.

[9] C.A. Balaras, G. Grossman, H.-M. Henning, C.A. Infante Ferreira, E. Podesser, L. Wang, E. Wiemken, Solar air conditioning in Europe—an overview, Renewable and sustainable energy reviews, 11 (2007) 299-314.

[10] J.M. Abdulateef, K. Sopian, M.A. Alghoul, M.Y. Sulaiman, Review on solar-driven ejector refrigeration technologies, Renewable and sustainable energy reviews, 13 (2009) 1338-1349.

[11] K.R. Ullah, R. Saidur, H.W. Ping, R.K. Akikur, N.H. Shuvo, A review of solar thermal refrigeration and cooling methods, Renewable and sustainable energy reviews, 24 (2013) 499-513.

[12] Z. Aidoun, M. Ouzzane, The effect of operating conditions on the performance of a supersonic ejector for refrigeration, International Journal of Refrigeration, 27 (2004) 974-984.

[13] H.E. González Bravo, R. Dorantes Rodríguez, J. Hernández Gutiérrez, R. Best y Brown, R. Román Aguila, H. Terres Peña, State of art of simple and hybrid jet compression refrigeration systems and the working fluid influence, International Journal of Refrigeration, 35 (2012) 386-396

[14] European Parliament and European Council, Directive 2009/28/EC, (2009).

[15] Solair, Market Report for Small and Medium-Sized Solar Air-Conditioning Appliance, (2008).

[16] V. Vakiloroaya, B. Samali, A. Fakhar, K. Pishghadam, A review of different strategies for HVAC energy saving, Energy Conversion and Management, 77 (2014) 738-754.

[17] T. Otanicar, R.A. Taylor, P.E. Phelan, Prospects for solar cooling–An economic and environmental assessment, Solar Energy, 86 (2012) 1287-1299.

[18] H. Vidal, S. Colle, Simulation and economic optimization of a solar assisted combined ejector-vapor compression cycle for cooling applications, Applied Thermal Engineering, 30 (2010) 478-486.

[19] R. Ben Mansour, M. Ouzzane, Z. Aidoun, Numerical Evaluation of Ejector-Assisted Mechanical Compression Systems for Refrigeration Applications, International Journal of Refrigeration, (2014).

Chapter 1

[1] K.R. Ullah, R. Saidur, H.W. Ping, R.K. Akikur, N.H. Shuvo, A review of solar thermal refrigeration and cooling methods, Renewable and sustainable energy reviews, 24 (2013) 499-513.

[2] C. Koroneos, E. Nanaki, G. Xydis, Solar air conditioning systems and their applicability—An exergy approach, Resources, Conservation and Recycling, 55 (2010) 74-82.

[3] G. Angelino, C. Invernizzi, Thermodynamic optimization of ejector actuated refrigerating cycles, International Journal of Refrigeration, 31 (2008) 453-463.

[4] I. Sarbu, C. Sebarchievici, Review of solar refrigeration and cooling systems, Energy and Buildings, 67 (2013) 286-297.

[5] Solair, Survey of Available Technical Solutions and Successful Running Systems, (2009).

[6] European Parliament and European Council, Directive 2009/28/EC, (2009).

[7] M.A. Produttive, Scenario tendenziale dei consumi e del fabbisogno al 2020, (2005).

[8] C. Bovo, Esercizio e sicurezza, in: Dipartimento di Energia, Politecnico di Milano, 2012.

[9] D.S. Kim, C.A. Infante Ferreira, Solar refrigeration options–a state-of-the-art review, International Journal of Refrigeration, 31 (2008) 3-15.

[10] J.M. Abdulateef, K. Sopian, M.A. Alghoul, M.Y. Sulaiman, Review on solar-driven ejector refrigeration technologies, Renewable and sustainable energy reviews, 13 (2009) 1338-1349.

[11] A. Mani, Solar refrigeration: current status and future trends, in: Mechanical Engineering, Indian Institute of Technology Madras, 2013.

[12] T. Otanicar, R.A. Taylor, P.E. Phelan, Prospects for solar cooling–An economic and environmental assessment, Solar Energy, 86 (2012) 1287-1299.

[13] J. Chen, H. Havtun, B. Palm, Investigation of ejectors in refrigeration system: Optimum performance evaluation and ejector area ratios perspectives, Applied Thermal Engineering, 64 (2014) 182-191.

[14] G. Besagni, R. Mereu, E. Colombo, CFD study of ejector efficiencies, Proceedings of the ASME, (2014).

[15] B.J. Huang, J.M. Chang, C.P. Wang, V.A. Petrenko, A 1-D analysis of ejector performance, International Journal of Refrigeration, 22 (1999) 354-364.

[16] K. Chunnanond, S. Aphornratana, Ejectors: applications in refrigeration technology, Renewable and sustainable energy reviews, 8 (2004) 129-155.

[17] K. Pianthong, W. Seehanam, M. Behnia, T. Sriveerakul, S. Aphornratana, Investigation and improvement of ejector refrigeration system using computational fluid dynamics technique, Energy Conversion and Management, 48 (2007) 2556-2564.

[18] I.W. Eames, A new prescription for the design of supersonic jet-pumps: the constant rate of momentum change method, Applied Thermal Engineering, 22 (2002) 121-131.

[19] V. Kumar, G. Singhal, P.M.V. Subbarao, Study of supersonic flow in a constant rate of momentum change (CRMC) ejector with frictional effects, Applied Thermal Engineering, 60 (2013) 61-71.

[20] A.E. Ablwaifa, A theoretical and experimental investigation of jet-pump refrigeration system, in, University of Nottingham, 2006.

[21] Y. Zhu, Y. Li, New theoretical model for convergent nozzle ejector in the proton exchange membrane fuel cell system, Journal of Power Sources, 191 (2009) 510-519.

[22] J. He, J. Ahn, S.-Y. Choe, Analysis and control of a fuel delivery system considering a two-phase anode model of the polymer electrolyte membrane fuel cell stack, Journal of Power Sources, 196 (2011) 4655-4670.

[23] V. Spallina, M.C. Romano, P. Chiesa, G. Lozza, Integration of coal gasification and packed bed CLC process for high efficiency and near-zero emission power generation, Energy Procedia, 37 (2013) 662-670.

[24] V. Spallina, M.C. Romano, P. Chiesa, F. Gallucci, M. van Sint Annaland, G. Lozza, Integration of coal gasification and packed bed CLC for high efficiency and near-zero emission power generation, International Journal of Greenhouse Gas Control, 27 (2014) 28-41.

[25] S. Elbel, Historical and present developments of ejector refrigeration systems with emphasis on transcritical carbon dioxide air-conditioning applications, International Journal of Refrigeration, 34 (2011) 1545-1561.

[26] K. Sumeru, H. Nasution, F.N. Ani, A review on two-phase ejector as an expansion device in vapor compression refrigeration cycle, Renewable and sustainable energy reviews, 16 (2012) 4927-4937.

[27] A.B. Little, S. Garimella, A review of ejector technology for refrigeration applications, International Journal of Air-Conditioning and Refrigeration, 19 (2011) 1-15.

[28] F. Marsano, L. Magistri, A.F. Massardo, Ejector performance influence on a solid oxide fuel cell anodic recirculation system, Journal of Power Sources, 129 (2004) 216-228.

[29] F. Trasino, M. Bozzolo, L. Magistri, A.F. Massardo, Modeling and performance analysis of the Rolls-Royce fuel cell systems limited: 1 MW plant, Journal of engineering for gas turbines and power, 133 (2011) 021701.

[30] B. Kim, D.H. Kim, J. Lee, S.W. Kang, H.C. Lim, The operation results of a 125 kW molten carbonate fuel cell system, Renewable Energy, 42 (2012) 145-151.

[31] B. Kim, D.H. Kim, J. Lee, S.W. Kang, H.C. Lim, The ejector performance of a 75 kW Molten carbonate fuel cell system, Journal of Fuel Cell Science and Technology, 8 (2011) 014503.

[32] G. Angelino, C. Invernizzi, Ejector-assisted liquid metal topping cycles, Proceedings of the Institution of Mechanical Engineers, Part A: Journal of Power and Energy, 218 (2004) 111-121.

[33] B.Z. Freedman, N. Lior, A novel high-temperature ejector-topping power cycle, Journal of engineering for gas turbines and power, 116 (1994) 1-7.

[34] X. Li, C. Zhao, X. Hu, Thermodynamic analysis of organic Rankine cycle with ejector, Energy, 42 (2012) 342-349.

[35] X. Chen, S. Omer, M. Worall, S. Riffat, Recent developments in ejector refrigeration technologies, Renewable and sustainable energy reviews, 19 (2013) 629-651.

[36] H.E. González Bravo, R. Dorantes Rodríguez, J. Hernández Gutiérrez, R. Best y Brown, R. Román Aguila, H. Terres Peña, State of art of simple and hybrid jet compression refrigeration systems and the working fluid influence, International Journal of Refrigeration, 35 (2012) 386-396

[37] G. Besagni, An integrated thermodynamic CFD approach to ejector modeling, in, Politecnico di Milano, 2012.

[38] J.T. Munday, D.F. Bagster, A new ejector theory applied to steam jet refrigeration, Industrial & Engineering Chemistry Process Design and Development, 16 (1977) 442-449.

[39] B.J. Huang, C.B. Jiang, F.L. Hu, Ejector performance characteristics and design analysis of jet refrigeration system, Journal of engineering for gas turbines and power, 107 (1985) 792-802.

[40] B.J. Huang, J.M. Chang, Empirical correlation for ejector design, International Journal of Refrigeration, 22 (1999) 379-388.

[41] S.M.V. Rao, G. Jagadeesh, Observations on the non-mixed length and unsteady shock motion in a two dimensional supersonic ejector, Physics of Fluids, 26 (2014).

[42] S. Elbel, P. Hrnjak, Ejector Refrigeration: an overview of historical and present developments with an emphasis on air-conditioning applications, (2008).

[43] D. Schmidt, M. Colarossi, M.J. Bergander, Multidimensional modeling of condensing two-phase ejector flow, (2009).

[44] E.K. Levy, Investigation of liquid-vapour interactions in a constant area condensing ejector, in, Massachusetts Institute of Technology, 1967.

[45] G. Grazzini, A. Milazzo, S. Piazzini, Prediction of condensation in steam ejector for a refrigeration system, International Journal of Refrigeration, 34 (2011) 1641-1648.

[46] K. Ariafar, D. Buttsworth, N. Sharifi, R. Malpress, Ejector Primary Nozzle Steam Condensation: Area Ratio Effects and Mixing Layer Development, Applied Thermal Engineering, (2014).

[47] T. Marynowski, P. Desevaux, Y. Mercadier, Experimental and numerical visualizations of condensation process in a supersonic ejector, Journal of visualization, 12 (2009) 251-258.

[48] Y. Yang, S. Shen, S. Zhou, R. Liu, H. Yu, Numerical investigation for the supersonic steam jetting flow in the thermal vapor compressor, Desalination and Water Treatment, 51 (2013) 4684-4693.

[49] ASHRAE, Designation and Safety Classification of Refrigerants, (2007).

[50] J. Chen, H. Havtun, B.r. Palm, Screening of working fluids for the ejector refrigeration system, International Journal of Refrigeration, (2014).

[51] Z. Aidoun, M. Ouzzane, The effect of operating conditions on the performance of a supersonic ejector for refrigeration, International Journal of Refrigeration, 27 (2004) 974-984.

[52] A. Khalil, M. Fatouh, E. Elgendy, Ejector design and theoretical study of R134a ejector refrigeration cycle, International Journal of Refrigeration, 34 (2011) 1684-1698.

[53] W.C. Holton, Effect of molecular weight of entrained fluid on the perfromance of steam-jet ejectors, Trans. Am. Soc. Mech. Eng, 73 (1951) 905-910.

[54] D.-W. Sun, Comparative study of the performance of an ejector refrigeration cycle operating with various refrigerants, Energy Conversion and Management, 40 (1999) 873-884.

[55] K. Chunnanond, S. Aphornratana, An experimental investigation of a steam ejector refrigerator: the analysis of the pressure profile along the ejector, Applied Thermal Engineering, 24 (2004) 311-322.

[56] G.K. Alexis, Exergy analysis of ejector-refrigeration cycle using water as working fluid, International journal of energy research, 29 (2005) 95-105.

[57] X. Ma, W. Zhang, S.A. Omer, S.B. Riffat, Experimental investigation of a novel steam ejector refrigerator suitable for solar energy applications, Applied Thermal Engineering, 30 (2010) 1320-1325.

[58] R.H. Yen, B.J. Huang, C.Y. Chen, T.Y. Shiu, C.W. Cheng, S.S. Chen, K. Shestopalov, Performance optimization for a variable throat ejector in a solar refrigeration system, International Journal of Refrigeration, 36 (2013) 1512-1520.

[59] S. Varga, A.C. Oliveira, B. Diaconu, Analysis of a solar-assisted ejector cooling system for air conditioning, International Journal of Low-Carbon Technologies, (2009).

[60] V.M. Nguyen, S.B. Riffat, P.S. Doherty, Development of a solar-powered passive ejector cooling system, Applied Thermal Engineering, 21 (2001) 157-168.

[61] S. Shen, X. Qu, B. Zhang, S. Riffat, M. Gillott, Study of a gas–liquid ejector and its application to a solar-powered bi-ejector refrigeration system, Applied Thermal Engineering, 25 (2005) 2891-2902.

[62] J. Kasperski, Two kinds of gravitational ejector refrigeration stimulation, Applied Thermal Engineering, 29 (2009) 3380-3385.

[63] J. Kasperski, Rotational type of a gravitational ejector refrigerator–A system balance of the refrigerant analysis, International Journal of Refrigeration, 33 (2010) 3-11.

[64] S.B. Riffat, A. Holt, A novel heat pipe/ejector cooler, Applied Thermal Engineering, 18 (1998) 93-101.

[65] B.M. Ziapour, A. Abbasy, First and second laws analysis of the heat pipe/ejector refrigeration cycle, Energy, 35 (2010) 3307-3314.

[66] D.-W. Sun, I.W. Eames, S. Aphornratana, Evaluation of a novel combined ejector-absorption refrigeration cycle, International Journal of Refrigeration, 19 (1996) 172-180.

[67] A. Sözen, M. Özalp, Solar-driven ejector-absorption cooling system, Applied Energy, 80 (2005) 97-113.

[68] D. Hong, G. Chen, L. Tang, Y. He, A novel ejector-absorption combined refrigeration cycle, International Journal of Refrigeration, 34 (2011) 1596-1603

[69] J. Wang, Y. Dai, T. Zhang, S. Ma, Parametric analysis for a new combined power and ejector-absorption refrigeration cycle, Energy, 34 (2009) 1587-1593.

[70] C.H. Li, R.Z. Wang, Y.Z. Lu, Investigation of a novel combined cycle of solar powered adsorption–ejection refrigeration system, Renewable Energy, 26 (2002) 611-622.

[71] X.J. Zhang, R.Z. Wang, A new combined adsorption-ejector refrigeration and heating hybrid system powered by solar energy, Applied Thermal Engineering, 22 (2002) 1245-1258.

[72] D.-W. Sun, Solar powered combined ejector-vapour compression cycle for air conditioning and refrigeration, Energy Conversion and Management, 38 (1997) 479-491.

[73] D.W. Sun, Evauation of a combined ejector-vapour-compression refrigeration system, International journal of energy research, 22 (1998) 333-342.

[74] S. Aphornratana, I.W. Eames, A small capacity steam-ejector refrigerator: experimental investigation of a system using ejector with movable primary nozzle, International Journal of Refrigeration, 20 (1997) 352-358.

[75] D.-W. Sun, Variable geometry ejectors and their applications in ejector refrigeration systems, Energy, 21 (1996) 919-929.

[76] I.W. Eames, M. Worall, S. Wu, An experimental investigation into the integration of a jet-pump refrigeration cycle and a novel jet-spray thermal ice storage system, Applied Thermal Engineering, 53 (2013) 285-290.

[77] D.K. Gupta, R. Kumar, N. Kumar, First and second law analysis of solar operated combined Rankine and ejector refrigeration cycle, Applied Solar Energy, 50 (2014) 113-121.

[78] Y.-M. Chen, C.-Y. Sun, Experimental study of the performance characteristics of a steam-ejector refrigeration system, Experimental Thermal and Fluid Science, 15 (1997) 384-394.

[79] W. Martynowsky, Use of waste heat for refrigeration, Refrigeration Eng., 62 (1954).

[80] K.P. Tyagi, K.N. Murty, Ejector-compression systems for cooling: Utilising low grade waste heat, Journal of heat recovery systems, 5 (1985) 545-550.

[81] F.C. Chen, C.T. Hsu, Performance of ejector heat pumps, International journal of energy research, 11 (1987) 289-300.

[82] R. Dorantes, A. Lallemand, Influence de la nature des fluides, purs ou en mélanges non-azéotropiques, sur les performances d'une machine de climatisation à éjecto-compresseur, International Journal of Refrigeration, 18 (1995) 21-30.

[83] A.A. Kornhauser, The use of an ejector as a refrigerant expander, (1990).

[84] J. Mizrahi, M. Solomiansky, T. Zisner, W. Resnick, Ejector refrigeration from low temperature energy sources, Bull. Res. Counc. of Israel, 6 (1957) 1-8.

[85] L.-T. Chen, A new ejector-absorber cycle to improve the COP of an absorption refrigeration system, Applied Energy, 30 (1988) 37-51.

[86] Y. Zhu, P. Jiang, Hybrid vapor compression refrigeration system with an integrated ejector cooling cycle, International Journal of Refrigeration, 35 (2012) 68-78.

[87] N. Al-Khalidy, An experimental study of an ejector cycle refrigeration machine operating on R113: Etude expérimentale d'une machine frigorifique à éjecteur au R113, International Journal of Refrigeration, 21 (1998) 617-625.

[88] L.-T. Chen, A heat driven mobile refrigeration cycle analysis, Energy Conversion, 18 (1978) 25-29.

[89] M. Sokolov, D. Hershgal, Enhanced ejector refrigeration cycles powered by low-grade heat, International Journal of Refrigeration, (1990).

[90] M. Sokolov, D. Hershgal, Solar-powered compression-enhanced ejector air conditioner, Solar Energy, 51 (1993) 183-194.

[91] K. Cizungu, A. Mani, M. Groll, Performance comparison of vapour jet refrigeration system with environment friendly working fluids, Applied Thermal Engineering, 21 (2001) 585-598.

[92] R. Yapıcı, Experimental investigation of performance of vapor ejector refrigeration system using refrigerant R123, Energy Conversion and Management, 49 (2008) 953-961.

[93] D.W. Sun, I.W. Eames, Performance characteristics of HCFC‐123 ejector refrigeration cycles, International journal of energy research, 20 (1996) 871-885.

[94] H.K. Ersoy, S. Yalcin, R. Yapici, M. Ozgoren, Performance of a solar ejector cooling-system in the southern region of Turkey, Applied Energy, 84 (2007) 971-983.

[95] F. Wang, S. Shen, A novel solar bi-ejector refrigeration system and the performance of the added injector with different structures and operation parameters, Solar Energy, 83 (2009) 2186-2194.

[96] M. Elakdhar, E. Nehdi, L. Kairouani, Analysis of a compression/ejector cycle for domestic refrigeration, Ind. Eng. Chem. Res., 46 (2007) 4639-4644.

[97] R. Yapıcı, H.K. Ersoy, A. Aktoprakoğlu, H.S. Halkacı, O. Yiğit, Experimental determination of the optimum performance of ejector refrigeration system depending on ejector area ratio, International Journal of Refrigeration, 31 (2008) 1183-1189.

[98] A. Selvaraju, A. Mani, Analysis of an ejector with environment friendly refrigerants, Applied Thermal Engineering, 24 (2004) 827-838.

[99] A. Selvaraju, A. Mani, Experimental investigation on R134a vapour ejector refrigeration system, International Journal of Refrigeration, 29 (2006) 1160-1166.

[100] G.K. Alexis, E.K. Karayiannis, A solar ejector cooling system using refrigerant R134a in the Athens area, Renewable Energy, 30 (2005) 1457-1469.

[101] E. Nehdi, L. Kairouani, M. Elakhdar, A solar ejector air-conditioning system using environment-friendly working fluids, International journal of energy research, 32 (2008) 1194-1201.

[102] J. Guo, H.G. Shen, Modeling solar-driven ejector refrigeration system offering air conditioning for office buildings, Energy and Buildings, 41 (2009) 175-181.

[103] Z. Dai, Y. He, Y. Huang, L. Tang, G. Chen, Ejector Performance of a Pump-less Ejector Refrigeration System Driven by Solar Thermal Energy, (2012).

[104] P.V.J.P. Reddy, S.S. Murthy, Studies on an Ejector-Absorption Refrigeration Cycle with New Working Fluid Pairs, in, 2005.

[105] R. Ben Mansour, M. Ouzzane, Z. Aidoun, Numerical Evaluation of Ejector-Assisted Mechanical Compression Systems for Refrigeration Applications, International Journal of Refrigeration, (2014).

[106] J. Yu, H. Chen, Y. Ren, Y. Li, A new ejector refrigeration system with an additional jet pump, Applied Thermal Engineering, 26 (2006) 312-319.

[107] J. Yu, H. Zhao, Y. Li, Application of an ejector in autocascade refrigeration cycle for the performance improvement, International Journal of Refrigeration, 31 (2008) 279-286.

[108] R. Roman, J.I. Hernandez, Performance of ejector cooling systems using low ecological impact refrigerants, International Journal of Refrigeration, 34 (2011) 1707-1716

[109] L. Kairouani, M. Elakhdar, E. Nehdi, N. Bouaziz, Use of ejectors in a multi-evaporator refrigeration system for performance enhancement, International Journal of Refrigeration, 32 (2009) 1173-1185.

[110] P. Chaiwongsa, S. Wongwises, Experimental study on R-134a refrigeration system using a two-phase ejector as an expansion device, Applied Thermal Engineering, 28 (2008) 467-477.

[111] N. Bilir, H.K. Ersoy, Performance improvement of the vapour compression refrigeration cycle by a two‐phase constant area ejector, International journal of energy research, 33 (2009) 469-480.

[112] S. Disawas, S. Wongwises, Experimental investigation on the performance of the refrigeration cycle using a two-phase ejector as an expansion device, International Journal of Refrigeration, 27 (2004) 587-594.

[113] E. Nehdi, L. Kairouani, M. Bouzaina, Performance analysis of the vapour compression cycle using ejector as an expander, International journal of energy research, 31 (2007) 364-375.

[114] P. Chaiwongsa, S. Wongwises, Effect of throat diameters of the ejector on the performance of the refrigeration cycle using a two-phase ejector as an expansion device, International Journal of Refrigeration, 30 (2007) 601-608.

[115] B.J. Huang, J.M. Chang, V.A. Petrenko, K.B. Zhuk, A solar ejector cooling system using refrigerant R141b, Solar Energy, 64 (1998) 223-226.

[116] H. Vidal, S. Colle, G.d.S. Pereira, Modelling and hourly simulation of a solar ejector cooling system, Applied Thermal Engineering, 26 (2006) 663-672

[117] M. Dennis, K. Garzoli, Use of variable geometry ejector with cold store to achive high solar fraction for solar cooling, International Journal of Refrigeration, 34 (2011) 1626-1632.

[118] B.J. Huang, S.S. Hu, S.H. Lee, Development of an ejector cooling system with thermal pumping effect, International Journal of Refrigeration, 29 (2006) 476-484

[119] B.J. Huang, V.A. Petrenko, J.M. Chang, C.P. Lin, S.S. Hu, A combined-cycle refrigeration system using ejector-cooling cycle as the bottom cycle, International Journal of Refrigeration, 24 (2001) 391-399.

[120] H. Vidal, S. Colle, Simulation and economic optimization of a solar assisted combined ejector-vapor compression cycle for cooling applications, Applied Thermal Engineering, 30 (2010) 478-486.

[121] J. Yu, Y. Li, A theoretical study of a novel regenerative ejector refrigeration cycle, International Journal of Refrigeration, 30 (2007) 464-470.

[122] J. Chen, H. Havtun, B. Palm, Parametric analysis of ejector working characteristics in the refrigeration system, Applied Thermal Engineering, 69 (2014) 130-142.

[123] L. Boumaraf, A. Lallemand, Modeling of an ejector refrigerating system operating in dimensioning and off-dimensioning conditions with the working fluids R142b and R600a, Applied Thermal Engineering, 29 (2009) 265-274.

[124] R. Dorantes, C.A. Estrada, I. Pilatowsky, Mathematical simulation of a solar ejector-compression refrigeration system, Applied Thermal Engineering, 16 (1996) 669-675.

[125] A. Arbel, M. Sokolov, Revisiting solar-powered ejector air conditioner—the greener the better, Solar Energy, 77 (2004) 57-66

[126] J.I. Hernández, R.J. Dorantes, R. Best, C.A. Estrada, The behaviour of a hybrid compressor and ejector refrigeration system with refrigerants 134a and 142b, Applied Thermal Engineering, 24 (2004) 1765-1783.

[127] J. Yu, Y. Ren, H. Chen, Y. Li, Applying mechanical subcooling to ejector refrigeration cycle for improving the coefficient of perfromance, Energy Conversion and Management, 48 (2007) 1193-1199.

[128] I.W. Eames, A.E. Ablwaifa, V. Petrenko, Results of an experimental study of an advanced jet-pump refrigerator operating with R245fa, Applied Thermal Engineering, 27 (2007) 2833-2840.

[129] I. Sarbu, A review on substitution strategy of non-ecological refrigerants from vapour compression-based refrigeration, air-conditioning and heat pump systems, International Journal of Refrigeration, (2014).

[130] Montreal Protocol, Montreal protocol on substances that deplete the ozone layer, Washington, DC: US Government Printing Office, (1987).

[131] M. Heymann, W. Resnick, Optimum ejector design for ejector-operated refrigeration cycle, Israel J. of Tech, 2 (1964) 242.

[132] J. Kasperski, B. Gil, Performance estimation of ejector cycles using heavier hydrocarbon refrigerants, Applied Thermal Engineering, (2014).

[133] J. Sarkar, Geometric parameter optimization of ejector ‐ expansion refrigeration cycle with natural refrigerants, International journal of energy research, 34 (2010) 84-94.

[134] W. Pridasawas, P. Lundqvist, An exergy analysis of a solar-driven ejector refrigeration system, Solar Energy, 76 (2004) 369-379.

[135] V.O. Petrenko, B.J. Huang, V.O. Ierin, Design-theoretical study of cascade CO2 sub-critical mechanical compression/butane ejector cooling cycle, International Journal of Refrigeration, 34 (2011) 1649-1656.

[136] K. Śmierciew, J. Gagan, D. Butrymowicz, J. Karwacki, Experimental investigations of solar driven ejector air-conditioning system, Energy and Buildings, (2014).

[137] D. Butrymowicz, K. Śmierciew, J. Karwacki, J. Gagan, Experimental investigations of low-temperature driven ejector refrigeration cycle operating with isobutane, International Journal of Refrigeration, 39 (2014) 196-209.

[138] W. Pridasawas, P. Lundqvist, A year-round dynamic simulation of a solar-driven ejector refrigeration system with iso-butane as a refrigerant, International Journal of Refrigeration, 30 (2007) 840-850

[139] Y. Liu, T. Xin, L. Cao, C. Wan, M. Zhang, Compression-injection hybrid refrigeration cycles in household refrigerators, Applied Thermal Engineering, 30 (2010) 2442-2447.

[140] T. Zhang, S. Mohamed, Conceptual Design and Analysis of Hydrocarbon-based Solar Thermal Power and Ejector Cooling Systems in Hot Climates, Journal of Solar Energy Engineering, (2014).

[141] B. Palm, Hydrocarbons as refrigerants in small heat pump and refrigeration systems–a review, International Journal of Refrigeration, 31 (2008) 552-563.

[142] T. Sankarlal, A. Mani, Experimental investigations on ejector refrigeration system with ammonia, Renewable Energy, 32 (2007) 1403-1413.

[143] K. Cizungu, M. Groll, Z.G. Ling, Modelling and optimization of two-phase ejectors for cooling systems

, Applied Thermal Engineering, 25 (2005) 1979-1994.

[144] R. Sirwan, M.A. Alghoul, K. Sopian, Y. Ali, J. Abdulateef, Evaluation of adding flash tank to solar combined ejector–absorption refrigeration system, Solar Energy, 91 (2013) 283-296.

[145] D.A. Dokandari, A.S. Hagh, S.M.S. Mahmoudi, Thermodynamic investigation and optimization of novel ejector-expansionCO2/ NH3cascade refrigeration cycles (novel CO2/NH3 cycle), International Journal of Refrigeration, (2014).

[146] S.B. Riffat, S.A. Omer, CFD modelling and experimental investigation of an ejector refrigeration system using methanol as the working fluid, International journal of energy research, 25 (2001) 115-128.

[147] G.K. Alexis, J.S. Katsanis, Performance characteristics of a methanol ejector refrigeration unit, Energy Conversion and Management, 45 (2004) 2729-2744.

[148] L. Jiang, Z. Gu, X. Feng, Y. Li, Thermo-economical analysis between new absorption–ejector hybrid refrigeration system and small double-effect absorption system, Applied Thermal Engineering, 22 (2002) 1027-1036.

[149] M. Worall, S. Omer, S. Riffat, Design analysis of a hybrid jet-pump CO2 compression system, (2010).

[150] D. Li, E.A. Groll, Transcritical CO2 refrigeration cycle with ejector-expansion device, International Journal of Refrigeration, 28 (2005) 766-773.

[151] J.-q. Deng, P.-x. Jiang, T. Lu, W. Lu, Particular characteristics of transcritical CO2 refrigeration cycle with an ejector, Applied Thermal Engineering, 27 (2007) 381-388.

[152] M. Yari, M. Sirousazar, Cycle improvement to ejector-expansion transcritical CO2 two-stage refrigeration cycle, International journal of energy research, 32 (2008) 677-687.

[153] M. Yari, Performance analysis and optimization of a new two-stage ejector-expansion transcritical CO2 refrigeration cycle, International Journal of Thermal Sciences, 48 (2009) 1997-2005.

[154] M. Nakagawa, A.R. Marasigan, T. Matsukawa, A. Kurashina, Experimental investigation on the effect of mixing length on the performance of two-phase ejector for CO2 refrigeration cycle with and without heat exchanger, International Journal of Refrigeration, 34 (2011) 1604-1613.

[155] M.E. Ahammed, S. Bhattacharyya, M. Ramgopal, Thermodynamic design and simulation of a CO2 based transcritical vapour compression refrigeration system with an ejector, International Journal of Refrigeration, (2014).

[156] S. Fangtian, M. Yitai, Thermodynamic analysis of transcritical CO2 refrigeration cycle with an ejector, Applied Thermal Engineering, 31 (2011) 1184-1189.

[157] J.M. Calm, G.C. Hourahan, Physical, safety and environmental data for current and alternative refrigerants, in, 2011, pp. 21-26.

[158] I.H. Bell, J. Wronski, S. Quoilin, V. Lemort, Pure and Pseudo-pure Fluid Thermophysical Property Evaluation and the Open-Source Thermophysical Property Library CoolProp, Industrial & Engineering Chemistry Research, 53 (2014) 2498-2508.

[159] H. El-Dessouky, H. Ettouney, I. Alatiqi, G. Al-Nuwaibit, Evaluation of steam jet ejectors, Chemical Engineering and Processing: Process Intensification, 41 (2002) 551-561.

[160] T. Sriveerakul, S. Aphornratana, K. Chunnanond, Performance prediction of steam ejector using computational fluid dynamics: Part 1. Validation of the CFD results, International Journal of Thermal Sciences, 46 (2007) 812-822.

[161] D. Maddiotto, Analysis of the behavior of an ejector in off-design conditions, in, Politecnico di Milano, 2013.

[162] H. Giffard, Injector, in: E. Patent (ed.), Vol. English Patent, No. 1,665, 1858.

[163] C.A. Parsons, Condenser, in: U.S.P.a.T. Office (ed.), Vol. U.S. Patent No. 1,197,148, Washington, DC, 1903.

[164] M. Leblanc, Cooling apparatus for houses, in: U.S.P.a.T. Office (ed.), Vol. U.S. Patent No. 967,024, Washington, DC, 1910.

[165] M. Leblanc, Refrigerating-machine, in: U.S.P.a.T. Office (ed.), Vol. U.S. Patent No. 1,029,201, Washington, DC, 1912.

[166] J.H. Keenan, E.P. Neumann, A simple air ejector, Journal of Applied Mechanics, 9 (1942) A75-A81.

[167] J.H. Keenan, An investigation of ejector design by analysis and experiment, Journal of Applied Mechanics, 17 (1950).

[168] L.A. DeFrate, A.E. Hoerl, Optimum design of ejectors using digital computers, in, Vol. 21, 1959.

[169] C.M. Ashley, Mixed refrigerant system, in, Vol. U.S. Patent No. 2,492,725, 1949.

[170] X. Liu, Efficiency of Non-Azeotropic Refrigerant Cycle, (1998).

[171] S. Varga, A.C. Oliveira, B. Diaconu, Influence of geometrical factors on steam ejector performance–a numerical assessment, International Journal of Refrigeration, 32 (2009) 1694-1701.

[172] Y. Zhu, W. Cai, C. Wen, Y. Li, Numerical investigation of geometry parameters for design of high performance ejectors, Applied Thermal Engineering, 29 (2009) 898-905.

[173] Y. Bartosiewicz, Z. Aidoun, P. Desevaux, Y. Mercadier, Numerical and experimental investigations on supersonic ejectors, International Journal of Heat and Fluid Flow, 26 (2005) 56-70.

[174] E. Rusly, L. Aye, W.W.S. Charters, A. Ooi, CFD analysis of ejector in a combined ejector cooling system, International Journal of Refrigeration, 28 (2005) 1092-1101

[175] S. Varga, A.C. Oliveira, B. Diaconu, Numerical assessment of steam ejector efficiencies using CFD, International Journal of Refrigeration, 32 (2009) 1203-1211.

[176] S.B. Riffat, P. Everitt, Experimental and CFD modelling of an ejector system for vehicle air conditioning, Journal of the Institute of Energy, 72 (1999) 41-47.

[177] P.G. Charalambous, G.G. Maidment, S.A. Kalogirou, K. Yiakoumetti, Photovoltaic thermal (PV/T) collectors: A review, Applied Thermal Engineering, 27 (2007) 275-286.

[178] B.J. Huang, V.A. Petrenko, I.Y. Samofatov, N.A. Shchetinina, Collector selection for solar ejector cooling system, Solar Energy, 71 (2001) 269-274.

[179] B.M. Diaconu, S. Varga, A.C. Oliveira, Numerical simulation of a solar-assisted ejector air conditioning system with cold storage, Energy, 36 (2011) 1280-1291.

[180] B.M. Diaconu, Energy analysis of a solar-assisted ejector cycle air conditioning system with low temperature thermal energy storage, Renewable Energy, 37 (2012) 266-276

[181] A. Bejan, J.V.C. Vargas, M. Sokolov, Optimal allocation of a heat-exchanger inventory in heat driven refrigerators, International journal of heat and mass transfer, 38 (1995) 2997-3004.

[182] H. Müller-Steinhagen, F. Trieb, Concentrating solar power, A review of the technology. Ingenia Inform QR Acad Eng, 18 (2004) 43-50.

[183] J.H. Wang, J.H. Wu, S.S. Hu, B.J. Huang, Performance of ejector cooling system with thermal pumping effect using R141b and R365mfc, Applied Thermal Engineering, 29 (2009) 1904-1912

[184] P. Srikhirin, S. Aphornratana, S. Chungpaibulpatana, A review of absorption refrigeration technologies, Renewable and sustainable energy reviews, 5 (2001) 343-372.

[185] C.A. Balaras, G. Grossman, H.-M. Henning, C.A. Infante Ferreira, E. Podesser, L. Wang, E. Wiemken, Solar air conditioning in Europe—an overview, Renewable and sustainable energy reviews, 11 (2007) 299-314.

[186] J. Sarkar, Ejector enhanced vapor compression refrigeration and heat pump systems—A review, Renewable and sustainable energy reviews, 16 (2012) 6647-6659.

[187] N.H. Gay, Refrigerating system, in: U.S.P.a.T. Office (ed.), Vol. U.S. Patent No. 1,836,318, Washington, DC, 1931.

[188] A.A. Kornhauser, P. Menegay, Method of reducing flow metastability in an ejector nozzle, in: U.S.P.a.T. Office (ed.), Vol. U.S. Patent No. 5,343,711, Washington, DC, 1994.

[189] M. Nakagawa, H. Takeuchi, Performance of two-phase ejector in refrigeration cycle, in, Vol. 382, 1998, pp. 1-8.

[190] H.K. Ersoy, N. Bilir, The influence of ejector component efficiencies on performance of ejector expander refrigeration cycle and exergy analysis, International Journal of Exergy, 7 (2010) 425-438.

[191] C. Lin, W. Cai, Y. Li, J. Yan, Y. Hu, Pressure recovery ratio in a variable cooling loads ejector-based multi-evaporator refrigeration system, Energy, 44 (2012) 649-656.

[192] C. Li, Y. Li, W. Cai, Y. Hu, H. Chen, J. Yan, Analysis on performance characteristics of ejector with variable area-ratio for multi-evaporator refrigeration system based on experimental data, Applied Thermal Engineering, 68 (2014) 125-132.

[193] J. Yu, Z. Du, Theoretical study of a transcritical ejector refrigeration cycle with refrigerant R143a, Renewable Energy, 35 (2010) 2034-2039.

[194] J.P. Liu, J.P. Chen, Z.J. Chen, Thermodynamic analysis on transcritical R744 vapor compression/ejector hybrid refrigeration cycle, (2002).

[195] S. Elbel, P. Hrnjak, Experimental validation of a prototype ejector designed to reduce throttling losses encountered in transcritical R744 system operation, International Journal of Refrigeration, 31 (2008) 411-422.

[196] R.P. Braden, K.S. Nagaraja, H.J.P. Von Ohain, Proceedings: ejector workshop for aerospace applications, in: Flight Dynamics Laboratory, University of Dayton Research Institute, 1982.

[197] S.A. Sherif, W.E. Lear, J.M. Steadham, P.L. Hunt, J.B. Holladay, Analysis and modeling of a two-phase jet pump of a thermal management system for aerospace applications, International journal of mechanical sciences, 42 (2000) 185-198.

[198] Maritime Diesel Electric Inc., http://www.mardiesel.com.

[199] Ellehammer, http://www.hellehammer.dk.

[200] SAMHWA Mixing Tech Co., http://www.samhwamix.com.

[201] GD Nash, http://www.gdnash.com.

[202] Körting Hannover AG, http://www.koerting.de.

[203] Global DENSO, http://www.globaldenso.com.

[204] S.A. Tassou, J.S. Lewis, Y.T. Ge, A. Hadawey, I. Chaer, A review of emerging technologies for food refrigeration applications, Applied Thermal Engineering, 30 (2010) 263-276.

Chapter 2

[1] G. Besagni, An integrated thermodynamic CFD approach to ejector modeling, in, Politecnico di Milano, 2012.

[2] D. Maddiotto, Analysis of the behavior of an ejector in off-design conditions, in, Politecnico di Milano, 2013.

[3] H.K. Versteeg, W. Malalasekera, An introduction to computational fluid dynamics: the finite volume method, Pearson Education, 2007.

[4] P.K. Kundu, I.M. Cohen, D.R. Dowling, Fluid mechanics 5th ed, in, Academic Press, 2011.

[5] C. Osnaghi, Teoria delle turbomacchine, Società Editrice Esculapio, 2013.

[6] F. Inzoli, Course notes for "Termo-fluidodinamica computazionale per l'ingegneria", (2013-2014).

[7] S. He, Y. Li, R.Z. Wang, Progress of mathematical modeling on ejectors, Renewable and sustainable energy reviews, 13 (2009) 1760-1780.

[8] H. El-Dessouky, H. Ettouney, I. Alatiqi, G. Al-Nuwaibit, Evaluation of steam jet ejectors, Chemical Engineering and Processing: Process Intensification, 41 (2002) 551-561.

[9] K. Cizungu, A. Mani, M. Groll, Performance comparison of vapour jet refrigeration system with environment friendly working fluids, Applied Thermal Engineering, 21 (2001) 585-598.

[10] A.B. Little, S. Garimella, A review of ejector technology for refrigeration applications, International Journal of Air-Conditioning and Refrigeration, 19 (2011) 1-15.

[11] N.S. Kumar, K.T. Ooi, One dimensional model of an ejector with special attention to Fanno flow within the mixing chamber, Applied Thermal Engineering, 65 (2014) 226-235.

[12] T. Sriveerakul, S. Aphornratana, K. Chunnanond, Performance prediction of steam ejector using computational fluid dynamics: Part 1. Validation of the CFD results, International Journal of Thermal Sciences, 46 (2007) 812-822.

[13] S. Alimohammadi, T. Persoons, D.B. Murray, M.S. Tehrani, B. Farhanieh, J. Koehler, A Validated Numerical-Experimental Design Methodology for a Movable Supersonic Ejector Compressor for Waste-Heat Recovery, Journal of Thermal Science and Engineering Applications, 6 (2014) 021001.

[14] S.M.V. Rao, G. Jagadeesh, Observations on the non-mixed length and unsteady shock motion in a two dimensional supersonic ejector, Physics of Fluids, 26 (2014).

[15] B.J. Huang, C.B. Jiang, F.L. Hu, Ejector performance characteristics and design analysis of jet refrigeration system, Journal of engineering for gas turbines and power, 107 (1985) 792-802.

[16] Y.-M. Chen, C.-Y. Sun, Experimental study of the performance characteristics of a steam-ejector refrigeration system, Experimental Thermal and Fluid Science, 15 (1997) 384-394.

[17] I.W. Eames, S. Wu, M. Worall, S. Aphornratana, An experimental investigation of steam ejectors for applications in jet-pump refrigerators powered by low-grade heat, Proceedings of the Institution of Mechanical Engineers, Part A: Journal of Power and Energy, 213 (1999) 351-361.

[18] T. Sriveerakul, S. Aphornratana, K. Chunnanond, Performance prediction of steam ejector using computational fluid dynamics: Part 2. Flow structure of a steam ejector influenced by operating pressures and geometries, International Journal of Thermal Sciences, 46 (2007) 823-833.

[19] J.H. Keenan, An investigation of ejector design by analysis and experiment, Journal of Applied Mechanics, 17 (1950).

[20] J. Fabri, R. Siestrunck, Supersonic air ejectors, Advances in applied mechanics, 5 (1958) 1-34.

[21] J.T. Munday, D.F. Bagster, A new ejector theory applied to steam jet refrigeration, Industrial & Engineering Chemistry Process Design and Development, 16 (1977) 442-449.

[22] Y. Zhu, W. Cai, C. Wen, Y. Li, Shock circle model for ejector performance evaluation, Energy Conversion and Management, 48 (2007) 2533-2541.

[23] J. Chen, H. Havtun, B. Palm, Investigation of ejectors in refrigeration system: Optimum performance evaluation and ejector area ratios perspectives, Applied Thermal Engineering, 64 (2014) 182-191.

[24] B.J. Huang, J.M. Chang, C.P. Wang, V.A. Petrenko, A 1-D analysis of ejector performance, International Journal of Refrigeration, 22 (1999) 354-364.

[25] W. Chen, M. Liu, D. Chong, J. Yan, A.B. Little, Y. Bartosiewicz, A 1D model to predict ejector performance at critical and sub-critical operational regimes, International Journal of Refrigeration, 36 (2013) 1750-1761.

[26] G. Besagni, R. Mereu, E. Colombo, CFD study of ejector efficiencies, in: ASME 2014 12th Biennal Conference on Engineering Systems Design and Analysis, Vol. Dynamics, Vibration and Control; Energy; Fluid Engineering; MIcro and Nano Manufacturing, ESDA2014-20053, Copenhagen, Denmark, July 25-27, 2014, 2014, pp. V02T11A004.

[27] J. Kasperski, B. Gil, Performance estimation of ejector cycles using heavier hydrocarbon refrigerants, Applied Thermal Engineering, (2014).

[28] J. Yu, H. Zhao, Y. Li, Application of an ejector in autocascade refrigeration cycle for the performance improvement, International Journal of Refrigeration, 31 (2008) 279-286.

[29] S. Varga, A.C. Oliveira, B. Diaconu, Numerical assessment of steam ejector efficiencies using CFD, International Journal of Refrigeration, 32 (2009) 1203-1211.

[30] A.L. Addy, J.C. Dutton, C.C. Mikkelsen, Supersonic ejector-diffuser theory and experiments, in, DTIC Document, 1982.

[31] S. Aphornratana, Theoretical and experimental investigation of a combined ejector-absorption refrigerator, in, University of Sheffield, Department of Mechanical and Process Engineering, 1995.

[32] H.K. Abdel-Aal, A.S. Al-Zakri, M.E. El-Sarha, M.E. El-Swify, G.M. Assassa, Other options of mass and energy input for steam jet refrigeration systems, The Chemical Engineering Journal, 45 (1990) 99-110.

[33] J.M. Cardemil, S. Colle, A general model for evaluation of vapor ejectors performance for application in refrigeration, Energy Conversion and Management, 64 (2012) 79-86.

[34] I.W. Eames, S. Aphornratana, H. Haider, A theoretical and experimental study of a small-scale steam jet refrigerator, International Journal of Refrigeration, 18 (1995) 378-386.

[35] N.H. Aly, A. Karameldin, M.M. Shamloul, Modelling and simulation of steam jet ejectors, desalination, 123 (1999) 1-8.

[36] X. Chen, S. Omer, M. Worall, S. Riffat, Recent developments in ejector refrigeration technologies, Renewable and sustainable energy reviews, 19 (2013) 629-651.

[37] M. Yazdani, A.A. Alahyari, T.D. Radcliff, Numerical Modeling and Validation of Supersonic Two-Phase Flow of CO2 in Converging-Diverging Nozzles, Journal of Fluids Engineering, 136 (2014) 014503.

[38] N. Ruangtrakoon, T. Thongtip, S. Aphornratana, T. Sriveerakul, CFD simulation on the effect of primary nozzle geometries for a steam ejector in refrigeration cycle, International Journal of Thermal Sciences, 63 (2013) 133-145.

[39] K. Chunnanond, S. Aphornratana, An experimental investigation of a steam ejector refrigerator: the analysis of the pressure profile along the ejector, Applied Thermal Engineering, 24 (2004) 311-322.

[40] S. Varga, A.C. Oliveira, B. Diaconu, Influence of geometrical factors on steam ejector performance–a numerical assessment, International Journal of Refrigeration, 32 (2009) 1694-1701.

[41] A. Fluent, 12.0 User's guide, User Inputs for Porous Media, 6 (2009).

[42] R.D. Zucker, O. Biblarz, Fundamentals of gas dynamics, John Wiley & Sons, 2002.

[43] V. Babu, Fundamentals of gas dynamics, Ane Books Pvt Ltd, 2008.

[44] G. Grazzini, A. Mariani, A simple program to design a multi-stagejet-pump for refrigeration cycles, Energy Conversion and Management, 39 (1998) 1827-1834.

[45] R.B. Power, Steam jet ejectors for the process industries.[Glossary included], (1994).

[46] E.D. Rogdakis, G.K. Alexis, Design and parametric investigation of an ejector in an air-conditioning system, Applied Thermal Engineering, 20 (2000) 213-226.

[47] M. Ouzzane, Z. Aidoun, Model development and numerical procedure for detailed ejector analysis and design, Applied Thermal Engineering, 23 (2003) 2337-2351.

[48] A. Selvaraju, A. Mani, Analysis of an ejector with environment friendly refrigerants, Applied Thermal Engineering, 24 (2004) 827-838.

[49] R. Yapıcı, H.K. Ersoy, Performance characteristics of the ejector refrigeration system based on the constant area ejector flow model, Energy Conversion and Management, 46 (2005) 3117-3135.

[50] J. Yu, H. Chen, Y. Ren, Y. Li, A new ejector refrigeration system with an additional jet pump, Applied Thermal Engineering, 26 (2006) 312-319.

[51] S. Aphornratana, S. Chungpaibulpatana, P. Srikhirin, Experimental investigation of an ejector refrigerator: effect of mixing chamber geometry on system performance, International journal of energy research, 25 (2001) 397-411.

[52] A. Hemidi, F. Henry, S. Leclaire, J.-M. Seynhaeve, Y. Bartosiewicz, CFD analysis of a supersonic air ejector. Part I: experimental validation of single-phase and two-phase operation, Applied Thermal Engineering, 29 (2009) 1523-1531.

[53] R. Yapıcı, H.K. Ersoy, A. Aktoprakoğlu, H.S. Halkacı, O. Yiğit, Experimental determination of the optimum performance of ejector refrigeration system depending on ejector area ratio, International Journal of Refrigeration, 31 (2008) 1183-1189.

[54] H. Lund, T. Flatten, Equilibrium conditions and sound velocities in two-phase flows, in, Vol. 112, 2010.

[55] K. Banasiak, A. Hafner, Mathematical modelling of supersonic two-phase R744 flows through converging–diverging nozzles: The effects of phase transition models, Applied Thermal Engineering, 51 (2013) 635-643.

[56] N. Deberne, J.F. Leone, A. Duque, A. Lallemand, A model for calculation of steam injector performance, International Journal of Multiphase Flow, 25 (1999) 841-855.

[57] S.A. Sherif, W.E. Lear, J.M. Steadham, P.L. Hunt, J.B. Holladay, Analysis and modeling of a two-phase jet pump of a thermal management system for aerospace applications, International journal of mechanical sciences, 42 (2000) 185-198.

[58] N. Beithou, H.S. Aybar, A mathematical model for steam-driven jet pump, International Journal of Multiphase Flow, 26 (2000) 1609-1619.

[59] G. Cattadori, L. Galbiati, L. Mazzocchi, P. Vanini, A single-stage high pressure steam injector for next generation reactors: test results and analysis, International Journal of Multiphase Flow, 21 (1995) 591-606.

[60] D. Li, E.A. Groll, Transcritical CO2 refrigeration cycle with ejector-expansion device, International Journal of Refrigeration, 28 (2005) 766-773.

[61] F. Liu, E.A. Groll, Analysis of a Two Phase Flow Ejector For Transcritical CO2 Cycle, (2008).

[62] Y. Zhu, Y. Li, Novel ejector model for performance evaluation on both dry and wet vapors ejectors, International Journal of Refrigeration, 32 (2009) 21-31.

[63] K. Banasiak, A. Hafner, 1D Computational model of a two-phase R744 ejector for expansion work recovery, International Journal of Thermal Sciences, 50 (2011) 2235-2247.

[64] X.-x. Xu, G.-m. Chen, L.-m. Tang, Z.-j. Zhu, S. Liu, Experimental evaluation of the effect of an internal heat exchanger on a transcritical CO2 ejector system, Journal of Zhejiang University-SCIENCE A, 12 (2011) 146-153.

[65] F. Mazzelli, A. Milazzo, Performance analysis of a supersonic ejector cycle working with R245fa, International Journal of Refrigeration.

[66] S.B. Riffat, S.A. Omer, CFD modelling and experimental investigation of an ejector refrigeration system using methanol as the working fluid, International journal of energy research, 25 (2001) 115-128.

[67] Y. Bartosiewicz, Z. Aidoun, P. Desevaux, Y. Mercadier, Cfd-experiments integration in the evaluation of six turbulence models for supersonic ejector modeling, in, 2003.

[68] P. Desevaux, O. Aeschbacher, Numerical and experimental flow visualizations of the mixing process inside an induced air ejector, International Journal of Turbo and Jet Engines, 19 (2002) 71-78.

[69] P. Desevaux, F. Lanzetta, Y. Bailly, CFD modelling of shock train inside a supersonic ejector: Validation against flow visualizations and pressure measurements in the case of zero-secondary flow, in, 2002.

[70] V. Dvorak, P. Safarik, Supersonic flow structure in the entrance part of a mixing chamber of 2D model ejector, Journal of Thermal Science, 12 (2003) 344-349.

[71] E. Rusly, L. Aye, W.W.S. Charters, A. Ooi, CFD analysis of ejector in a combined ejector cooling system, International Journal of Refrigeration, 28 (2005) 1092-1101

[72] V. Dvorak, P. Safarik, Transonic instability in entrance part of mixing chamber of high-speed ejector, Journal of Thermal Science, 14 (2005) 258-264.

[73] Y. Bartosiewicz, Z. Aidoun, P. Desevaux, Y. Mercadier, Numerical and experimental investigations on supersonic ejectors, International Journal of Heat and Fluid Flow, 26 (2005) 56-70.

[74] Y. Bartosiewicz, Z. Aidoun, Y. Mercadier, Numerical assessment of ejector operation for refrigeration applications based on CFD, Applied Thermal Engineering, 26 (2006) 604-612.

[75] K. Pianthong, W. Seehanam, M. Behnia, T. Sriveerakul, S. Aphornratana, Investigation and improvement of ejector refrigeration system using computational fluid dynamics technique, Energy Conversion and Management, 48 (2007) 2556-2564.

[76] D. Scott, Z. Aidoun, O. Bellache, M. Ouzzane, CFD simulations of a supersonic ejector for use in refrigeration applications, (2008).

[77] I.W. Eames, A.E. Ablwaifa, V. Petrenko, Results of an experimental study of an advanced jet-pump refrigerator operating with R245fa, Applied Thermal Engineering, 27 (2007) 2833-2840.

[78] C. Bao, M. Ouyang, B. Yi, Modeling and control of air stream and hydrogen flow with recirculation in a PEM fuel cell system—I. Control-oriented modeling, International journal of hydrogen energy, 31 (2006) 1879-1896.

[79] Y. Zhu, W. Cai, C. Wen, Y. Li, Numerical investigation of geometry parameters for design of high performance ejectors, Applied Thermal Engineering, 29 (2009) 898-905.

[80] M. Ji, T. Utomo, J. Woo, Y. Lee, H. Jeong, H. Chung, CFD investigation on the flow structure inside thermo vapor compressor, Energy, 35 (2010) 2694-2702.

[81] S. Varga, A.C. Oliveira, X. Ma, S.A. Omer, W. Zhang, S.B. Riffat, Experimental and numerical analysis of a variable area ratio steam ejector, International Journal of Refrigeration, 34 (2011) 1668-1675.

[82] J. Yan, W. Cai, Y. Li, Geometry parameters effect for air-cooled ejector cooling systems with R134a refrigerant, Renewable Energy, 46 (2012) 155-163.

[83] X. Yang, X. Long, X. Yao, Numerical investigation on the mixing process in a steam ejector with different nozzle structures, International Journal of Thermal Sciences, 56 (2012) 95-106.

[84] C. Lin, W. Cai, Y. Li, J. Yan, Y. Hu, K. Giridharan, Numerical investigation of geometry parameters for pressure recovery of an adjustable ejector in multi-evaporator refrigeration system, Applied Thermal Engineering, 61 (2013) 649-656.

[85] J. Smolka, Z. Bulinski, A. Fic, A.J. Nowak, K. Banasiak, A. Hafner, A computational model of a transcritical R744 ejector based on a homogeneous real fluid approach, Applied Mathematical Modelling, 37 (2013) 1208-1224.

[86] C. Lucas, H. Rusche, A. Schroeder, J. Koehler, Numerical investigation of a two-phase CO2 ejector, International Journal of Refrigeration, (2014).

[87] M.T. Kandakure, V.G. Gaikar, A.W. Patwardhan, Hydrodynamic aspects of ejectors, Chemical Engineering Science, 60 (2005) 6391-6402.

[88] S.R. Bhutada, V.G. Pangarkar, Gas induction and hold-up characteristics of liquid jet loop reactors, Chemical Engineering Communications, 61 (1987) 239-258.

[89] M.I. Kim, O. Sin Kim, D.H. Lee, S. Done Kim, Numerical and experimental investigations of gas–liquid dispersion in an ejector, Chemical Engineering Science, 62 (2007) 7133-7139.

[90] R.L. Yadav, A.W. Patwardhan, Design aspects of ejectors: Effects of suction chamber geometry, Chemical Engineering Science, 63 (2008) 3886-3897.

[91] S. Balamurugan, V.G. Gaikar, A.W. Patwardhan, Effect of ejector configuration on hydrodynamic characteristics of gas–liquid ejectors, Chemical Engineering Science, 63 (2008) 721-731.

[92] C. Li, Y.Z. Li, Investigation of entrainment behavior and characteristics of gas–liquid ejectors based on CFD simulation, Chemical Engineering Science, 66 (2011) 405-416.

[93] M. Colarossi, N. Trask, D.P. Schmidt, M.J. Bergander, Multidimensional modeling of condensing two-phase ejector flow, International Journal of Refrigeration, 35 (2012) 290-299.

[94] M. Nakagawa, A.R. Marasigan, T. Matsukawa, A. Kurashina, Experimental investigation on the effect of mixing length on the performance of two-phase ejector for CO2 refrigeration cycle with and without heat exchanger, International Journal of Refrigeration, 34 (2011) 1604-1613.

[95] M. Yazdani, A.A. Alahyari, T.D. Radcliff, Numerical modeling of two-phase supersonic ejectors for work-recovery applications, International journal of heat and mass transfer, 55 (2012) 5744-5753.

[96] M. Nakagawa, M.S. Berana, A. Kishine, Supersonic two-phase flow of CO2 through converging–diverging nozzles for the ejector refrigeration cycle, International Journal of Refrigeration, 32 (2009) 1195-1202.

[97] C. Lucas, A. Schroeder, J. Koehler, W. Tegethoff, Experimental investigation of the performance curve of a CO2 ejector on the expansion side of a vapour compression refrigeration system, 2nd IIR International Conference on Sustainability and Cold Chain, (2013).

Chapter 3

[1] J. Kasperski, B. Gil, Performance estimation of ejector cycles using heavier hydrocarbon refrigerants, Applied Thermal Engineering, (2014).

[2] J. Chen, H. Havtun, B. Palm, Investigation of ejectors in refrigeration system: Optimum performance evaluation and ejector area ratios perspectives, Applied Thermal Engineering, 64 (2014) 182-191.

[3] W. Chen, M. Liu, D. Chong, J. Yan, A.B. Little, Y. Bartosiewicz, A 1D model to predict ejector performance at critical and sub-critical operational regimes, International Journal of Refrigeration, 36 (2013) 1750-1761.

[4] Y. Zhu, W. Cai, C. Wen, Y. Li, Shock circle model for ejector performance evaluation, Energy Conversion and Management, 48 (2007) 2533-2541.

[5] N.S. Kumar, K.T. Ooi, One dimensional model of an ejector with special attention to Fanno flow within the mixing chamber, Applied Thermal Engineering, 65 (2014) 226-235.

[6] R.D. Zucker, O. Biblarz, Fundamentals of gas dynamics, John Wiley & Sons, 2002.

[7] V. Babu, Fundamentals of gas dynamics, Ane Books Pvt Ltd, 2008.

[8] J.M. Cardemil, S. Colle, A general model for evaluation of vapor ejectors performance for application in refrigeration, Energy Conversion and Management, 64 (2012) 79-86.

[9] MathWorks, MATLAB R2013a.

[10] B.J. Huang, J.M. Chang, C.P. Wang, V.A. Petrenko, A 1-D analysis of ejector performance, International Journal of Refrigeration, 22 (1999) 354-364.

[11] A.E. Ablwaifa, A theoretical and experimental investigation of jet-pump refrigeration system, in, University of Nottingham, 2006.

[12] X.-x. Xu, G.-m. Chen, L.-m. Tang, Z.-j. Zhu, S. Liu, Experimental evaluation of the effect of an internal heat exchanger on a transcritical CO2 ejector system, Journal of Zhejiang University-SCIENCE A, 12 (2011) 146-153.

[13] I.H. Bell, J. Wronski, S. Quoilin, V. Lemort, Pure and Pseudo-pure Fluid Thermophysical Property Evaluation and the Open-Source Thermophysical Property Library CoolProp, Industrial & Engineering Chemistry Research, 53 (2014) 2498-2508.

[14] E.W. Lemmon, M.L. Huber, M.O. McLinden, NIST reference fluid thermodynamic and transport properties–REFPROP, in, Version, 2002.

[15] H.Y. Afeefy, J.F. Liebman, S.E. Stein, P.J. Linstrom, W.G. Mallard, NIST Chemistry WebBook, NIST Standard Reference Database, 69 (2005).

[16] S.A. Klein, F.L. Alvarado, Engineering Equation Solver (EES), FChart Software, in, 2010.

[17] R. Yapıcı, H.K. Ersoy, A. Aktoprakoğlu, H.S. Halkacı, O. Yiğit, Experimental determination of the optimum performance of ejector refrigeration system depending on ejector area ratio, International Journal of Refrigeration, 31 (2008) 1183-1189.

[18] A. Hemidi, F. Henry, S. Leclaire, J.-M. Seynhaeve, Y. Bartosiewicz, CFD analysis of a supersonic air ejector. Part I: experimental validation of single-phase and two-phase operation, Applied Thermal Engineering, 29 (2009) 1523-1531.

[19] S. Aphornratana, S. Chungpaibulpatana, P. Srikhirin, Experimental investigation of an ejector refrigerator: effect of mixing chamber geometry on system performance, International journal of energy research, 25 (2001) 397-411.

[20] H. Schlichting, Boundary-layer theory, (1968).

[21] H. Lund, T. Flatten, Equilibrium conditions and sound velocities in two-phase flows, in, Vol. 112, 2010.

[22] R. Saurel, F. Petitpas, R. Abgrall, Modelling phase transition in metastable liquids: application to cavitating and flashing flows, Journal of Fluid Mechanics, 607 (2008) 313-350.

[23] I.W. Eames, S. Aphornratana, H. Haider, A theoretical and experimental study of a small-scale steam jet refrigerator, International Journal of Refrigeration, 18 (1995) 378-386.

[24] G. Grazzini, A. Milazzo, S. Piazzini, Prediction of condensation in steam ejector for a refrigeration system, International Journal of Refrigeration, 34 (2011) 1641-1648.

[25] V.P. Cary, Liquid–Vapor Phase-Change Phenomena: An Introduction to the Thermophysics of Vaporization and Condensation Process in Heat Transfer Equipment, Bristol, by Taylor & Francis, (1992).

[26] T. Zhang, S. Mohamed, Conceptual Design and Analysis of Hydrocarbon-based Solar Thermal Power and Ejector Cooling Systems in Hot Climates, Journal of Solar Energy Engineering, (2014).

[27] A. Selvaraju, A. Mani, Experimental investigation on R134a vapour ejector refrigeration system, International Journal of Refrigeration, 29 (2006) 1160-1166.

[28] S. Varga, A.C. Oliveira, B. Diaconu, Influence of geometrical factors on steam ejector performance–a numerical assessment, International Journal of Refrigeration, 32 (2009) 1694-1701.

[29] D.W. Sun, I.W. Eames, Performance characteristics of HCFC‐123 ejector refrigeration cycles, International journal of energy research, 20 (1996) 871-885.

[30] W. Pridasawas, Solar-driven refrigeration systems with focus on the ejector cycle, (2006).

[31] D.S. Kim, C.A. Infante Ferreira, Solar refrigeration options–a state-of-the-art review, International Journal of Refrigeration, 31 (2008) 3-15.

[32] I. Sarbu, C. Sebarchievici, Review of solar refrigeration and cooling systems, Energy and Buildings, 67 (2013) 286-297.

[33] R. Yapıcı, Experimental investigation of performance of vapor ejector refrigeration system using refrigerant R123, Energy Conversion and Management, 49 (2008) 953-961.

[34] A. Selvaraju, A. Mani, Analysis of an ejector with environment friendly refrigerants, Applied Thermal Engineering, 24 (2004) 827-838.

[35] D.-W. Sun, Variable geometry ejectors and their applications in ejector refrigeration systems, Energy, 21 (1996) 919-929.

[36] G. Besagni, R. Mereu, E. Colombo, CFD study of ejector efficiencies, in: ASME 2014 12th Biennal Conference on Engineering Systems Design and Analysis, Vol. Dynamics, Vibration and Control; Energy; Fluid Engineering; MIcro and Nano Manufacturing, ESDA2014-20053, Copenhagen, Denmark, July 25-27, 2014, 2014, pp. V02T11A004.

[37] S. Varga, A.C. Oliveira, B. Diaconu, Numerical assessment of steam ejector efficiencies using CFD, International Journal of Refrigeration, 32 (2009) 1203-1211.

[38] G. Besagni, An integrated thermodynamic CFD approach to ejector modeling, in, Politecnico di Milano, 2012.

Chapter 4

[1] E. Colombo, F. Inzoli, R. Mereu, A methodology for qualifying industrial CFD: The Q-3 approach and the role of a protocol, Computers & Fluids, 54 (2012) 56-66.

[2] G. Comini, G. Croce, E. Nobile, E. Colombo, F. Inzoli, Fondamenti di termofluidodinamica computazionale, SGE editoriali, Padova, (2008).

[3] F. Inzoli, Course notes for "Termo-fluidodinamica computazionale per l'ingegneria", (2013-2014).

[4] T. European Research Community on Flow, Q. Combustion. Special Interest Group on, C.F.D. Trust in Industrial, M. Casey, T. Wintergerste, Best practice guidelines, Ercoftac, 2000.

[5] C. Hirsh, The QNET-CFD Project, QNET-CFD Network Newsletter, 1 (2001) 4-5.

[6] G. Besagni, An integrated thermodynamic CFD approach to ejector modeling, in, Politecnico di Milano, 2012.

[7] Y. Bartosiewicz, Z. Aidoun, P. Desevaux, Y. Mercadier, Numerical and experimental investigations on supersonic ejectors, International Journal of Heat and Fluid Flow, 26 (2005) 56-70.

[8] A. Hemidi, F. Henry, S. Leclaire, J.-M. Seynhaeve, Y. Bartosiewicz, CFD analysis of a supersonic air ejector. Part I: experimental validation of single-phase and two-phase operation, Applied Thermal Engineering, 29 (2009) 1523-1531.

[9] G. Besagni, R. Mereu, E. Colombo, CFD study of ejector efficiencies, in: ASME 2014 12th Biennal Conference on Engineering Systems Design and Analysis, Vol. Dynamics, Vibration and Control; Energy; Fluid Engineering; MIcro and Nano Manufacturing, ESDA2014-20053, Copenhagen, Denmark, July 25-27, 2014, 2014, pp. V02T11A004.

[10] T. Sriveerakul, S. Aphornratana, K. Chunnanond, Performance prediction of steam ejector using computational fluid dynamics: Part 1. Validation of the CFD results, International Journal of Thermal Sciences, 46 (2007) 812-822.

[11] H.K. Versteeg, W. Malalasekera, An introduction to computational fluid dynamics: the finite volume method, Pearson Education, 2007.

[12] A. Fluent, 12.0 User's guide, User Inputs for Porous Media, 6 (2009).

[13] T. Sriveerakul, S. Aphornratana, K. Chunnanond, Performance prediction of steam ejector using computational fluid dynamics: Part 2. Flow structure of a steam ejector influenced by operating pressures and geometries, International Journal of Thermal Sciences, 46 (2007) 823-833.

[14] X.-D. Wang, J.-L. Dong, Numerical study on the performances of steam-jet vacuum pump at different operating conditions, Vacuum, 84 (2010) 1341-1346.

[15] N. Ruangtrakoon, T. Thongtip, S. Aphornratana, T. Sriveerakul, CFD simulation on the effect of primary nozzle geometries for a steam ejector in refrigeration cycle, International Journal of Thermal Sciences, 63 (2013) 133-145.

[16] E. Rusly, L. Aye, W.W.S. Charters, A. Ooi, CFD analysis of ejector in a combined ejector cooling system, International Journal of Refrigeration, 28 (2005) 1092-1101

[17] K. Pianthong, W. Seehanam, M. Behnia, T. Sriveerakul, S. Aphornratana, Investigation and improvement of ejector refrigeration system using computational fluid dynamics technique, Energy Conversion and Management, 48 (2007) 2556-2564.

[18] B. Zhang, X. Song, J. Lv, J. Zuo, Study on the key ejector structures of the waste heat-driven ejector air conditioning system with R236fa as working fluid, Energy and Buildings, 49 (2012) 209-215.

[19] N. Sharifi, M. Sharifi, Reducing energy consumption of a steam ejector through experimental optimization of the nozzle geometry, Energy, 66 (2014) 860-867.

[20] M. Yazdani, A.A. Alahyari, T.D. Radcliff, Numerical Modeling and Validation of Supersonic Two-Phase Flow of CO2 in Converging-Diverging Nozzles, Journal of Fluids Engineering, 136 (2014) 014503.

[21] F. Mazzelli, A. Milazzo, Performance analysis of a supersonic ejector cycle working with R245fa, International Journal of Refrigeration.

[22] Y. Bartosiewicz, Z. Aidoun, P. Desevaux, Y. Mercadier, Cfd-experiments integration in the evaluation of six turbulence models for supersonic ejector modeling, in, 2003.

[23] C. Li, Y.Z. Li, Investigation of entrainment behavior and characteristics of gas–liquid ejectors based on CFD simulation, Chemical Engineering Science, 66 (2011) 405-416.

[24] Y. Zhu, P. Jiang, Experimental and numerical investigation of the effect of shock wave characteristics on the ejector performance, International Journal of Refrigeration, 40 (2014) 31-42.

[25] K. Chunnanond, S. Aphornratana, An experimental investigation of a steam ejector refrigerator: the analysis of the pressure profile along the ejector, Applied Thermal Engineering, 24 (2004) 311-322.

[26] I.W. Eames, S. Wu, M. Worall, S. Aphornratana, An experimental investigation of steam ejectors for applications in jet-pump refrigerators powered by low-grade heat, Proceedings of the Institution of Mechanical Engineers, Part A: Journal of Power and Energy, 213 (1999) 351-361.

[27] S. Alimohammadi, T. Persoons, D.B. Murray, M.S. Tehrani, B. Farhanieh, J. Koehler, A Validated Numerical-Experimental Design Methodology for a Movable Supersonic Ejector Compressor for Waste-Heat Recovery, Journal of Thermal Science and Engineering Applications, 6 (2014) 021001.

[28] J.G. del Valle, J.M.S. Jabardo, F.C. Ruiz, J.F.S.J. Alonso, An experimental investigation of a R-134a ejector refrigeration system, International Journal of Refrigeration, 46 (2014) 105-113.

[29] J.T. Munday, D.F. Bagster, A new ejector theory applied to steam jet refrigeration, Industrial & Engineering Chemistry Process Design and Development, 16 (1977) 442-449.

[30] J.J. Ginoux, Supersonic Ejectors, in, DTIC Document, 1972.

[31] J. Chen, H. Havtun, B. Palm, Investigation of ejectors in refrigeration system: Optimum performance evaluation and ejector area ratios perspectives, Applied Thermal Engineering, 64 (2014) 182-191.

[32] W. Chen, M. Liu, D. Chong, J. Yan, A.B. Little, Y. Bartosiewicz, A 1D model to predict ejector performance at critical and sub-critical operational regimes, International Journal of Refrigeration, 36 (2013) 1750-1761.

[33] Y. Zhu, W. Cai, C. Wen, Y. Li, Shock circle model for ejector performance evaluation, Energy Conversion and Management, 48 (2007) 2533-2541.

[34] N.S. Kumar, K.T. Ooi, One dimensional model of an ejector with special attention to Fanno flow within the mixing chamber, Applied Thermal Engineering, 65 (2014) 226-235.

[35] J.M. Cardemil, S. Colle, A general model for evaluation of vapor ejectors performance for application in refrigeration, Energy Conversion and Management, 64 (2012) 79-86.

[36] J. Kasperski, B. Gil, Performance estimation of ejector cycles using heavier hydrocarbon refrigerants, Applied Thermal Engineering, (2014).

Chapter 5

[1] G. Besagni, An integrated thermodynamic CFD approach to ejector modeling, in, Politecnico di Milano, 2012.

[2] J. Chen, H. Havtun, B. Palm, Investigation of ejectors in refrigeration system: Optimum performance evaluation and ejector area ratios perspectives, Applied Thermal Engineering, 64 (2014) 182-191.

[3] W. Chen, M. Liu, D. Chong, J. Yan, A.B. Little, Y. Bartosiewicz, A 1D model to predict ejector performance at critical and sub-critical operational regimes, International Journal of Refrigeration, 36 (2013) 1750-1761.

[4] R. Yapıcı, H.K. Ersoy, Performance characteristics of the ejector refrigeration system based on the constant area ejector flow model, Energy Conversion and Management, 46 (2005) 3117-3135.

[5] C. Osnaghi, Teoria delle turbomacchine, Società Editrice Esculapio, 2013.

[6] G. Besagni, R. Mereu, E. Colombo, CFD study of ejector efficiencies, in: ASME 2014 12th Biennal Conference on Engineering Systems Design and Analysis, Vol. Dynamics, Vibration and Control; Energy; Fluid Engineering; MIcro and Nano Manufacturing, ESDA2014-20053, Copenhagen, Denmark, July 25-27, 2014, 2014, pp. V02T11A004.